
Establishing membrane mimetics for the mass spectrometric analysis of membrane proteins

Dissertation
zur Erlangung des
Doktorgrades der Naturwissenschaften (Dr. rer. nat)

der
Naturwissenschaftlichen Fakultät I - Biowissenschaften -

der Martin-Luther-Universität
Halle-Wittenberg,

vorgelegt
von Frau **Melissa Frick**
geboren am 17.01.1993 in Bad Homburg v. d. Höhe

eingereicht am: 25.07.2022

verteidigt am: 17.10.2022

Gutachter*innen

1. Jun.-Prof. Dr. Carla Schmidt, Martin-Luther-Universität Halle-Wittenberg
2. PD Annette Meister, Martin-Luther-Universität Halle-Wittenberg
3. Prof. Dr. Michael T Marty, University of Arizona, USA

“We cross that bridge when we get to it”

A quote from my dad who always believed in me.

Table of Contents

List of abbreviations	I
List of figures	IV
List of tables	VII
Summary	IX
Zusammenfassung	XI
1 Introduction	1
1.1 Membrane proteins, lipids and their interactions	1
1.1.1 Membrane proteins	1
1.1.2 The importance of lipids.....	3
1.1.3 Protein-lipid interactions	5
1.2 Membrane mimetics	7
1.2.1 Liposomes	7
1.2.2 Nanodiscs	9
1.3 Biophysical analysis of liposomes and nanodiscs	10
1.3.1 Dynamic light scattering.....	10
1.3.2 Negative-stain transmission electron microscopy	11
1.4 Mass spectrometry.....	11
1.4.1 Lipidomics.....	13
1.4.2 Native MS.....	14
1.4.3 Cross-linking MS	17
1.4.4 Instruments	19
1.4.4.1 The Q Exactive Plus Hybrid-Quadrupole-Orbitrap mass spectrometer	19
1.4.4.2 The Q-ToF Ultima mass spectrometer	20
2 Aim of this thesis	22
3 Materials & methods	24
3.1 Materials.....	24
3.1.1 Reagents	24
3.1.2 Plasmids, bacterial strains and enzymes.....	26
3.1.3 Lipids, peptides and proteins	26

3.1.4	Instruments, consumables and software	27
3.2	Methods	29
3.2.1	Molecular biological methods	29
3.2.1.1	Bacterial transformation	29
3.2.1.2	Plasmid purification.....	30
3.2.1.3	Determination of cell density	30
3.2.1.4	Cell culture and protein expression	30
3.2.1.5	Cell disruption	31
3.2.1.6	Protein purification of the p40phox (1-144) protein domain.....	32
3.2.1.7	Protein purification of MSP1E3D1	33
3.2.1.8	Protein purification of Syntaxin-1A	34
3.2.2	Protein biochemical methods	35
3.2.2.1	Protein concentration determination.....	35
3.2.2.2	Gel electrophoresis	35
3.2.2.3	Western blot analysis.....	35
3.2.2.4	Chemical cross-linking	36
3.2.3	Biophysical methods	37
3.2.3.1	Preparation of liposomes	37
3.2.3.2	Preparation of proteoliposomes with membrane-associated proteins	37
3.2.3.3	Preparation of nanodiscs.....	38
3.2.3.4	Reconstitution of an integral membrane protein into nanodiscs	38
3.2.3.5	DLS analysis.....	39
3.2.3.6	Liposome flotation assay	39
3.2.3.7	Negative-stain TEM of nanodiscs	39
3.2.3.8	Monolayer measurements.....	40
3.2.4	Mass spectrometric methods	40
3.2.4.1	Nano-ESI emitters for MS analysis.....	40
3.2.4.2	Sample preparation and direct infusion MS analysis	41
3.2.4.3	MS analysis of peptides.....	41
3.2.4.4	Buffer exchange for native MS	44
3.2.4.5	Native MS analysis.....	45
3.2.5	Data analysis.....	45
4	Results.....	46
4.1	Establishing liposomes for MS analysis of membrane-associated proteins	46

4.1.1	Preparation and characterization of liposomes	46
4.1.1.1	Characterization of single-component liposomes.....	48
4.1.1.2	Characterization of multi-component liposomes.....	49
4.1.2	MS analysis of liposomes.....	50
4.1.2.1	MS analysis of single-component liposomes	50
4.1.2.2	MS analysis of multi-component liposomes	52
4.1.3	Complementary investigation of liposomes by DLS and native MS	54
4.1.3.1	Analysis of multi-component liposomes with different sizes.....	54
4.1.3.2	Analysis of multi-component liposomes with a higher concentration	55
4.1.3.3	MS analysis of multi-component liposomes analyzed at different collisional voltages..	56
4.2	Analysis of liposomes in the presence of soluble peptides/proteins.....	57
4.2.1	MS Analysis of soluble peptides/proteins	57
4.2.2	MS analysis of peptides/proteins mixed with liposomes.....	60
4.3	Analysis of peptides/proteins associated with liposomes	63
4.3.1	Preparation and characterization of proteoliposomes.....	63
4.3.2	Analysis of the p40phox (1-144) protein domain associated with liposomes	64
4.3.2.1	Expression and purification of p40phox.....	65
4.3.2.2	Preparation and characterization of p40phox-proteoliposomes	65
4.3.2.3	MS analysis of p40phox	68
4.3.2.4	MS analysis of p40phox-proteoliposomes	69
4.3.3	Analysis of Melittin associated with liposomes	71
4.3.3.1	Preparation and characterization of Melittin-proteoliposomes.....	71
4.3.3.2	MS analysis of Melittin	74
4.3.3.3	MS analysis of Melittin-proteoliposomes (eukaryotic membrane composition).....	75
4.3.3.4	MS analysis of Melittin-proteoliposomes (prokaryotic membrane composition)	77
4.3.3.5	Complementary investigation of oligomeric states of Melittin	80
4.3.3.6	Complementary investigation of lipid preferences of Melittin.....	81
4.4	Establishing nanodiscs for MS analysis of membrane proteins	84
4.4.1	Preparation of nanodiscs.....	84
4.4.1.1	Expression and purification of MSP1E3D1	85
4.4.1.2	Preparation and purification of single-component nanodiscs.....	86
4.4.1.3	Preparation and purification of multi-component nanodiscs.....	86
4.4.2	DLS analysis and negative-stain TEM of nanodiscs	88
4.4.3	Establishing Syntaxin-1A nanodiscs	89

4.4.3.1	Expression and purification of Syntaxin-1A	90
4.4.3.2	Preparation and characterization of Syntaxin-1A nanodiscs.....	90
4.4.4	DLS analysis and negative-stain TEM of Syntaxin-1A nanodiscs.....	92
4.5	Chemical cross-linking of Syntaxin-1A nanodiscs	93
4.5.1	Manual validation of Syntaxin-1A nanodisc cross-links.....	94
5	Discussion and outlook.....	99
5.1	Choosing the right membrane mimetics for analyzing membrane proteins	99
5.2	Establishing liposomes for the analysis of membrane-associated proteins by MS	100
5.2.1	Selection of liposomes as membrane mimetics	100
5.2.2	Methodological considerations.....	101
5.2.3	MS analysis of liposomes.....	103
5.2.4	MS analysis of membrane proteins associated with liposomes.....	106
5.3	Establishing nanodiscs for the analysis of protein-protein interactions	111
5.3.1	Selection of nanodiscs as membrane mimetics	111
5.3.2	Methodological aspects - Chemical cross-linking of nanodiscs.....	112
5.3.3	Biological aspects - Chemical cross-linking of Syntaxin-1A in nanodiscs.....	113
6	References	115
7	Appendix	132
7.1	Supplementary figures.....	132
7.2	Supplementary Tables	142
	Acknowledgment	148
	Curriculum vitae	150
	Publication list	151
	Oral presentations	153
	Poster presentations	156
	Affidavit.....	156
	Eidesstattliche Erklärung	157

List of abbreviations

AmAc	ammonium acetate
ATP	adenosine triphosphate
BS3	bis(sulfosuccinimidyl)suberate
CE	collision energy
CEM	chain ejection model
CHAPS	3-[(3-cholamidopropyl)-dimethylammonio]-1-propane sulfonate
CID	collision-induced dissociation
CMC	critical micelle concentration
CRM	charged residue model
CSI	cesium iodide
DC	direct current
ddH ₂ O	double-distilled water
DHPC	1,2-diheptanoyl- <i>sn</i> -glycero-3-phosphocholine
DIBMA	diisobutylene-maleic acid
DLS	dynamic light scattering
DMPC	1,2-dimyristoyl- <i>sn</i> -glycero-3-phosphocholine
EDC	1-ethyl-3-[3-dimethylaminopropyl] carbodiimide-hydrochloride
EM	electron microscopy
ESI	electrospray ionization
FAIMS	high field asymmetric waveform ion mobility spectrometry
FDR	false discovery rate
GC	gas chromatography
GPL	glycerophospholipids
GUVs	giant unilamellar vesicles
HCD	High-energy collisional dissociation
HDX	hydrogen-deuterium exchange
HILIC	hydrophilic liquid chromatography
IEM	ion evaporation model
LC-MS/MS	liquid chromatography-coupled mass spectrometry
LUVs	large unilamellar vesicles
<i>m/z</i>	mass-to-charge ratio
MLVs	multilamellar vesicles

List of abbreviations

MS	mass spectrometry
MSP	membrane scaffolding protein
MVV	multivesicular vesicles
Nano-ESI	nano-electrospray ionization
NHS	N-hydroxysuccinimide
NMR	nuclear magnetic resonance
PA	phosphatidic acid
PC	phosphatidylcholine
PC-18:1/18:1 (DOPC)	1,2-dioleoyl- <i>sn</i> -glycero-3-phosphocholine
PE	phosphatidylethanolamine
PE-18:1/18:1 (DOPE)	1,2-dioleoyl- <i>sn</i> -glycero-3-phosphoethanolamine
PG-18:1/18:1 (DOPG)	1,2-dioleoyl- <i>sn</i> -glycero-3-phospho-(1'- <i>rac</i> -glycerol)
PG	phosphatidylglycerol
PI	phosphatidylinositol
PI(3)P - 18:1	1,2-dioleoyl- <i>sn</i> -glycero-3-phospho-(1'- <i>myo</i> -inositol-3'-phosphate)
PS	phosphatidylserine
PS-18:1/18:1	1,2-dioleoyl- <i>sn</i> -glycero-3-phospho-L-serine
Q	quadrupole
Q-ToF	quadrupole time-of-flight
RF	radio frequency
SapNPs	saposin-derived lipid nanoparticles
SDA	succinimidyl-4,4-azipentanoate
SDS-PAGE	sodium dodecyl sulphate-polyacrylamide gel electrophoresis
SM	sphingomyelin
SMA	styrene maleic-acid
SMALPs	Styrene maleic-acid lipid particles
SNARE	soluble N-ethylmaleimide-sensitive factor attachment receptor
SPL	sphingophospholipids
SUVs	small unilamellar vesicles
TEM	transmission electron microscopy
TOF	time-of-flight
ULVs	unilamellar vesicles
XL-MS	cross-linking MS

Code for amino acids

amino acid	one letter code	three-letter code
alanine	A	Ala
arginine	R	Arg
asparagine	N	Asn
aspartic acid	D	Asp
cysteine	C	Cys
glutamic acid	E	Glu
glutamine	Q	Gln
glycine	G	Gly
histidine	H	His
isoleucine	I	Ile
leucine	L	Leu
lysine	K	Lys
methionine	M	Met
phenylalanine	F	Phe
proline	P	Pro
serine	S	Ser
threonine	T	Thr
tryptophan	W	Trp
tyrosine	Y	Tyr
valine	V	Val

List of figures

Figure 1: Structure of a biological membrane and function of membrane proteins	2
Figure 2: Structure and composition of lipids in membranes	4
Figure 3: Types of lipids in biological membranes	6
Figure 4: Classification of liposomes	8
Figure 5: Classification of nanodiscs	9
Figure 6: ESI process and mechanism in positive ion mode	12
Figure 7: Sample preparation and interpretation of native MS data.....	16
Figure 8: Cross-linking mass spectrometry	18
Figure 9: The Q Exactive Plus Hybrid-Quadrupole-Orbitrap mass spectrometer.....	20
Figure 10: The Q-ToF Ultima mass spectrometer.....	21
Figure 11: Workflow of liposome preparation, characterization and analysis	47
Figure 12: DLS analysis of single-component liposomes	49
Figure 13: DLS analysis of multi-component liposomes	50
Figure 14: MS analysis of single-component liposomes.....	51
Figure 15: MS analysis of multi-component liposomes.....	53
Figure 16: DLS and native MS analysis of multi-component liposomes differing in size and concentration	54
Figure 17: Native MS analysis of multi-component liposomes at increasing collisional voltages	56
Figure 18: MS analysis of soluble peptides/proteins.....	58
Figure 19: MS analysis of soluble peptides/proteins mixed with liposomes.....	62
Figure 20: Workflow of proteoliposome preparation, characterization and analysis.....	64
Figure 21: Flotation assay of p40 ^{phox} -proteoliposomes	66
Figure 22: Preparation of p40 ^{phox} -proteoliposomes for MS analysis	68
Figure 23: MS analysis of p40 ^{phox}	69
Figure 24: MS analysis of p40 ^{phox} -proteoliposomes.....	70
Figure 25: Flotation assay and DLS analysis of Melittin-proteoliposomes resembling a eukaryotic membrane composition	72
Figure 26: Flotation assay and DLS analysis of Melittin-proteoliposomes resembling a prokaryotic membrane composition	73
Figure 27: MS analysis of Melittin.....	75

Figure 28: MS analysis of Melittin-proteoliposomes resembling a eukaryotic membrane composition	76
Figure 29: MS analysis of Melittin-proteoliposomes resembling a prokaryotic membrane composition	78
Figure 30: Chemical cross-linking of Melittin and Melittin-proteoliposomes	80
Figure 31: Binding study of Melittin to single-component liposomes	81
Figure 32: Lipid monolayer studies of Melittin	83
Figure 33: Nanodisc preparation and characterization	84
Figure 34: SEC purification of single-component nanodiscs	86
Figure 35: SEC purification of multi-component nanodiscs	87
Figure 36: DLS analysis and negative-stain TEM of nanodiscs	89
Figure 37: Preparation, characterization and cross-linking of Syntaxin-1A nanodiscs	91
Figure 38: SEC purification and western blot analysis of Syntaxin-1A nanodiscs	92
Figure 39: DLS analysis and negative-stain TEM of Syntaxin-1A nanodiscs	93
Figure 40: Cross-linking of Syntaxin-1A nanodiscs	94
Figure 41: Example spectrum of an intra-molecular cross-link of Syntaxin-1A	95
Figure 42: Example spectrum of an intra-molecular cross-link of MSP1E3D1	96
Figure 43: Example spectrum of an inter-molecular cross-link of Syntaxin-1A and MSP1E3D1	97
Figure 44: Syntaxin-1A and MSP1E3D1 constructs and network plot of cross-links	98
Figure 45: Overview of commonly used membrane mimetics	99
Figure 46: p40 ^{phox} interactions and the p40 ^{phox} binding pocket	107
Figure 47: Melittin association with the membrane	110
Figure 48: Dynamics of Syntaxin-1A in nanodiscs	114
Supplementary Figure 1: DLS analysis of multi-component liposomes differing in size	132
Supplementary Figure 2: Protein purification of p40 ^{phox}	133
Supplementary Figure 3: DLS analysis of multi-component liposomes with different compositions ..	134
Supplementary Figure 4: MS analysis of liposomes resembling a eukaryotic membrane composition incubated with phospholipase A2	135
Supplementary Figure 5: MS analysis of liposomes resembling a prokaryotic membrane composition incubated with phospholipase A2	136
Supplementary Figure 6: Protein purification of MSP1E3D1	137
Supplementary Figure 7: DLS analysis of single-component nanodiscs	138

Supplementary Figure 8: DLS analysis of multi-component nanodiscs	139
Supplementary Figure 9: Protein purification of Syntaxin-1A	140
Supplementary Figure 10: DLS analysis of Syntaxin-1A nanodiscs	141

List of tables

Table 1: Chemicals.....	24
Table 2: Solvents.....	25
Table 3: Reagent kits.....	25
Table 4: Gel electrophoresis and Western Blot reagents.....	25
Table 5: Antibodies for western blot analysis	26
Table 6: Plasmids	26
Table 7: Bacterial strains.....	26
Table 8: Enzymes.....	26
Table 9: Lipids.....	26
Table 10: Peptides and Proteins	27
Table 11: Instruments.....	27
Table 12: Consumables	28
Table 13: Software	29
Table 14: LB medium composition.....	30
Table 15: dYT medium composition.....	31
Table 16: TB medium composition.....	31
Table 17: 10 x TB salts composition.....	31
Table 18: Parameters protein expression.....	31
Table 19: Protein properties	35
Table 20: Composition, diameter and concentration of liposomes.	37
Table 21: Composition, diameter and concentration of nanodiscs.....	38
Table 22: Settings of the micropipette puller	41
Table 23: Buffer for in-gel proteolysis.....	42
Table 24: Liquid-chromatography gradient.....	44
Supplementary Table S1: m/z ratios of single-component liposomes in denaturing MS experiments	142
Supplementary Table S2: m/z ratios of single-component liposomes in native MS experiments.....	143
Supplementary Table S3: Results of MaxQuant search for protein identification.....	144
Supplementary Table S4: m/z ratios of p40 ^{phox} -proteoliposomes in denaturing MS experiments.....	144
Supplementary Table S5: m/z ratios of p40 ^{phox} -proteoliposomes in native MS experiments.....	144

Supplementary Table S6: <i>m/z</i> ratios of Melittin (M)-proteoliposomes in denaturing MS experiments	145
Supplementary Table S7: <i>m/z</i> ratios of Melittin (M)-proteoliposomes in native MS experiments....	145
Supplementary Table S8: Cross-links Syntaxin-1A.....	146
Supplementary Table S9: Cross-links MSP1E3D1	146
Supplementary Table S10: Cross-links MSP1E3D1 and Syntaxin-1A.....	147

Summary

In this thesis, the application of liposomes and nanodiscs to study membrane proteins in their native-like lipid environment was explored by employing different mass spectrometry-based (MS-based) methods. Although detergents are commonly used for the solubilization and purification of membrane proteins they do not resemble a natural phospholipid bilayer and often cannot preserve the native state of the proteins. In the last decade, membrane mimetics, therefore, gained more importance as they allow the analysis of membrane proteins in the presence of lipids. Of these, liposomes and nanodiscs have proven to be promising, although their application for MS is still limited.

In the first part of this thesis, liposomes and proteoliposomes were studied by MS under denaturing and native gas phase conditions. The overall aim of these experiments was to dissociate liposomes in the gas phase of the mass spectrometer and to release membrane-associated proteins allowing the structural investigation in their lipid environment. For this, liposomes without proteins were first investigated. Single-component liposomes dissociated into lipid clusters under denaturing and native gas phase conditions. Similar dissociation patterns were also obtained for multi-component liposomes; however, these lipid clusters contained different lipids. Importantly, by applying native MS experiments liposomes differing in composition, size and concentration revealed comparable mass spectra. The dissociation of liposomes is, therefore, independent on composition, size and concentration. Further experiments showed that the dissociation of liposomes was improved by increasing the collision voltages under native gas phase conditions resulting in smaller lipid clusters. These initial experiments highlighted that single- and multi-component liposomes dissociate under denaturing and native gas phase conditions and are, therefore, promising for our application to study membrane proteins in a native lipid environment.

To continue investigating the usage of liposomes they were in next step mixed with soluble peptides/proteins to prove whether peptides/proteins and lipids can be analyzed simultaneously or protein signals are suppressed. These experiments showed that peptides/proteins and lipids are detectable in the same mass spectrum. This was confirmed using three different model proteins ranging in molecular weight from small (approximately 1 kDa) to large (approximately 25 kDa) proteins.

Next, the application of liposomes to study membrane-associated proteins was explored. For this, p40^{phox} and Melittin were investigated. The binding of the proteins to liposomes was verified by flotation analysis. MS spectra acquired under denaturing and native gas phase conditions revealed signals for p40^{phox} and lipids.

Finally, Melittin was incubated with liposomes differing in lipid composition (i.e. eukaryotic and prokaryotic membrane composition). Surprisingly, the mass spectra revealed protein-lipid interactions

under denaturing and native gas phase conditions. Moreover, under native gas phase conditions, Melittin oligomers were preserved, showing that liposomes successfully transfer membrane-associated proteins into the gas phase while preserving their oligomeric states and lipid interactions. Accordingly, by comparing MS analyses under denaturing and native gas phase conditions, we gained insights into the dissociation of liposomes and the binding of peptides/proteins to the phospholipid bilayer. Liposomes, therefore, represent a valuable alternative to study membrane-associated peptides and proteins and their interactions by MS.

In the second part of this thesis, the application of nanodiscs for chemically cross-linking of membrane proteins in a native-like membrane environment was investigated. For this, single- and multi-component nanodiscs were prepared and their size, as well as shape, were validated by dynamic light scattering (DLS) and negative-stain transmission electron microscopy (TEM). Subsequently, an integral membrane protein (Syntaxin-1A) was reconstituted into nanodiscs and cross-linked with bis(sulfosuccinimidyl)suberate (BS3). Cross-links were analyzed using a standardized cross-linking protocol. By following this protocol, cross-links of Syntaxin-1A, as well as membrane-scaffolding protein (MSP) cross-links were identified. In future applications, chemical cross-linking and subsequent MS analysis of proteins reconstituted into nanodiscs will then allow the structural analysis of membrane proteins in the presence of lipids.

In summary, this work shows that liposomes and nanodiscs are important tools to analyze membrane proteins and their interactions using different MS-based methods. The investigation of membrane proteins and their lipid interactions in a well-defined environment resembling a biological membrane will certainly be of great value for the structural elucidation of membrane proteins in the future.

Zusammenfassung

In dieser Arbeit wurde die Anwendung von Liposomen und Nanodiscs zur Untersuchung von Membranproteinen in ihrer nativen Lipidumgebung untersucht, indem verschiedene Massenspektrometrie-basierte (MS-basierte) Methoden eingesetzt wurden. Obwohl Detergenzien üblicherweise für die Solubilisierung und Reinigung von Membranproteinen verwendet werden, ähneln sie nicht einer natürlichen Phospholipid-Doppelschicht und können daher oft den nativen Zustand von Proteinen nicht erhalten. Aufgrund dessen haben Membranmimetika in den letzten Jahren zunehmend an Bedeutung gewonnen, da sie die Analyse von Membranproteinen in Gegenwart von Lipiden ermöglichen. Liposomen und Nanodiscs erwiesen sich bereits als vielversprechend für die Analyse von Membranproteinen, ihre Anwendung für die Massenspektrometrie (MS) ist allerdings bis heute noch begrenzt.

Im ersten Teil dieser Arbeit wurden Liposomen und Proteoliposomen mittels MS unter denaturierenden und nativen Gasphasenbedingungen untersucht. Das übergeordnete Ziel dieser Experimente war es, Liposomen im Massenspektrometer zu dissoziieren und membranassoziierte Proteine in die Gasphase freizusetzen. Dadurch sollte die strukturelle Untersuchung von membranassoziierten Proteinen in ihrer natürlichen Lipidumgebung ermöglicht werden. Hierfür wurden zunächst Liposomen ohne Proteine untersucht. Einzelkomponenten Liposomen dissoziierten unter denaturierenden und nativen Gasphasenbedingungen in Lipidcluster. Ähnliche Dissoziationsmuster wurden auch für multikomponenten Liposomen erhalten, allerdings enthielten diese Lipidcluster auch unterschiedliche Lipide. Außerdem zeigten die nativen MS-Experimente von Liposomen, die sich in Zusammensetzung, Größe und Konzentration unterscheiden, ähnliche Massenspektren. Die Dissoziation von Liposomen ist demnach unabhängig von Zusammensetzung, Größe und Konzentration. Weitere Experimente zeigten zudem, dass die Dissoziation durch Erhöhung der Kollisionsspannungen unter nativen Gasphasenbedingungen verbessert werden kann, was zu kleineren Lipidclustern führt. Zusammenfassend zeigten diese ersten Experimente, dass einzel- und mehrkomponenten Liposomen unter denaturierenden und nativen Gasphasenbedingungen dissoziieren und daher vielversprechende Membranmimetika für die Analyse von Membranproteinen in einer natürlichen Umgebung sind.

Um die Anwendung von Liposomen weiter zu untersuchen, wurden sie als nächstes mit löslichen Peptiden/Proteinen gemischt und mittels MS analysiert, um zu beweisen, dass sich Peptide/Proteine und Lipide gleichzeitig analysiert werden oder die Proteinsignale unterdrückt werden. Diese Versuche zeigten, dass Peptide/Proteine in Gegenwart von Lipiden nachweisbar sind. Dies wurde durch Verwendung von drei verschiedenen Modellproteinen bestätigt, deren Molekulargewicht von kleinen (ca. 1 kDa) bis zu großen (ca. 25 kDa) Proteinen reichte.

Um nun zu untersuchen, ob Liposomen als Überträger von membranassoziierten Proteinen in die Gasphase des Massenspektrometers dienen können, wurde zwei unterschiedliche membran-assoziierte Modellproteine (p40^{phox}, Melittin) näher untersucht. Die Bindung der Proteine an Liposomen wurde durch Flotationsanalyse bestätigt. Die MS-Spektren zeigten, dass die Ionisierung der Lipide begünstigt ist, wodurch p40^{phox} mit geringerer Intensität beobachtet wurde. Dennoch konnten wir bestätigen, dass Proteine, die spezifisch mit Liposomen Membranen assoziiert sind, sich mittels MS analysieren lassen.

Melittin wurde mit Liposomen inkubiert, die sich in der Lipidzusammensetzung unterscheiden (eukaryotische und prokaryotische Membranzusammensetzung). Interessanterweise zeigten die MS Spektren, dass Protein-Lipid-Wechselwirkungen unter denaturierenden und nativen Gasphasen Bedingungen nachgewiesen werden konnten. Darüber hinaus blieben Melittin-Oligomere unter nativen Gasphasenbedingungen erhalten. Mit Hilfe von Liposomen können membranassoziierte Proteine erfolgreich in die Gasphase überführt werden, wodurch sowohl die oligomeren Zustände des Peptides als auch Lipidinteraktionen erhalten bleiben. Zusammenfassend wurden durch den Vergleich der MS-Analyse unter denaturierenden und nativen Gasphasenbedingungen Einblicke in die Dissoziation von Liposomen und die Bindung von Peptiden/Proteinen an die Phospholipid-Doppelschicht gewonnen. Dementsprechend stellen Liposomen eine wertvolle Alternative dar, um membranassoziierte Peptide und Proteine und ihre Wechselwirkungen mittels MS zu untersuchen.

Im zweiten Teil dieser Arbeit wurde die Anwendung von Nanodiscs für die chemische Quervernetzung von Membranproteinen in ihrer natürlichen Membranumgebung untersucht. Dazu wurden einzel- und mehrkomponenten Nanodiscs mit unterschiedlichen Zusammensetzungen hergestellt und ihre Größe sowie Form mittels dynamische Lichtstreuung (DLS) und Transmissionselektronenmikroskopie (TEM) validiert. Anschließend wurde ein integrales Membranprotein (Syntaxin-1A) in Nanodiscs rekonstituiert und mittels Bis(sulfosuccinimidyl)suberat (BS3) quervernetzt. Die Quervernetzungen wurden anhand eines standardisierten Quervernetzungsprotokolls analysiert. Auf Grundlage dieses Protokolls konnten Quervernetzungen von Syntaxin-1A und des Nanodisc Gerüstproteins nachgewiesen werden. Insgesamt zeigen diese Experimente, dass chemisches Quervernetzen von Proteinen, die in Nanodisc rekonstituiert wurden, möglich ist. In Zukunft könnten diese ersten Studien dabei helfen eine erweiterte Strukturanalyse von Membranproteinen mit Hilfe von Nanodiscs zu ermöglichen.

Zusammenfassend zeigt diese Arbeit, dass Liposomen und Nanodiscs wichtige Werkzeuge sind, um Membranproteine und ihre Wechselwirkungen mittels MS zu analysieren. Die Untersuchung von Membranproteinen und ihren Lipidwechselwirkungen in einer wohldefinierten Umgebung, die einer biologischen Membran ähnelt, wird sicherlich in naher Zukunft von großem Wert für die Strukturaufklärung von Membranproteinen sein.

1 Introduction

1.1 Membrane proteins, lipids and their interactions

1.1.1 Membrane proteins

Biological membranes separate the interior of organelles from their external environment and function as permeability barriers¹. Accordingly, biological membranes are involved in sending, receiving and processing information in form of chemical and electrical signals². The organization of biological membranes was previously described by the fluid mosaic model postulated by Singer and Nicolson in 1972³. This model defines membranes as fluid phospholipid bilayers in which membrane proteins and lipids are highly dynamic and freely float. Over the last decade, this model was refined, and it was proposed that biological membranes contain microdomains consisting of different lipids and proteins. These domains are essential for the organization of the membrane and it is, accordingly, assumed that the lipid bilayer is divided into so-called lipid rafts that coordinate the function of proteins⁴. Lipid rafts are initially described as detergent-resistant membrane fractions that usually contain a high content of cholesterol, glycolipids and sphingolipids. In addition, the fatty acid side chains of the phospholipids present in lipid rafts are highly saturated compared to the rest of the membrane⁵. Although controversially discussed to date, lipid rafts are nowadays thought to play important roles in membrane signaling and trafficking⁶.

Most biological membranes have a protein content $\geq 50\%$ ⁷. Membrane proteins penetrate the phospholipid bilayer depending on their hydrophobicity and, therefore, determine the function and structure of biological membranes. There are two types of proteins associated with biological membranes: peripheral (extrinsic), and integral (intrinsic) membrane proteins (**Figure 1A**). Peripheral membrane proteins are transiently bound to the phospholipid bilayer and are easily released by changes in ionic strength or pH⁸. They associate with biological membranes by forming electrostatic and other non-covalent interactions with lipid head groups or the hydrophilic surface of other proteins⁹. Other peripheral membrane proteins are covalently linked to the membrane through a lipid anchor. Accordingly, lipid anchored membrane proteins are located on either side of the phospholipid bilayer⁷. The various lipid groups that anchor proteins to the membrane can also play a central role in the interaction and function of proteins¹⁰.

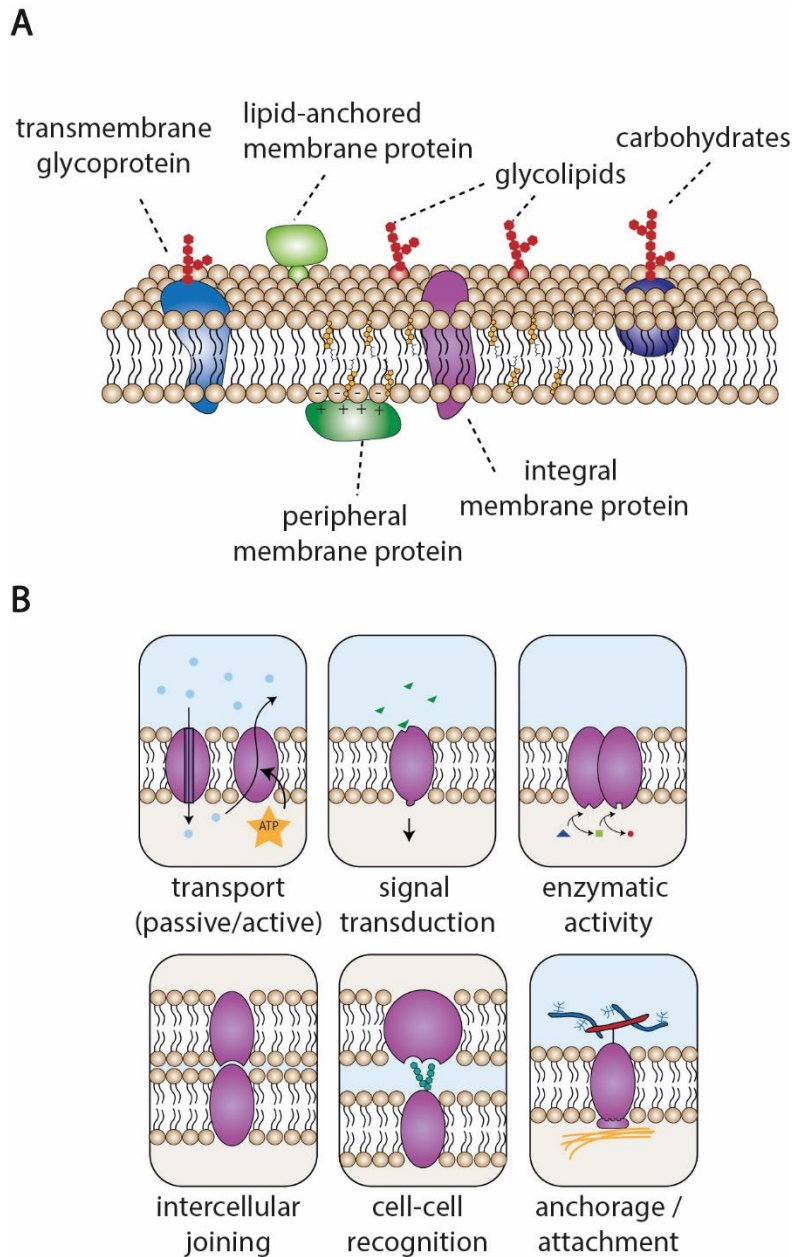


Figure 1: Structure of a biological membrane and function of membrane proteins. (A) Organization of a biological membrane. The membrane consists of a phospholipid bilayer containing a variety of proteins. Proteins are classified as peripheral (dark green) and integral (pink) membrane proteins. Peripheral membrane proteins are either associated with the membrane through electrostatic interactions (dark green) or through a lipid-anchor (light green). Transmembrane glycoproteins (blue) and glycolipids (red) are also displayed. (B) Different functions of membrane proteins. Membrane proteins contribute to the transport of molecules (passive and active transport), signal transduction, enzymatic activity, intercellular joining, cell-cell recognition and association of the cytoskeleton.

Integral membrane proteins contain a relatively large number of hydrophobic amino acids and are, therefore, embedded into the phospholipid bilayer. They interact with the fatty-acid chains or head groups of phospholipids through hydrophobic, hydrophilic or ionic interactions. The ionic interactions are mostly formed between positively (Lys, Arg and His) or negatively charged residues (Asp and Glu) and phospholipid head groups. Integral membrane proteins are, therefore, not easily released from the phospholipid bilayer⁷. A subset of integral membrane proteins are glycoproteins, which contain oligosaccharide chains (glycans) covalently attached to their amino acid side chains¹¹.

Membrane proteins have a variety of functions in biological membranes (**Figure 1B**). For instance, transport proteins enable the transfer of ions, small molecules or macromolecules across the cell membrane¹². Transport mechanisms are divided into passive and active transport. During the passive transport, molecules are transferred across the cell membrane through a concentration gradient without the use of energy. In active transport mechanisms molecules are pumped against a concentration gradient^{13,14}. This mechanism is driven by the release of energy e.g. through the hydrolysis of adenosine triphosphate¹⁵. Furthermore, enzymatic membrane proteins, such as oxidoreductases, transferases and hydrolases are particularly involved in metabolic pathways and catalyze the transfer of electrons from one molecule to another¹⁶. Other membrane proteins are responsible for cell junctions (tight junctions, desmosomes and gap junctions), providing contact adhesion between neighboring cells or between cells and the extracellular matrix⁷. Glycoproteins are, for instance, involved in the identification and recognition between cells and have shown to be particularly important for the immune system to support the detection of foreign cells that cause infections¹¹. Some membrane proteins are also associated with the cytoskeleton or extracellular matrix and, therefore, maintain the shape of a cell¹⁷. Based on these functions, membrane proteins are often associated with diseases and are, therefore, important biological and pharmaceutical targets.

1.1.2 The importance of lipids

The membranes of organelles are composed of a variety of different lipids that form the phospholipid bilayer. Lipids are amphipathic molecules consisting of a hydrophilic head group and a hydrophobic carbon chain. Accordingly, they spontaneously self-associate in aqueous solutions so that their hydrophobic carbon chains face inwards forming the hydrophobic core and their hydrophilic head groups face outwards towards the aqueous surrounding¹⁸.

There are three main classes of lipids found in biological membranes: phospholipids, glycolipids and sterols¹⁹ (**Figure 2**). Phospholipids are classified, according to their head group structure, as glycerophospholipids (GPL) and sphingophospholipids (SPL). Glycerophospholipids, including phosphatidic acid (PA), phosphatidylethanolamine (PE), phosphatidylcholine (PC), phosphatidylglycerol (PG), phosphatidylserine (PS) and phosphatidylinositol (PI) are considered to be the most abundant lipids in biological membranes²⁰. GPLs consist of two fatty acyl chains linked by a glycerol and a phosphate group (**Figure 2A**). The two fatty acyl chains of GPLs usually consist of an even number of carbon atoms (between 14 and 24 carbon atoms) and cis carbon-carbon double bonds (unsaturated GPLs). Accordingly, the fluidity of a membrane is determined by the degree of saturation of the hydrocarbon chain.

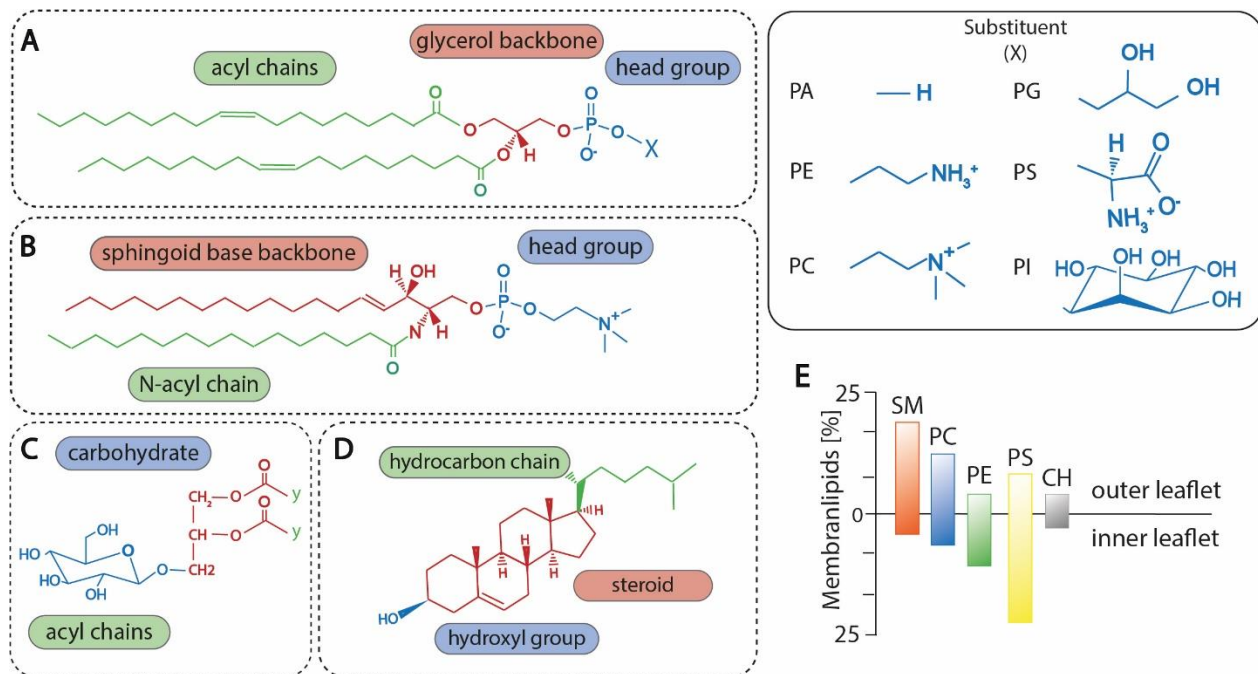


Figure 2: Structure and composition of lipids in membranes. (A) Glycerophospholipids contain two fatty acyl chains which are linked to the phosphate group through a glycerol backbone. Common headgroups (X) of glycerophospholipids are displayed. (B) Sphingophospholipids consist of a sphingoid base backbone, an N-acyl chain linked by an amide bond. SM is shown as a representation of a sphingophospholipid. (C) Glycolipids contain fatty acyl chains (y) which are glycosidically attached to one or more mono- or oligosaccharides. (D) Cholesterol is the major sterol of eukaryotic cell membranes and consists of a four-ring steroid, a hydroxyl group and a hydrocarbon chain. (E) Distribution of lipids in the outer leaflet and inner leaflet of plasma membranes.

Unsaturated fatty acids with one or more double bonds, therefore, influence the packing arrangement of biological membranes and increase membrane fluidity while saturated fatty acyl chains lead to a higher membrane rigidity²¹. SPLs consist of a sphingoid base and an N-acyl side chain linked by an amide bond²² (**Figure 2B**).

A typical SPL found in biological membranes is sphingomyelin (SM). Glycolipids are the second largest group of lipids and are mostly found on the surface of eukaryotic membranes²³. Structurally, glycolipids are phosphate-free lipids that are glycosidically attached to one or more mono- or oligosaccharides (**Figure 2C**). Cerebrosides, which are typical glycolipids found in nerve cell membranes, are involved in different biological and pathological processes suggesting to play important roles in cell recognition²⁴.

Sterols, which are important components of eukaryotic membranes contain a four-ring steroid, a hydroxyl group and a short hydrocarbon side chain²² (**Figure 2D**). Cholesterol, the basic building block of hormones and vitamins, contributes to membrane stiffness and, therefore, reduces membrane fluidity at high temperatures²⁵. At low temperatures, however, the bending of the cholesterol-hydrocarbon chain prevents the formation of an ordered structure and membrane fluidity is increased²⁰.

The lipid composition of biological membranes is very diverse¹⁹. Plasma membranes, for instance, contain a high proportion of PC, PE and SM, but less PI or PS lipids. The cholesterol content in plasma membranes is high compared to other membranes²⁶. Mitochondrial membranes, however, have the lowest cholesterol content but high levels of PC, PE and PI¹⁹. The structural differences of organelles also define the compositions of the inner and outer leaflets of membranes²⁷. In plasma membranes, for example, the outer leaflet is composed of sphingolipids and PC while the inner leaflet contains mostly PE and PS lipids (**Figure 2E**)^{28,29}. Interestingly, cholesterol is equally distributed in the outer and inner leaflets of the plasma membrane³⁰. The different lipid compositions and distributions in membranes, therefore, result in different membrane fluidity, curvature, lateral pressure and transition temperature.

1.1.3 Protein-lipid interactions

Protein-lipid interactions are important for membrane organization. Early studies considered lipids to be essential for anchoring membrane proteins in the phospholipid bilayer^{7,31}. However, lipids also showed significant effects on protein activity³² and it is nowadays generally accepted that lipids are crucial for analyzing the structure and function of membrane proteins.

The lipids that interact with proteins are divided into three groups including bulk lipids, annular lipids and non-annular lipids (**Figure 3**). Bulk lipids, the majority of membrane lipids, do not interact with membrane-bound proteins, but are responsible for membrane assembly. Accordingly, these lipids, affect the physical properties of the membrane, including fluidity, lateral pressure and curvature⁸. The lipid envelope surrounding membrane proteins is usually referred to the lipid annulus³³. These lipids interact with membrane proteins mostly through hydrophobic interactions between the amino acid side chains of the protein and the fatty acid chains of lipids.

In addition, they also interact through hydrophilic interactions between polar amino acid chains and the polar lipid head groups. Accordingly, the lipid annulus mediates between proteins and the lipid environment and is responsible for the vertical positioning of the protein in the membrane³⁴. Note that, annular lipids exchange more rapidly with their lipid environment compared to bulk lipids and their interactions with membrane proteins are, therefore, difficult to detect³⁵. Nevertheless, studies applying electron paramagnetic resonance spin labeling and other biophysical methods were able to provide information on lipid stoichiometry, selectivity and exchange dynamics³⁶ and the interactions of annular lipids were also preserved in high-resolution structures³⁷⁻³⁹. Non-annular lipids, also known as lipid cofactors or structural lipids, interact with proteins with high affinity. These lipids are often found at protein surface cavities, between transmembrane helices or at the protein-protein interfaces of protein complexes³⁴. Accordingly, the association of non-annular lipids with membrane proteins is based on non-covalent interactions⁴⁰. Non-annular lipids are important for modulating the structure, conformation and localization of membrane protein complexes as well as their enzymatic functions⁴¹.

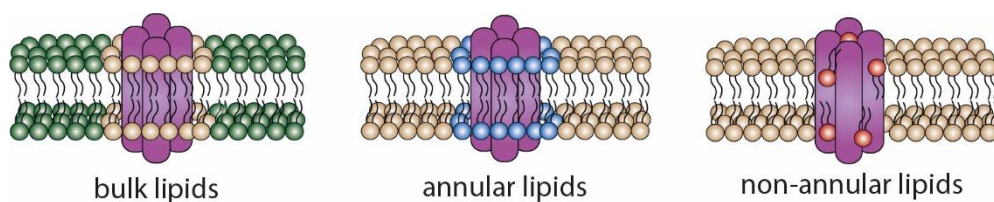


Figure 3: Types of lipids in biological membranes. Bulk lipids (green) do not interact with the proteins embedded in the membrane and represent the bulk lipid composition of the protein's membrane environment. Annular lipids (blue) mediate between the protein and the lipid environment and are important for the vertical positioning of the protein in the lipid bilayer. Non-annular lipids (red) are bound in protein surface cavities, between transmembrane helices of a protein or at the protein-protein interfaces of protein complexes containing multiple subunits.

1.2 Membrane mimetics

For many years, the major challenge in the analysis of membrane proteins was their purification from membranes while preserving their native structure and function. To date, detergents are mostly used for solubilizing membrane proteins^{42,43}. Amphiphilic detergent molecules contain a hydrophilic head group and a hydrophobic tail, allowing them to form, above the critical micelle concentration (CMC), a spherical micelle with a hydrophobic interior and a hydrophilic exterior. The CMC is defined as the concentration used for spontaneous micelle formation⁴⁴.

Although detergents seem to be valuable for solubilizing membrane proteins, recent studies proved that detergents also tend to destabilize the native structure of membrane proteins and lead to unfolding⁴⁵. In addition, extensive screening of detergents is often required to achieve successful extraction of membrane proteins^{46,47}. Accordingly, the search for a suitable detergent is often time-consuming and expensive. Detergents are, therefore, considered unsuitable for the analysis of membrane proteins. However, the importance of the membrane environment on protein structure and function has led to the development of new membrane mimetics.

Nowadays, the most commonly employed membrane mimetics for the analysis of membrane proteins in their native-like environment are bicelles, amphipoles, nanodiscs and liposomes. Bicelles consist of a mixture of short-chain detergents and long-chain phospholipids that result in a planar lipid bilayer. However, as bicelles are polydisperse and contain detergents they do not represent a proper native environment for membrane proteins⁴⁸. Amphipoles are short amphipathic polymers that keep proteins soluble in the absence of detergents. However, they are heterogeneous and do not represent a phospholipid bilayer. Recently, biophysical studies also showed that the oligomeric states and protein-lipid interactions of membrane proteins are difficult to be maintained in bicelles and amphipols, hence they are not suitable for structural analysis of membrane proteins⁴⁹. In this thesis, liposomes and nanodiscs were, therefore, employed for the analysis of membrane proteins in their native-like environment. A more detailed description of these membrane mimetics is given in the following sections:

1.2.1 Liposomes

Liposomes are artificial spherical vesicles composed of one or more phospholipid bilayers surrounding an aqueous interior. Accordingly, similar to biological membranes, liposomes spontaneously assemble in aqueous solutions. Liposomes are able to encapsulate hydrophilic and hydrophobic drugs and were, therefore, increasingly used as drug carriers for biomedical research⁵⁰. Nowadays, they also proved to be useful model membranes for the structural analysis of membrane proteins^{51,52}.

Liposomes are easily prepared, for instance, by rotary evaporation, paired with extrusion or ultrasonication⁵³. In other protocols, liposomes were prepared by the ether or ethanol injection method⁵⁰. Liposomes are classified by their lamellarity and, accordingly, divided into multilamellar vesicles (MLVs) and unilamellar vesicles (ULVs) (**Figure 4A**). MLVs have an onion-like structure and contain multiple lipid bilayers, whereas ULVs consist of only one phospholipid bilayer⁵⁴. Depending on their size and incorporated vesicles, MLVs are further divided into multivesicular vesicles (MVs) including centrally arranged vesicle-in-vesicle systems (**Figure 4B**).

ULVs are further classified as giant unilamellar vesicles (GUVs), large unilamellar vesicles (LUVs) and small unilamellar vesicles (SUVs) (**Figure 4B**)^{55,56}. Smaller sized vesicles have an increased curvature compared to larger vesicles. As some proteins and peptides are negatively affected by a high curvature, larger vesicles (~100 nm vesicles) are often employed as model mimetics to study the structure and function of membrane proteins. Liposomes of different sizes are prepared from a variety of natural and non-natural lipids including cholesterol. Nowadays it is well accepted that the physical properties, such as surface charge and particle size of liposomes strongly depend on the lipid composition. In addition, the composition of lipids also mediates phospholipid bilayer stiffness and fluidity and, therefore, interferes with vesicle formation and might lead to the destabilization of the associated proteins⁵⁰.

For the incorporation of integral membrane proteins into liposomes, purified membrane proteins, dissolved in detergents, are incubated with lipid-detergent micelles. During the reconstitution process and detergent removal by dialysis, gel filtration or bio bead adsorption, the proteins spontaneously reconstitute into liposomes and form so-called proteoliposomes⁵⁷. A major drawback when preparing proteoliposomes is the difficulty to control the final orientation of proteins in liposomes and different populations are detected⁵⁸.

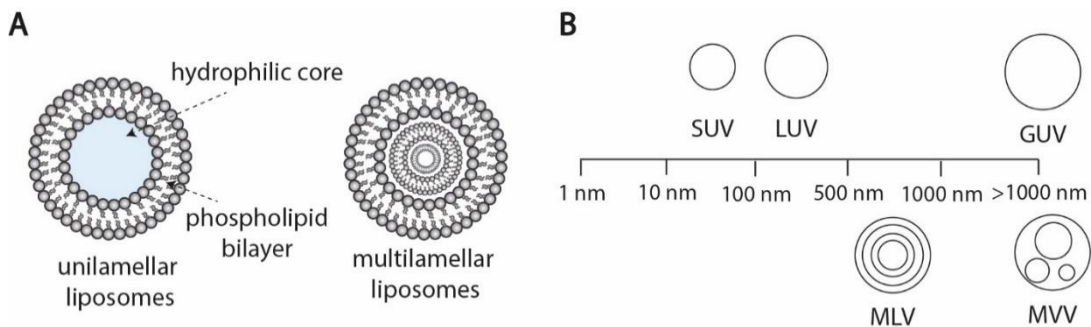


Figure 4: Classification of liposomes. (A) Liposomes are spherical vesicles consisting of a hydrophilic core surrounded by a phospholipid bilayer. Liposomes are either unilamellar or multilamellar. (B) Liposomes are classified into subgroups based on their size: SUVs (10-1000 nm), LUVs (100-500 nm), MLVs (500-1000 nm), GUVs and MVV (>1000 nm).

In contrast to integral membrane proteins, peripheral membrane proteins associate with liposomes without the use of detergents. However, one should keep in mind that the composition of liposomes plays a major role in the association of proteins and specific lipids are often necessary for successful attachment of the peripheral membrane protein.

1.2.2 Nanodiscs

Nanodiscs are nanoscale disc-shaped lipid bilayers enclosed by proteins or polymers which are well-defined and relatively monodisperse. Due to their size, stability and homogeneity, they were successfully used as membrane mimetics for functional and structural studies of membrane proteins⁵⁹.

To date, two different types of nanodiscs including protein nanodiscs (**Figure 5, i**) and polymer nanodiscs (**Figure 5, ii**) were developed for membrane protein studies. Classical protein nanodiscs contain two copies of an amphipathic membrane scaffold protein (MSP)⁶⁰. MSPs are truncated forms of apolipoprotein that allow stabilizing the phospholipid bilayer⁶¹. The different scaffold proteins define the diameter of the nanodisc complex, while the type of lipid determines the composition of the bilayer.

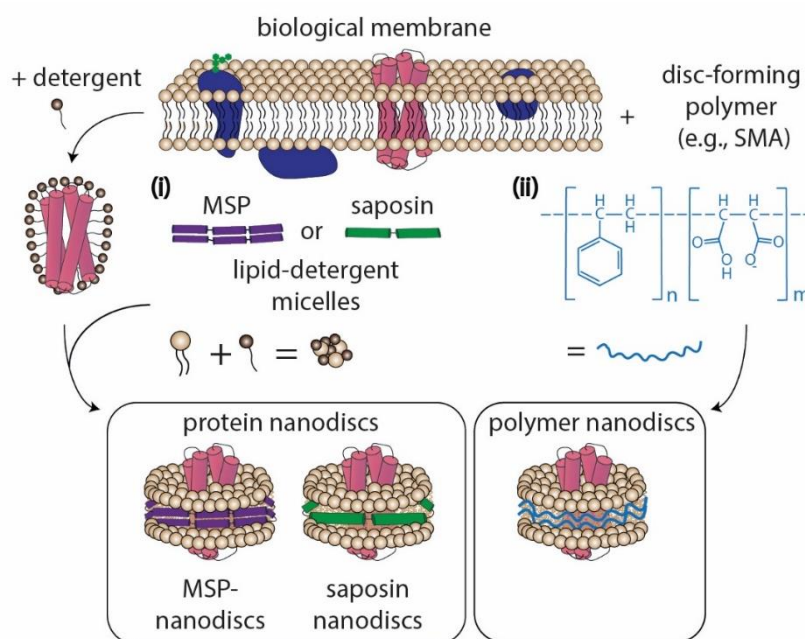


Figure 5: Classification of nanodiscs. Nanodiscs are classified into protein nanodiscs, including MSP-nanodiscs and SapNPs as well as polymer nanodiscs. MSP and SapNPs are assembled in detergents, either using a membrane scaffolding or a saposin protein. Polymer nanodiscs, for instance SMALPs are assembled without detergent

An alternative to the MSP nanodiscs is provided by the recently developed saposin-derived lipid nanoparticles (SapNPs)⁶². Saposin proteins A, B, C or D form disc-shaped constructs in the presence of lipids thus enabling the solubilization of membrane proteins in their lipid environment. However, as this method is relatively new, an extensive application of saposins for the structural analysis of membrane proteins is still missing. Nevertheless, SapNPs were recently employed for hydrogen-deuterium exchange (HDX)-MS and fast photochemical oxidation of proteins to study the structure of membrane proteins in their native environment⁶³.

Polymer lipid disc nanoparticles were recently described as an alternative to protein nanodiscs⁶⁴. Accordingly, copolymers such as styrene maleic acid (SMA) or diisobutylene-maleic acid (DIBMA) were used. Styrene maleic acid nanoparticles (SMALPs) are then formed by adding the amphiphilic SMA copolymer to membranes, which allows membrane proteins to be directly extracted from the native membrane along with their surrounding lipid environment^{65,66}. As detergents can lead to destabilization of protein-protein and protein-lipid interactions, SMALPs have the advantage that they do not need to be solubilized in detergents and membrane proteins are, therefore, comparatively stable⁶⁷. Nevertheless, one should keep in mind that the stoichiometry and diameter of copolymer nanodiscs cannot be defined, resulting in higher heterogeneity.

1.3 Biophysical analysis of liposomes and nanodiscs

1.3.1 Dynamic light scattering

Dynamic light scattering (DLS) is an analytical technique used to determine the diffusion coefficient and thus the diameter of particles in a suspension^{68,69}. In a typical DLS experiment, a particle-containing solution is irradiated with a monochromatic light beam (e.g a laser) causing light scattering in different directions. Light from different scattering centers interferes and variations in light intensity fluctuations are observed indicating that particles freely move in a suspension (Brownian motion). Accordingly, the smaller the molecules are, the faster they move and larger fluctuations are observed. In contrast, larger particles generate comparatively low-frequency signals. From these frequencies the diffusion coefficient is determined, which is then used to calculate the particle size using the Stokes-Einstein equation^{70,71}. In this thesis, DLS was used to investigate the diameter of liposomes, proteoliposomes and MSP-nanodiscs.

1.3.2 Negative-stain transmission electron microscopy

Negative-stain of specimen was initially developed by Brenner and Home in 1959 for the study of viruses⁷². Since then, this method was further developed and, nowadays, a wide variety of biological samples is stained by an electron-dense staining solution including heavy metal ions such as uranyl acetate or uranyl formate⁷³. Negative-stain transmission electron microscopy (TEM) is used to provide structural information on a range of biological specimens including cells and macromolecules^{74,75} and is also used to characterize the shape and size of nanoparticles⁷⁶. In negative-stain the background is stained and the specimen remains unstained as the staining solution, due to negative charge repulsion does not bind to the specimen on the grid. Negatively stained specimen are then visualized by TEM.

A TEM microscope underlies the same principle as a light microscope where an electron beam is applied to illuminate a biological sample⁷⁷. Accordingly, a high-energy electron beam hits the stained specimen on a grid. Most electrons pass through the sample, however, some electrons scatter, caused by the atoms of the sample. Negative-stain TEM then produces high contrast images as heavy metal stains cause a higher scattering than the atoms in proteins. Although high-resolution structures cannot be achieved, this method is well suited to determine sample quality and is, therefore, mostly used for initial screening of protein samples. In this thesis, negative-stain TEM was used to investigate the shape and size of MSP-nanodiscs.

1.4 Mass spectrometry

In the last decade, a variety of analytical methods was used to investigate proteins and their interactions with lipids. Of these, cryo-electron microscopy (EM), nuclear magnetic resonance (NMR) and X-ray crystallography are techniques that provide high-resolution structural information⁷⁸. However, the analysis of some proteins and protein complexes is still challenging and the detection of protein-lipid interactions is often restricted by the complex nature of biological membranes. Accordingly, intrinsic disorder, low abundance and heterogeneity of protein samples hinder proper analysis⁷⁹. In this thesis, mass spectrometry (MS) was employed to elucidate the structure of membrane proteins. MS is a technique used to determine the mass-to-charge (m/z) ratio of ions in the gas phase and has increasingly provided information in the field of proteomics, lipidomics and metabolomics⁸⁰. In the last decade, with new developments in instrumentation and methodology, MS has also shown great potential for the analysis of protein-lipid interactions^{81,82}. Most importantly, MS is advantageous compared to other structural techniques, as it is applicable to samples that vary in mass and polydispersity. Moreover, multiple oligomeric states are analyzed simultaneously, allowing to study the structure of proteins in real-time. Lastly, MS is highly sensitive and can, therefore, be applied for limited sample quantities⁸³.

Electrospray ionization

Electrospray ionization (ESI) is a gentle ionization method used in MS-based approaches such as proteomics and lipidomics⁸⁴. In ESI, an analyte solution is ionized by applying a strong electric field between the capillary and the sample cone (**Figure 6A**)⁸⁵. At the tip of the capillary, charges accelerate and induce the formation of a Taylor cone⁸⁶. A mist of highly charged droplets with the same polarity as the capillary voltage is emitted from the Taylor cone in form of a fine spray. As the solvent evaporates, the droplet size continuously decreases, resulting in an increase in surface charge. When the size and charge of the droplet reaches its stability limit (so-called the Rayleigh limit), droplet jet fission occurs (Coulomb explosion)⁸⁷.

The generation of ions is described by three commonly accepted theories, namely the ion evaporation model (IEM), the charged residue model (CRM) and the chain ejection model (CEM) (**Figure 6B**). The IEM model proposes that solvent evaporation leads to a higher surface charge density in the droplet. Accordingly, as coulombic repulsion overcomes the surface charges, ions undergo an electrostatically driven release from the droplet surface⁸⁸. This mechanism describes ionization of smaller ions; however, it is underestimated for charged ions of larger complexes. The CRM model describes that ongoing evaporation and fission events lead to droplet shrinkage until the surface charge is close to the Rayleigh limit and only a single analyte molecule remains in the droplet. Upon complete evaporation of the solvent, the charge is transferred to the analyte resulting in a charged molecule⁸⁹. The ionization of unfolded proteins is most likely described by the CEM. In this model, long chains are ejected out of the droplet by coulombic repulsion⁹⁰. Although the models do not explain all experimental observations, it is generally expected that for larger ions the CRM seems to be the most dominant mechanism^{91,92}.

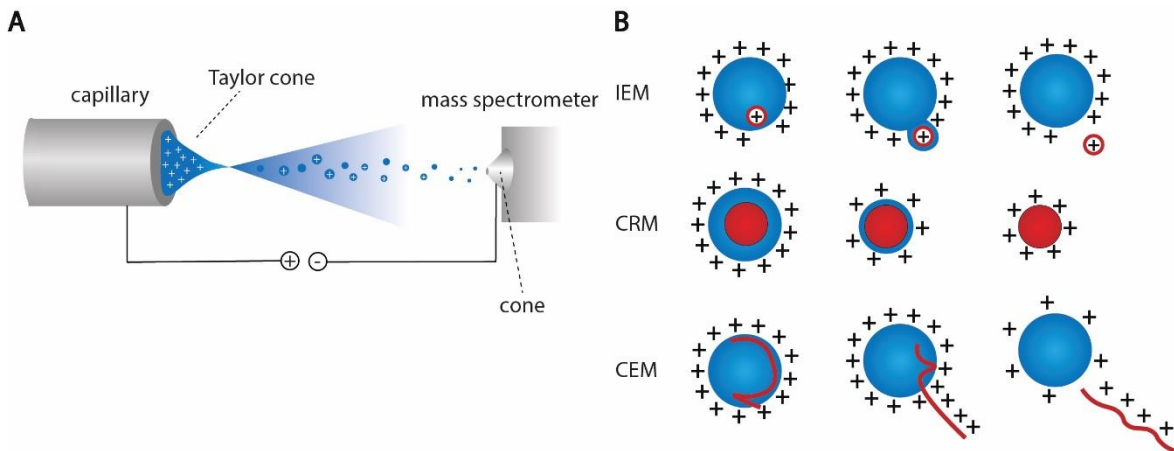


Figure 6: ESI process and mechanism in positive ion mode. (A) The sample is injected through a capillary at high voltage. At the tip of the capillary the charges accumulate and a Taylor cone is formed. The Taylor cone ejects a fine jet towards the counter electrode. (B) ESI mechanism. Ejection of small ions from a charged nanodroplet is described by the IEM. Globular proteins are most likely released into the gas phase by the CRM and the release of an unfolded protein is proposed by the CEM. Figures adapted from Göth et al. 2013 and Konermann et al. 2012.

Nano ESI (nESI) is based on the same ionization process as ESI⁹³. However, compared to conventional ESI, thinner capillaries and lower flow rates are employed, resulting in smaller electrospray droplets. In addition, by using nESI, it is possible to acquire mass spectra by only using a few picomoles of sample. Previous studies showed that nESI is also more tolerant toward salt contaminants which is especially important when analyzing proteins by native MS (see below) since these compounds are often only stable in solutions containing buffer salts⁹¹. These advantages, therefore, make nESI well-suited for peptide and protein analysis.

Ion transmission, selection and detection

Ions generated by nESI are separated in the mass analyzer according to their m/z ratios. The most commonly used mass analyzers are the quadrupole⁹⁴, time-of-flight (TOF)⁹⁵, and Orbitrap⁹⁶ mass analyzers. Subsequently, the ions are detected in a detector e.g. an Orbitrap, a secondary electron multiplier⁹⁷, or a microchannel plate⁹⁸. The m/z ratios are displayed in an MS1 spectrum. For tandem MS (MS2) experiments, triple quadrupole, quadrupole TOF or quadrupole Orbitrap mass spectrometers are employed to enable the selection of a specific ion (precursor ion) and subsequent fragmentation⁹⁹. Ion fragmentation is usually achieved by collision-induced dissociation (CID)¹⁰⁰ or high-energy collisional dissociation (HCD)¹⁰¹, electron transfer dissociation¹⁰² or electron capture dissociation¹⁰³. During CID, the collisions between the sample ions and the inert buffer gas convert the kinetic energy of the ions into their internal energy, leading to the dissociation and fragmentation of the ions¹⁰⁴.

1.4.1 Lipidomics

The lipidome is nowadays understood as the entirety of all lipids of a cell or an organism under certain conditions and at a defined point in time. Accordingly, lipidomics describes the identification and quantification of all lipid species in a lipidome. Lipidomics is often used to study lipid metabolic pathways, signaling pathways, and other physiological functions of lipid molecules¹⁰⁵. Due to its high sensitivity and quantitative as well as qualitative capabilities, MS has recently become the method of choice for lipid analysis. In MS-based lipidomic approaches, lipids are identified by their intact and fragment masses.

Three different methods were established¹⁰⁶: chromatography-coupled MS methods, including gas chromatography-coupled MS (GC-MS)¹⁰⁷ or liquid chromatography-coupled MS (LC-MS)¹⁰⁸ as well as direct infusion shotgun MS¹⁰⁹ and MS imaging¹¹⁰. In this thesis, shotgun lipidomics was applied for the analysis of lipids in liposomes and proteoliposomes.

Direct infusion shotgun lipidomics

Shotgun lipidomics, which was first proposed in 1994 by Han et al¹¹¹, describes that lipid extracts without prior chromatographic separation are injected directly into the mass spectrometer. Accordingly, samples are analyzed time-efficiently. In addition, certain analysis parameters, such as collisional energy are directly adjusted and optimized during each analysis. Accordingly, shotgun lipidomics has the great advantage that lipid species are directly compared and quantified.

A major drawback of this method is, however, that signal intensities of the same lipids from two different samples cannot be directly compared as the signals are often affected by other molecules present in the sample. For separation of lipid isomers and enrichment of lipid molecules, GC-MS and LC-MS MS methods were, therefore, described¹¹². Nowadays, the coupling of LC with MS offers a sophisticated method for studying lipids, as the restriction to volatile lipids limits the use of GC-MS based approaches. Accordingly, during normal phase LC and hydrophilic liquid chromatography (HILIC) lipid compounds are separated based on their hydrophilicity, allowing lipids with identical head groups to elute together and lipid classes to be separated¹¹³.

Shotgun lipidomics analysis includes MS/MS experiments, which are used to identify individual lipid species. To quantify lipid species within a lipidome, internal standards, which co-ionize with the lipids, are added. Internal standards are used for chromatographic-coupled as well as direct infusion lipidomics. The most commonly used internal standards are lipids containing acyl chains with odd carbon numbers (e.g., 17:1 or 19:0), as these are rarely found in eukaryotes. Other commonly employed internal standards are lipids with shorter carbon chains (e.g., 12:0 or 14:0) or deuterated lipid analogs. For quantification the abundance ratios of the lipid peak areas of the analytes and the respective internal standards are calculated¹¹⁴.

1.4.2 Native MS

Native MS allows the investigation of proteins in their ‘native’ (non-denatured) state in the gas phase and is, therefore, used for the determination of precise stoichiometries, protein interactions, topology as well as stability of protein complexes^{115,116}. In this thesis, native MS was employed to analyze the oligomeric states and protein-lipid interactions of membrane-associated proteins. Native MS of large protein complexes is dependent on two prerequisites. Accordingly, sample preparation has to be adapted to a non-denaturing buffer for native MS analysis and an optimal instrument environment for the transmission of high-mass complexes under non-denaturing conditions must be established¹¹⁷.

Sample preparation of protein complexes

For native MS experiments, the sample buffer has to be exchanged to a volatile solution such as ammonium acetate or ammonium bicarbonate solution which are known to provide the necessary ionic strength and pH for proteins and their complexes, allowing non-covalent interactions to be preserved in the gas phase^{118,119}. In contrast, high concentrations of non-volatile salts present in protein samples, can, for instance, cause the mass peaks to broaden resulting in a loss of resolution, mass accuracy and sensitivity. To remove salts prior to MS analysis, proteins and their complexes are, therefore, transferred into ammonium acetate using gel filtration columns, centrifugal filters or dialysis devices (**Figure 7A**)¹²⁰.

Interpretation of native MS data

According to the charged residue model, ions of folded proteins or protein complexes generated by nESI typically follow Gaussian distributions in the mass spectra (**Figure 7B**)¹²⁰. By determining the mass of intact protein complexes, the stoichiometry of the protein complex is calculated. Monomeric proteins exhibit lower m/z values, while protein complexes are detected at higher m/z ratios. The charge state distribution of a protein ion leads to a series of signals with different m/z . When several charge state distributions are observed, the molecular weight of a complex can then be calculated from the m/z of two adjacent peaks that differ by one proton (**Figure 7B**). The calculation of the molecular weight of the protein assembly is facilitated by different deconvolution software tools^{121,122}.

The observed charge state distribution correlates with the folded state of the protein. By increasing the collisional voltages, the individual subunits of the protein complexes are dissociated and identified. Since the weakest bound peripheral subunit typically dissociates first, this provides information about the topology of protein complexes as well as the binding affinities of the subunits.

The dissociated subunits are usually highly charged, while the remaining complex, also called the ‘stripped-complex’, carries fewer charges due to the asymmetrical charge partitioning of the original complex¹²³. As the charge states are affected by the geometry and folding state of a protein, the charge state of membrane proteins is also affected by their detergent/lipid environment¹²⁴. For instance, the mass spectra of membrane proteins solubilized in tetramethylene glycol monoethyl ether (C8E4) reveal lower charge states compared to membrane proteins solubilized in n-Octyl β -d-glucopyranoside. As C8E4 dissociates from the protein-detergent complex, positive charges are captured, leading to a charge reduction effect¹²⁵.

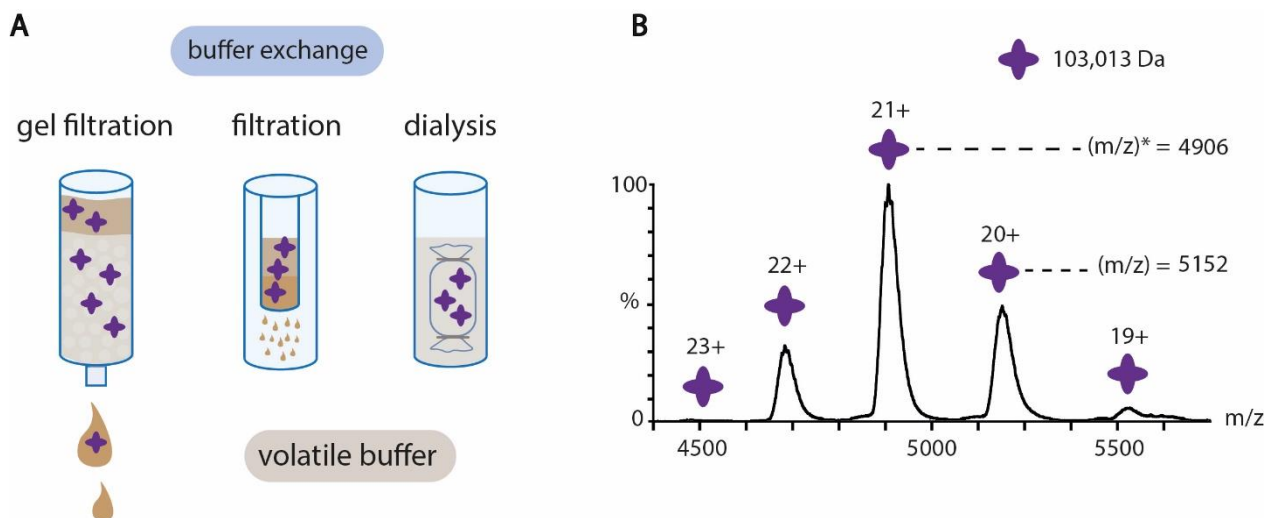


Figure 7: Sample preparation and interpretation of native MS data. (A) Sample preparation for native MS. The buffer is exchanged against an aqueous volatile solution following gel filtration, filtration or dialysis. (B) Native MS of tetrameric Concanavalin A reveals a Gaussian distribution of charge states (19+ to 23+). The molecular weight of the protein complex is calculated from two neighboring m/z . A molecular weight of 103,013 Da was calculated for the Concanavalin A tetramer. Figure adapted from Barth. et al. 2020.

Native MS for studying protein complexes and protein-lipid interactions

Due to its unique ability to preserve non-covalent interactions in the gas phase, native MS has emerged as a powerful technique to study membrane protein complexes. Accordingly, the stoichiometries and topologies of many membrane proteins including ion channels and transporters¹²⁶ or ATP synthases^{127–130} and enzymes of the electron transport chain^{53,131} were investigated. Moreover, native MS also delivers insights into the activities of proteins, for instance, it was shown that the structure of the *E. coli* translocon complex mediates the translocation of colicin E9 across the bacterial outer membrane¹³².

In recent years, native MS has also provided important insights into the interactions between membrane proteins and lipids. Accordingly, with native MS the selectivity and specificity of various lipid species towards membrane proteins were determined¹³³.

In addition, the effects of lipid binding on the structure and function of membrane proteins, as well as interactions with other lipids at binding sites were evaluated^{134,135}. Native MS was, for instance, used to study the functional and structural effects of lipid interactions on the ATP-binding cassette transporter TmrAB¹³⁶. In this study, a controlled delipidation protocol was developed and specialized bound lipids were retained after the delipidation process. By combining quantitative lipidomics and native MS, tightly bound lipids were, therefore, revealed.

Most importantly, however, new approaches using artificial membrane systems highlight the versatility of native MS. In particular, studies on membrane proteins embedded into nanodiscs showed that several types of lipid-binding sites with different specificity are preserved in the gas phase^{137–139}. In addition, native MS is also capable to detect fragile interactions and polydisperse complexes within lipid membranes^{140,141}.

A recent breakthrough revealed the analysis of protein-lipid assemblies directly from native membrane vesicles by native MS¹⁴². In this study, native membranes were purified, followed by sonication in ammonium acetate solution allowing to directly analyze mitochondrial membrane proteins and transporters by native MS. Recently, native MS was also employed in combination with other high-resolution structural techniques such as X-ray crystallography¹⁴³ and cryo-EM¹⁴⁴ allowing an even more detailed understanding of protein-lipid interactions.

1.4.3 Cross-linking MS

In the last years, cross-linking (XL) MS emerged as a powerful and alternative technique to study the three-dimensional structure of proteins and their complexes^{129,145,146}. XL-MS is also be applied to investigate proteins present in organelles and whole organisms such as cells^{147–149}. Within these organelles or organisms, it allows to capture protein interactions in a native environment and, therefore, derive structural information on large and transient protein complexes.

Cross-linking reagents

Most cross-linking reagents contain two reactive groups, which are either identical (homobifunctional) or different (heterobifunctional) connected by a spacer with a length between 6 and 25 Å (**Figure 8A**). The reactive groups introduce the covalent linkage while the length of the spacer determines the maximum distance of the two cross-linked amino acid side chains. The most commonly employed cross-linkers are homobifunctional active esters, for instance, the amine-reactive cross-linker bis(sulfosuccinimidyl)suberate (BS3)¹⁵⁰ containing a spacer length of 11.5 Å, which was also used in this thesis. The cross-linking reaction mechanism is shown in **Figure 8B**. This cross-linker contains an N-hydroxysuccinimide group that reacts with primary amines, resulting in the formation of a covalent isopeptide bond. Some protein cross-linkers are, however, bifunctional and, therefore, carry two functional groups allowing a linkage between different amino acid residues. Succinimidyl 4,4'-azipentanoate (SDA)¹⁵¹, for instance, contains an N-hydroxysuccinimide (NHS) group and a diazirine group. The NHS ester reacts with primary amines of amino acid residues and the diazirine group is photoactivated and can unspecifically react with any amino acid residue of the protein.

Other cross-linkers like 1-ethyl-3-(3-dimethyl aminopropyl)carbodiimide hydrochloride (EDC) are zero-length crosslinkers and allow an amino and carboxyl group to covalently bind to each other without insertion of a spacer¹⁵². Zero-length cross-linkers obtain a distance restrained in the length of a salt bridge. Tri- and multifunctional reagents were also described in the literature, which contain additional functional groups that facilitate the identification and enrichment of cross-linked interaction partners^{153,154}.

Cross-linking workflow

In a typical cross-linking experiment, two amino acids in close proximity of purified proteins or protein complexes are covalently linked by a cross-linker. For this, two different approaches are described, namely photo-induced or chemical cross-linking. Chemical cross-linking MS is performed by a bottom-up. Accordingly, the cross-linked samples are enzymatically hydrolyzed to generate covalently linked peptides (**Figure 8C**). After hydrolysis, a mixture of peptides including mono-linked peptides, loop-linked linear peptides as well as intra- and intermolecular cross-links is obtained. Cross-linked peptide pairs, although they are of particular interest usually have a low abundance.

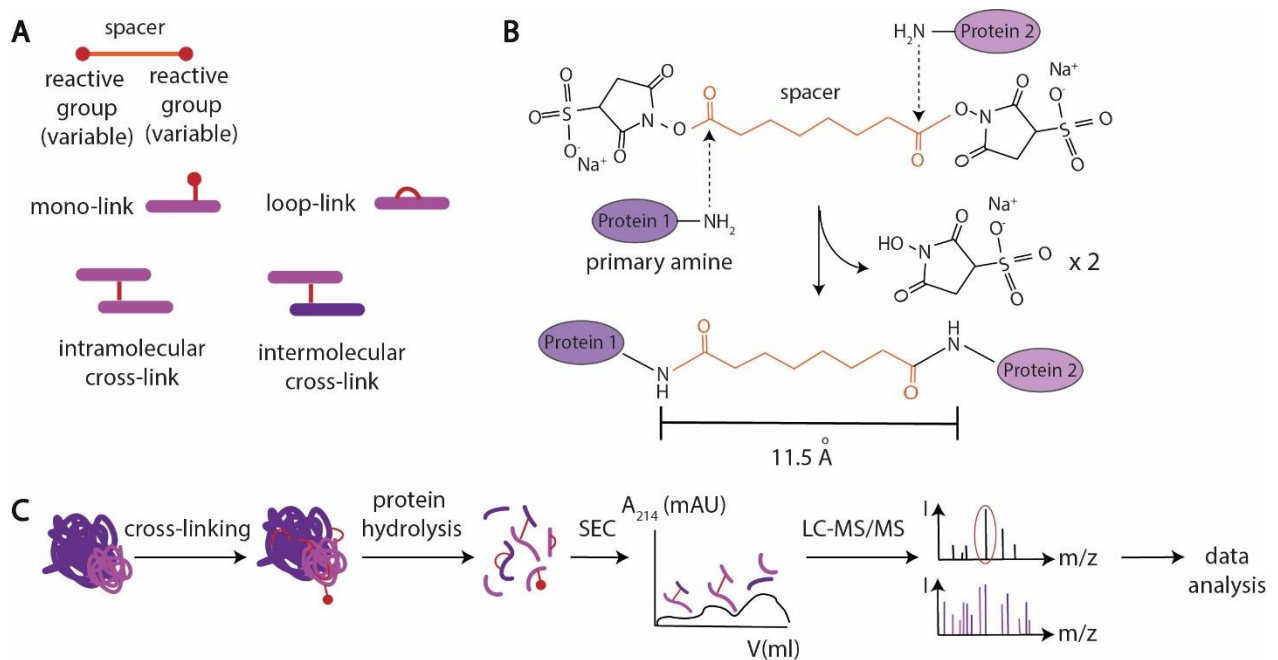


Figure 8: Cross-linking mass spectrometry. (A) Cross-linkers consist of two reactive groups that are connected by a linker. After cross-linking and protein hydrolysis, linear peptides, loop-links as well as inter- and intra-molecular cross-linked peptide pairs are obtained. (B) The reaction mechanism of the cross-linker BS3, containing a spacer of 11.5 Å. (C) Bottom-up cross-linking workflow is shown. After cross-linking, the proteins are hydrolyzed followed by SEC enrichment of cross-linked peptide pairs and LC-MS/MS analysis. The acquired data is then further analyzed using different software.

Accordingly, various strategies, such as size exclusion chromatography¹⁵⁵ and strong cation exchange chromatography¹⁵⁶, are employed to enrich the cross-linked peptide pairs. Additional affinity tags of trifunctional cross-linkers can also be used for selective enrichment of cross-links. The fractions that contain the highest amount of cross-linked peptide pairs are then analyzed by LC-MS. For MS analysis, the ions with lower charges are often excluded since the cross-linked peptide pairs carry higher charges compared to mono- and loop-linked peptides and linear peptides. A new and innovative approach for selecting specific ions with lower charge states was recently introduced by the high-field asymmetric waveform ion mobility (FAIMS) device which is added to the front end of the mass spectrometer¹⁵⁷.

After MS analysis, the cross-linked peptide pairs are identified by comparing MS cross-link data with possible cross-link predictions *in silico*. As the identification is very complex, specialized software such as Kojak¹⁵⁸, pLink2¹⁵⁹, xQuest¹⁵⁶, Xlink¹⁶⁰ identifier, XiSearch¹⁶¹, MeroX¹⁶² and LinX¹⁶³ was developed to identify cross-linked peptide pairs. However, to reduce the potential of false positives manual validation of spectra and the application of a false discovery rate (FDR) are highly recommended. Once intra- as well as inter-protein cross-links are obtained, the cross-linked peptide pairs are visualized using bar-, circle- or network plots¹⁶⁴. In addition, if high-resolution structures of proteins are available, cross-links are also mapped to these structures and cross-linked peptide pairs are validated.

1.4.4 Instruments

1.4.4.1 The Q Exactive Plus Hybrid-Quadrupole-Orbitrap mass spectrometer

In this thesis, the Thermo Scientific Q Exactive Plus Hybrid-Quadrupole-Orbitrap mass spectrometer was used for the analysis of lipids and proteins of liposomes and proteoliposomes under denaturing gas phase conditions (**Figure 9**). In the Q Exactive mass spectrometer, ions are generated at atmospheric pressure using an nESI source. Subsequently, ions are focused and guided through an S-lens and the bent flatpole, which operates in radio frequency (RF) mode. The configuration of the bent flatpole reduces noise by preventing the transfer of neutral molecules during this process allowing only charged molecules to be transmitted to the quadrupole¹⁶⁵. The quadrupole separates ions based on their flight trajectories through an electric field. This field is generated when RF and direct-current (DC) voltages are applied to opposite metal rods of the quadrupole. At a given DC/RF voltage specific m/z ions travel on stable flight paths through the quadrupole and, therefore, reach the detector¹⁶⁶.

The quadrupole can operate in two modes: In scanning mode, all ions differing in their m/z are transferred from the quadrupole through the C-trap into the Orbitrap and a full scan mass spectrum (MS1 spectrum) is recorded. In filtering mode, a fixed set of DC and RF voltages is applied to the quadrupole allowing the selection of a specific ion, that is then transferred to the C-trap¹⁶⁷ and directed to the HCD cell for fragmentation¹⁰¹. In this mode, an MS2 spectrum is recorded. Subsequently, the fragment ions are transferred back to the C-trap and ejected into the Orbitrap. Inside the Orbitrap, the ions oscillate laterally at frequencies determined by their m/z ratios. The oscillation of the ions induces an electric current that is simultaneously detected and converted into m/z values by Fourier transformation. The resolution of a mass spectrum is determined by the lateral oscillation time of the ions in the trap. Therefore, higher resolution of the mass spectra is achieved if the ions remain longer in the Orbitrap^{96,167}.

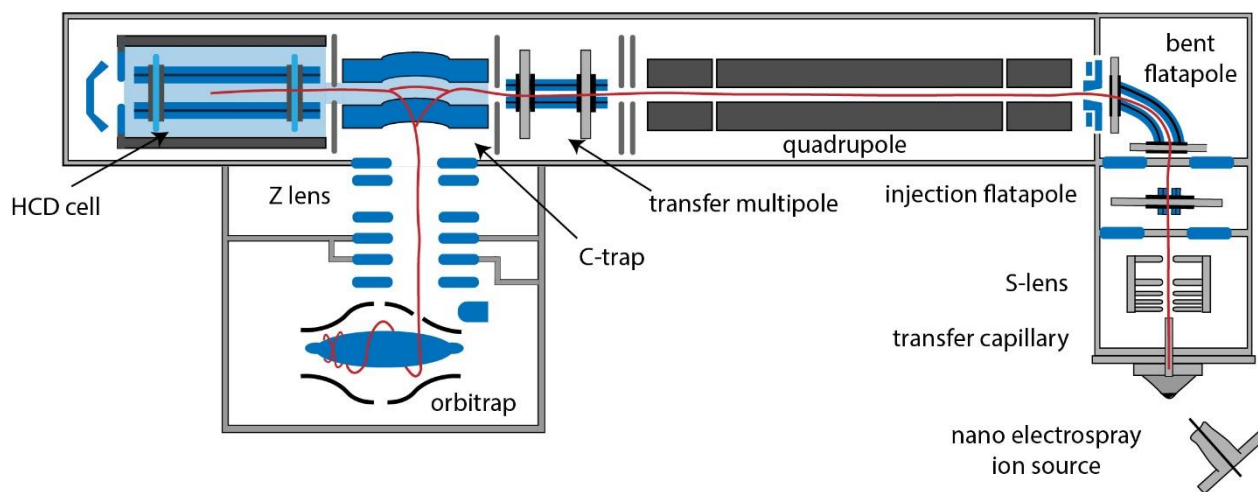


Figure 9: The Q Exactive Plus Hybrid-Quadrupole-Orbitrap mass spectrometer. After the ions are generated using an nESI source, they are transmitted through the mass spectrometer by several lenses until they reach the quadrupole. In MS1 experiments, the quadrupole acts as a scanning device and all ions pass to the C-trap where they are stored and transferred into the Orbitrap. In MS2 experiments an ion with a specific m/z value is selected and fragmented inside the HCD cell. The fragment ions are then detected in the Orbitrap (Schematic adapted from Thermo Fisher Scientific).

1.4.4.2 The Q-ToF Ultima mass spectrometer

In this thesis, a modified Q-ToF Ultima mass spectrometer was employed for native MS analysis of liposomes and proteoliposomes (**Figure 10**). In this mass spectrometer, a quadrupole, a collision cell and a TOF are arranged in series. Ions are generated by nESI and then transmitted by a set of ion guides optimized for ion transmission and focusing.

To analyze protein complexes, modifications of the MS instrument were proposed. For instance, the pressure in the first pumping stages of the instrument is manipulated by adding an inert gas. The increased pressure then leads to the reduced kinetic energy of ions, leading to a better ion transmission by collisional cooling and collisional focusing¹⁶⁸⁻¹⁷⁰. Furthermore, the RF of the quadrupole is reduced allowing transmission of ions up to a m/z ratio of 32,000. In the last stage of the mass spectrometer, the precursor and product ions are then sent to the TOF analyzer which separates the ions according to their m/z ratios on the traveling time through the analyzer^{83,171}.

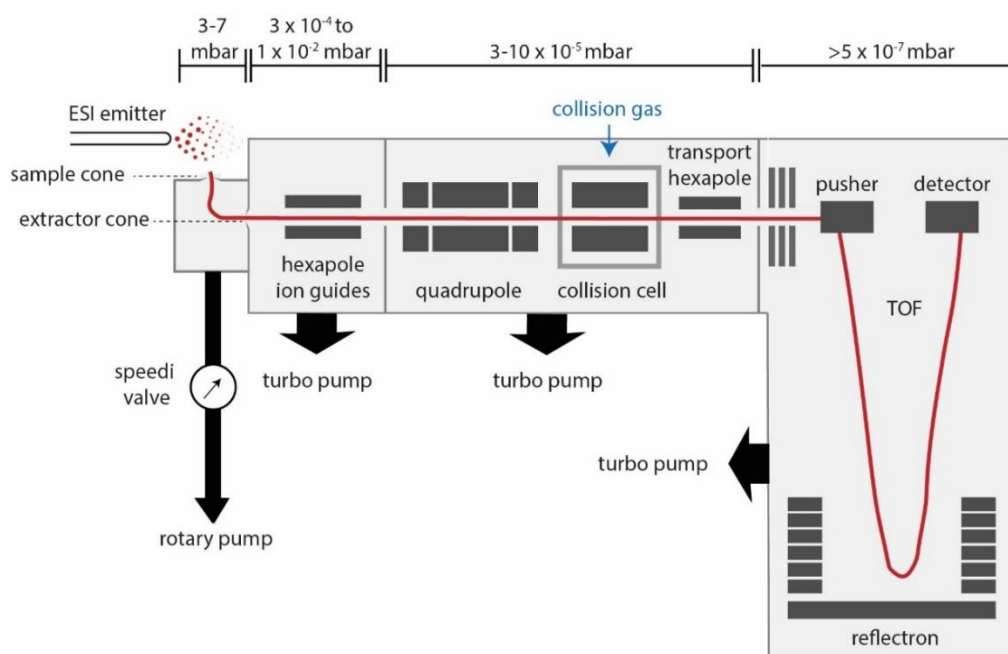


Figure 10: The Q-ToF Ultima mass spectrometer. Ions are generated from a nESI source and transmitted to the quadrupole. Ions with certain m/z ratios are selected in the quadrupole and then transferred into the collision cell. Here, the pressure is increased by an inert gas and ions depending on the applied voltage are fragmented. Finally, the ions are sent to the TOF analyzer for mass analysis (adapted from Sharon and Robinson, 2007).

2 Aim of this thesis

Until today, it has been an ongoing challenge for biophysical methods to analyze membrane proteins and their interactions with lipids. To facilitate the analysis of membrane proteins in their natural lipid environment, the aim of this thesis is to establish membrane mimetics for the analysis of membrane proteins for MS-based methods. MS will then be used to study the oligomeric states as well as protein-lipid interactions of membrane proteins. In this thesis, MS includes the analysis of liposomes and proteoliposomes as well as the analysis of an integral membrane protein reconstituted into nanodiscs. Accordingly, the MS-based methods should then enable the structural elucidation of proteins in a native-like lipid environment.

In the first part of this thesis, liposomes will be established for the analysis of membrane-associated proteins. We hypothesized, that in the gas phase of a mass spectrometer, liposomes dissociate and intact proteins or peptides are released allowing their structural analysis in the presence of lipids. By comparing the analysis of liposomes and proteoliposomes under denaturing and native gas phase conditions, a detailed analysis of proteins associated with the phospholipid bilayer should be enabled. Accordingly, under denaturing gas phase conditions, the dissociation of liposomes is studied, whereas, under native gas phase conditions, protein-protein and protein-lipid interactions are investigated.

As there has not yet been a sophisticated approach to study membrane proteins in liposomes by MS, an initial analysis of liposomes without proteins is desirable. In previous experiments during my Master's thesis, I was able to show that liposomes dissociate in the gas phase of a mass spectrometer under denaturing gas phase conditions allowing to identify and quantify lipids directly from a phospholipid bilayer¹⁷². In this thesis, these initial experiments will be complemented and liposomes will be analyzed under native gas phase conditions. For this, liposomes differing in composition, size and concentration will be investigated by MS. The dissociation of liposomes will also be monitored by applying increasing collisional voltages under native gas phase conditions.

Next, liposomes will be analyzed in the presence of soluble peptides/proteins differing in molecular weight by MS (Angiotensin I, Ubiquitin, ConA) to investigate whether lipids and peptides/proteins are detectable in the same mass spectrum. Finally, the application of liposomes for the analysis of membrane-associated proteins is investigated by MS under denaturing and native gas phase conditions, assuming that protein-lipid interactions, as well as the oligomeric states of these proteins are preserved in native MS experiments. In summary, these experiments will demonstrate that liposomes can be applied as a new and innovative approach to study membrane proteins in their native environment by MS.

The aim of the second project is to establish nanodiscs for the analysis of Syntaxin-1A. In the past, nanodiscs proved to be valuable membrane mimetics for the analysis of membrane proteins in their natural environment. Although MSP-nanodiscs have been increasingly studied using various structural methods, a sophisticated approach employing XL-MS to study specific protein-protein interactions in the membrane is missing. In this thesis, nanodiscs will, therefore, be established for MS-based chemical cross-linking. For this, “empty” nanodiscs will first be established, followed by the analysis of an integral membrane protein reconstituted into nanodiscs. This thesis will, therefore, apply various MS-based methods to elucidate the structure of membrane proteins associated with liposomes and nanodiscs. Taken together, these studies will allow us to extend the toolbox for a more simplified approach to study membrane proteins in their native lipid environment using biophysical methods.

3 Materials & methods

3.1 Materials

3.1.1 Reagents

Table 1: Chemicals.

chemicals	manufacturer
2-(4-(2-Hydroxyethyl)-1-piperazinyl)-ethansulfonsäure (HEPES)	Sigma Aldrich, St. Louis, USA
Ammoniumhydrogencarbonate	Sigma Aldrich, St. Louis, USA
Ampicillin	Carl Roth, Karlsruhe, Germany
Bis-(sulfosuccinimidyl)-suberat-do (BS3-do)	Fisher Scientific, Hampton, USA
Calcium chloride	Sigma Aldrich, St. Louis, USA
Cesium iodide	Sigma Aldrich, St. Louis, USA
CHAPS	Carl Roth, Karlsruhe, Germany
Cholic acid sodium salt	Anatrace, Maumee, USA
cOmplete TM , EDTA- free Protease Inhibitor	Sigma Aldrich, St. Louis, USA
Dikaliumhydrogenphosphate	Carl Roth, Karlsruhe, Germany
D (+)-Saccharose	Carl Roth, Karlsruhe, Germany
Dimethylsulfoxid	Sigma Aldrich, St. Louis, USA
Dithiothreitol (DTT)	Sigma Aldrich, St. Louis, USA
Ethylendiamin-tetraessigsäure	Carl Roth, Karlsruhe, Germany
Glycerol	Sigma Aldrich, St. Louis, USA
Hydrochloric acid (HCl) fuming 37%	Carl Roth, Karlsruhe, Germany
Hydrochloric acid volumeric solution 0.1 N	Neolab, Heidelberg, Germany
Imidazole	Carl Roth, Karlsruhe, Germany
Iodoacetamide (IAA)	Sigma Aldrich, St. Louis, USA
Isopropyl β -D-thiogalactopyranosid (IPTG)	Carl Roth, Karlsruhe, Germany
Kaliumchlorid	Carl Roth, Karlsruhe, Germany
Kaliumdihydrogenphosphate	Carl Roth, Karlsruhe, Germany
L-Glutathione reduced	Sigma Aldrich, St. Louis, USA
Magnesium sulfate	Carl Roth, Karlsruhe, Germany
Milk powder	Carl Roth, Karlsruhe, Germany
n-Octyl β -D-glucopyranoside (OG)	Glycon, Luckenwalde, Germany
Phenylmethysulfonylfluoride (PMSF)	Carl Roth, Karlsruhe, Germany
Phosphate Buffered Saline Tablet	Sigma Aldrich, St. Louis, USA
Pierce TM BS3 No-weight format	Thermo Fisher Scientific, Waltham, USA
RapiGest SF Surfactant	Waters, Milford, USA
Sodium dodecyl sulfate (SDS)	Sigma Aldrich, St. Louis, USA
Sodiumdihydrogenphosphate	VWR, Radnor, USA
Sodium chloride	Carl Roth, Karlsruhe, Germany
Sodium hydroxide	Merck, Darmstadt, Germany
Trifluoroacetic acid, LC-MS Grade (TFA)	Thermo Fisher Scientific, Waltham, USA
Tris(hydroxymethyl)aminomethan	Biofroxx, Einhausen, Germany
Tris-(2-carboxyethyl)-phosphin-hydrochlorid (TCEP)	Carl Roth, Karlsruhe, Germany
Triton-X-100	Sigma Aldrich, St. Louis, USA
Trypton (Pepton of Casein)	Sigma Aldrich, St. Louis, USA

Tween 20	Carl Roth, Karlsruhe, Germany
Yeast extract	Sigma Aldrich, St. Louis, USA

Table 2: Solvents.

solvent	manufacturer
2-propanol	Fisher Scientific, Hampton, USA
Acetic acid	Sigma Aldrich, St. Louis, USA
Acetone	Sigma Aldrich, St. Louis, USA
Acetonitril (ACN), Optima LC/MS	Fisher Scientific, Hampton, USA
Chloroform for HPLC	Sigma Aldrich, St. Louis, USA
Ethanol	Carl Roth, Karlsruhe, Germany
Formic acid	Sigma Aldrich, St. Louis, USA
Methanol	Thermo Fisher Scientific, Waltham, USA
Water for HPLC	Fisher Scientific, Hampton, USA

Table 3: Reagent kits.

reagent kit	manufacturer
Plasmid Mini-prep Kit	Thermo Fisher Scientific, Waltham, USA

Table 4: Gel electrophoresis and Western Blot reagents.

Gel electrophoresis chemicals and buffers	manufacturer
InstantBlue™ solution	Expedeon Ltd., Cambridge, UK
NuPAGE™ Antioxidant	Thermo Scientific, Dreieich, Germany
NuPAGE™ Bis-Tris Gels (4-12%)	Thermo Scientific, Dreieich, Germany
NuPAGE™ LDS sample buffer (4x)	Thermo Scientific, Dreieich, Germany
NuPAGE™ MES SDS running buffer	Thermo Scientific, Hampton, USA
NuPAGE™ Sample Reducing Agent (10x)	Thermo Scientific, Hampton, USA
SeeBlue Plus2 Pre-Stained Protein Marker	Thermo Scientific, Hampton, USA
Western Blot reagent	manufacturer
Pierce ECL Western Blotting Detection Reagent 1 (peroxide solution)	Thermo Scientific, Dreieich, Germany
Pierce ECL Western Blotting Detection Reagent 2 (luminol enhancer solution)	Thermo Scientific, Dreieich, Germany

Table 5: Antibodies for western blot analysis.

antibody	dilution	manufacturer
Mouse anti-Syntaxin-1A IgG polyclonal antibody	1:200	Synaptic Systems, Göttingen, Germany
Rabbit anti-mouse IgG polyclonal antibody	1:3000	Merck, Darmstadt, Germany
Mouse anti-His IgG polyclonal antibody	1:2500	Synaptic Systems Göttingen, Germany

3.1.2 Plasmids, bacterial strains and enzymes.

Table 6: Plasmids.

plasmid	producer
pGEX4T2-p40 ^{phox}	Brett Collins, Queensland, Australia
pET28a-MSP1E3D1	Stephen Sligar, Illinois, USA
pET3a-Syntaxin-1A	Reinhard Jahn, Göttingen, Germany

Table 7: Bacterial strains.

bacterium	strain
<i>E. coli</i>	BL21 (DE3)
<i>E. coli</i>	NEB5-alpha competent (High efficiency)

Table 8: Enzymes.

enzyme	manufacturer
Dnase I (from bovine pancreas)	Sigma Aldrich, St. Louis, USA
Thrombin	GE Healthcare, Chicago, USA
Trypsin (sequencing grade)	Roche Diagnostics, Mannheim, Germany
Trypsin (sequencing grade modified)	Promega, Mannheim, Germany
TEV protease	Sigma Aldrich, St. Louis, USA

3.1.3 Lipids, peptides and proteins

Table 9: Lipids

All lipids were purchased from Avanti Polar Lipids, Alabaster, USA.

lipids	nomenclature according to Liebisch et al. ¹⁷³
1,2-dioleoyl- <i>sn</i> -glycero-3-phosphocholine (DOPC)	PC-18:1/18:1
1,2-dioleoyl- <i>sn</i> -glycero-3-phosphoethanolamine (DOPE)	PE-18:1/18:1

1,2-dioleoyl- <i>sn</i> -glycero-3-phospho-L-serine (DOPS)	PS-18:1/18:1
1,2-dioleoyl- <i>sn</i> -glycero-3-phospho-(1- <i>rac</i> -glycerol) (DOPG)	PG-18:1/18:1
1-palmitoyl-2-linoleoyl- <i>sn</i> -glycero-3-phospho-(1- <i>rac</i> -glycerol) (POPG)	PG-16:1/18:2
1,2-dioleoyl- <i>sn</i> -glycero-3-phospho-(1'-myo-inositol-3'-phosphate) (PI(3)P)	PI(3)P-18:1/18:1
1-palmitoyl-2-oleoyl- <i>sn</i> -glycero-3-phosphoethanolamine (POPE)	PE-16:0/18:1
1-palmitoyl-2-oleoyl- <i>sn</i> -glycero-3-phosphocholine (POPC)	PC-16:0/18:1

Table 10: Peptides and proteins.

Peptides/Proteins	manufacturer
Albumin Fraction V	Carl Roth, Karlsruhe, Germany
Angiotensin I human acetate	Sigma Aldrich, St. Louis, USA
Bovine serum albumin (BSA)	Sigma Aldrich, St. Louis, USA
Conalbumin A	Sigma Aldrich, St. Louis, USA
Melittin from bee venom (approx. 85% purity)	Sigma Aldrich, St. Louis, USA
Phospholipase A2 from bee venom	Sigma Aldrich, St. Louis, USA
Ubiquitin	Sigma Aldrich, St. Louis, USA

3.1.4 Instruments, consumables and software.

Table 11: Instruments.

instruments	type	manufacturer
Cell disrupter	Cell disruptor French Press	Constant Sytems, Low March, UK Gaulin, Amicon, Silver Spring, MD
Dynamic light scattering	Zeta sizer Nano-s DLS Particle Analyzer Litesizer 500	Malvern instruments, Malvern, UK Anton Paar, Graz, Austria
Extruder	Avanti Mini Extruder	Avanti® Polar Lipids, Alabaster, USA
Film balance	deltaPi-4x Tensiometer	Kibron Inc., Helsinki, Finland
Gel electrophoresis	Xcell Surlock Mini-cell Electrophoresis system	Thermo Fisher Scientific, Waltham, USA
Gel scanner	Viewpix 700	Epson biostep®, Suwa, Japan
Glow chamber for grids	PELCO easy glow chamber	Ted Pella Inc., Redding, USA
Luminescent image analyser	LAS-4000	Fujifilm Corporation, Tokyo, Japan
Mass spectrometer	Q Exactive Plus Hybrid- Quadrupole-Orbitrap Q-ToF Ultima mass spectrometer, MS Vision, high mass upgrade	Thermo Fisher Scientific, Waltham, USA Waters Corporation Milford, USA
pH Meter	pH 1100 L pHenomenal	VWR GmbH, Radnor, USA
Purification systems	Äkta™ purifier Äkta™ pure Ultimate Dionex, 300 nano-LC system	GE Healthcare, Chicago, USA GE Healthcare, Chicago, USA Thermo Fisher Scientific, Waltham, USA
Rotary evaporator	Hei-VAP Advantage	Heidolph, Schwabach, Germany

Sputter Coater	P-1000	Quorum Technologies, Lewes, UK
UV/Vis-Spectrometer	DS-11 + spectrophotometer	DeNovix [®] , Wilmington, USA

Table 12: Consumables.

type	consumable	manufacturer
Affinity columns	HisTrap [™] HP HiTrap [™] Q HP HiTrap [™] SP HP GSTTrap [™] HP	Cytiva, Marlborough, USA GE Healthcare, Chicago, USA GE Healthcare, Chicago, USA GE Healthcare, Chicago, USA
Amicon	Amicon Ultra-15 Ultracel-3K, 10K filter	Merck, Darmstadt, Germany
Benchtop columns	PD MiniTrap G25 column	GE Healthcare, Chicago, USA
Biobeads	SM-2 Absorbant Media	Bio-rad, Hercules, USA
Bio-Spins	Micro Bio-Spin TM 6 column	Biorad Laboratories, München, Germany
EM grids	300 mesh size	Quantifoil Micro Tools, Großlobichau, Germany
ESI-Emitter (Q Exactive plus Hybrid-Quadrupole-Orbitrap)	Stainless Steel Emitters (40 mm, OD 1/32)	Thermo Fisher Scientific, Waltham, USA
ESI-Emitter (Q-ToF Ultima)	GC 100-TF-100	HAVARD Apparatus, Massachusetts, USA
Filter support	Whatman, 10 mm, 1 EA	Sigma Aldrich, St. Louis, USA
HPLC column	Acclaim [™] PepMap [™] 100 C18-LC-column (300 µm x 5 mm, particlesize 5 µm, poresize 100 Å)	Thermo Fisher Scientific, Waltham, USA
HPLC precolumn	Acclaim [™] PepMap [™] 100 C18-LC-column (75 µm x 500 mm, particlesize 3 µm, poresize 100 Å)	Thermo Fisher Scientific, Waltham, USA
Micro UV cuvettes	Brand, center H 15 mm, volume 70-550 µL, pack of 100 ea	Sigma Aldrich, St. Louis, USA
Native MS capillaries	Flaming/Brown Micropipette puller	Sutter Instruments, Novato, USA
PMMA cuvettes	Brand, disposable cuvettes	Sigma Aldrich, St. Louis, USA
Polycarbonate membrane	Whatman Nucleopore Track-Etched membranes 0.05 µm, 0.1 µm, 0.2 µm, 0.4 µm	Sigma Aldrich, St. Louis, USA
SEC-column (protein purification)	Superdex HiLoad [™] 16/600 75 pg	GE Healthcare, Chicago, USA
SEC-column (purification nanodiscs)	Superdex 200 Increase [™] 10/300 GL	Cytiva, Marlborough, USA
SEC-column (enrichment of cross-linked peptides)	Superdex Peptide 3.2/300	GE Healthcare, Chicago, USA

TLC plates	aluminum plates, layer thickness 0.25 mm, particle size 10-12 μm	Merck, Darmstadt, Germany
Western Blot filter paper	Rotilabo - Blottingpaper (thickness: 1.5 mm)	Carl Roth, Karlsruhe, Germany
Western Blot membrane	Amersham TM Protran Nitrocellulose Blotting membrane (pore size 0.2 μm)	GE Healthcare, Chicago, USA

Table 13: Software.

software	reference	version
Croco	J. Bender, C. Schmidt 2020 ¹⁷⁴	croco_wx_0_7_1
DTS nano	Malvern Instruments	5.00
Mascot	www.matrixscience.com ¹⁷⁵	V 2.7
MassLynx	Waters ¹⁷⁶	V 4.0 SP4
Max Quant	J. Cox, M. Mann 2008 ¹⁷⁷	1.5.5.1
Masssign	N. Morgner, C. Robinson 2012 ¹⁷⁸	14.11.2014
Origin	OriginLab ¹⁷⁹	Origin 2020 (9.7)
PLabel	Li et al. 2005 ¹⁸⁰	3.2.1
PLink2	Yang et al. 2012 ¹⁸¹	2.3.2
Xcalibur	Thermo scientific	4.0 SP1
xVis	http://xvis.genzentrum.lmu.de ¹⁸²	V 4.0

3.2 Methods

3.2.1 Molecular biological methods

3.2.1.1 Bacterial transformation

Bacterial *E. coli* (BL21) DE3 cells and NEB5-alpha cells were thawed on ice for 5 minutes. *E. coli* BL21 cells were used for protein expression and NEB5-alpha cells were employed for cryo-stocks and long-term storage. 3 μl of plasmid DNA were added to the cells, following incubation for 30 min on ice. The cells were then heated at 42 °C for 10 sec (BL21 cells) or 30 sec (NEB5-alpha cells) and afterward placed back on ice without mixing for 5 minutes. 950 μl of pre-heated lysogeny broth (LB) medium (**Table 14**) were added to the cells, followed by incubation at 37 °C and 250 rpm for 1 h. Cells were centrifuged for 2 minutes at 5000 x g and the pellet was resuspended in 100 μl fresh LB medium. Bacteria were plated on agar plates containing the appropriate antibiotic (ampicillin f.c. 100 mg/ml for pGEX4T2, kanamycin f.c. 30 mg/ml for pET28a and pET3a plasmids) and incubated overnight at 37 °C.

Table 14: LB medium composition.

reagent	amount
Tryptone	10 g
NaCl	10 g
Yeast extract	5 g
ddH ₂ O	ad 1000 ml

3.2.1.2 Plasmid purification

Plasmid DNA was isolated from 3-5 ml of an overnight culture of *E. coli* (BL21) DE3 cells containing the DNA of interest and the appropriate antibiotic (ampicillin f.c. 100 mg/ml for pGEX4T2, kanamycin f.c. 30 mg/ml for pET28a and pET3a plasmids). The cells were harvested and DNA was isolated using the Plasmid Mini-Prep Kit (Thermo Fisher Scientific, Waltham, USA). The plasmid was eluted with 40 μ l of elution buffer. The plasmid concentration was determined at a wavelength of 280 nm by UV-Vis spectroscopy. The ideal concentration for sequencing should be between 30 and 100 ng/ μ l DNA. Sequencing was performed by Eurofins, Genomics, Luxembourg. The results were analyzed using the Benchling software¹⁸³.

3.2.1.3 Determination of cell density

The cell density of bacterial cultures was determined during cell cultivation by measuring the optical density at a wavelength of 590 nm (OD₅₉₀). Cell density measurements were performed using the Ultrospec 10 cell density meter.

3.2.1.4 Cell culture and protein expression

The plasmid encoding the corresponding proteins was transformed into *E. coli* BL21 (DE3) cells and the pre-culture with the corresponding antibiotic (ampicillin f.c. 100 mg/ml for pGEX4T2, kanamycin f.c. 30 mg/ml for pET28a and pET3a plasmids) was incubated overnight in 150 ml LB medium (**Table 14**) at 37 °C and 180 rpm. Four main cultures of 500 ml double-strength yeast extract/tryptone (dYT) medium (**Table 15**) or terrific broth (TB) medium (**Table 16**) enriched with 10 x TB salts (**Table 17**) were each spiked with the appropriate antibiotic and inoculated with the pre-culture to an OD of 0.05. The cells were cultured while shaking at 200 rpm and 37 °C. When an OD of approximately 0.8 - 1.0 was reached, protein expression was induced by adding 1 mM isopropyl β -D-1-thiogalactopyranoside (IPTG). Depending on the expressed protein, cells were cultured at different temperatures and times (**Table 18**).

The cells were harvested by centrifugation at 4000 x g for 20 min and 4 °C. The pellets were resuspended with approximately 10 ml buffer and were either directly used for purification or snap frozen in liquid nitrogen and stored at -80 °C.

Table 15: dYT medium composition.

reagent	amount
Tryptone	16 g
NaCl	5 g
Yeast extract	10 g
ddH ₂ O	ad 1000 ml

Table 16: TB medium composition.

reagent	amount
Tryptone	12 g
Glycerol	4 ml
Yeast extract	24 g
ddH ₂ O	ad 900 ml, ad 100 ml of sterile 10 x TB salts

Table 17: 10 x TB salts composition.

reagent	amount	concentration [M]
KH ₂ PO ₄	23.1 g	0.17
K ₂ HPO ₄	125.4 g	0.72
ddH ₂ O	ad 1000 ml	

Table 18: Parameters protein expression.

proteins	temperature	time	antibiotic resistance
p40 ^{phox} (1-144) protein domain	25 °C	16 h	ampicillin
MSP1E3D1	25 °C	3 h	kanamycin
Syntaxin-1A	22 °C	16 h	kanamycin

3.2.1.5 Cell disruption

Cell disruption with cell disrupter/french press. Cell pellets of approximately 9 g bacterial cell culture were mixed with 5 mM magnesium sulfate (MgSO₄) and 10 µg/ml DNase I. Cell lysis was performed mechanically using a cell disrupter (Constant Sytems LTD, Low March, UK) by repeatedly applying a pressure of 2 kbar on cells with the expressed p40^{phox} (1-144) protein domain. Note that, for full-length Syntaxin-1A cell lysis was performed on a French press (Gaulin Amicon, Silver Spring, MD). Accordingly, the buffer contained 2% OG.

Immediately after cell disruption, the cell lysate was mixed with an ethylenediaminetetraacetic acid (EDTA)-free protease inhibitor cocktail tablet dissolved in 2 ml water and 1 mM phenylmethylsulfonyl fluoride (PMSF). The lysate was centrifuged at 4 °C and 25,000 rpm for 60 min. The supernatant was either directly purified chromatographically or snap frozen in liquid nitrogen and stored at -80 °C.

Cell disruption by sonication. This protocol was adapted from Malhotra and Alder¹⁸⁴. For cell lysis, cell pellets with expressed membrane-scaffolding protein E3D1 (MSP1E3D1) were thawed on ice, followed by the addition of 20 ml buffer (20 mM Na₃PO₄, pH 7.5) containing 1 mM PMSF. Triton-X-100 was added to a final concentration of 1% (v/v). Cells were disrupted by 5 rounds of ultrasonication on ice, using a microtip at 50% amplitude for 60 sec with pauses of 60 sec between pulses. The lysate was centrifuged at 25,000 x g for 60 min.

3.2.1.6 Protein purification of the p40^{phox} (1-144) protein domain

Purification of the p40^{phox} (1-144) protein domain was adopted from Chandra et al¹⁸⁵. All purification steps were carried out at 4 °C using a liquid chromatography system ÄktaTM purifier (GE Healthcare, Chicago, USA). Purification of the p40^{phox} (1-144) protein domain was performed using a glutathione-sepharose (GST) high-performance column. Buffer compositions and concentrations are given below. The cell lysate was first loaded onto the GST column pre-equilibrated in binding buffer (50 mM HEPES, 150 mM NaCl, 0.1 mM TCEP, pH 7.4), followed by a washing step until a constant UV signal below 200 mAU was detected. Stepwise elution (20%, 75%, 100%) of the protein was performed with GST elution buffer containing 10 mM reduced glutathione. Gel electrophoresis was performed to identify elution fractions containing the protein. Protein-containing fractions were combined and the GST tag was cleaved during dialysis overnight in 5 L dialysis buffer with 100 U - 150 U thrombin. Subsequently, the p40^{phox} (1-144) protein domain was subjected to size-exclusion chromatography (SEC) using a high loading Superdex 16/600 column pre-equilibrated in gel filtration buffer. The protein was loaded at a flow rate of 1 ml/min onto the SEC column and eluted isocratically over a volume of 80 ml. After elution and analysis of the fractions by gel electrophoresis, the purified protein was concentrated at 4000 rpm to 1.5 mg/ml. The concentration of the protein was determined by UV-Vis spectroscopy (**Section 3.2.2.1**).

p40^{phox} (1-144) protein domain buffers**Binding buffer:**

50 mM HEPES, 150 mM NaCl, 0.1 mM TCEP, pH 7.4

Elution buffer:

50 mM HEPES, 150 mM NaCl, 0.1 mM TCEP, 10 mM Glutathion reduced, pH 7.4

Dialysis buffer:

50 mM HEPES, 150 mM NaCl, 0.1 mM TCEP, pH 7.4

SEC buffer:

50 mM HEPES, 150 mM NaCl, 0.1 mM TCEP, pH 7.4

3.2.1.7 Protein purification of MSP1E3D1

Purification of MSP1E3D1 was carried out following a protocol from Malhotra and Alder¹⁸⁴. All purification steps were performed at 4 °C. The N-terminally hexahistidine-tagged protein was extracted from the cell lysate by immobilized metal affinity chromatography (IMAC). Buffer compositions and concentrations are given below. The cell lysate was loaded onto the IMAC column, preequilibrated in resuspension buffer. A washing step with four column volumes of wash buffer 1 followed. The IMAC column was washed with four column volumes of wash buffer 2 and four column volumes of wash buffer 3. The MSP1E3D1 protein was eluted with 3 column volumes of elution buffer. For washing and elution of the protein, a protein-dependent imidazole concentration was used. After inspecting the elution fractions for MSP1E3D1 by gel electrophoresis, protein-containing fractions were pooled and concentrated to 5 ml for SEC purification. For this, the protein was loaded onto a Superdex 16/600 column preequilibrated with SEC buffer and was eluted isocratically over a volume of 80 ml. After elution protein containing fractions were combined and subsequently concentrated at 4000 rpm to a concentration of 4.5 mg/ml using. The protein concentration was determined by UV-Vis spectroscopy (**Section 3.2.2.1**). The protein was aliquoted and either snap frozen in liquid nitrogen and stored at -80 °C or directly used for the preparation of nanodiscs.

MSP1E3D1 buffers**Resuspension buffer:**

20 mM Na₃PO₄, pH 7.5

Wash buffer 3:

20 mM HEPES, 300 mM NaCl, 50 mM Imidazol, pH 8.0

Wash buffer 1:

20 mM HEPES, 300 mM NaCl, 1% (v/v) Triton-X-100, pH 8.0

Elution buffer:

20 mM HEPES, 300 mM NaCl, 400 mM Imidazol, pH 8.0

Wash buffer 2:

20 mM HEPES, 300 mM NaCl, 20 mM Imidazol, 50 mM Na-cholate, pH 8.0

SEC buffer:

20 mM HEPES, 100 mM NaCl, 0.5 mM EDTA, pH 8.0

3.2.1.8 Protein purification of Syntaxin-1A

The purification of full-length Syntaxin-1A was performed as previously described^{186,187}. Purification steps were performed at 4 °C. Buffers compositions and concentrations are given below. Purification buffers for full-length Syntaxin-1A contained 2% OG. The proteins were first extracted from the cell lysate by IMAC. For this, the IMAC column was equilibrated with 3 column volumes of Ni-A buffer.

The lysate was loaded onto the column followed by a washing step until a constant UV signal below 200 mAU is obtained. Note that, different imidazole concentrations were used for the washing and elution steps (see below). The protein was eluted with 3 column volumes of Ni-B buffer. Gel electrophoresis was used to identify which elution fractions contained the protein. Fractions containing the appropriate protein were combined, mixed with 50 -100 U thrombin and dialyzed overnight at 4 °C against dialysis buffer 1 to cleave the hexahistidine-tag (His-tag). To remove the His-tag from the protein sample, the dialysate was repeatedly loaded onto the IMAC column. The column was washed with three column volumes of Ni-A buffer until a constant UV signal was obtained. Subsequently, to elute the His-tag, the column was washed with Ni-B buffer. After inspecting the elution fractions for protein by gel electrophoresis, fractions containing the protein were combined and dialyzed at 4 °C against dialysis buffer 2 to prepare the sample for anion-exchange chromatography with a salt concentration of 50 mM. The protein was then loaded onto a Superdex 16/600 equilibrated in SEC buffer and the protein was eluted isocratically over a volume of 80 ml. After elution, protein-containing fractions were combined and subsequently concentrated at 400 rpm to a volume of 1.5 ml. The protein concentration was determined by UV-Vis spectroscopy (**Section 3.2.2.1**). Aliquots were snap frozen in liquid nitrogen and stored at -80 °C.

Buffers for purification of full-length Syntaxin-1A

Ni-A buffer:

20 mM HEPES, 500 mM NaCl, 10 mM Imidazol, 0.1 mM TCEP, 2% OG, pH 7.4

Dialysis buffer:

20 mM HEPES, 50 mM NaCl, 1 mM EDTA, 0.1 mM TCEP, 2% OG, pH 7.4

Ni-B buffer:

20 mM HEPES, 500 mM NaCl, 500 mM Imidazol, 0.1 mM TCEP, 2% OG, pH 7.4

SEC buffer:

20 mM HEPES, 150 mM KCl, 0.1 mM TCEP, 1mM EDTA, 2% OG, pH 7.4

3.2.2 Protein biochemical methods

3.2.2.1 Protein concentration determination

Protein concentrations were measured by UV-Vis-spectroscopy at a wavelength of 280 nm. All measurements were performed three times. The protein concentration was calculated according to the Lambert-Beers law using the extinction coefficient of the specific protein. The molecular weight and extinction coefficients were calculated using the Expasy Protparam Tool^{188,189}. The molecular weight and the extinction coefficient of each protein used in this thesis are given in **Table 19**:

Table 19: Protein properties. They were calculated using the Expasy tool^{188,189}.

protein	molecular weight [Da]	extinction coefficient [$l \cdot mol^{-1} \cdot cm^{-1}$]
Angiotensin I	1046.18	1490
Conalbumin A	69366.68	41435
Melittin	2846.46	5500
p40 ^{phox} (1-144) protein domain	16424.88	15930
Phospholipase A2	19057.62	29045
Syntaxin-1A	33348.75	7450
Ubiquitin	8565.00	1280

3.2.2.2 Gel electrophoresis

Protein-containing samples (5-12 μ g) were incubated with 4 x sample buffer and 10 x reducing agent. The samples were centrifuged for 1 min at 14,000 x g and then heated to 70 °C for 10 min to achieve denaturation. Proteins were separated by gel electrophoresis using the NuPAGE system (Thermo Fisher Scientific, Waltham, USA) according to the manufacturer's protocol. Protein samples and 5 μ l of Protein2 Pre-stained Protein standard marker were loaded onto 4-12 % Bis-Tris protein gels and separated at 200 V for 30 min. Protein gels were stained with Coomassie using InstantBlue Protein solution and incubated at room temperature on a horizontal shaker. For destaining, the gel was washed with double-distilled water (ddH₂O) until the background was clear.

3.2.2.3 Western blot analysis

After protein separation by gel electrophoresis, the gel was subjected to western blot analysis. For this, filter papers were drained in transfer buffer and the blotting membrane was incubated with phosphate buffer saline containing Tween 20 (PBS-T). Following incubation for 5 minutes, the NuPAGE Bis-Tris gel was stacked between two filter papers and the blotting membrane.

Air bubbles were removed using a glass rod. The proteins were then transferred to a nitrocellulose membrane for 2 h at 55 mAU. The membrane was blocked for 1 h at room temperature with blocking solution. Subsequently, the membrane was washed at least 3 times for 5 minutes following incubation at 4 °C for 16 h with the primary antibody solution. The membrane was repeatedly washed with PBS-T buffer to remove unspecifically bound primary antibodies. The membrane was then incubated with horseradish-peroxidase marked secondary antibody for 1 h at room temperature. Finally, ECL Western Blotting Detergent Reagents 1 and 2 were added at a 1:1 ratio and the chemiluminescent was detected by a LAS-4000 analyzer. The marker was detected by fluorescence.

Western blot buffers

Transfer buffer:

25 mM Tris base pH 8.8, 193 mM Glycin, 0.1 % (m/v) SDS, 10 % (v/v) Methanol

PBS buffer:

1.76 mM KH₂PO₄, 10 mM Na₂HPO₄ pH 7.4, 2.7 mM KCl, 137 mM NaCl

PBS-T:

(PBS- Tween 20) PBS, 0.02 % (v/v) Tween 20

Blocking solution:

PBST, 5 % (m/v) Milkpowder

Primary antibody solution:

PBST, 1 % (m/v) BSA, Anti-syx IgG 1:1000, Anti-6xHis-tag IgG 1:1000

Secondary antibody solution:

PBST, 1 % (m/v) BSA, Anti-mouse IgG 1:10.000

3.2.2.4 Chemical cross-linking

For chemical cross-linking, BS3 was dissolved in ddH₂O directly before the reaction to minimize hydrolysis of NHS esters. Proteins, proteoliposomes and nanodiscs were cross-linked with varying BS3 concentrations. Samples were incubated with BS3 for 30 minutes at 25 °C in a thermomixer at 300 rpm. The cross-linked proteins were separated by gel electrophoresis (**Section 3.2.2.2**) and stained with InstantBlue staining solution. Non-crosslinked proteins were used as control samples. For in-solution hydrolysis of the cross-links, samples were precipitated in 100 % ethanol, hydrolyzed in solution and cross-linked peptides were enriched by SEC (**Section 3.2.4.3**), followed by the analysis by liquid chromatography-coupled mass spectrometry (LC-MS/MS) and evaluation of the cross-links (**Section 3.2.5**).

3.2.3 Biophysical methods

3.2.3.1 Preparation of liposomes

Liposomes were prepared by mixing different lipids at different concentrations. The solvent was evaporated by rotary evaporation at 40 °C for 1 h. The resulting dry lipid film was rehydrated for 1 h at room temperature with an aqueous buffer e.g. 200 mM ammonium acetate (AmAc). The resulting multi-lamellar vesicles were subjected to sonication followed by extrusion through polycarbonate membranes with pore sizes of 50 nm, 100 nm, 200 nm and 400 nm. Diameter and homogeneity of the liposomes were analyzed by DLS (Section 3.2.3.5). All preparations were performed in triplicate. **Table 20** shows the composition, diameter and final concentration of prepared liposomes.

Table 20: Composition, diameter and concentration of liposomes.

lipid composition liposomes	diameter [nm]	final concentration [mM]
DOPC	50	0.5
DOPE	50	0.5
DOPS	50	0.5
DOPG	50	0.5
DOPC/DOPG (1:1)	50	0.5
DOPC/DOPE (1:1)	50	0.5
DOPG/DOPE (1:1)	50	0.5
DOPC/DOPE/DOPS (5:2:2)	50	5
DOPC/DOPE/DOPS/cholesterol (5:2:2:1)	100	0.5
DOPC/DOPE/DOPS/cholesterol (5:2:2:1)	50	0.5
lipid composition proteoliposomes	diameter [nm]	final concentration [mM]
DOPG/DOPE	100	2.0
DOPC/DOPE/DOPS/cholesterol (5:2:2:1)	100	2.0
DOPC/DOPE/PI(3)P (8:1:1)	100	2.0
DOPC/DOPE (8:2)	100	2.0

3.2.3.2 Preparation of proteoliposomes with membrane-associated proteins

The p40^{phox} (1-144) protein domain (concentration approx. 5 mg/ml, solubilized in SEC buffer or 200 mM AmAc solution) was associated with liposomes by incubating the protein with liposomes (1.5 mM - 2.5 mM) for 1 h at room temperature at protein-to-lipid ratios of 1:50 and 1:100. Melittin (concentration approx. 1 mg/ml, solubilized in 200 mM AmAc solution) was associated to liposomes by incubating the protein with liposomes (1.5 mM - 2.5 mM) for 1 h at room temperature at a protein-to-lipid molar ratio of 1:50. Protein binding to the liposomes, was verified by liposome flotation analysis (Section 3.2.3.6).

3.2.3.3 Preparation of nanodiscs

Nanodiscs were prepared by solubilizing a dry lipid film of DMPC or POPC, POPE and DOPS lipid at a molar ratio of 45:15:40 in 20 mM sodium cholate buffer. After heating at 37°C, vortexing, and sonicating the lipid solution for 30 minutes, MSP1E3D1 was added at the desired protein-to-lipid molar ratio (1:150 for DMPC, 1:120 for POPC, POPE and DOPS) and the mixtures were incubated for 1 h at 4 °C. The detergent concentration was adjusted to 12-40 mM after the addition of the protein. Bio-beads SM-2, which are used for detergent removal, were washed with methanol (1x), water (3x), and buffer (1x). 0.5 - 0.8 g of washed Bio-beads were added to 1 ml of the lipid/protein mixture and incubated overnight at 4 °C with gentle shaking on an orbital shaker. The mixture was then filtrated and nanodiscs were purified by SEC using a Superdex 200 GL increase 30/200 column. Fractions were evaluated by gel electrophoresis and nanodisc diameter and homogeneity was determined by DLS (**Section 3.2.3.5**). The shape of the nanodiscs was visualized by negative-stain TEM (**Section 3.2.3.7**). **Table 16** shows the composition, size and concentration of the prepared nanodiscs.

Buffer nanodisc preparation

SEC buffer:

20 mM HEPES, 100 mM NaCl, 0.5 mM EDTA, pH 7.4

Table 21: Composition, diameter and concentration of prepared nanodiscs.

lipid composition nanodiscs	diameter [nm]	final concentration [mM]
DMPC	13	5.0
POPC/POPE/DOPS (45:15:40)	13	2.5

3.2.3.4 Reconstitution of an integral membrane protein into nanodiscs

Reconstitution of Syntaxin-1A into nanodiscs was performed as described previously^{190,191}. Lipid mixtures were prepared by rehydrating the dry lipid film containing POPC, POPE and DOPS in 20 mM cholate buffer to a final concentration of 10 mM total lipid. Phospholipid-detergent mixtures, Syntaxin-1A and MSP1E3D1 were then mixed at a molar ratio of 120:0.25:1 and incubated on ice for 1 h. The cholate concentration was adjusted to 12-40 mM and 0.5 - 0.8 g of Bio-beads were then added to the solution, followed by incubation at 4 °C overnight with gentle shaking on an orbital shaker. Syntaxin-1A nanodiscs were purified on a Superdex 200 GL 10/300 column. Diameter and homogeneity of the reconstituted nanodiscs were determined by DLS (**Section 3.2.3.5**) followed by an additional characterization of the nanodiscs by western blot analysis (**Section 3.2.2.3**) and negative-stain TEM (**Section 3.2.3.7**).

3.2.3.5 DLS analysis

DLS measurements of liposomes and proteoliposomes were performed using a Zetasizer Nano S instrument (Malvern Instruments, Worcestershire, UK) equipped with a helium-neon laser of 633 nm and a scattering angle of 173°. 70 µl of liposome or proteoliposome samples were pipetted into micro-UV cuvettes and heated for 2 min at 25 °C before they were analyzed 10 times for 60 sec at 22 °C in an aqueous buffer. Data was collected with the software DTS Nano and data analysis was performed using the Origin software.

The size distributions of nanodiscs were determined by DLS using a Litesizer 500 instrument (Anton Paar, Graz, Austria) equipped with a 633-nm helium-neon laser and a detection angle of 90°. Samples were heated for 2 min at 25 °C and analyzed 5 times for 15 seconds at 22 °C in an aqueous buffer. Autocorrelation functions were fitted by applying the Kalliope software (Anton Paar, Graz, Austria) and data analysis was later performed using the Origin software.

3.2.3.6 Liposome flotation assay

For flotation analysis, proteoliposomes were mixed with sucrose to a final concentration of 1M and overlaid with $\frac{3}{4}$ volumes of 0.75 M sucrose solubilized in the appropriate liposome buffer. 0.175 volumes of the liposome buffer without sucrose were added on top and the samples were centrifuged at 268,000 x g for 2 h or overnight to separate liposome-associated proteins from free protein. Top, middle, and bottom fractions were collected and subsequently evaluated by gel electrophoresis. Liposomes and proteoliposomes are observed in the top fraction due to their lower density (**Section 3.2.2.2**).

3.2.3.7 Negative-stain TEM of nanodiscs

For the preparation of negative-stain TEM samples, quantifoil carbon support film grids were coated with low-energy hydrogen plasma to improve hydrophilicity. For this, grids were discharged in a PELCO easy glow chamber for 25 sec at a pressure of 0.39 mbar. Following discharging, EM grids were loaded with 10 µL of nanodiscs suspension (0.05 mg/ml or 0.1 mg/ml lipid). Excess liquid was blotted off with a strip of filter paper after 45 sec followed by two washing steps with 10 µl ddH₂O. Grids were stained with 10 µL 1% (w/v) aqueous uranyl acetate solution for 1 min. Excess staining solution was again removed by blotting with a clean filter paper. Specimens were dried, examined on an EM 900 transmission electron microscope and micrographs were recorded with an SM-1k-120 slow-scan charge-coupled camera. Sample preparation was performed together with Jennifer Zierath. TEM measurements were performed by PD Dr. Annette Meister.

3.2.3.8 Monolayer measurements

Monolayer measurements were performed utilizing a deltaPi-4x Tensiometer (Kibron, Helsinki, Finland), which consists of 4 Wilhelmy pressure sensors (Kibron, Helsinki, Finland) placed over Langmuir troughs. Before sample analysis, each trough was cleaned thoroughly with 1% Helmanex® detergent solution, following several washing steps with ddH₂O until all detergent was removed.

Wilhelmy pressure sensors were cleaned with ddH₂O and then heated to remove residual molecules. Troughs were maintained at 20 °C and filled with 1100 µl PBS buffer as a subphase. Calibration of the pressure sensors was achieved by hanging the sensor freely in air and setting the surface pressure (Π) to 72.6 mNm⁻¹ followed by the insertion of the sensor into PBS buffer and setting Π to 0 mNm⁻¹. After equilibrating for >30 minutes and pressure stabilization, lipid mixtures in chloroform/methanol (3:1, vol/vol) were added dropwise to the air/buffer interface until the desired surface pressure was reached. The solvent was subsequently allowed to evaporate for at least 10 min and the lipid film was equilibrated for at least 30 min. Protein solutions were injected underneath the equilibrated lipid monolayer through the injection port into the subphase. To ensure homogeneous distribution of the peptides, the subphase was gently stirred during injection and measurement. After injection, the surface pressure was recorded for approximately 4 hours as a function of time until a constant value was reached. Monolayer experiments were performed together with Dr. Christian Schwieger. Data analysis was performed by Dr. Christian Schwieger.

3.2.4 Mass spectrometric methods

3.2.4.1 Nano-ESI emitters for MS analysis

Thin wall borosilicate capillaries without filament, with an inner diameter of 0.78 mm were used for in-house preparation of nESI emitters with a Fleming/Brown micropipette puller. Program settings are described in **Table 22**. Program settings (1) were used for the preparation of nano-ESI emitters for native MS experiments using a Q-ToF Ultima instrument. Program settings (2) were used for the preparation of nano-ESI emitters for direct infusion experiments using a Q Exactive instrument. Capillaries were gold-coated using a Sputter, Quorum Q150RS with a sputter current of 80 mA, sputter time of 150 seconds and a tooling factor of 1.00. Before MS analysis, the tip of the needle was opened with tweezers.

Table 22: Settings of the micropipette puller.

Program 1	heat	pull	velocity	time	pressure	ramp
	514	0	100	60		
	514	0	70	40	500	514
	514	100	100	60		
Program 2	heat	pull	velocity	time	pressure	ramp
	475	90	70	70	200	475

3.2.4.2 Sample preparation and direct infusion MS analysis

Liposomes and proteoliposomes were analyzed by direct infusion nESI MS using a Q Exactive mass spectrometer. For this, 2-4 μl of the liposome/proteoliposome samples prepared in 200 mM AmAc were loaded into borosilicate offline emitters coated with gold/palladium or into self-prepared capillaries (**Section 3.2.4.1**). Mass spectra were recorded in positive ion mode. An electrospray capillary voltage of 1.70 - 4.0 kV was applied and the capillary temperature was set to 250 °C. The resolution was 70,000 and the AGC target was set to 3×10^6 . RF lens was set to 50 and the MS scan range was 500 - 6000 m/z . The minimum injection time was 100 ms and MS/MS fragmentation was performed in the HCD cell applying a normalized collision energy of 10 - 40 NCE. The isolation window was set to 2.00 m/z . Data acquired on the Q Exactive mass spectrometer was analyzed using the Xcalibur software.

3.2.4.3 MS analysis of peptides

In-gel hydrolysis of proteins. In-gel hydrolysis of proteins was performed as previously described by Shevchenko et al. 1996⁹³. All steps were carried out at 26 °C and 1050 rpm unless otherwise indicated. Gel bands were excised, cut into 1 x 1 mm pieces, and washed with 150 μl of water for 5 min. After each incubating step, the samples were centrifuged (for 1 min at 16,200 x g) and the supernatant was discarded. The gel pieces were then incubated with 150 μL acetonitrile (ACN) for 15 min. The gel pieces were spun down (for 1 min at 16,200 x g), the supernatant was discarded and the gel pieces were dried in a vacuum centrifuge. Disulfide bridges were reduced by the addition of 100 μl 10 mM dithiothreitol (DTT; in 100 mM ammonium hydrogen carbonate (NH_4HCO_3), pH 8.0) at 56 °C for 50 minutes. The gel pieces were centrifuged (1 min at 16,200 x g) and the supernatant was removed. After washing with 150 μl ACN for 15 min the gel pieces were spun down (for 1 min at 16,200 x g) and the supernatant was removed. Free cysteine residues were alkylated by adding 100 μl 55 mM iodacetamide (IAA, in 100 mM NH_4HCO_3 , pH 8.0). The reaction was performed in the dark at 37 °C for 30 minutes. The gel pieces were incubated with 150 μl of 100 mM NH_4HCO_3 for 15 min followed by the addition of 150 μl ACN.

The gel pieces were centrifuged for 1 min at 16,200 x g and the supernatant was discarded. After the addition of 150 μ l ACN, gel pieces were dried for 5-10 min in a vacuum centrifuge and rehydrated on ice for 45 min by adding approximately 20 μ l proteolytic buffer 1 (**Table 23**). The gel pieces were covered with 50 μ l proteolytic buffer 2 (**Table 23**) and incubated at 37 °C overnight.

Table 23: Buffer for in-gel proteolysis. All buffers were freshly prepared.

Chemical	Proteolytic buffer 1	Proteolytic buffer 2
0.1 μ g/ μ l Trypsin	0.0125 μ g/ μ l	-
100 mM NH_4HCO_3	41.64 mM	47.62 mM
100 mM CaCl_2	4.17 mM	4.76 mM

After incubating the gel pieces overnight with trypsin, they were centrifuged (for 1 min at 16,200 x g) and mixed with 50 μ l of water followed by the addition of 50 μ l ACN. The supernatant containing tryptic peptides was removed and collected in a new sample tube. 50 μ l of 5% (v/v) formic acid was added followed by the addition of 50 μ l of ACN for the second round of extraction of the peptides from the gel pieces. The gel pieces were spun down (for 1 min at 16,200 x g), the supernatant was removed and pooled with the supernatant from the previous extraction steps. The peptides were dried in a vacuum centrifuge and the pellet was stored at -20 °C until analysis by LC-MS/MS.

Ethanol precipitation. Proteins were precipitated by the addition of 20 μ l 3M sodium acetate (pH 5.3) and 600 μ l ice-cold 100% (v/v) ethanol incubated overnight at -20 °C. The proteins were then centrifuged for 30 min at 4 °C, 13,000 rpm. The supernatant was removed and the pellet was washed with 80% (v/v) ethanol and subjected to another centrifugation step at 4 °C, 13,000 rpm. The pellet was then dried in a vacuum centrifuge. The proteins were hydrolyzed in solution and cross-linked peptides were enriched by size exclusion chromatography (SEC) and analyzed by LC-MS/MS.

In-solution hydrolysis. After ethanol precipitation, the protein pellet was dissolved in 10 μ l 1% (w/v) Rapigest (in 25 mM NH_4HCO_3 , pH 8.5) followed by the addition of 10 μ l 50 mM DTT (in 25 mM NH_4HCO_3 , pH 8.5) for reducing disulfide bonds and addition of 10 μ l 100 mM IAA (in 25 mM NH_4HCO_3 , pH 8.5) for alkylation for 1 h at 37 °C. Proteins were hydrolyzed by incubation with 0.1 μ g/ μ l trypsin solution (in 25 mM NH_4HCO_3 , pH 8.5) at a molar ratio of 1:20 (trypsin: protein), following incubation overnight at 37 °C. To inactivate Rapigest, 20 μ l 5% (v/v) trifluoroacetic acid (TFA) was added and the sample was incubated at 37 °C for 2 h followed by centrifugation for 30 min at 13,000 rpm. The peptide containing supernatant was dried by vacuum centrifugation.

Enrichment of cross-linked peptides by SEC. Enrichment of cross-linked peptides was performed by SEC using an Äkta™ system (GE Healthcare, Chicago, USA). The peptide pellet was rehydrated with 60 µl SEC-buffer 30% (v/v) ACN, 0.1 % (v/v) TFA, sonicated for 1 min, and centrifuged for 5 min at 13,000 rpm. Following this, 50 µl of the supernatant were loaded with a flow rate of 0.05 ml/min onto a Superdex™ peptide 3.2/300 column and eluted. Fractions, which contain the cross-linked peptides were dried by vacuum centrifugation and subsequently analyzed by LC-MS/MS.

LC-MS/MS. Peptides were analyzed by nano-flow reverse-phase liquid chromatography on a DionexUltiMate 3000 RSLnano System coupled with a Q Exactive mass spectrometer. For liquid chromatography 0.1% (v/v) formic acid (FA) was used as mobile phase A and 80% (v/v) ACN/0.1% (v/v) FA was used as mobile phase B. The dried peptides were diluted in 2% (v/v) ACN, 0.1% (v/v) formic acid and subjected to ultrasonication for 1-2 min. Following this, the samples were centrifuged at 10,000 rpm and 4 °C. The supernatant was transferred into injection vials for LC-MS/MS analysis. 5 µL of the sample were loaded onto the Acclaim PepMap 100 C18-LC precolumn (µ-precolum C18 Acclaim™ PepMap™ 100, C18, 300 µm, I.D., particle size 5 µm) at a flow rate of 10 µl/min. Subsequently, the peptides were separated on an Acclaim PepMap 100 C18-LC analytical column (50 cm, HPLC, column Acclaim™ PepMap™ 100, C18, 75 µm I.D., particle size 3 µm) at a flow rate of 300 nl/min over a gradient of 4-90% (v/v) running buffer B (see **Table 24** for details).

Samples from in-gel hydrolysis are separated by a 90 min gradient, while samples from the SEC enriched cross-linked peptides are separated by a 120 min gradient. Depending on the peptide hydrophobicity different analysis methods were used. For larger, strongly hydrophobic, cross-linked peptides (first 5 peptide-containing fractions of SEC) methods 1 to 3 were used. Method 2 (peptide-containing fractions 6-10 of SEC) and method 3 (peptide-containing fractions 11-13) were used to separate smaller, cross-linked peptides with lower hydrophobicity.

Table 24: Liquid-chromatography gradient. The gradient consisting of 0.1% (v/v) formic acid as mobile phase A and 80% (v/v) ACN/ 0.1% (v/v) FA as mobile phase B is shown at different gradient length. For protein identification, a gradient of 90 minutes was used. Identification of cross-linked peptides was achieved by step-wise adjusting the 120 min gradient according to the hydrophobicity of the samples:

Running buffer A [%]	Running buffer B [%]	Time [min]			
		Method 1	Method 2	Method 3	Method 4
96	4	0	0	0	0
92	8	3	3	3	3
85	15	-	15	-	75
75	25	60	90	90	90
50	50	64	94	94	94
10	90	65	95	95	95
10	90	69	99	99	99
96	4	70	100	100	100
96	4	90	120	120	120

Peptides were directly eluted into the Q Exactive mass spectrometer and analyzed in positive ion mode (MS1). Typical mass spectrometric standard conditions were: data-dependent mode; capillary voltage, 2.8 kV; capillary temperature, 275 °C and polarity, positive. Survey full scan MS spectra were acquired in a mass range of 350 - 1600 m/z , with a resolution of 70,000 and an automatic gain control (AGC) target of $3e6$. The maximum injection time was set to 100 ms. The "top 20" method was used to isolate the 20 most intense precursor ions with charge states ranging von 1 and >8 in the quadrupole mass filter. These precursor ions were transferred into the HCD cell for fragmentation with an AGC target of $1e5$ and a fixed mass of 105 m/z . The resolution of MS2 spectra was 17,500 and for cross-linking samples 35,000. The maximum injection time (MS2 spectra) was 150 ms (for proteomic samples) and 200 ms (for cross-linked samples). For cross-linking samples charge states 1-3 and >8 were excluded.

3.2.4.4 Buffer exchange for native MS

Liposome and proteoliposome samples were prepared in 200 mM AmAc buffer before MS analysis. For measurement of protein complexes by native MS, protein buffers were exchanged to 200 mM AmAc buffer. Buffer exchange was achieved by SEC using Micro Bio-Spin columns. For this, the Bio-Spin column was first equilibrated in 500 μ l 200 mM AmAc solution, followed by 1 min centrifugation at 1000 x g at 4 °C. This step was repeated three times. After equilibration, at least 20 μ l of sample were loaded onto the Bio-Spin column, followed by centrifugation for 4 min at 1000 x g at 4 °C.

3.2.4.5 Native MS analysis

Liposomes and proteoliposomes were analyzed by native MS utilizing a Q-ToF mass spectrometer modified for the transmission of high mass complexes¹⁹². For this, 2-4 μ l of liposomes or proteoliposomes were loaded into in-house prepared capillaries and injected into the mass spectrometer. Mass spectra were recorded in positive ion mode. Measurements were carried out at a capillary voltage of 1.50 - 1.70 kV and a cone voltage of 80 - 100 V. The RF lens energy was 80 V and the source temperature was set to 80 °C. Collision voltages of 20 - 200 V were applied. Mass spectra were calibrated externally using 100 mg/ml CSI dissolved in water.

3.2.5 Data analysis

Data analysis of direct infusion MS spectra. Data obtained on the Q Exactive instrument was processed and analyzed using the Xcalibur software. At least 100 scans were combined.

Data analysis of native MS spectra. Data obtained from the Q-ToF mass spectrometer was processed using MassLynx 4.0¹⁷⁶ and analyzed using the Massign software¹²². At least 100 scans were combined. Acquired mass spectra were calibrated externally using cesium iodide solution (100 mg were dissolved in 1 ml). Calibrated mass spectra were linearized, smoothed and the peak list was transferred to the Massign software¹⁷⁸. Peaks were assigned and the masses of the protein complexes were determined.

Identification of cross-linked peptides. Cross-links were identified using the software pLink2 version 2.3.9¹⁵⁸. Raw data were searched against a FASTA database of Syntaxin-1A and MSP1E3D1. The search parameters for pLink2 were set to trypsin as the protease; trypsin cleavage sites, 3; fixed modification, oxidation of methionine; variable modification, methionine; mass accuracy, 20 ppm. Charge states were set to a maximum of 7+. Filtered spectra were manually inspected for cross-linked dipeptides using the pLink2 visualization software pLabel. The filtering of manually validated cross-links was performed using the software CroCo¹⁷⁴. Cross-links were visualized in network plots using xVis¹⁸².

Database search using MaxQuant. The search engine MaxQuant¹⁷⁷ was used for protein identification and quantification. Raw data was searched against amino acid sequences of proteins of Syntaxin-1A (Uniprot Q16623), p40^{phox}, MSP1E3D1 and contaminations. Standard search parameters included: trypsin/P as a protease (trypsin cleavage C-terminal of lysine or arginine, also when C-terminal amino acid is proline); fixed modification, carbamidomethyl (cysteine); variable modifications, oxidation (methionine) and acetylation (protein N-terminus); missed trypsin cleavage sites, 2; minimal peptide length, 7; and maximal peptide mass 6,000 Da. The Orbitrap was specified as the instrument used.

4 Results

4.1 Establishing liposomes for MS analysis of membrane-associated proteins¹

4.1.1 Preparation and characterization of liposomes

Liposomes are phospholipid vesicles that resemble biological membranes. Due to their variability in size, composition, and amphiphilic character, they are suitable membrane mimetics for a variety of membrane proteins. Although liposomes are considered the simplest artificial membrane system, a sophisticated application for MS analysis of membrane proteins is still missing. In this work, liposomes were explored for the mass spectrometric analysis of membrane-associated proteins to allow their analysis in a native-like lipid environment.

To establish an MS-based workflow liposomes without associated proteins were first prepared and characterized. For this, lipids of natural membranes were selected (**Figure 11A**). These lipids contain head groups of different sizes and charges as well as fatty acyl chains with the same number of carbon atoms (18 carbon atoms). In addition, they are unsaturated, including one double bond. The workflow for liposome preparation, characterization and analysis is shown in **Figure 11B**. The following considerations were taken into account: (i) buffer conditions, (ii) DLS and (iii) MS analysis.

- (i) For liposome preparation, an MS-compatible buffer, such as ammonium acetate (AmAc) solution, is chosen. AmAc solution is preferred in MS analysis, as it is a volatile electrolyte which allows to preserve non-covalent interactions and the native structure of proteins as well as their complexes in the gas phase¹⁹³. In this thesis, liposomes, if not specified differently, are directly prepared in 200 mM AmAc solution for MS analysis (**Figure 11B, i**).
- (ii) Prior to MS analysis, all liposomes are characterized by DLS to determine their size distributions and homogeneities (see **Section 3.2.3.5** for details). In the DLS graphs, the particle diameter is plotted to the weighted intensity (**Figure 11B, ii**). The diameter is then indicative of the size of the liposomes.
- (iii) Following DLS analysis, liposomes are subsequently investigated by MS (**Figure 11B, iii**). For this, two different mass spectrometers are employed: first, a conventional Q Exactive mass spectrometer, which is typically utilized for the identification of lipids and peptides

¹ The results presented in this chapter were published in **Frick M**, Schwieger C, Schmidt C. Liposomes as Carriers of Membrane-Associated Proteins and Peptides for Mass Spectrometric Analysis. *Angew Chem Int Ed Engl.* 2021;60(20):11523-11530. doi:10.1002/anie.202101242

(see **Section 1.8.1** for details). The conditions in this mass spectrometer are rather harsh and non-covalent bonds are most likely not preserved. Gas phase conditions of this mass spectrometer are, therefore, considered to be denaturing. Second, a Q-ToF mass spectrometer (see **Section 1.8.2** for details), which was modified for the transfer of high-mass complexes so that non-covalent interactions are preserved in the gas phase, was employed. Accordingly, this mass spectrometer allows the analysis of intact protein complexes and their interactions with ligands, such as lipids. Gas phase conditions of this mass spectrometer are, therefore, considered to be native. By comparing denaturing and native gas phase conditions, liposome dissociation was investigated.

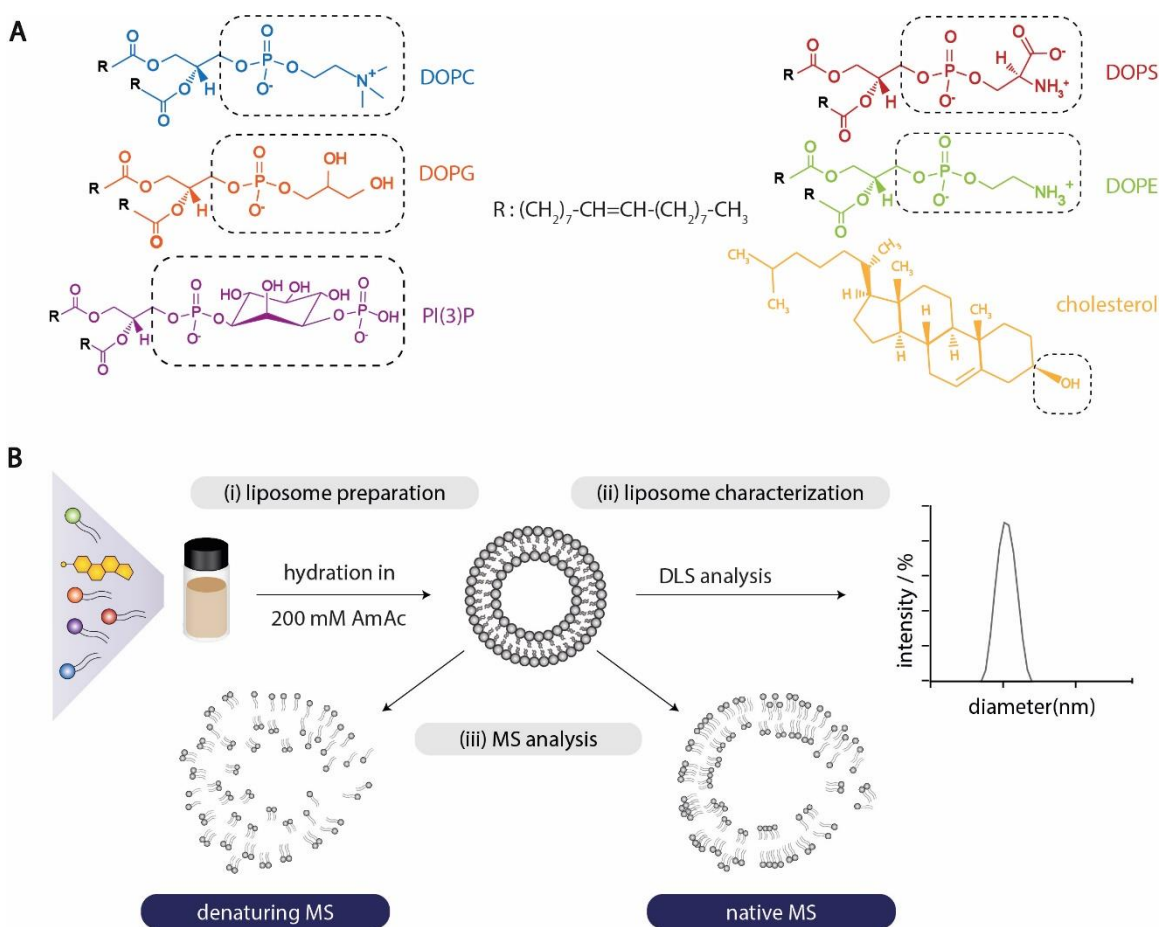


Figure 11: Workflow of liposome preparation, characterization and analysis. (A) Structures of lipids used in this thesis. The headgroups are labeled and lipids are highlighted with different colors: DOPC (blue), DOPG (orange), PI(3)P (purple), DOPS (red), DOPE (green) and cholesterol (yellow). Note that these colors will stay the same throughout this thesis. (B) Liposomes composed of different lipids were prepared in 200 mM AmAc solution (i) followed by DLS analysis to determine the mean size distribution and homogeneity of liposomes (ii). Liposomes were analyzed by MS under denaturing and native gas phase conditions (iii).

4.1.1.1 Characterization of single-component liposomes²

Single-component liposomes were first prepared and characterized (see **Section 3.2.3.1** for detailed information). By investigating liposomes containing only one lipid, the influence of individual lipids on the size and homogeneity of liposomes was explored. For this, liposomes were prepared containing either DOPC, DOPG, DOPS or DOPE lipids at a final concentration of 0.5 mM and subsequently extruded through a polycarbonate membrane of 100 nm. Note that, previous studies employing small-angle neutron scattering and TEM revealed that a mixture of liposomes of various lamellarities is often obtained after extrusion¹⁹⁴. However, we could previously show that lamellarity does not influence the dissociation behavior of liposomes in the gas phase of a mass spectrometer¹⁷². For subsequent MS analyses, we, therefore, did not investigate liposome lamillarity further in this thesis.

After preparation of single-component liposomes, homogeneity and diameter of the liposomes were inspected by DLS revealing a homogeneous size distribution with a mean diameter of approximately 68 nm for DOPC or DOPG liposomes (**Figure 12A&B**). DOPS liposomes were also found to be homogeneous with a mean diameter of approximately 79 nm (**Figure 12C**). DOPE liposomes, however, did not demonstrate a homogeneous size distribution (**Figure 12D**). Instead, larger and smaller size distributions were observed. Previous studies showed that DOPE lipids, which have a smaller head group than DOPC, DOPG and DOPS lipids exhibit different behavior in membranes^{195,196}. Accordingly, DOPE liposomes do not form phospholipid bilayers in aqueous solutions and rather adopt a more energetically favorable hexagonal structure. Hydrophobic interactions, stabilizing the phospholipid bilayer are, therefore, limited¹⁹⁷. To study this effect further, DOPE liposomes were prepared and their diameters were monitored by DLS immediately after preparation ($t = 0$) and after 5, 24, 28, 48 and 78 hours. The resulting size distributions were compared. Interestingly, DOPE liposomes size distributions change over time. (**Figure 12E**). Compared to the starting point of analysis ($t=0$), broader size distributions and larger aggregates were observed after 5 h and 24 h (**Figure 12E, $t = 5$ h, 24 h**). Smaller size distributions (<10 nm) were detected after 28 h, 48 h and 78 h, emphasizing the unstable nature of DOPE liposomes (**Figure 12E, $t=28$ h, 48 h, 78 h**). For comparison, DOPC liposomes were also analyzed by DLS at different time points (0 h, 5 h, 24 h, 28 h, 48 h, 78 h). Importantly, DOPC liposomes are homogeneous and do not show time-dependent changes in size (**Figure 12F**). In summary, single-component liposomes containing DOPC, DOPG or DOPS lipids form stable, homogeneous liposomes, while DOPE liposomes were not sufficiently stabilized due to their head group structure.

² DLS analyses of longer time periods of DOPE and DOPC liposomes were carried out together with Danny Knobloch-Sperlich as part of his bachelor thesis.

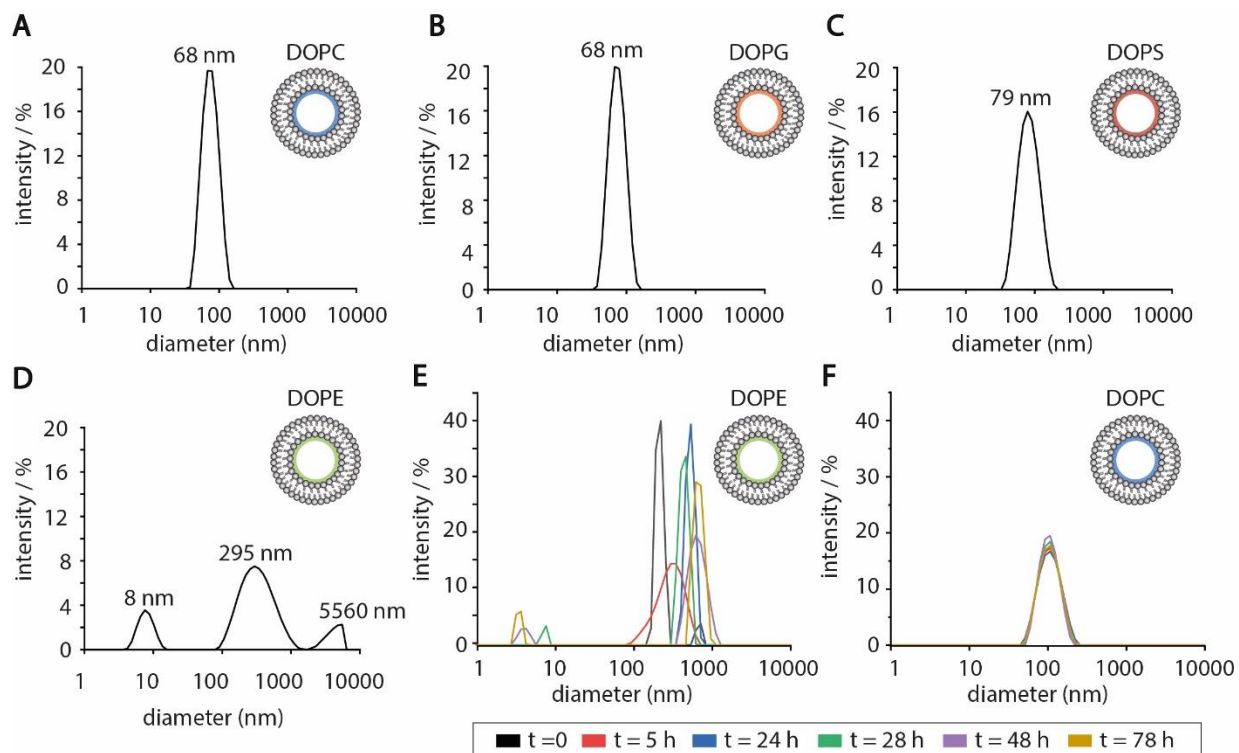


Figure 12: DLS analysis of single-component liposomes. DLS spectra show the mean size values for each peak. Liposomes were prepared at a concentration of 0.5 mM and extruded through polycarbonate membranes of 100 nm. DLS analysis of (A) DOPC liposomes, (B) DOPG liposomes, (C) DOPS liposomes reveal homogeneous size distributions. (D) Multiple size distributions were observed for DOPE liposomes. (E) Time-dependent DLS analysis of DOPE liposomes. (F) Size distributions of DOPC liposomes at different time points. See figure legend for time points.

4.1.1.2 Characterization of multi-component liposomes

Next, liposomes with natural and more complex membrane compositions resembling a eukaryotic plasma membrane¹⁹ were investigated. For this, liposomes containing DOPC, DOPE and DOPS at a molar ratio of 5:2:2 were prepared and characterized by DLS. As cholesterol is a typical component of natural membranes affecting fluidity, elasticity, permeability and curvature of membranes¹⁹⁸, multi-component liposomes of the same composition containing cholesterol were also explored. DLS analysis of liposomes containing DOPC, DOPE and DOPS at a molar ratio of 5:2:2 revealed a homogeneous size distribution with a mean diameter of approximately 105 nm (**Figure 13A**). This is comparable to the DLS analysis of liposomes containing cholesterol (**Figure 13B**). DLS analysis, therefore, verified that DOPE lipids do not influence the stability of multi-component liposomes as observed for single-component DOPE liposomes. Moreover, DLS analysis also revealed that cholesterol does not influence the diameter and homogeneity of liposomes. In conclusion, complex liposome compositions, also allow the formation of stable and monodisperse vesicles.

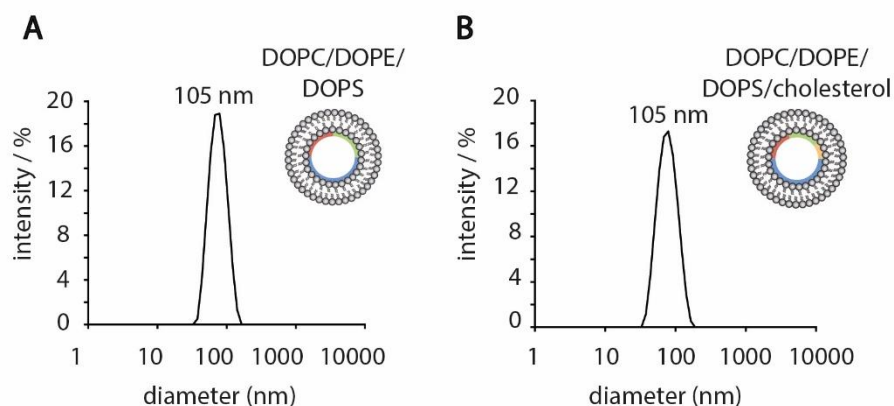


Figure 13: DLS analysis of multi-component liposomes. DLS spectra show the mean size values for each peak. Liposomes were prepared at a concentration of 0.5 mM and extruded through a polycarbonate membrane of 100 nm. **(A)** Liposomes containing DOPC, DOPE and DOPS (molar ratio 5:2:2) revealed a homogeneous size distribution. **(B)** Likewise, liposomes containing DOPC, DOPE, DOPS and cholesterol (5:2:2:1) showed a homogenous size distribution at a mean diameter of approximately 105 nm diameter.

4.1.2 MS analysis of liposomes

4.1.2.1 MS analysis of single-component liposomes

In the next step, to verify the application of liposomes for the analysis of membrane-associated proteins by MS, liposome dissociation was explored in the gas phase under denaturing and native gas phase conditions. Again, single-component liposomes were first analyzed. After their injection into the Q Exactive mass spectrometer, dissociation of liposomes was observed under denaturing gas phase conditions. The mass spectra showed similar dissociation patterns for liposomes composed of DOPC, DOPG, DOPS and DOPE lipids (**Figure 14A**). Namely, singly-charged monomers of DOPC (m/z 786.60), DOPG (m/z 775.55), DOPS (m/z 788.54) and DOPE (m/z 744.55) were observed with the highest signal intensities in these mass spectra. Singly-charged dimers were also observed, albeit at lower intensities. The mass spectrum of DOPC liposomes revealed lipid clusters consisting of up to 12 lipid molecules carrying different numbers of charges (**Figure 14A, i**). Interestingly, DOPG liposomes dissociate into smaller lipid clusters containing up to eight lipid molecules and exhibiting additional ammonium adducts (**Figure 14A, ii**). Ammonium adducts are known to be products of the ionization process when samples for MS analysis are analyzed in AmAc solution^{193,199}. DOPS liposomes dissociate comparable to DOPC liposomes into large lipid clusters of up to 16 lipid molecules, carrying different numbers of charges (**Figure 14A, iii**). For DOPE liposomes, lipid clusters with up to 15 lipid molecules were identified (**Figure 14A, iv**).

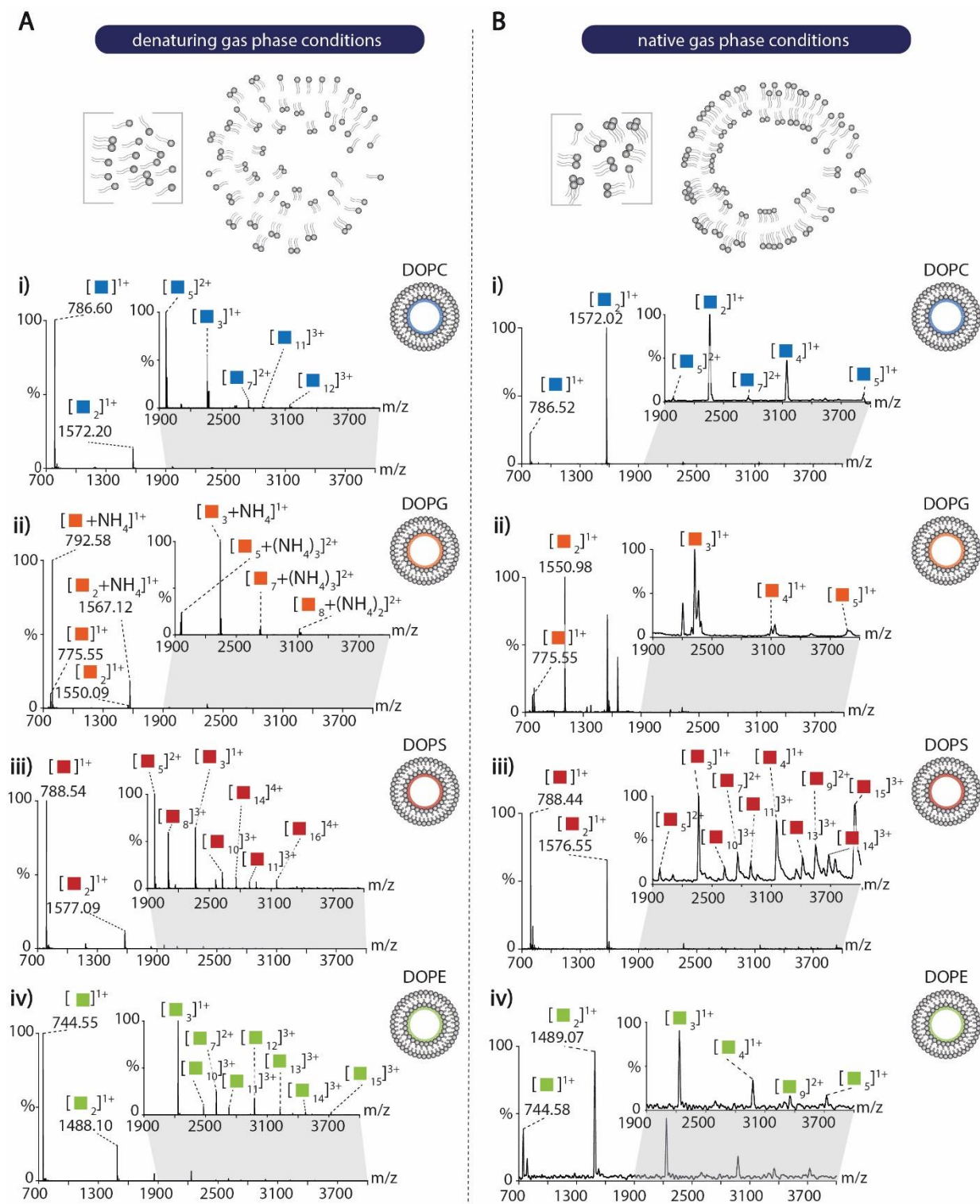


Figure 14: MS analysis of single-component liposomes. Liposomes composed of different lipids are highlighted: DOPC (blue), DOPG (orange), DOPS (red), DOPE (green). (A) Dissociation of liposomes under denaturing gas phase conditions. (i) DOPC, (ii) DOPG, (iii) DOPS, (iv) DOPE liposomes. See **Supplementary Table S1 and Table S2** for m/z values. (B) Native MS spectra of liposomes acquired at collisional voltages of 100 V. (i) DOPC, (ii) DOPG, (iii) DOPS, (iv) DOPE liposomes. See **Supplementary Table S2** for m/z values.

Next, single-component liposomes were analyzed under native gas phase conditions (**Figure 14B**). For this, liposomes were injected into the Q-ToF mass spectrometer and analyzed at a collision voltage of 100 V to create conditions similar to those in the Q Exactive mass spectrometer used above. Under native gas phase conditions, high intense signals corresponding in mass to singly-charged dimers of DOPC (m/z 1572.72), DOPG (m/z 1550.98), DOPS (m/z 788.44) and DOPE (m/z 1489.07) were detected, suggesting that non-covalent interactions are maintained in the Q-ToF mass spectrometer. Larger singly-, doubly- and triply-charged lipid clusters containing up to 15 lipid molecules at lower intensities were also observed. Note that, in the mass spectrum of DOPS, the highest signal intensity is observed m/z 788.44 suggesting that DOPS liposomes are readily destabilized under native gas phase conditions (**Figure 14B, iii**). To conclude, these studies show that single-component liposomes are sufficiently dissociated into lipid clusters.

4.1.2.2 MS analysis of multi-component liposomes

Subsequently, liposomes containing a complex lipid composition resembling eukaryotic membranes¹⁹ were investigated by MS. For this, multi-component liposomes containing DOPC, DOPE and DOPS (molar ratio 5:2:2) or DOPC, DOPE, DOPS and cholesterol (molar ratio 5:2:2:1) were first analyzed under denaturing gas phase conditions. The mass spectra of liposomes without cholesterol (**Figure 15A**) and with cholesterol (**Figure 15B**) show intense signals at m/z 786.60 corresponding to singly-charged DOPC monomers, which is also the major component of these liposomes. Moreover, at lower intensities, signals for singly-charged DOPE monomers (m/z 744.55), singly-charged DOPC dimers (m/z 1530.15) and DOPE dimers (m/z 1488.10) as well as mixed lipid dimers, were detected. Interestingly, even though liposome preparations contained DOPS and cholesterol, these lipids were not observed under denaturing gas phase conditions.

For comparison, multi-component liposomes were analyzed under native gas phase conditions. The mass spectra of liposomes without (**Figure 15C**) and with (**Figure 15D**) cholesterol showed similar results with intense signals predominantly observed for singly-charged DOPC monomers (m/z 786.64), and dimers (m/z 1573.64). Again, at lower intensities, mixed lipid clusters of DOPC and DOPE were observed. DOPS and cholesterol were also not detected under native gas phase conditions.

As signals for DOPS lipids were not observed in any of the mass spectra of multi-component liposomes acquired under denaturing or under native gas phase conditions, we suggest that DOPS lipids possess a lower ionization efficiency compared to DOPC or DOPE lipids. Likewise, cholesterol was also not observed in the mass spectra of multi-component liposomes, suggesting that effective ionization of neutral lipid species in ESI-MS experiments is difficult. Nevertheless, these experiments show that multi-component liposomes containing different lipid species are dissociated under denaturing and native gas phase conditions.

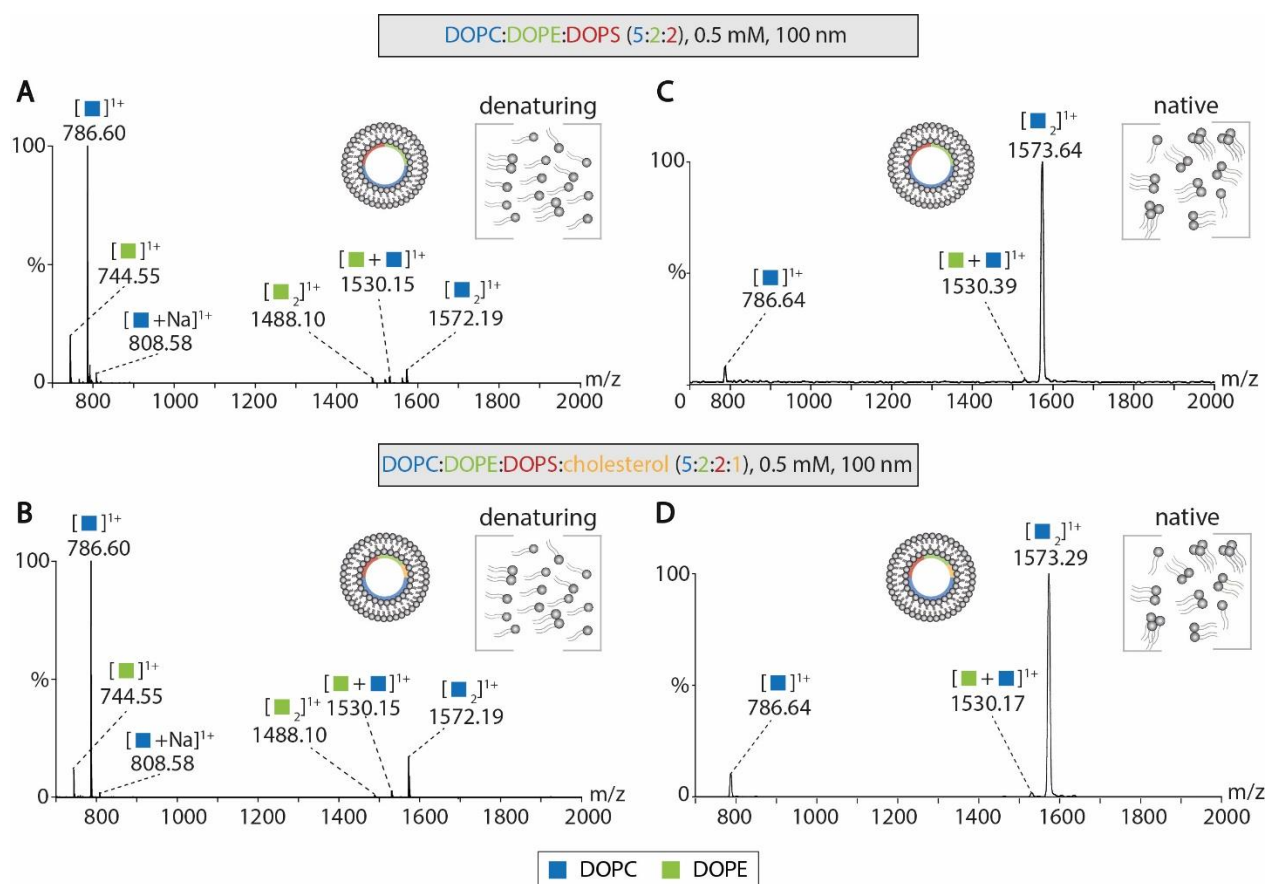


Figure 15: MS analysis of multi-component liposomes. See legend for color scheme. (A) Mass spectrum of DOPC, DOPE, DOPS (molar ratio: 5:2:2) acquired under denaturing gas phase conditions. (B) Denaturing MS of liposomes composed of DOPC, DOPE, DOPS and cholesterol (5:2:2:1) liposomes (C) Native MS of liposomes containing DOPC, DOPE and DOPS (molar ratio 5:2:2). (D) Mass spectrum of DOPC, DOPE, DOPS and cholesterol (5:2:2:1) liposomes analyzed under native gas phase conditions. Collisional voltage: 100 V. The mass spectra of liposomes with and without cholesterol acquired under denaturing and native gas phase conditions revealed DOPC and DOPE monomers and dimers as well as mixed lipid clusters.

4.1.3 Complementary investigation of liposomes by DLS and native MS

4.1.3.1 Analysis of multi-component liposomes with different sizes

Next, we aimed to obtain smaller lipid clusters for a sufficient analysis of proteins in the presence of lipids. Accordingly, liposomes differing in size and concentration were further investigated. In addition, different collisional energies were applied to monitor the dissociation of the lipid clusters. Note that, these experiments were exclusively carried out under native gas phase conditions applying a Q-ToF instrument as collisional energies can be adjusted.

To investigate whether the size of liposomes influences their homogeneity and dissociation in the gas phase, liposomes were extruded through different membrane pore sizes and analyzed by DLS and native MS. Native MS was applied, as For this, liposomes containing DOPC, DOPE and cholesterol (molar ratio: 5:2:2:1) were first prepared and extruded through membrane pore sizes of 50 nm, 200 nm, 400 nm and 800 nm followed by determination of their size distributions by DLS.

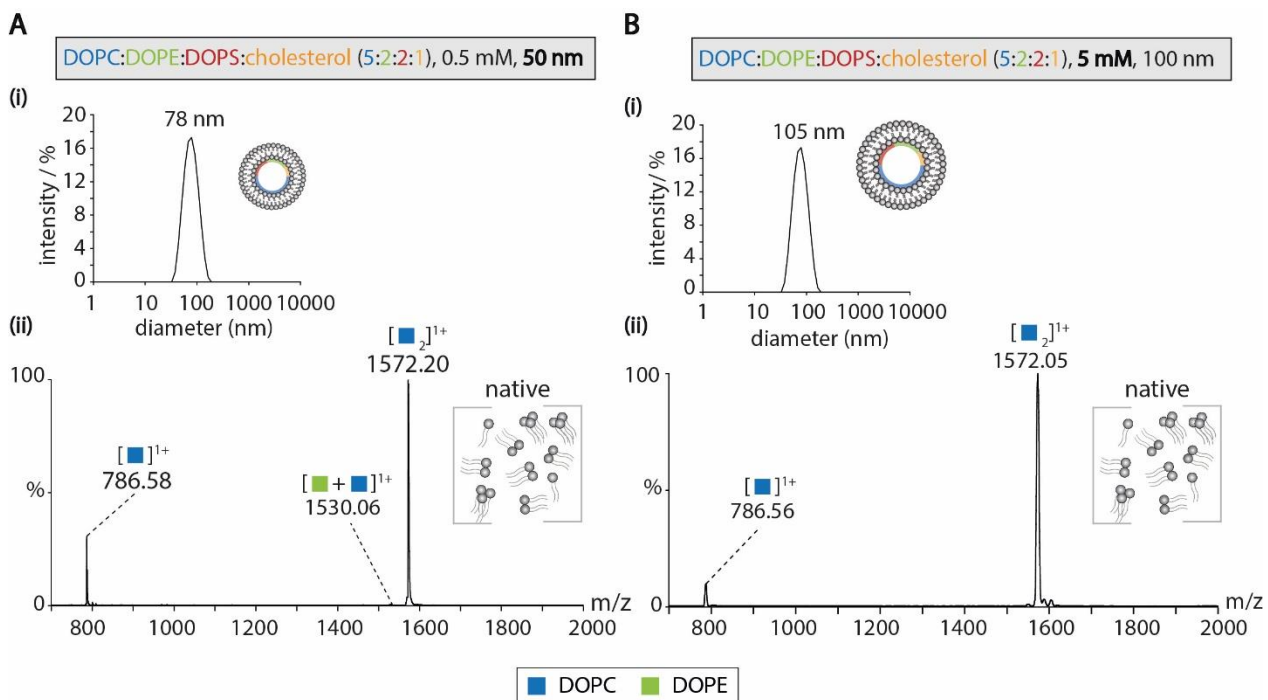


Figure 16: DLS and native MS analysis of multi-component liposomes differing in size and concentration. DLS spectra show the mean size values for each peak. See legend for color scheme. (A) Liposomes containing DOPC, DOPE, DOPS and cholesterol (molar ratio: 5:2:2:1) were prepared at a concentration of 0.5 mM and extruded through a polycarbonate membrane of 50 nm. (i) DLS analysis revealed a homogeneous size distribution. (ii) In the mass spectrum, singly-charged monomers of dimers of DOPC as well as clusters of DOPC and DOPE were assigned. (B) DOPC, DOPE, DOPS and cholesterol liposomes (molar ratio: 5:2:2:1) were prepared at a concentration of 5 mM and extruded through a polycarbonate membrane of 100 nm. (i) DLS analysis revealed a homogeneous size distribution. (ii) The native MS spectrum revealed singly-charged monomers and dimers of DOPC. Collisional voltage: 100 V.

Liposomes extruded through a membrane of 50 nm pore size revealed a homogeneous size distribution with a mean diameter of approximately 80 nm diameter (**Figure 16A, i**). Interestingly, liposomes extruded through membranes of 200 nm, 400 nm and 800 nm pore size showed much smaller size distributions than expected (**Supplementary Figure S1**).

These liposomes revealed mean size distributions of approximately 100 nm diameter, suggesting that a diameter of 100 nm represents an energetically favored state. Interestingly, liposomes (i.e. containing cholesterol at a molar ratio of 5:2:2:1) are monodisperse and the liposome diameter does not influence homogeneity.

Next, liposomes were analyzed by MS to explore whether the size of liposomes affects the formation and composition of lipid clusters in the gas phase. For this, multi-component liposomes were first extruded through a polycarbonate membrane of 50 nm pore size, followed by their analysis under native gas phase conditions (**Figure 16A, ii**). The mass spectrum is comparable to the previously shown mass spectrum of multi-component liposomes shown before (**Figure 15D**). Accordingly, intense peaks at m/z 1572.20 were observed, corresponding to singly-charged dimeric DOPC. Signals for singly-charged monomeric DOPC at approximately m/z 786.58 and signals for mixed lipid clusters of DOPC and DOPE were observed at lower intensities. The size of liposomes does, therefore, not influence the formation and composition of lipid clusters in the gas phase.

4.1.3.2 Analysis of multi-component liposomes with a higher concentration

Next, liposomes with a higher concentration were prepared to investigate whether the concentration of lipids affects homogeneity and the dissociation of the liposomes in the gas phase. For this, multi-component liposomes containing DOPC, DOPE, DOPS and cholesterol at a molar ratio of 5:2:2:1 and a concentration of 5 mM were first prepared and extruded through a polycarbonate membrane of 100 nm pore size, followed by DLS analysis. DLS analysis revealed a homogeneous size distribution with a mean diameter of 105 nm diameter (**Figure 16B, i**) confirming that liposome homogeneity is not affected by the lipid concentration.

Subsequently, the liposomes were analyzed under native gas phase conditions to determine whether the lipid concentration affects cluster formation in the gas phase. For this, liposomes were prepared at a concentration of 5 mM and explored by MS under native gas phase conditions. Again, these results are comparable to the mass spectrum of multi-component liposomes prepared at a concentration of 0.5 mM and extruded through polycarbonate membranes of 100 nm (**Figure 15D**). Accordingly, peaks of singly-charged monomers (m/z 786.56) and dimers (m/z 1572.05) of DOPC were shown (**Figure 16B, ii**). To conclude, MS analysis

confirms that liposomes dissociate under native gas phase conditions and cluster formation is independent of the lipid concentration.

4.1.3.3 MS analysis of multi-component liposomes analyzed at different collisional voltages

In a final step, liposome dissociation was monitored in the gas phase. For this, liposomes with cholesterol and without cholesterol were investigated at increasing collision voltages (20 V to 200 V) under native gas phase conditions. During MS analysis, collisional voltages were adjusted in the collision cell and mass spectra were recorded and compared (**Figure 17**).

As expected, the mass spectra showed that lower collision voltages result in mass spectra containing larger lipid clusters, whereas smaller lipid clusters were obtained with increasing collision voltages (**Figure 17A**). At a collision voltage of 100 V, signals were observed for singly-charged trimers and tetramers of DOPC. In the mass spectra of liposomes containing cholesterol additional lipid clusters were revealed corresponding to mixed clusters of DOPC and DOPE (**Figure 17B**).

To conclude, liposome dissociation in the gas phase under denaturing or native gas phase conditions is not influenced by their composition, size or concentration, suggesting that liposomes can indeed be valuable tools for the analysis of membrane proteins embedded into various membranes.

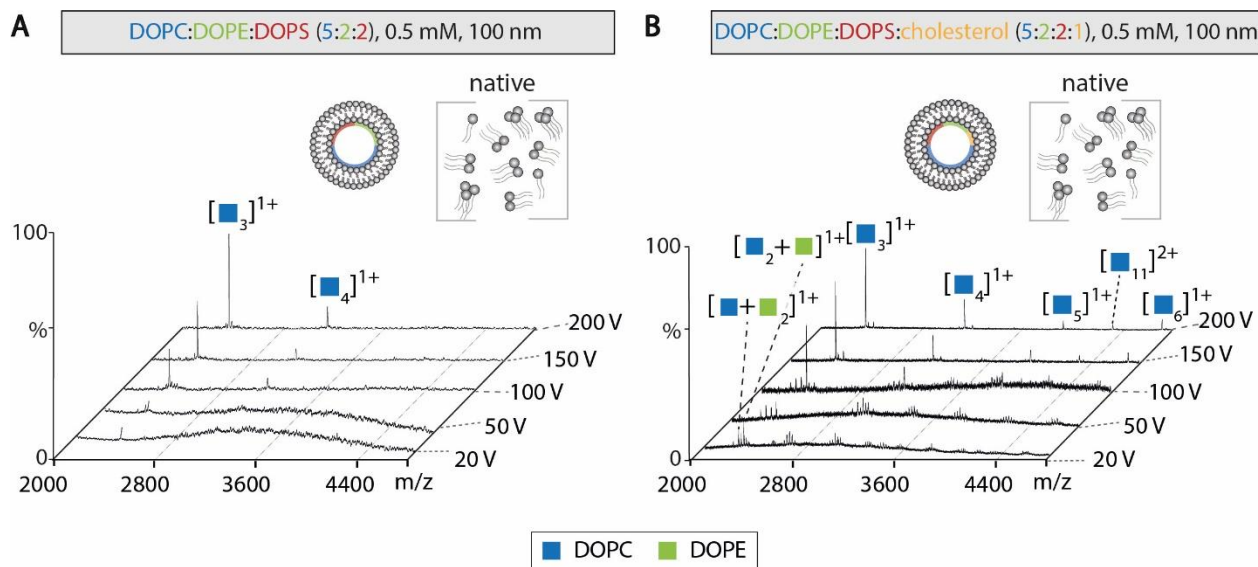


Figure 17: Native MS analysis of multi-component liposomes at increasing collisional voltages (20- 200 V). See legend for color scheme. **(A)** Mass spectra of liposomes containing DOPC, DOPE and DOPS (molar ratio 5:2:2) revealed clusters of DOPC at increasing collisional voltages. **(B)** Mass spectra of liposomes containing DOPC, DOPE, DOPS and cholesterol (molar ratio 5:2:2:1) at increasing collisional voltages. The mass spectra showed DOPC, and mixed lipid clusters composed of DOPC and DOPE.

4.2 Analysis of liposomes in the presence of soluble peptides/proteins

Next, the application of liposomes for the analysis of proteins was investigated. In nano-ESI experiments, the presence of more ionizable compounds or concentration differences often results in ion suppression, and low abundant signals or less ionizable species are buried in the baseline^{200,201}. As liposomes dissociate into high intense lipid clusters, the question remains whether lipids suppress peptide/protein signals in the gas phase. To investigate this, liposomes were, therefore, mixed with soluble peptides/proteins that do not interact with phospholipids or biological membranes in general. Peptides/proteins with different molecular weight (Angiotensin I 1 kDa, Ubiquitin 10 kDa, ConA 25 kDa) were used to analyze protein-liposome mixtures at different mass ranges. Peptide/protein-mixtures were subjected to MS analysis under denaturing and native gas phase conditions employing a Q Exactive and Q-ToF mass spectrometer. The resulting mass spectra were inspected for peptide/protein signals to verify whether proteins and lipids can be analyzed simultaneously in the same mass spectrum.

4.2.1 MS Analysis of soluble peptides/proteins

Initially, the different model peptides/proteins (Angiotensin I, Ubiquitin, and ConA) without liposomes were analyzed by MS under denaturing and native gas phase conditions. Understanding how peptides/proteins ionize in the gas phase in the absence of liposomes is essential to compare these mass spectra with the mass spectra of protein/peptide-liposomes mixtures.

Angiotensin I plays a key role in the renin-angiotensin-aldosterone system and is responsible for maintaining blood pressure and water balance in the body^{202,203}. Angiotensin I is a small peptide of 1.3 kDa and was initially used for MS analyses as it has a similar molecular weight compared to the lipids in this study. Under denaturing gas phase conditions (**Figure 18A**), peaks at m/z 648.85 and m/z 1296.68, corresponding to doubly-charged and singly-charged monomeric Angiotensin I, were observed. Under native gas phase conditions, the most intense signal was detected at m/z 1296.72, corresponding to singly-charged monomeric Angiotensin I (**Figure 18B**). The doubly-charged monomer of Angiotensin I was also observed (m/z 648.86). By comparing the mass spectra under denaturing and native gas phase conditions, it was shown that the 2+- charge state of Angiotensin I has a much higher intensity under denaturing gas phase conditions. The mass spectrum under native gas phase conditions, however, reveals that the 1+-charge state of Angiotensin I has a much higher intensity compared to denaturing gas phase conditions.

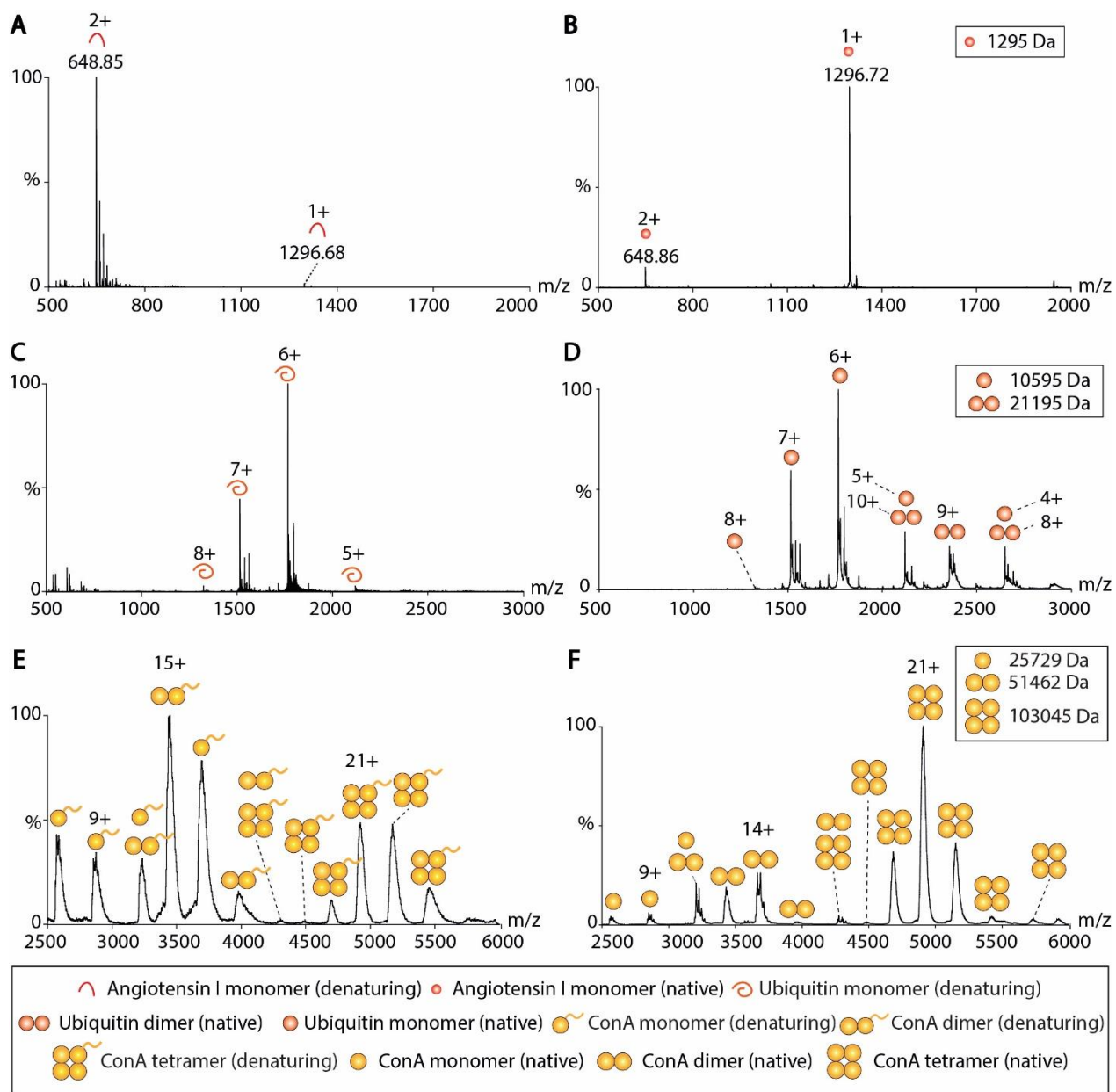


Figure 18: MS analysis of soluble peptides/proteins. See figure legend for colors and symbols. **(A)** The mass spectrum of Angiotensin I obtained under denaturing gas phase conditions revealed signals for monomeric Angiotensin I. **(B)** Native MS analysis of Angiotensin I showed signals for monomeric Angiotensin I. Collisional voltage: 50 V. **(C)** Ubiquitin analyzed under denaturing gas phase conditions. Charge state series corresponding to monomeric (5+ to 8+) Ubiquitin were assigned. **(D)** Native MS analysis revealed charge state series corresponding to monomeric (4+ to 8+) and dimeric (8+ to 10+) Ubiquitin. Collisional voltage: 50 V. **(E)** Mass spectrum of ConA acquired under denaturing gas phase conditions. Charge state distributions for monomeric, dimeric and tetrameric ConA were assigned. **(F)** Native MS analysis of ConA showed charge state series for monomeric, dimeric and tetrameric ConA. Collisional voltage: 50 V.

As non-covalent bonds are most likely not preserved due to the harsh conditions of the Q Exactive mass spectrometer, Angiotensin I is presumably unfolded under denaturing gas phase conditions and, therefore, contains more sites accessible for protonation. Therefore, a higher charge state is detected in this mass spectrum. In contrast, as the mass spectrum obtained under native gas phase conditions reveals a lower charge state for Angiotensin I indicating that fewer protonation sites are available. Accordingly, we suggest that non-covalent bonds are preserved in the Q-ToF mass spectrometer and the protein remains folded.

Ubiquitin is a small protein with a molecular weight of approximately 10 kDa and functions in targeting proteins for degradation by the proteasome^{204,205}. It further plays a key role in transcription and translation processes as well as signal transduction and DNA repair²⁰⁶. Ubiquitin was chosen as a model protein because it has a slightly larger molecular weight than Angiotensin I (**see above**). Ubiquitin was first inspected under denaturing gas phase conditions revealing charge states of 5+ to 8+ corresponding to monomeric Ubiquitin (**Figure 18C**). The mass spectrum of Ubiquitin obtained under native gas phase conditions revealed charge state series from 4+ to 8+ and 8+ to 10+ corresponding to monomeric and dimeric Ubiquitin (**Figure 18D**).

By comparing the mass spectra of Ubiquitin under denaturing and native gas phase conditions, similar charge states for monomeric Ubiquitin were obtained suggesting that the harsh conditions of the Q Exactive mass spectrometer do not lead to protein unfolding. This agrees with previous studies showing that the native structure and conformation of Ubiquitin are maintained under certain ESI-MS conditions⁹⁰. Importantly, Ubiquitin oligomers are detected under native gas phase conditions, suggesting that non-covalent bonds that stabilize dimeric Ubiquitin are only preserved in the gas phase of the Q-ToF mass spectrometer.

ConA binds mannose residues of various glycoproteins and activates lymphocytes²⁰⁷. It was used as a model protein in this thesis as it has a molecular weight of approximately 25 kDa and forms pH- and temperature-dependent oligomers in solution^{208,209}. Previous studies showed that, at a pH > 7, ConA is found predominantly as a tetramer, while at a pH of 5.5 ConA exists as a dimer^{208,210}. MS analysis of ConA under denaturing (**Figure 18E**) and native gas phase conditions (**Figure 18F**) revealed similar charge state distributions for monomeric, dimeric and tetrameric ConA. However, as the charge states differ we, therefore, assume that ConA is slightly unfolded under denaturing gas phase conditions. The 15+-charge state of the dimeric complex has the highest signal intensity under denaturing conditions, suggesting that the ConA dimer is the most stable conformation. This is consistent with previous studies showing that dimeric ConA is the most commonly observed conformation in nano-ESI experiments²¹¹. The fact that non-covalent interactions were preserved during denaturing MS analysis is surprising.

However, similar effects were also observed for peptides in a previous study supporting the observation that protein interactions, at least partially, are preserved under denaturing gas phase conditions when using a Q Exactive mass spectrometer²¹¹. In contrast, the charge states (18+ to 24+) of the tetrameric ConA exhibit the highest signal intensities under native gas phase conditions, suggesting that non-covalent interactions stabilizing the ConA tetramer are predominantly preserved under these conditions. The signal intensities of the oligomeric states observed under denaturing and native gas phase conditions, therefore, confirm that the environment of the Q Exactive mass spectrometer is harsher than that of the Q-ToF mass spectrometer.

In summary, Angiotensin I, Ubiquitin and ConA can be analyzed under denaturing and native gas phase conditions. The different charge state distributions reflect the solution conformations of the proteins and represent their stability. Accordingly, the higher charge states observed under denaturing gas phase conditions indicate unfolding of the proteins, while lower charges and oligomeric states observed under native gas phase conditions suggest a more folded conformation.

4.2.2 MS analysis of peptides/proteins mixed with liposomes

In the next step, peptide/protein-liposome mixtures were explored to investigate whether peptides/proteins can be analyzed by MS in the presence of lipids. For this, liposomes containing DOPC, DOPE, DOPS and cholesterol (molar ratio 5:2:2:1) were prepared as described (**Section 4.1.1.2**). Subsequently, liposomes were mixed with Angiotensin I, Ubiquitin, or ConA followed by incubation at room temperature for 1 hour prior to MS analysis.

Angiotensin I-liposome mixtures were first analyzed under denaturing gas phase conditions (**Figure 19A**). The mass spectrum revealed that liposomes dissociate as described before (**Figure 15B**). Accordingly, the most abundant signal was observed at m/z 786.60 corresponding in mass to monomeric DOPC. A peak for monomeric DOPE at m/z 744.55 was also detected. In addition, singly-charged dimers containing DOPC and DOPE were observed, albeit at lower intensities. Most importantly, however, doubly-charged monomeric Angiotensin I was observed at m/z 648.84.

For comparison, Angiotensin I-liposome mixtures were analyzed under native gas phase conditions revealing lipid clusters with the most intense signals at m/z 1572.30, corresponding in mass to the DOPC dimer (**Figure 19B**). Singly-charged monomeric Angiotensin I was also detected, however, at a lower intensity compared to the lipids. Again, the mass spectrum acquired under denaturing gas phase conditions showed a higher charge state for monomeric Angiotensin I suggesting protein unfolding.

In contrast, the native MS spectrum revealed a 1+-charge state for Angiotensin I which again indicates a ore folded conformation. When comparing the mass spectra of Angiotensin I without and with liposomes only protein charge states with the highest signal intensities were observed in the presence of lipids suggesting that lower charge states are suppressed by intense lipid signals.

As the mass spectra of Angiotensin I revealed low intense protein signals, in the next step a protein with a higher molecular weight was investigated. For this, Ubiquitin-liposome mixtures were first analyzed under denaturing gas phase conditions revealing high-intense lipid signals for singly-charged dimeric DOPC as well as clusters containing DOPC and DOPE. A series of charge states ranging from 5+ to 8+ corresponding to monomeric Ubiquitin was also observed (**Figure 19C**). For comparison, Ubiquitin-liposome mixtures were analyzed under native gas phase conditions. Again, the most intense signals corresponding to singly-charged monomeric and dimeric DOPC were detected under these conditions.

Most importantly, under native gas phase conditions, charge states for monomeric Ubiquitin (4+ to 6+) were obtained (**Figure 19D**). Accordingly, the mass spectra under denaturing and native gas phase conditions showed similar charge states for monomeric Ubiquitin. Interestingly, however, the 5+-charge state has a higher signal intensity under native gas phase conditions, suggesting that the 6+-charge state is suppressed due to the high intense signal of the DOPC dimer. Compared to the mass spectra without liposomes, oligomeric states of Ubiquitin were not detected and proteins show much lower signal intensities, suggesting that low abundant protein signals are again suppressed due to high intense lipid signals.

Finally, the ConA tetramer was analyzed in the presence of liposomes by MS to investigate whether a large protein, which also forms oligomers can be analyzed in the presence of lipids. For this, ConA-liposome mixtures were first analyzed under denaturing gas phase conditions which showed high intense signals for singly-charged monomeric and dimeric DOPC (**Figure 19E**). In addition, singly-charged and higher-charged mixed lipid clusters were observed at lower intensities. Charge state series from 13+ to 15+ and 20+ to 22+ corresponding to dimeric and tetrameric ConA were also detected. For comparison, ConA-liposome mixtures were analyzed under native gas phase conditions (**Figure 19F**). High intense signals were observed for singly-charged DOPC dimers and mixed lipid clusters. Most importantly, charge state series from 12+ to 16+ and 18+ to 22+ corresponding to dimeric and tetrameric ConA were assigned.

The mass spectra under denaturing and native gas phase conditions, therefore, revealed similar charge states for dimeric and tetrameric ConA which is consistent with the ConA experiments described before (**Figure 18**). However, compared to the mass spectra without liposomes monomeric ConA was not detected under denaturing or native gas phase conditions suggesting that high lipid signals suppress the signals for monomeric ConA.

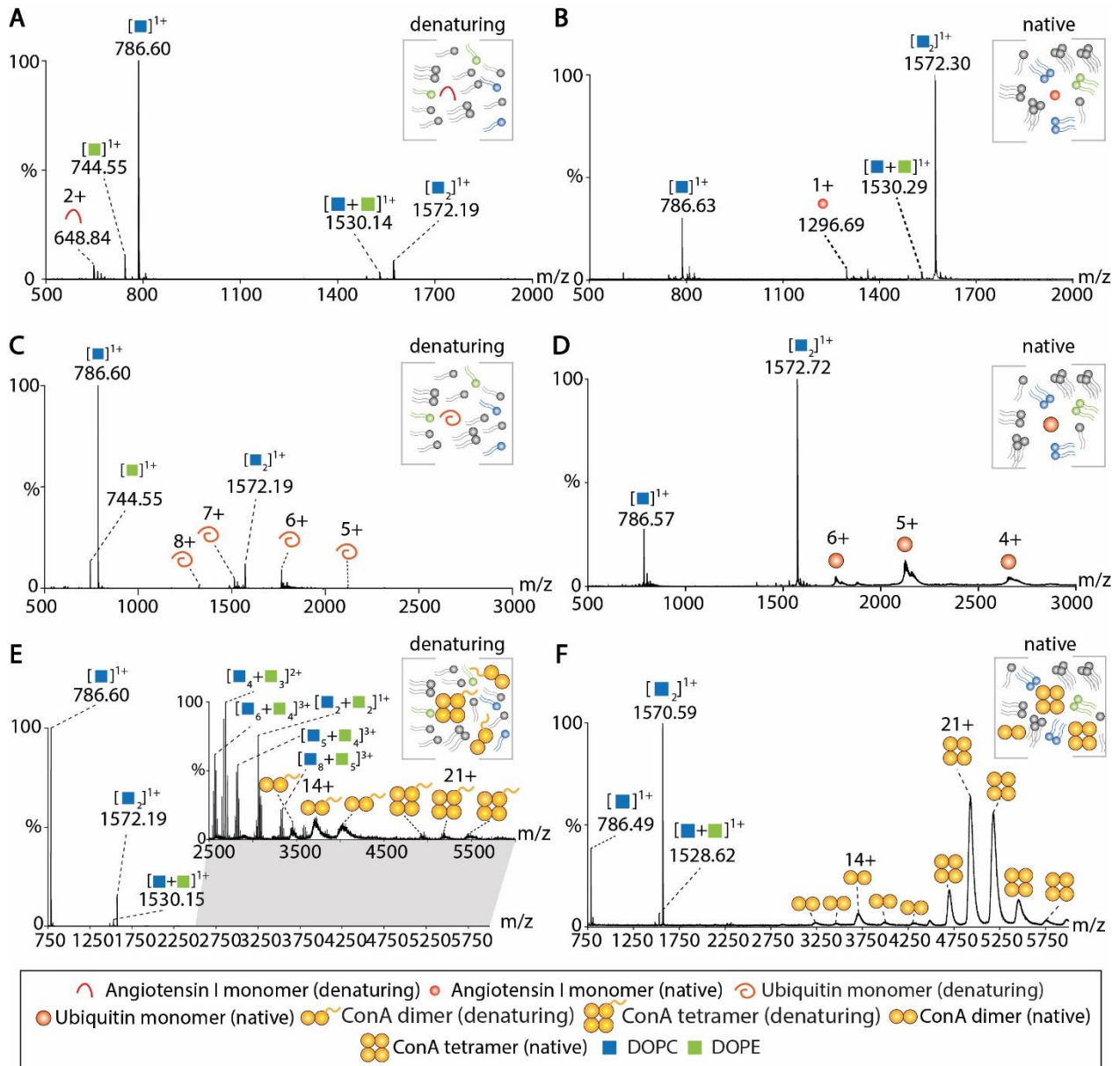


Figure 19: MS analysis of soluble peptides/proteins mixed with liposomes. Liposomes contained DOPC, DOPE, DOPS and cholesterol at a molar ratio of 5:2:2:1. See figure legend for color scheme and symbols. **(A)** Mass spectrum of Angiotensin I mixed with liposomes under denaturing gas phase conditions. Doubly-charged monomeric Angiotensin I, dimers of DOPC and mixed lipid clusters were assigned. **(B)** The native mass spectrum of Angiotensin I mixed with liposomes revealed singly-charged monomeric Angiotensin I, dimers of DOPC and mixed clusters containing DOPC and DOPE. Collisional voltage: 50 V. **(C)** MS analysis of Ubiquitin under denaturing gas phase conditions. DOPC and DOPE signals as well as charge state series for monomeric Ubiquitin were assigned. **(D)** Native MS of Ubiquitin-liposome mixtures revealed charge states of monomeric Ubiquitin as well as DOPC clusters. Collisional voltage: 50 V. **(E)** Denaturing MS of ConA mixed with liposomes. Charge states for dimeric and tetrameric ConA as well as signals for lipid clusters of DOPC and mixed clusters were detected. **(F)** ConA-liposome mixtures analyzed under native gas phase conditions. Charge states for dimeric and tetrameric ConA as well as signals for DOPC and mixed lipid clusters were assigned. Collisional voltage: 50 V.

Nevertheless, as dimeric and tetrameric ConA were detected, this indicates that large proteins and protein complexes can be analyzed in the presence of lipids.

In summary, these experiments highlight that peptides/proteins with different molecular weights are detectable under native and denaturing gas phase conditions in the presence of lipids. However, due to intense lipid signals, peptide/protein signals were comparably low in these mass spectra. Nevertheless, lipids and peptides/proteins are analyzed in the same mass spectrum and charge states are indicative of folded or unfolded conformations suggesting that protein-protein interactions can be at least partially maintained in the presence of lipids.

4.3 Analysis of peptides/proteins associated with liposomes

4.3.1 Preparation and characterization of proteoliposomes

To further assess liposomes as membrane mimetics for the mass spectrometric analysis of membrane proteins, proteins that associate with phospholipid membranes were investigated. The workflow of proteoliposome preparation, characterization and analysis is shown in **Figure 20**. Accordingly, liposomes are prepared (see **Section 3.2.3.2** for details) and incubated with the proteins of interest for 1h at room temperature (**Figure 20, i**). DLS analysis then confirms homogeneity and diameter of liposomes as well as proteoliposomes (**Figure 20, ii**). In addition, binding of the proteins is verified by flotation analysis, which is based on sucrose density ultracentrifugation (see **Section 3.2.3.6** for details) (**Figure 20, iii**). After ultracentrifugation, liposomes and associated proteins, due to their lower density, are expected to float on top of the sucrose gradient, while unbound protein remains at the bottom as evaluated by gel electrophoresis (**Figure 20, iv**). Subsequently, proteoliposomes are analyzed by MS under denaturing and native gas phase conditions utilizing a Q Exactive or Q-ToF mass spectrometer as described above (**Figure 20, v**).

During MS analysis, liposomes are assumed to dissociate in the gas phase of the mass spectrometer thereby releasing membrane-associated proteins and allowing their structural analysis in the presence of lipids. Under denaturing gas phase conditions liposome dissociation is assumed to be facilitated, while protein-lipid and protein-protein interactions are expected to be maintained under native gas phase conditions.

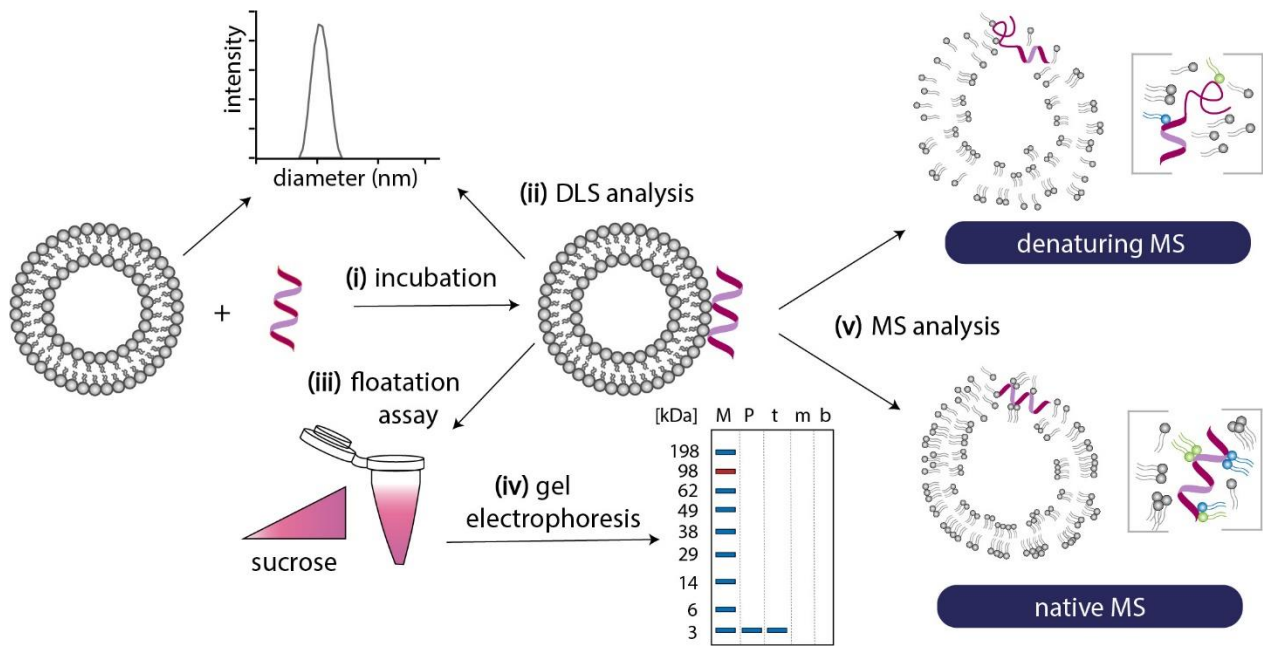


Figure 20: Workflow of proteoliposome preparation, characterization and analysis. (i) Preformed liposomes were incubated with proteins. (ii) Liposomes and proteoliposomes were analyzed by DLS to determine the mean size distribution. (iii) Liposomes and proteoliposomes were separated from unbound protein employing sucrose density flotation analysis. (iv) Top (t), middle (m), and bottom (b) fractions of the flotation analysis are evaluated by gel electrophoresis. (v) Liposomes and proteoliposomes are analyzed by MS under denaturing and native gas phase conditions.

4.3.2 Analysis of the p40^{phox} (1-144) protein domain associated with liposomes

In this thesis, the p40^{phox} (1-144) protein domain, here referred to as p40^{phox}, was first chosen as a model protein to investigate the application of liposomes to study membrane-associated proteins in the presence of lipids. P40^{phox} belongs to the human NADPH phagocyte oxidase and specifically interacts with PI(3)P-containing membranes^{212,213}. Previous studies showed that p40^{phox} only weakly associates with the phospholipid bilayer^{214,212}. We, therefore, assumed that p40^{phox} is readily released into the gas phase during liposome dissociation. Accordingly, p40^{phox} seems to be a well-suited target to study membrane proteins in their native-like lipid environment by MS.

4.3.2.1 Expression and purification of p40^{phox}

Before establishing p40^{phox}-proteoliposomes for MS analysis, p40^{phox} was first overexpressed and purified as described above (see **Sections 3.2.1.4 to 3.2.1.6** for details). After overexpression of the protein in *E.coli* cells, p40^{phox} was chromatographically purified following a protocol adapted from Chandra et al¹⁸⁵. In the first step, p40^{phox} was purified by GST-affinity chromatography.

The collected fractions were evaluated by gel electrophoresis and the GST-p40^{phox} fusion protein was observed at a molecular weight of 40 kDa (**Supplementary Figure S2A**). Next, the GST-tag was cleaved from the protein with thrombin during dialysis followed by reverse GST-affinity chromatography (**Supplementary Figure S2B**). The collected fractions contained cleaved p40^{phox} (MW 16 kDa), uncleaved p40^{phox} (MW 40 kDa) and the GST-tag (MW 26 kDa), suggesting insufficient thrombin cleavage or overloading of the column. In the final step, the protein was, therefore, subjected to SEC to allow further molecule separation based on the size. Gel electrophoresis after SEC purification revealed successful purification of p40^{phox} at a molecular weight of 16 kDa (**Supplementary Figure S2C**). Fractions containing the highest amount of purified p40^{phox} (fractions 22-25) were pooled and concentrated. Protein identification was performed by in-gel digestion and LC-MS/MS analysis. Raw data were searched against a human database using the MaxQuant software and p40^{phox} was identified with a sequence coverage of 100% (**Supplementary Table S3**).

4.3.2.2 Preparation and characterization of p40^{phox}-proteoliposomes

After purifying p40^{phox}, proteoliposomes were prepared to investigate p40^{phox} in a native-like lipid environment by MS. The protocol for p40^{phox} proteoliposome preparation was adapted from Chandra et al.²¹². For this, liposomes containing DOPC, DOPE and PI(3)P at a molar ratio of 8:1:1 were prepared as described. Liposomes containing DOPC and DOPE lipids at a molar ratio of 9:1 were prepared as a control. In both cases, liposomes were extruded through polycarbonate membranes of 100 nm pore size. Homogeneity and diameter of the liposomes were then verified by DLS analysis, showing that liposomes contained a homogeneous size distribution of approximately 100 nm diameter (**Supplementary Figure S3A**). As mentioned above, ammonium acetate is a volatile solution and allows in ESI-MS experiments to maintain non-covalent interactions in the gas phase^{118,119}. For MS analysis, p40^{phox} was, therefore, transferred to 200 mM AmAc solution prior to MS analysis. Subsequently, liposomes were incubated with p40^{phox} at protein-to-lipid ratios of 1:50 or 1:100. Flotation analysis was then performed to investigate whether p40^{phox} was bound to the liposomes.

However, gel electrophoresis showed, unexpectedly, that p40^{phox} was not observed in the top fractions (**Figure 21A**). Instead, p40^{phox} was detected in the bottom fractions of the sucrose gradient suggesting that 200 mM AmAc solution does not sufficiently stabilize the binding of p40^{phox} to PI(3)P-containing liposomes. As expected, p40^{phox} was observed in the bottom fractions of the control sample omitting PI(3)P lipids (**Figure 21A**). Additional optimization steps were, therefore, required to obtain sufficient association of p40^{phox} to liposomes.

To optimize p40^{phox} binding, buffer conditions during proteoliposome preparation were first adjusted. For this, liposomes containing DOPC, DOPE and PI(3)P at a molar ratio of 8:1:1 were prepared and incubated for 1 h with p40^{phox} solubilized in SEC buffer. Binding of p40^{phox} to liposomes was again investigated by flotation analysis. Compared to the experiments shown above, p40^{phox} was now observed in the top fractions of the sucrose gradient at protein-to-lipid ratios of 1:50 and 1:100 of liposomes containing PI(3)P lipids (**Figure 21B**). P40^{phox} did not associate with liposomes omitting PI(3)P and was, therefore, observed in the bottom fractions of the sucrose gradient. These results show that p40^{phox} is sufficiently stabilized in SEC buffer and is indeed able to associate with PI(3)P-containing membranes.

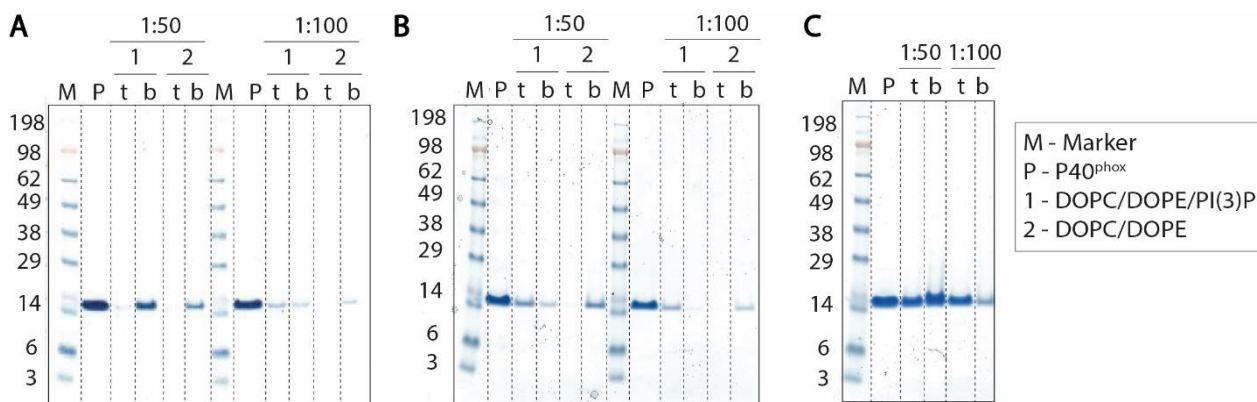


Figure 21: Flotation assay of p40^{phox}-proteoliposomes. Top (t) and bottom (b) fractions were evaluated by gel electrophoresis. Specific binding to PI(3)P-containing membranes was confirmed by comparing DOPC, DOPE and PI(3)P lipids (molar ratio 8:1:1) with DOPC and DOPE containing liposomes (molar ratio 9:1) prepared in 200 mM AmAc solution. Protein-to-lipid ratios of 1:50 and 1:100 were evaluated. **(A)** Gel electrophoresis of p40^{phox}-proteoliposomes prepared in 200 mM AmAc solution. P40^{phox} was observed in the bottom fractions of the sucrose gradient. **(B)** Gel electrophoresis of liposomes incubated with p40^{phox} solubilized in SEC buffer for 30 minutes. p40^{phox} was detected in the top fractions of the sucrose gradient of liposomes containing PI(3)P. **(C)** Gel electrophoresis of liposomes associated with p40^{phox}. Liposomes were incubated overnight with p40^{phox} solubilized in SEC buffer. P40^{phox} was predominantly observed in the top fractions of the sucrose gradient of liposomes containing PI(3)P, however, unbound p40^{phox} was also detected in the bottom fractions. Abbreviations: M (Marker), P (p40^{phox}).

Nevertheless, only a small amount of p40^{phox} binds to the liposomes, suggesting that p40^{phox} is only weakly associated with PI(3)P-containing membranes, which agrees with previous experiments¹⁸⁵. Therefore, in this thesis, additional experiments were performed next to optimize the binding of p40^{phox} to PI(3)P-containing membranes.

Next, p40^{phox} binding to liposomes was optimized by incubating proteoliposome mixtures overnight. For this, liposomes containing DOPC, DOPE and PI(3)P at a molar ratio of 8:1:1 were prepared as described before and subsequently incubated overnight with p40^{phox} at protein-to-lipid ratios of 1:50 and 1:100. Flotation analysis and gel electrophoresis demonstrated that high amounts of p40^{phox} bind to liposomes at protein-to-lipid ratios of 1:50 and 1:100 (**Figure 21C**), suggesting that a longer incubation time enhances protein association to liposomes.

Note that, employing both protein-to-lipid ratios, free protein is also detected in the bottom fractions. As p40^{phox} proteoliposome samples also contain free p40^{phox} we, therefore, assumed that only a certain amount of proteins was associated with PI(3)P-containing liposomes. As free p40^{phox} is present in the proteoliposome samples it is difficult to obtain accurate information on protein abundance, protein-protein and protein-lipid interactions of p40^{phox}-associated liposomes by MS analysis. Removal of free p40^{phox} is, therefore, required. For this, samples prepared at a molar ratio of 1:50 were further separated by SEC. Fractions were collected dropwise and visualized by gel electrophoresis. In the elution fractions 5 to 15, p40^{phox} (molecular weight 16 kDa) and associated lipids were detected (**Figure 22A**), showing that p40^{phox}-proteoliposomes were successfully separated from free p40^{phox} by SEC.

The protein concentration in the collected fractions was then determined by UV-Vis spectroscopy (**Figure 22B**). Fraction 15 contained the highest protein concentration. To verify that p40^{phox} is associated with the liposomes after SEC, a flotation analysis of fraction 15 was performed. Gel electrophoresis confirmed that a large proportion (approx. 95 %) of p40^{phox} was observed in the top fraction of the sucrose gradient (**Figure 22C**). DLS analysis of fraction 15 verified a homogeneous population and diameter of approximately 100 nm (**Figure 22D**). The mean size distribution of p40^{phox}-proteoliposomes was comparable to that observed for liposomes without protein (**Supplementary Figure S3A**).

In conclusion, these results indicate that p40^{phox} binding to liposomes is strongly dependent on the buffer composition and incubation time. Nevertheless, p40^{phox}-proteoliposomes could be prepared at high concentrations and are available for MS analysis.

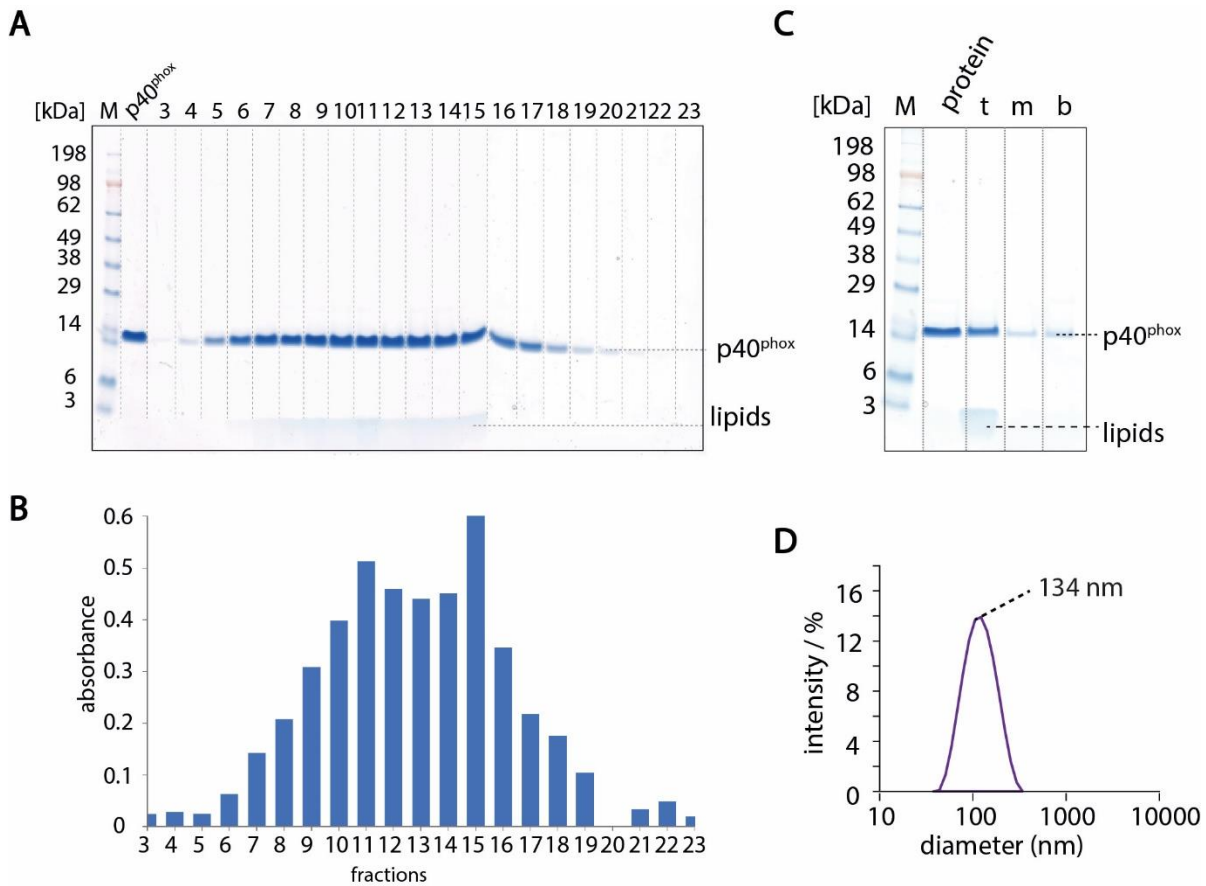


Figure 22: Preparation of p40^{phox}-proteoliposomes for MS analysis. Top (t), middle (m) and bottom (b) fractions of flotation analysis were evaluated by gel electrophoresis. Abbreviation: M (Marker) (A) Gel electrophoresis of SEC fractions 3 to 23 after buffer exchange. p40^{phox} was observed at approx. 16 kDa. The presence of lipids in these fractions confirmed the presence of liposomes. (B) The protein concentration of each SEC fraction was determined by UV-Vis spectroscopy. The absorbance of fractions 3 to 23 is plotted in a bar diagram. Fraction 15 shows the highest absorbance. (C) Flotation analysis of purified p40^{phox}-proteoliposomes. P40^{phox} was observed in the top fraction. (D) DLS analysis of p40^{phox}-proteoliposomes revealed a mean size distribution of approximately 100 nm diameter. The DLS spectrum shows the mean diameter value.

4.3.2.3 MS analysis of p40^{phox}

To compare the mass spectra of p40^{phox} with those of p40^{phox}-proteoliposomes, the protein was first analyzed without liposomes under denaturing and native gas phase conditions. For this, p40^{phox} was transferred into 200 mM AmAc solution (Section 3.2.4.4) and subsequently analyzed by MS under denaturing gas phase conditions. The mass spectrum revealed a charge state series from 6+ to 15+, corresponding to monomeric p40^{phox} (Figure 23A).

The native MS spectrum of p40^{phox} showed charge states from 5+ to 11+ of monomeric p40^{phox} (**Figure 23B**). Similar to the mass spectra of the soluble proteins (see above) we suggest that a higher charge state indicates a more folded conformation of the protein. As an extended charge state series was observed under denaturing gas phase conditions, we, accordingly, assume that non-covalent interactions of p40^{phox} are not maintained. In contrast, the lower charge states observed under native gas phase conditions indicate a more folded conformation of p40^{phox}. To conclude, p40^{phox} can be analyzed under denaturing and native gas phase conditions and non-covalent interactions are maintained by employing a modified Q-ToF mass spectrometer.

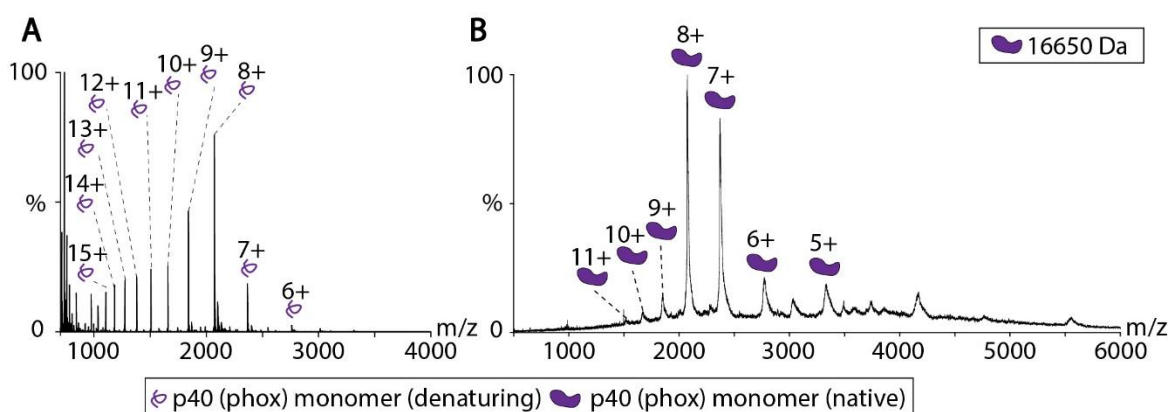


Figure 23: MS analysis of p40^{phox}. See legend for symbols. **(A)** Mass spectrum of p40^{phox} obtained under denaturing gas phase conditions. A charge state series from 6+ to 15+ corresponding to monomeric p40^{phox} was observed. **(B)** The mass spectrum of p40^{phox} obtained under native gas phase conditions. Collisional voltage: 50 V. Charge states from 5+ to 11+ were assigned to monomeric p40^{phox}.

4.3.2.4 MS analysis of p40^{phox}-proteoliposomes

Finally, p40^{phox}-proteoliposomes were analyzed by MS to investigate p40^{phox} in the presence of lipids. For this, p40^{phox}-proteoliposomes were prepared at a protein-to-lipid ratio of 1:50 as described above (**Section 4.3.2.2**). These proteoliposomes were then analyzed by MS under denaturing gas phase conditions (**Figure 24A**). Similar to the mass spectra of peptide/protein-liposome mixtures (see above), the denaturing mass spectrum showed high intense lipid signals for singly-charged monomeric and dimeric DOPC at m/z 786.60 and m/z 1572.19, respectively. In addition, doubly-charged lipid clusters of DOPC and DOPE as well as mixed clusters containing up to 6 lipid molecules were observed. Interestingly, signals for PI(3)P lipids were not detected. Notably, signals corresponding to the 8+ - and 9+-charge states of the p40^{phox} monomer (**compare Figure 23A**) were observed albeit at very low intensities. Protein-lipid interactions were not observed, which is most likely attributed to the weak interactions between p40^{phox} and PI(3)P lipids described in a previous study²¹².

The weak association of p40^{phox} with the membrane, therefore, suggests that p40^{phox}-PI(3)P interactions are lost during liposome dissociation. For comparison, p40^{phox}-proteoliposomes were also analyzed under native gas phase conditions (**Figure 24B**). Again, singly-charged dimeric DOPC at m/z 1573.72 was the highest signal observed in the mass spectrum. Singly-charged monomeric DOPC (m/z 786.60) and low intense lipid clusters with up to 6 lipids containing DOPC and DOPE were detected.

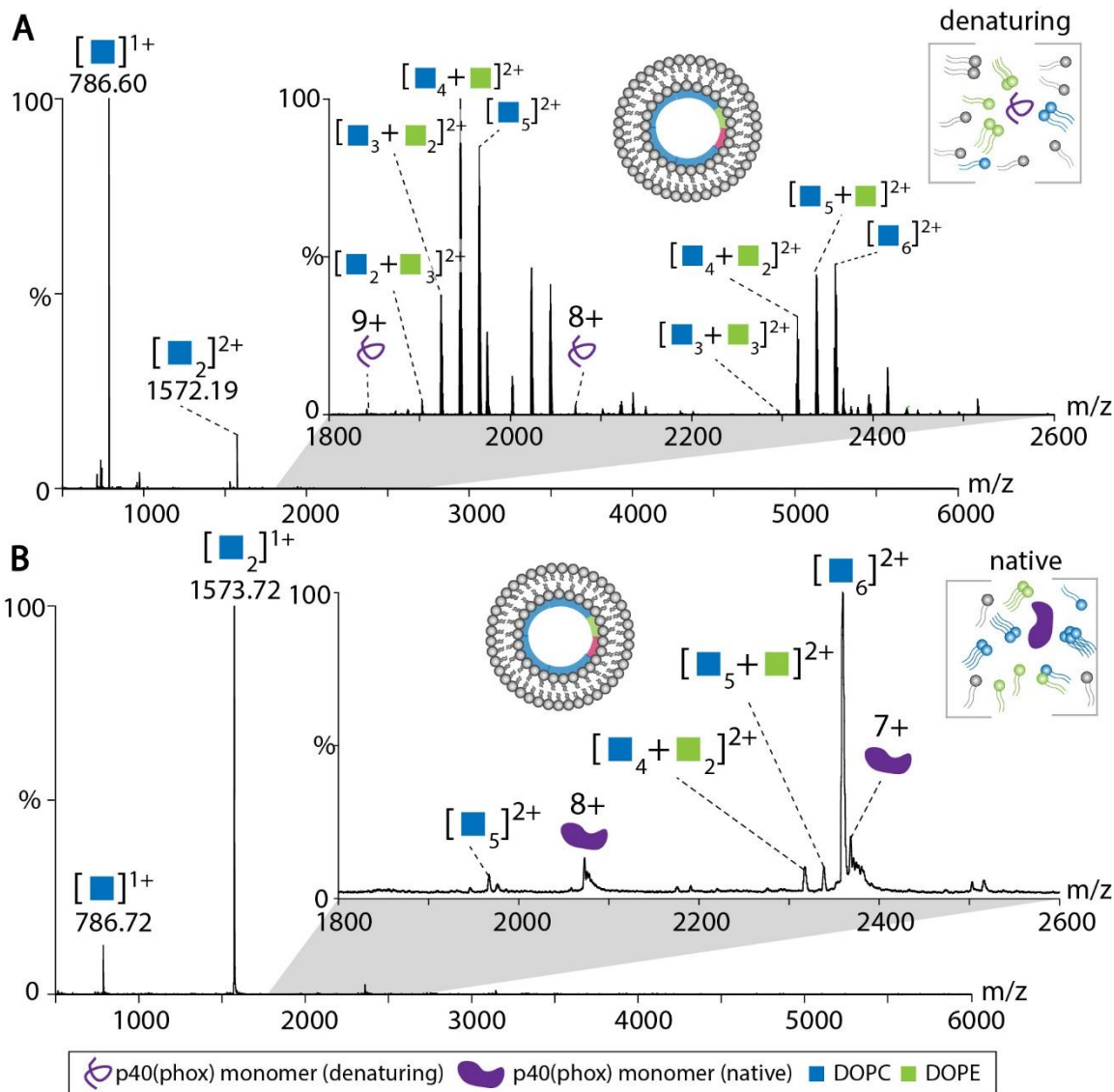


Figure 24: MS analysis of p40^{phox}-proteoliposomes. Liposomes composed of DOPC, DOPE, DOPS and PI(3)P at a molar ratio of 8:1:1. See figure legend for color scheme and symbols. **(A)** Mass spectrum of p40^{phox}-proteoliposomes obtained under denaturing gas phase conditions. DOPC and DOPE clusters as well as 8+ and 9+ charge states of monomeric p40^{phox} were assigned. See **Supplementary Table S4** for m/z values. **(B)** Native mass spectrum of p40^{phox}-proteoliposomes revealed signals for lipid clusters as well as charge states corresponding to monomeric p40^{phox}. Collisional voltage: 50 V. See **Supplementary Table S5** for m/z values.

Similar to the mass spectrum obtained under denaturing gas phase conditions (**compare Figure 24A**), PI(3)P was not observed. Importantly, the mass spectrum revealed signals for 7+ and 8+ charge states corresponding to monomeric p40^{phox} (**compare 23B**). Adduct peaks, most likely originating from insufficient desolvation of the protein during transfer into the gas phase were also observed in this mass spectrum. Protein-lipid interactions were not observed under native gas phase conditions, again suggesting that protein interactions are lost during the transfer from solution to the gas phase due to the weak binding of p40^{phox}.

In summary, these experiments show that p40^{phox} was successfully associated with liposomes. In addition, MS analysis revealed that p40^{phox} is released into the gas phase following liposome dissociation. The mass spectra of p40^{phox}-proteoliposomes showed that signals for p40^{phox} are comparably low suggesting that lipids are more efficiently ionized during electrospray ionization. Importantly, protein-lipid interactions were not observed in any of the acquired mass spectra, suggesting that during ionization in the gas phase, weak protein-lipid interactions are lost. Nevertheless, these experiments demonstrate that the structural analysis of proteins specifically bound to liposomes is possible.

4.3.3 Analysis of Melittin associated with liposomes

To further investigate the application of liposomes for the analysis of membrane-associated peptides/proteins Melittin was chosen as another model protein. Melittin is known to form oligomers upon association with phospholipid bilayers^{215–217} and has a molecular weight of 2.8 kDa which is comparable to the molecular weights of monomeric and dimeric lipids species. Moreover, its oligomeric mass is similar to the mass of p40^{phox} (**Section 4.3.2**). Liposomes resembling a eukaryotic and prokaryotic membrane composition were employed to study the structure of Melittin and Melittin-lipid interactions in different membrane environments.

4.3.3.1 Preparation and characterization of Melittin-proteoliposomes

To analyze the structure of Melittin in its natural lipid environment, Melittin binding to eukaryotic liposomes was first explored. The protocol for Melittin association with liposomes was adapted from Popplewell et al²¹⁸. Accordingly, liposomes containing DOPC, DOPE, DOPS and cholesterol (molar ratio of 5:2:2:1) were prepared in PBS buffer. DLS analysis of the liposomes revealed a homogenous size distribution of approximately 100 nm diameter (**Supplementary Figure S3B**).

Liposomes were then incubated with Melittin at protein-to-lipid ratios of 1:50, 1:100 or 1:1000. Melittin binding to the liposomes was verified by flotation on a sucrose gradient and evaluated by gel electrophoresis. Accordingly, Melittin was observed in the top fractions of the sucrose gradient at protein-to-lipid ratios of 1:50, 1:100 and 1:1000 (**Figure 25A**). As Melittin was not detected in the bottom fractions of the sucrose gradient, a tight association of Melittin with liposomes was assumed.

Interestingly, Melittin oligomers, which were not detected in the absence of liposomes were observed by gel electrophoresis and oligomeric states decreased with decreasing Melittin concentrations (**Figure 25A**). This agrees with previous studies²¹⁹, which proposed that Melittin oligomerization depends on the protein concentration. In summary, these experiments demonstrate that Melittin associates at different concentrations with liposomes resembling a eukaryotic membrane composition.

To achieve sufficient signals in the following MS experiments, proteoliposomes containing the highest Melittin concentration (protein-to-lipid ratio of 1:50) were prepared in 200 mM AmAc solution as described above. Subsequently, to investigate Melittin binding, Melittin-proteoliposomes were subjected to flotation analysis.

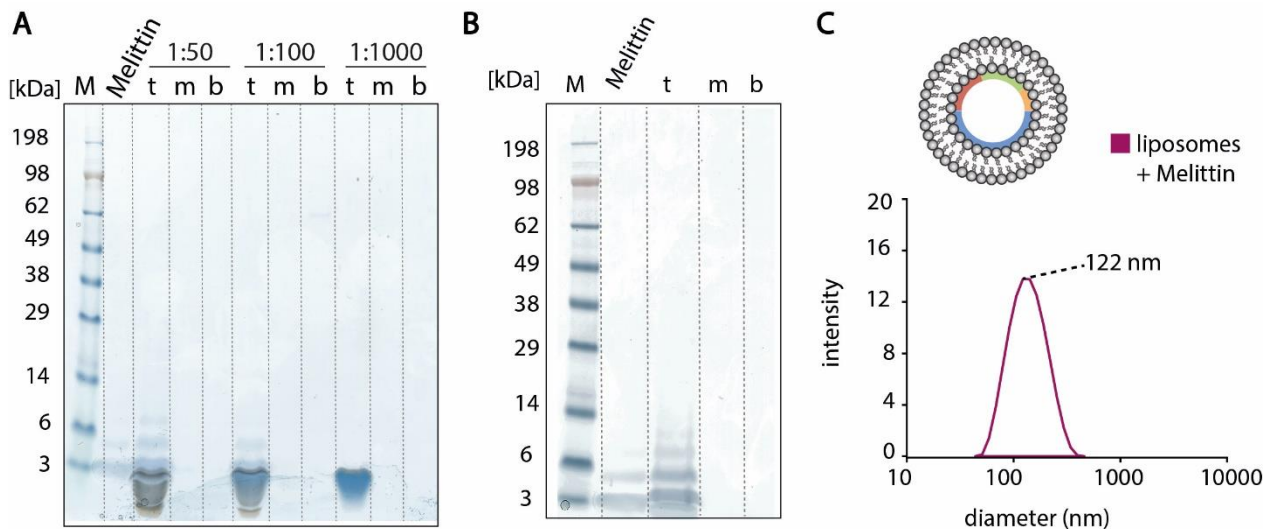


Figure 25: Flotation assay and DLS analysis of Melittin-proteoliposomes resembling a eukaryotic membrane composition. Liposomes were composed of DOPC, DOPE, DOPS and cholesterol (molar ratio: 5:2:2:1). Top (t), middle (m) and bottom (b) fractions were evaluated by gel electrophoresis. Abbreviation: M (Marker). (A) Gel electrophoresis of Melittin-proteoliposomes prepared in PBS buffer at protein-to-lipid ratios of 1:50, 1:100 and 1:1000 revealed the presence of Melittin in the top fractions of the sucrose gradient. (B) Gel electrophoresis of Melittin-proteoliposomes prepared in 200 mM AmAc solution at a protein-to-lipid ratio of 1:50. Melittin and its oligomers were detected in the top fraction of the sucrose gradient. (C) DLS analysis of Melittin-proteoliposomes showed a homogeneous size distribution at approximately 122 nm diameter. The DLS spectrum shows the mean size value.

Gel electrophoresis confirmed that Melittin associates with liposomes prepared in 200 mM AmAc solution (**Figure 25B**). Interestingly, compared to the Melittin-proteoliposomes inspected before, Melittin tetramers were observed, suggesting Melittin to be more stabilized in 200 mM AmAc solution.

Finally, diameter and homogeneity of Melittin-proteoliposomes were determined by DLS revealing a homogeneous size distribution at approximately 122 nm diameter (**Figure 25C**). Accordingly, the slightly larger size distribution compared to the size distributions of Melittin without liposomes (**Supplementary Figure S3B**) confirmed binding of Melittin, as protein association with the phospholipid bilayer presumably leads to an increase in liposome particle diameter. To conclude, homogeneous Melittin-proteoliposomes with a high concentration were established.

As Melittin plays a key role in the defense mechanism of honeybees against bacteria, additional studies were performed. Accordingly, Melittin-proteoliposomes resembling a prokaryotic membrane composition were prepared and the results were compared to Melittin-proteoliposomes resembling a eukaryotic membrane composition. For this, liposomes containing DOPE and DOPG at a molar ratio of 5:2 were prepared as described above in 200 mM AmAc solution (**Section 4.1.1**).

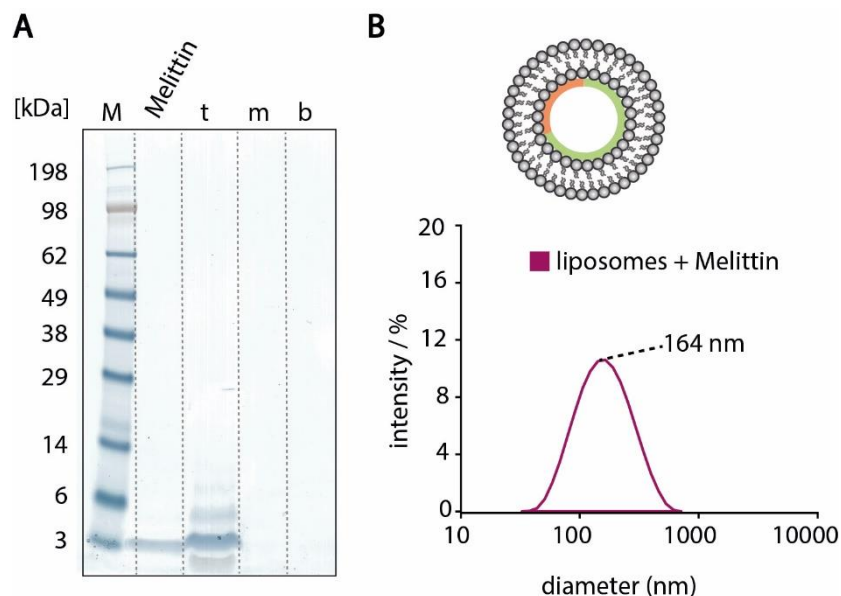


Figure 26: Flotation assay and DLS analysis of Melittin-proteoliposomes resembling a prokaryotic membrane composition. Liposomes were composed of DOPE and DOPG (molar ratio 5:2). Top (t), middle (m) and bottom (b) fractions were evaluated by gel electrophoresis. Abbreviation: M (Marker). **(A)** Gel electrophoresis of Melittin-proteoliposomes prepared in 200 mM AmAc solution at a protein-to-lipid ratio of 1:50 revealed the presence of Melittin in the top fraction. **(B)** DLS analysis of Melittin-proteoliposomes showed a homogenous size distribution of 164 nm diameter. The DLS spectrum reveals the mean size value.

DLS analysis of DOPE and DOPG liposomes revealed a homogenous diameter of approximately 100 nm (**Supplementary Figure S3C**). Subsequently, Melittin-proteoliposomes were prepared at a protein-to-lipid ratio of 1:50 and Melittin binding to liposomes was confirmed by flotation analysis and gel electrophoresis (**Figure 26A**). As expected, Melittin was only detected in the top fractions and not observed in the middle and bottom fractions of the sucrose gradient, suggesting that Melittin tightly binds to liposomes resembling a prokaryotic membrane composition.

Interestingly, Melittin-proteoliposomes showed less oligomeric states compared to Melittin-proteoliposomes resembling a eukaryotic liposome composition (**compare Figure 25B**). Notably, only Melittin oligomers up to trimers were detected by gel electrophoresis. Flotation analysis of Melittin-proteoliposomes composed of DOPG and DOPE, therefore, suggests that Melittin oligomers are not sufficiently stabilized. Nevertheless, DLS analysis revealed a slightly larger diameter for Melittin-proteoliposomes (164 nm diameter) (**Figure 26B**), compared to liposomes without Melittin (**Supplementary Figure S3C**), suggesting that Melittin is associated with liposomes containing DOPG and DOPE.

To conclude, Melittin was successfully associated with liposomes resembling eukaryotic and prokaryotic membrane compositions. Gel electrophoresis after flotation analysis revealed oligomeric states of Melittin, which are dependent on the protein concentration, buffer and lipid compositions used for liposome preparation. Nevertheless, all prepared Melittin-proteoliposomes revealed homogeneous size distributions and were, therefore, suitable for the following MS analyses.

4.3.3.2 MS analysis of Melittin

To allow later comparison to Melittin-proteoliposomes, Melittin was first investigated without liposomes. For this, Melittin, solubilized in 200 mM AmAc solution, was analyzed by MS under denaturing and native gas phase conditions. The mass spectrum obtained under denaturing gas phase conditions, revealed charge states from 2+ to 4+, corresponding to monomeric Melittin (**Figure 27A**). Under native gas phase conditions charge states corresponding to monomers (2+ to 4+), dimers (6+ to 8+) and trimers (6+ to 7+) of Melittin were observed (**Figure 27B**).

By comparing the mass spectra obtained under denaturing and native gas phase conditions similar charge states were observed for monomeric Melittin suggesting that Melittin remains stable even under the harsh conditions applied in the Q Exactive instrument. Under native gas phase conditions oligomeric states are

preserved suggesting that non-covalent interactions are preserved and Melittin forms a trimer in solution in the absence of lipids.

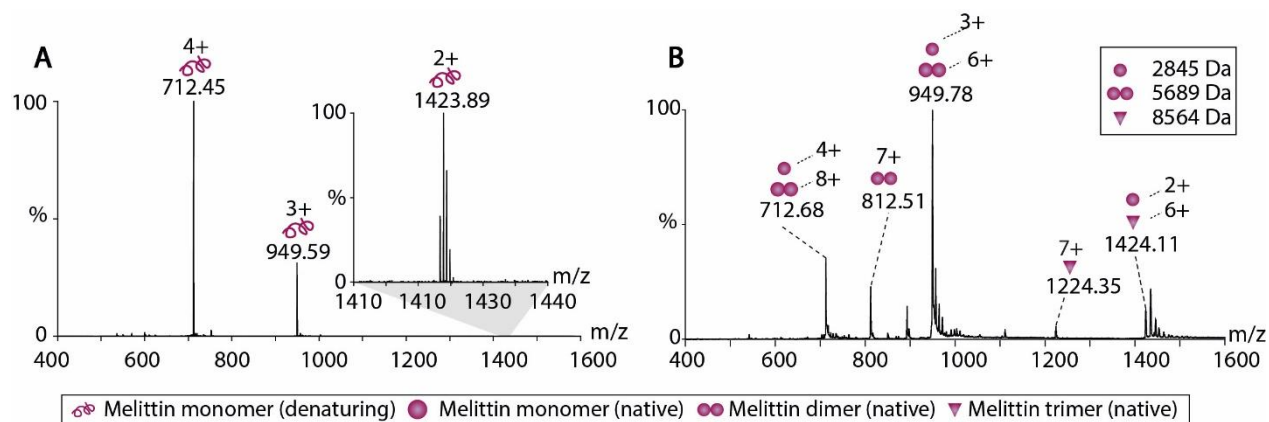


Figure 27: MS analysis of Melittin. See legend for symbols. **(A)** Melittin analyzed under denaturing gas phase conditions. A charge state distribution for monomeric Melittin was assigned. **(B)** Mass spectrum obtained under native gas phase conditions. Charge states for monomeric, dimeric and trimeric Melittin were assigned. Collisional voltage: 50 V.

4.3.3.3 MS analysis of Melittin-proteoliposomes (eukaryotic membrane composition)

Having prepared Melittin-proteoliposomes at different protein-to-lipid concentrations and lipid compositions, the next step was to verify the application of liposomes for the analysis of Melittin by MS under denaturing and native gas phase conditions. Specific binding properties of Melittin in the presence of various lipid environments should, therefore, be evaluated. For this, Melittin-proteoliposomes containing a eukaryotic membrane composition were first analyzed by MS under denaturing gas phase conditions (**Figure 28A**). The mass spectrum revealed signals for singly-charged monomeric DOPC. Charge states of monomeric Melittin and protein-lipid interactions were also detected at low intensities (**Figure 28A**). Interestingly, high-intense peaks at m/z 522.36 and m/z 480.31 corresponding in mass to lyso-PC and lyso-PE were observed. Mixed lipid clusters containing lyso-lipids were also observed, albeit at lower intensities. The signals for lyso-lipids most likely originate from cleavage with phospholipase A2 which is a typical component in Melittin preparations from bee venom²¹⁵. To validate this assumption, liposomes containing DOPC, DOPE, DOPS and cholesterol were incubated for 1h at room temperature with phospholipase A2 followed by MS analysis and MS/MS analysis under denaturing gas phase conditions (**Supplementary Figure S4A**). Indeed, the mass spectrum of liposome-phospholipase A2 mixtures shows signals corresponding to singly-charged lyso-PC (m/z 522.36) and lyso-PE (m/z 480.33). The MS/MS spectrum of lyso-PC (m/z 522.36) revealed several fragment ions confirming the loss of the head group and fatty acyl chains of PC (**Supplementary Figure S4B**).

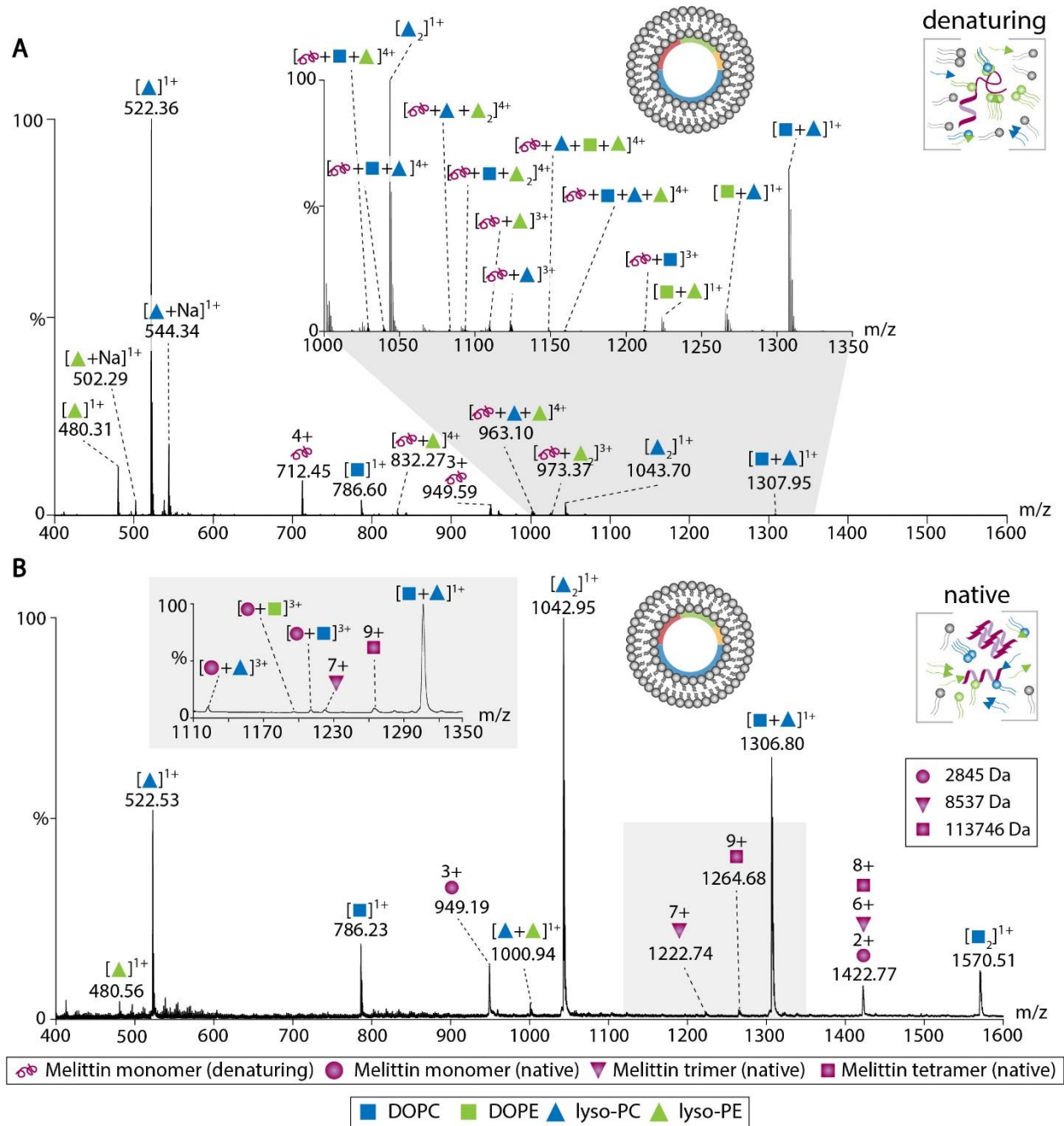


Figure 28: MS analysis of Melittin-proteoliposomes resembling a eukaryotic membrane composition. Liposomes composed of DOPC, DOPE, DOPS and cholesterol (molar ratio: 5:2:2:1). See **Supplementary Table S6** for m/z values of inserts. See figure legend for color scheme and symbols. **(A)** Mass spectrum of Melittin-proteoliposomes obtained under denaturing gas phase conditions. Signals for lyso-PC, lyso-PE, DOPC and DOPE as well as mixed clusters were observed. Monomeric Melittin and protein-lipid interactions are assigned. **(B)** Native MS of Melittin-proteoliposomes revealed signals for lyso-PC, lyso-PE, DOPC and DOPE as well as mixed lipid clusters. Oligomers of Melittin and protein-lipid interactions between monomeric Melittin and different lipids were assigned. Collisional voltage: 50 V. See **Supplementary Table S7** for m/z values of inserts.

Interactions of monomeric Melittin with up to three lyso-PC, lyso-PE, DOPE or DOPC were identified, suggesting that peptide-lipid interactions can be maintained under denaturing gas phase conditions. Next, Melittin-proteoliposomes were analyzed by MS under native gas phase conditions (**Figure 28B**). The mass spectrum revealed high intense signals for singly-charged dimeric lyso-PC at m/z 1042.95 and monomeric lyso-PC at m/z 522.23. Signals for singly-charged monomeric lyso-PE and DOPC as well as mixed lipid clusters in combination with lyso-lipids were also obtained, at low intensities.

To validate the cleavage of the lipids under native gas phase conditions, liposomes containing DOPC, DOPE, DOPS and cholesterol were again incubated with phospholipase A2 and injected into the Q-ToF instrument (**Supplementary Figure S4C**). The native mass spectrum showed similar results to the mass spectrum obtained under denaturing gas phase conditions (**compare Supplementary Figure S4A**), revealing clusters of lyso-PE, DOPE and lyso-PC.

The native mass spectrum of Melittin-proteoliposomes revealed charge states corresponding to monomers, trimers and tetramers of Melittin. This agrees well with the flotation analysis of Melittin-proteoliposomes shown above (**Figure 25B**). Importantly, protein-lipid interactions were also detected in this mass spectrum. However, these signals were of low abundance and protein-lipid interactions were only observed between monomeric Melittin and one DOPC or DOPE molecule (**Figure 28B, insert**). Nevertheless, these results show that Melittin-proteoliposomes containing a eukaryotic membrane composition are applicable to MS analysis and protein-protein as well as protein-lipid interactions are maintained in the gas phase under denaturing and native gas phase conditions.

4.3.3.4 MS analysis of Melittin-proteoliposomes (prokaryotic membrane composition)

Next, Melittin-proteoliposomes resembling a prokaryotic membrane composition were analyzed by MS. Again, Melittin-proteoliposomes were first investigated under denaturing gas phase conditions (**Figure 29A**). The acquired mass spectrum revealed high intense signals for singly-charge monomeric lyso-PE (m/z 480.31) as well as low intense signals for lyso-PG. The origin of these lyso-lipids was again verified by MS after incubation of the liposomes with phospholipase A2 (**Supplementary Figure S5A**). High intense signals for lyso-PE and singly-charged monomeric DOPE as well as mixed lipid clusters containing lyso-lipids and DOPE or DOPG, were observed. Most importantly, the mass spectrum of Melittin-proteoliposomes showed low intense charge states of 3+ and 4+ corresponding to monomeric Melittin.

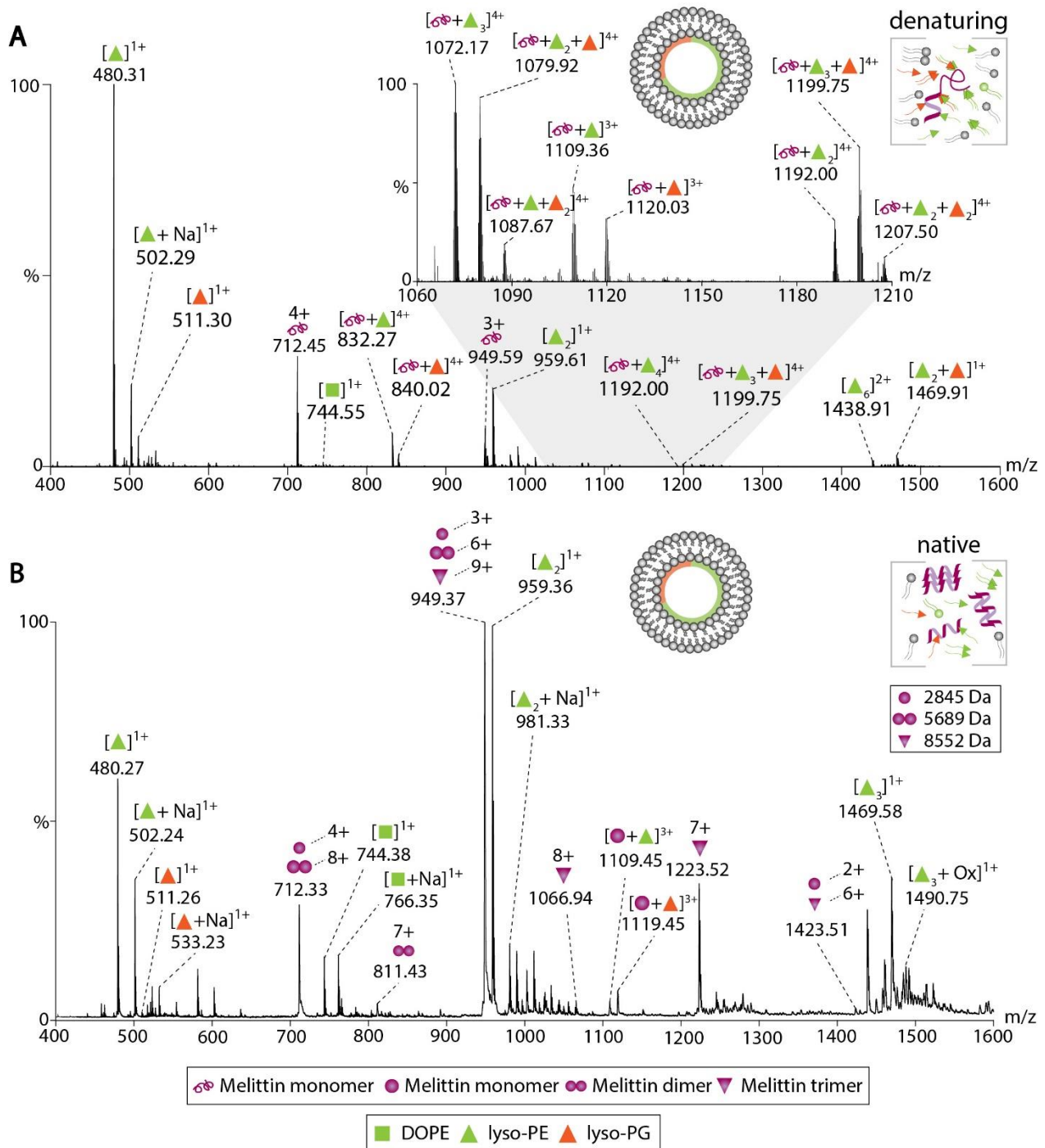


Figure 29: MS analysis of Melittin-proteoliposomes resembling a prokaryotic membrane composition. Liposomes composed of DOPE and DOPG (molar ratio: 5:2). See figure legend for color scheme and symbols. **(A)** Mass spectrum acquired under denaturing gas phase conditions. Lyso-PC, lyso-PE, DOPE and mixed clusters are assigned. Signals for monomeric Melittin and protein-lipid interactions were observed. **(B)** The mass spectrum acquired under native gas phase conditions reveals signals for lyso-PG, lyso-PE, DOPE and mixed lipid clusters. Melittin oligomers up to trimers and protein-lipid interactions were also detected. Collisional voltage: 50 V.

Protein-lipid interactions, as observed above in the mass spectrum of Melittin-proteoliposomes resembling a eukaryotic lipid composition (**Figure 28A**) were also observed between monomeric Melittin and up to four lyso-PG or lyso-PE lipids. Interestingly, these interactions comprise a much higher abundance compared to the protein-lipid interactions observed for Melittin-proteoliposomes containing DOPC, DOPE, DOPS and cholesterol.

For comparison, Melittin-proteoliposomes resembling a prokaryotic liposome composition were analyzed by MS under native gas phase conditions (**Figure 29B**). High intense signals for lyso-PE at m/z 480.27 and singly-charged dimeric lyso-PG at m/z 959.36 were observed. The presence of lyso-lipids was verified by native MS (**Supplementary Figure S5B**), revealing signals for monomeric lyso-PC and DOPE, as well as dimeric lyso-PE after the incubation with phospholipase A2. Mixed lipid clusters composed of lyso-PG and DOPG were also observed, at lower intensities.

The mass spectrum obtained under native gas phase conditions of Melittin-proteoliposomes further shows charge states for monomeric, dimeric and trimeric Melittin. This observation agrees well with the flotation analysis of Melittin-proteoliposomes resembling a prokaryotic membrane composition (**Figure 26A**). The absence of tetramers in this mass spectrum concludes again that Melittin oligomers are more stabilized in liposomes resembling a eukaryotic membrane composition. Protein-lipid interactions were observed between monomeric Melittin and one attached lyso-PG or lyso-PE.

In summary, these MS experiments showed that Melittin-proteoliposomes composed of different lipid compositions can be analyzed under denaturing and native gas phase conditions. As expected, peptide oligomers dissociate under the harsh conditions applied in the Q Exactive instrument. However, peptide-lipid interactions were maintained in the gas phase under both denaturing and native gas phase conditions.

As hydrophobic interactions are lost during desolvation in the gas phase²²⁰, we, therefore, suggest that the observed protein-lipid interactions are most likely ionic or polar interactions between lipid headgroups and amino acid side chains. Interestingly, protein-lipid interactions under native gas phase conditions were observed between only one lipid and monomeric Melittin, while the mass spectrum obtained under denaturing gas phase conditions revealed the association of multiple lipids. Accordingly, we suggest that unfolding during dissociation of liposomes under denaturing gas phase conditions, leads to binding of additional lipids. Of note, signals of oligomers were mostly observed in the mass spectra at low intensities and potential lipid adducts are presumably below the detection limit. Nonetheless, oligomers were preserved under native gas phase conditions and the oligomerization of Melittin differed when liposomes of different compositions were used. Higher stability of Melittin was, therefore, assumed when associated with eukaryotic membranes. Moreover, protein-lipid binding was only observed in the mass spectra between

DOPC, DOPE and lyso-PC, again suggesting that DOPS or lyso-lipids thereof, comprise lower ionization efficiencies.

4.3.3.5 Complementary investigation of oligomeric states of Melittin

The oligomeric states of Melittin and its interactions with lipids were previously described^{221,222}. In these studies, Melittin was thought to form a helical structure where it first orients parallel to the membrane and then inserts into the hydrophobic core and pore formation is initiated. However, other studies controversially discussed Melittin oligomerization in solution and the presence of phospholipid membranes^{223–225}. The experiments in this thesis also demonstrate that the oligomeric states depending on the liposome composition and protein concentration vary. Therefore, Melittin association with phospholipid bilayers was further investigated.

In the first step, Melittin and Melittin-proteoliposomes were analyzed by chemical cross-linking. For this, Melittin and Melittin-proteoliposomes resembling a eukaryotic membrane composition were incubated with BS3 and covalently linked oligomers were evaluated by gel electrophoresis (see **Section 3.2.2.4** for more details). In both samples, increasing the concentration of the cross-linker (35 μM , 87.5 μM , 175 μM , 262.5 μM , 350 μM , 525 μM of BS3) resulted in an increased number of Melittin oligomers (**Figure 30**).

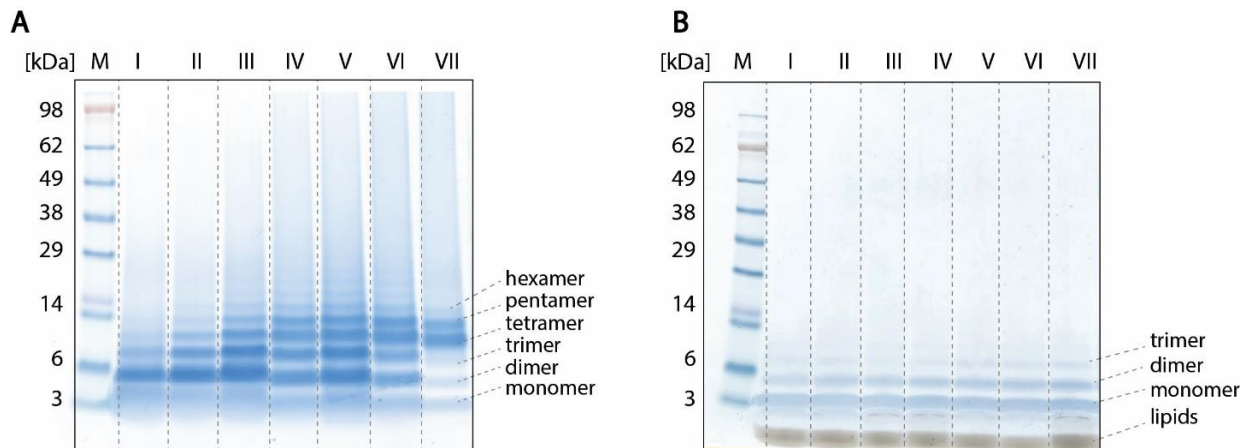


Figure 30: Chemical cross-linking of Melittin and Melittin-proteoliposomes. The molecular weight marker (M) indicates masses in kDa. **(A)** Melittin was cross-linked with BS3 and covalently linked Melittin oligomers were visualized by gel electrophoresis. Non-cross-linked Melittin was loaded as a control (I). Samples were cross-linked with increasing amounts of BS3: 35 μM (II), 87.5 μM (III), 175 μM (IV), 262.5 μM (V), 350 μM (VI), 525 μM (VII) BS3. Oligomers up to hexamers were observed. **(B)** Melittin-proteoliposomes were loaded as a control (I). Melittin-proteoliposomes were each cross-linked with increasing amounts of BS3: 35 μM (II), 87.5 μM (III), 175 μM (IV), 262.5 μM (V), 350 μM (VI), 525 μM (VII) BS3. Oligomers up to trimers were observed.

The non-cross-linked protein was used as a control. Chemical cross-linking of Melittin, therefore, showed that the oligomers exceed the tetrameric state and rather unspecifically aggregate (**Figure 30A**). However, in the presence of liposomes, a lower oligomerization propensity with oligomers up to trimers was observed (**Figure 30B**).

The unspecific oligomerization states of Melittin in solution and the presence of liposomes agree with previous studies describing different models for oligomerization and pore formation in the membrane²²⁵. In these models, Melittin associates with the membrane and subsequently undergoes various states before finally forming membrane pores. As previous studies show that membrane binding, oligomerization and pore formation is strongly dependent on the protein-to-lipid ratio²²⁶ we, therefore, assumed that at the protein-to-lipid ratio used in this thesis, the oligomeric states observed are presumably intermediate states of Melittin between oligomerization and pore formation.

4.3.3.6 Complementary investigation of lipid preferences of Melittin

Even though protein-lipid interactions of Melittin and DOPC, DOPE or even lyso-PC and lyso-PE were observed by MS, interactions with DOPS or DOPG were not observed in any of the acquired mass spectra obtained under denaturing or native gas phase conditions. Therefore, Melittin interactions with specific lipids were evaluated in additional experiments.

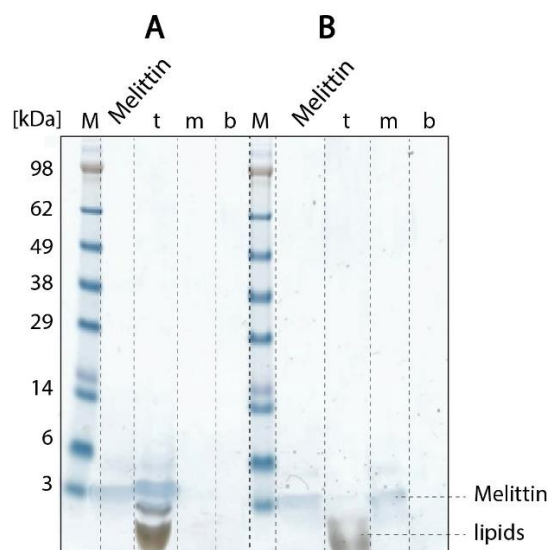


Figure 31: Binding study of Melittin to single-component liposomes. Liposomes contain DOPC or DOPG lipids. The molecular weight marker (M) indicates masses in kDa. Top (t), middle (m) and bottom (b) fractions of the sucrose gradient were evaluated by gel electrophoresis. Abbreviation: M (Marker). **(A)** Flotation assay of Melittin incubated with DOPC liposomes. Melittin was only observed in the top fraction confirming binding to the liposome membrane. **(B)** Flotation assay of Melittin incubated with DOPG liposomes. Melittin was only observed in the middle fraction.

To this end, Melittin-proteoliposomes using single-component liposomes containing DOPC or DOPG were prepared as described and Melittin-liposome interactions were analyzed by sucrose density flotation (**Section 3.2.3.6**) (**Figure 31**). Gel electrophoresis showed that Melittin was only observed in the top fractions of DOPC liposomes, indicating strong binding (**Figure 31A**). The presence of Melittin in the middle fraction of DOPG liposomes suggests that DOPG-bound Melittin dissociates from the liposome membrane during gradient centrifugation and binding to DOPG liposomes was significantly weaker (**Figure 31B**).

As a complementary study to determine lipid preferences of Melittin, lipid binding was monitored over time and Melittin was bound to various single-component lipid monolayers in a film balance³ (see **Section 3.2.3.8** for details). DOPC, DOPS or DOPG lipids were used to prepare lipid monolayers. After equilibration of the lipid film, Melittin was injected into the sub-phase at a concentration of 1 mg/ml. Binding curves for the different monolayers were then recorded. The synergy factor was obtained, by plotting the surface pressure increase ($\Delta\pi$) caused by Melittin binding as a function of the initial surface pressure (π_i) of the lipid monolayer. When comparing the binding curves of DOPC, DOPS and DOPG monolayers, Melittin showed a high affinity for the zwitterionic DOPC monolayer (**Figure 32A**). In contrast, binding to negatively charged DOPG and DOPS monolayers was notably weaker (**Figure 32B & C**). Differences in the shapes of the binding curves suggest remodeling of negatively charged lipid monolayers after Melittin injection presumably as a result of ionic interactions between the peptide and lipid head groups. A high synergy factor obtained for DOPC monolayers reflects a high binding affinity of Melittin while the low synergy factors of DOPG and DOPS monolayers reveal only moderate affinity for these lipids (**Figure 32D**).

In addition, the maximal insertion pressure (MIP) was determined, reflecting the maximal lipid density at which the monolayer is still being penetrated by the peptide. A higher MIP of DOPC monolayers compared to DOPS and DOPG monolayers, therefore, indicates a higher incorporation tendency of Melittin into zwitterionic lipid layers (**Figure 32E**). These results agree well with the MS analysis of Melittin-proteoliposomes shown above (**Figure 28**) suggesting that Melittin has a strong binding preference for DOPC and DOPE lipids, but not for DOPS or DOPG lipids. Lipid preferences of Melittin and zwitterionic or anionic lipids were previously controversially discussed^{216,227,228}. Nevertheless, the experiments in this thesis are in agreement with a recent lipid analysis showing that Melittin electrostatically interacts with anionic lipids and that insertion into the membrane is driven by the hydrophobic effect²²⁵, suggesting that Melittin interacts with anionic lipids, but stably associates with zwitterionic lipids.

³ Monolayer measurements and data analysis was performed by Dr. Christian Schwieger.

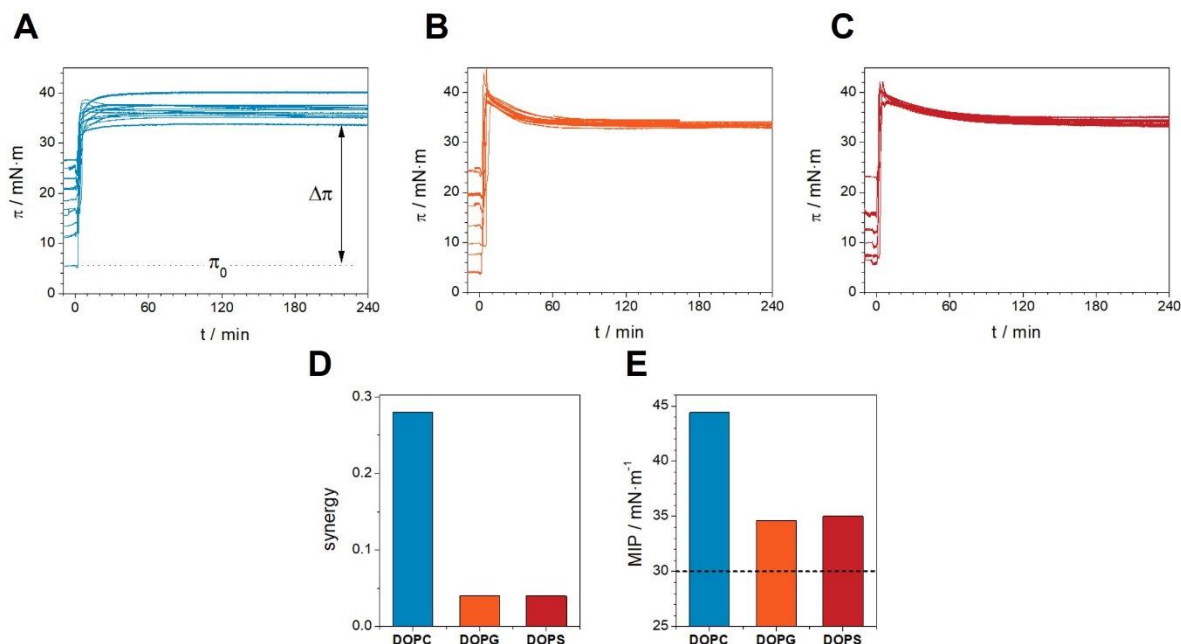


Figure 32: Lipid monolayer studies of Melittin. Adsorption of Melittin to DOPC, DOPG or DOPS monolayers at various initial surface pressures (π_0). The surface pressure (π) was recorded over time after injection of Melittin. Binding curves upon Melittin adsorption to (A) DOPC (blue), (B) DOPG (orange) and (C) DOPS (red). (D) The synergy of the interaction of Melittin with different lipids and (E) the maximum insertion pressure (MIP) of Melittin in the different lipid monolayers is displayed. The monolayer-bilayer equivalence pressure is indicated at $\Pi=30$ mN/m (dotted line).

To summarize the first part of this thesis, homogeneous liposomes were successfully established for MS analysis. When analyzing proteins mixed or associated with liposomes, lipids and proteins are detectable in the same mass spectrum and the charge states of the peptides/proteins represent folded or unfolded conformations. Most importantly, protein-protein as well as protein-lipid interactions were preserved in the gas phase by MS when analyzing Melittin associated with liposomes. These experiments, therefore, prove that liposomes are valuable tools for studying membrane-associated proteins in a native-like environment.

4.4 Establishing nanodiscs for MS analysis of membrane proteins

4.4.1 Preparation of nanodiscs

Nanodiscs are discoidal lipid bilayers with a diameter of 8–16 nm, which are stabilized in aqueous solutions by amphipathic membrane scaffold proteins (MSPs). The size of a nanodisc is defined by the length of the MSP and by the stoichiometry of lipids used in the self-assembly process^{229,230}. Nanodiscs are advantageous as they are stable and monodisperse even at high concentrations and can be employed for numerous biophysical and biochemical techniques providing an artificial lipid environment for membrane proteins²³¹.

In the past, nanodiscs were extensively applied for the MS analysis of membrane proteins in their natural lipid environment^{137,140,232,233}. However, even though these studies are promising, a sophisticated approach to capture specific protein-protein and protein-lipid interactions within their natural environment is not fully developed. In this thesis, nanodiscs were, therefore, established for chemical cross-linking to enable structure elucidation of membrane proteins in a native-like lipid environment.

To establish an MS-based nanodisc workflow for chemical cross-linking, nanodiscs were first prepared and characterized prior to reconstitution of proteins. The workflow for nanodisc preparation was adapted from Bayburt et al²²⁹ and is shown in **Figure 33** (see **Section 3.2.3.3** for details). Accordingly, lipids were first solubilized in detergent (**Figure 33, i**).

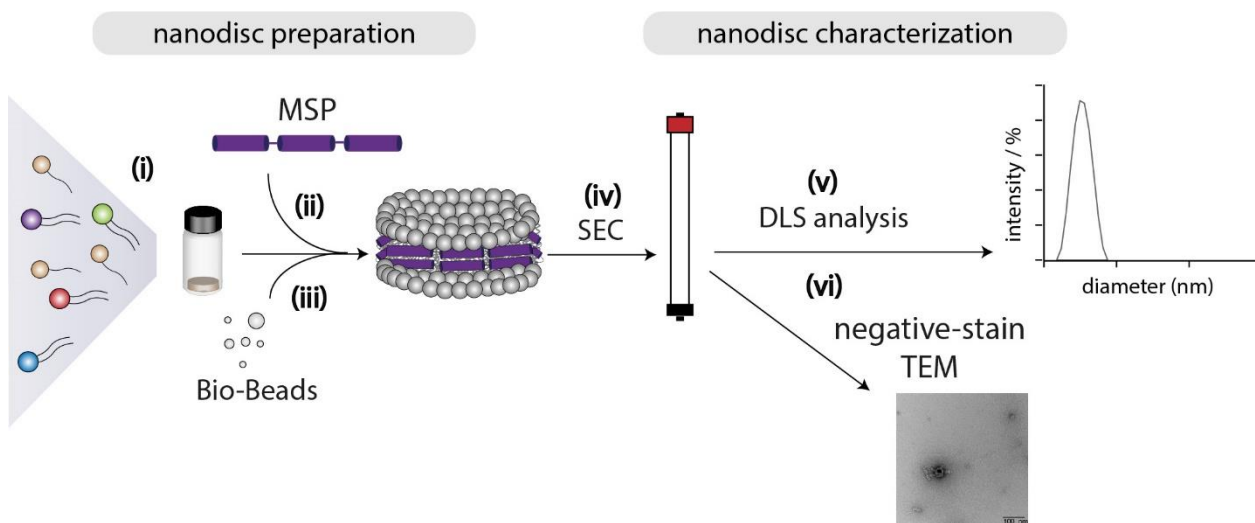


Figure 33: Nanodisc preparation and characterization. (i) Nanodiscs were prepared by solubilizing lipids in detergent, such as sodium cholate, followed by the addition of MSP in the appropriate lipid- to-MSP ratio (ii). Nanodisc assembly was initiated by detergent removal using Bio-Beads (iii). To remove aggregates nanodiscs were purified by SEC (iv), followed by DLS analysis (v) and negative-stain TEM (vi) for characterization of the nanodiscs.

Previous studies showed that the anionic detergent sodium cholate used for lipid solubilization improves the overall yield of nanodiscs^{234,235}. Based on this, detergent screening was omitted in this thesis, and sodium cholate was employed for nanodisc preparations.

Earlier studies also showed that lipid compositions are essential for nanodisc assembly^{230,231,236,237}. Accordingly, in this thesis, the lipid environment of the protein of interest was considered when choosing lipids for the preparation of nanodiscs. Lipids which are components of natural membranes were, therefore, selected.

After lipid solubilization in detergent, the MSP was added to the assembly mixture (**Figure 33, ii**) and nanodisc formation was initiated by detergent removal using Bio-Beads (**Figure 33, iii**). An essential step after nanodisc assembly is the purification of the nanodiscs by SEC (**Figure 33, iv**) to remove large aggregates containing unassembled lipids or MSP. As a homogeneous size distribution of nanodiscs is required for proper incorporation of membrane proteins into the nanodiscs, methods to determine homogeneity, size or shape evolved as important tools for nanodisc characterization. Accordingly, in this thesis, the assembled nanodiscs were analyzed by DLS (**Section 3.2.3.5**) (**Figure 33, v**) and visualized by negative-stain TEM (see **Section 3.2.3.7** for details) (**Figure 33, vi**).

4.4.1.1 Expression and purification of MSP1E3D1

For nanodisc assembly, the MSP was overexpressed and purified (see **Section 3.2.1.4 and 3.2.1.7** for details). In this thesis, MSP1E3D1, which is a variant of MSP containing three extended helices and a poly histidine tag, was used to assemble nanodiscs with a diameter of approximately 13 nm. The purification protocol was adapted from Ritchie et. al²³⁸.

After overexpression in *E.coli* cells, the N-terminally His-tagged MSP1E3D1 protein was purified by IMAC. Collected fractions after affinity chromatography were analyzed by gel electrophoresis to identify the His-MSP1E3D1 fusion protein at a molecular weight of approximately 30 kDa (**Supplementary Figure S6A**). To remove unspecifically bound proteins from the MSP1E3D1 sample, an additional SEC purification step was performed. Elution fractions from SEC were evaluated by gel electrophoresis (**Supplementary Figure S6B**). Note that MSP1E3D1 after purification still contained the His-tag. Fractions containing MSP (19-21) were pooled, concentrated and the protein was identified by LC-MS/MS analysis. Raw data were searched against a human database using the MaxQuant software and MSP1E3D1 was identified with a sequence coverage of 87.7% (**Supplementary Table S3**) confirming the successful purification of MSP1E3D1.

4.4.1.2 Preparation and purification of single-component nanodiscs

PC lipids are known to be a major component of plasma membranes¹⁹. The preparation of DMPC nanodiscs is, therefore, often a starting point for establishing native-like nanodiscs²³⁹. As a proof of principle, nanodiscs containing DMPC lipids were, therefore, investigated. The MSP1E3D1-to-lipid ratio for sufficient DMPC nanodisc assembly was previously determined^{230,235}.

Accordingly, nanodiscs were prepared by adding MSP1E3D1 to DMPC lipids solubilized in sodium cholate at a molar ratio of 1:150 followed by incubation at room temperature for 1h. Subsequently, assembled nanodiscs were purified by SEC (**Section 3.2.3.3**). The SEC purification revealed that nanodiscs are successfully eluted from the column and purified (**Figure 34A**). Subsequently, gel electrophoresis showed that MSP1E3D1 at a molar ratio of approximately 30 kDa was observed in fractions 19 to 29 (**Figure 34B**).

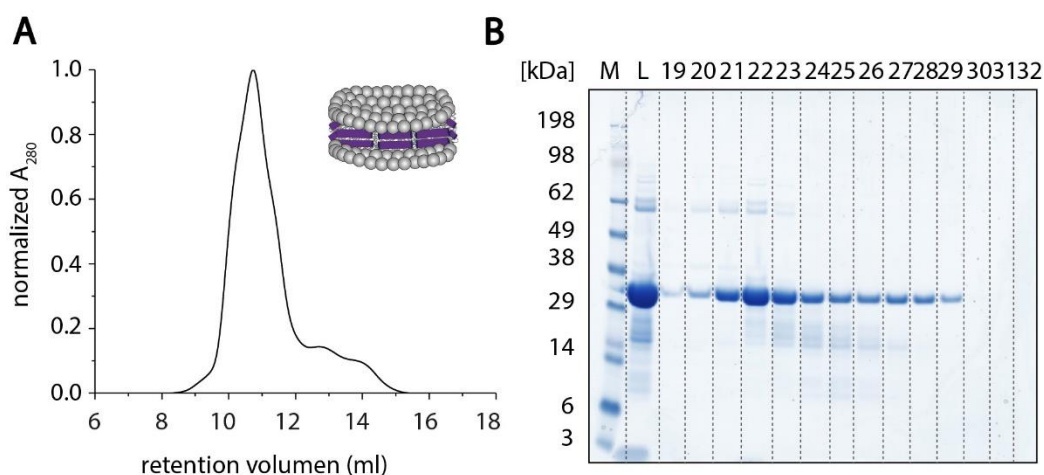


Figure 34: SEC purification of single-component nanodiscs. Nanodiscs are composed of DMPC lipids. **(A)** The SEC chromatogram revealed a peak corresponding to DMPC nanodiscs. **(B)** Gel electrophoresis after SEC purification (19 to 32). Fractions 19 to 29 show MSP1E3D1 at a molecular weight of approximately of 30 kDa. Abbreviations: M (Marker), L (Load).

4.4.1.3 Preparation and purification of multi-component nanodiscs

Mimicking the natural lipid environment of the protein of interest is essential for successful incorporation of the protein and subsequent analysis. Therefore, more complex nanodiscs representing the natural lipid environment of the protein of interest were prepared. For this, nanodiscs containing POPC, POPE, and DOPS at a molar ratio of 45:15:40, resembling a eukaryotic membrane were explored. The protocol for nanodisc assembly was adapted from Bayburt et al.²²⁹

Even though cholesterol is a major component of plasma membranes and affects its physical properties¹⁹⁸ previous studies showed that cholesterol tends to prevent nanodisc formation²⁴⁰. To guarantee proper nanodisc assembly, cholesterol was, therefore, not employed for the preparation of nanodiscs in this thesis.

As mentioned above, for sufficient nanodisc assembly, it is crucial to identify the appropriate MSP1E3D1-to-lipid ratio. MSP1E3D1-to-lipid ratios were, however, controversially discussed for complex lipid compositions^{241,242}. Nanodiscs containing POPC, POPE and DOPS were, therefore, prepared at two different lipid-to-MSP ratios.

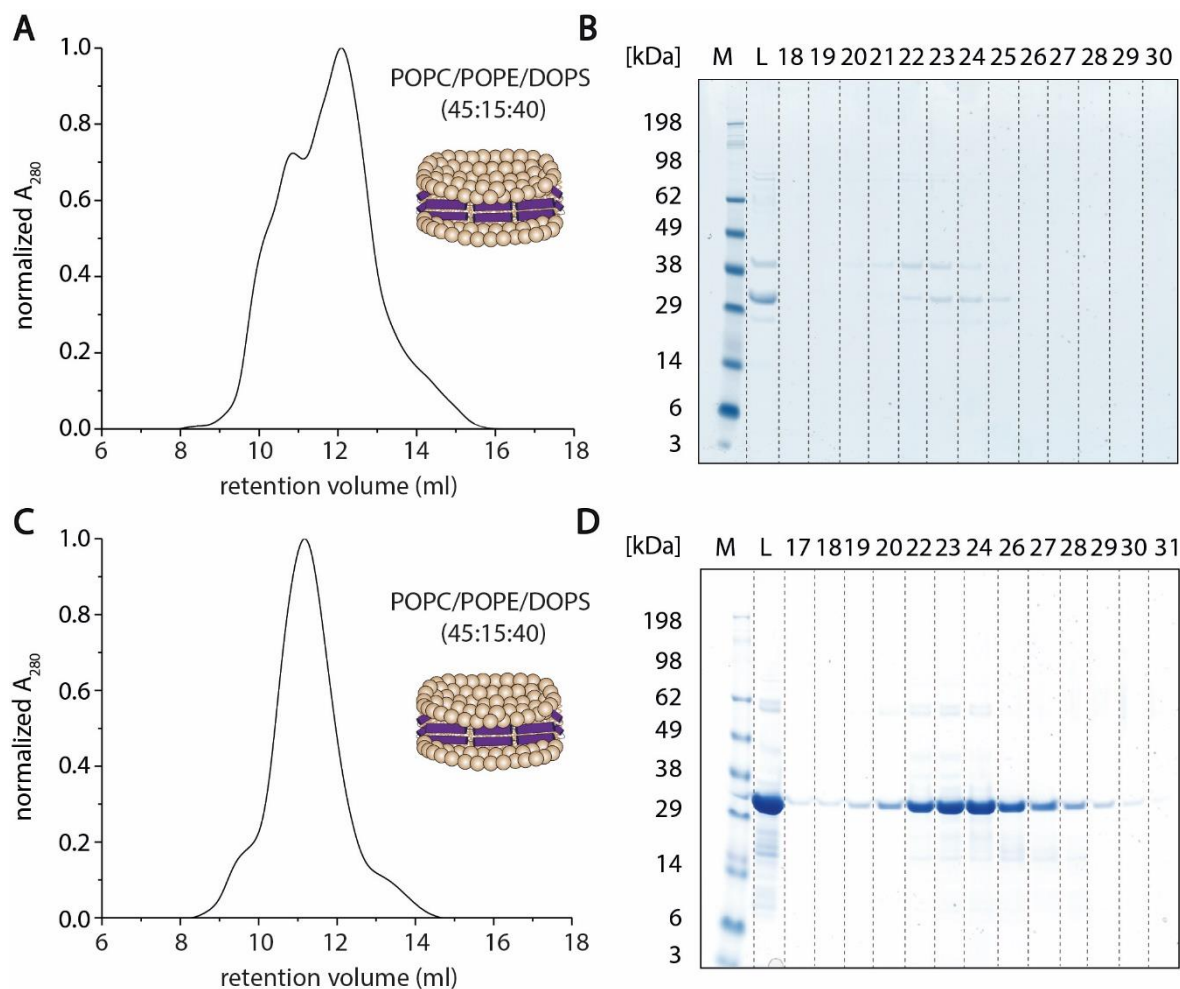


Figure 35: SEC purification of multi-component nanodiscs. Nanodiscs contained POPC, POPE and DOPS at a molar ratio of 45:15:40. For SEC purification the retention time is plotted against the normalized absorbance. **(A)** For SEC purification of nanodiscs prepared at a MSP1E3D1-to-lipid ratio of 1:60. **(B)** Gel electrophoresis after SEC purification at a MSP1E3D1-to-lipid ratio of 1:60. **(C)** Nanodiscs prepared at a MSP1E3D1-to-lipid ratio of 1:120 and purified by SEC. **(D)** Gel electrophoresis of SEC fractions revealed a protein band at approximately 30 kDa corresponding to MSP. Nanodiscs prepared at a MSP1E3D1-to-lipid ratio of 1:120. Abbreviations: M (Marker), L (Load).

Accordingly, lipids solubilized in sodium cholate were mixed with MSP1E3D1 at a protein-to-lipid ratio of 1:60 and 1:120 followed by SEC purification and evaluation of the collected fractions by gel electrophoresis. SEC (**Figure 35A**) and gel electrophoresis (**Figure 35B**) determined a low concentration of MSP1E3D1 at a protein-to-lipid ratio of 1:60 suggesting that nanodiscs were not sufficiently stabilized. These fractions were, therefore, not further analyzed. SEC (**Figure 35C**) and gel electrophoresis (**Figure 35D**) of nanodiscs prepared at an MSP1E3D1-to-lipid ratio of 1:120 revealed MSP1E3D1 at a molecular weight of 30 kDa confirming sufficient nanodisc assembly. Accordingly, these nanodiscs were subjected to further analysis.

4.4.2 DLS analysis and negative-stain TEM⁴ of nanodiscs

To verify the proper assembly of nanodiscs, homogeneity, diameter and shape of single- and multi-component nanodiscs were investigated by DLS analysis and negative-stain TEM, respectively. First, DMPC nanodiscs were targeted. For this, fractions after SEC purification containing the highest nanodisc concentration (fractions 21 to 28) were subjected to DLS analysis. DLS analysis revealed a size distribution at approximately 12 nm in all fractions, corresponding to the nanodiscs (**Supplementary Figure S7**). Moreover, higher size distributions were also observed presumably corresponding to liposomes or nanodisc aggregates. Of these, fraction 22 (**Figure 36A**), however, revealed the highest homogeneity and was, therefore subjected to negative-stain TEM analysis (**Figure 36B**). Negative-stain analysis of DMPC nanodiscs showed discoidal particles suggesting sufficiently nanodisc assembly (**Figure 36B**). Interestingly, large stacks of DMPC nanodiscs were also observed. Previous studies showed that these stacks are presumably staining artifacts, as they were not found in solution⁶⁰. The stacking of nanodiscs was, therefore, not explored further in this thesis.

Next, multi-component nanodiscs containing POPC, POPE and DOPS at a molar ratio of 45:15:40 and prepared at an MSP1E3D1-to-lipid ratio of 1:120 were verified by DLS analysis and negative-stain TEM. Again, fractions containing the highest concentration after SEC purification (fractions 22 to 27) were analyzed by DLS (**Supplementary Figure S8**). DLS analysis revealed a size distribution at approximately 13 nm diameter corresponding to nanodiscs as well as larger size distribution presumably originating from liposome species and insufficient nanodiscs assembly. Nevertheless, fraction 23 (**Figure 36C**) showed the highest homogeneity. Accordingly, the nanodiscs in fraction 23 containing POPC, POPE, and DOPS (molar ratio of 45:15:40) was then visualized by TEM analysis (**Figure 36D**). TEM of multi-component nanodiscs revealed discoidal particles as well as nanodisc stacks. However, in comparison to DMPC nanodiscs, these stacks were rather short, containing only up to ten nanodiscs.

⁴ Negative-stain TEM measurements were performed by PD Dr. Annette Meister.

In conclusion, DLS analysis and negative-stain TEM revealed that single- and multi-component nanodiscs were successfully assembled with a homogenous size distribution. Multi-component nanodiscs resembling a biological membrane composition were, therefore, employed in the following experiments in this thesis.

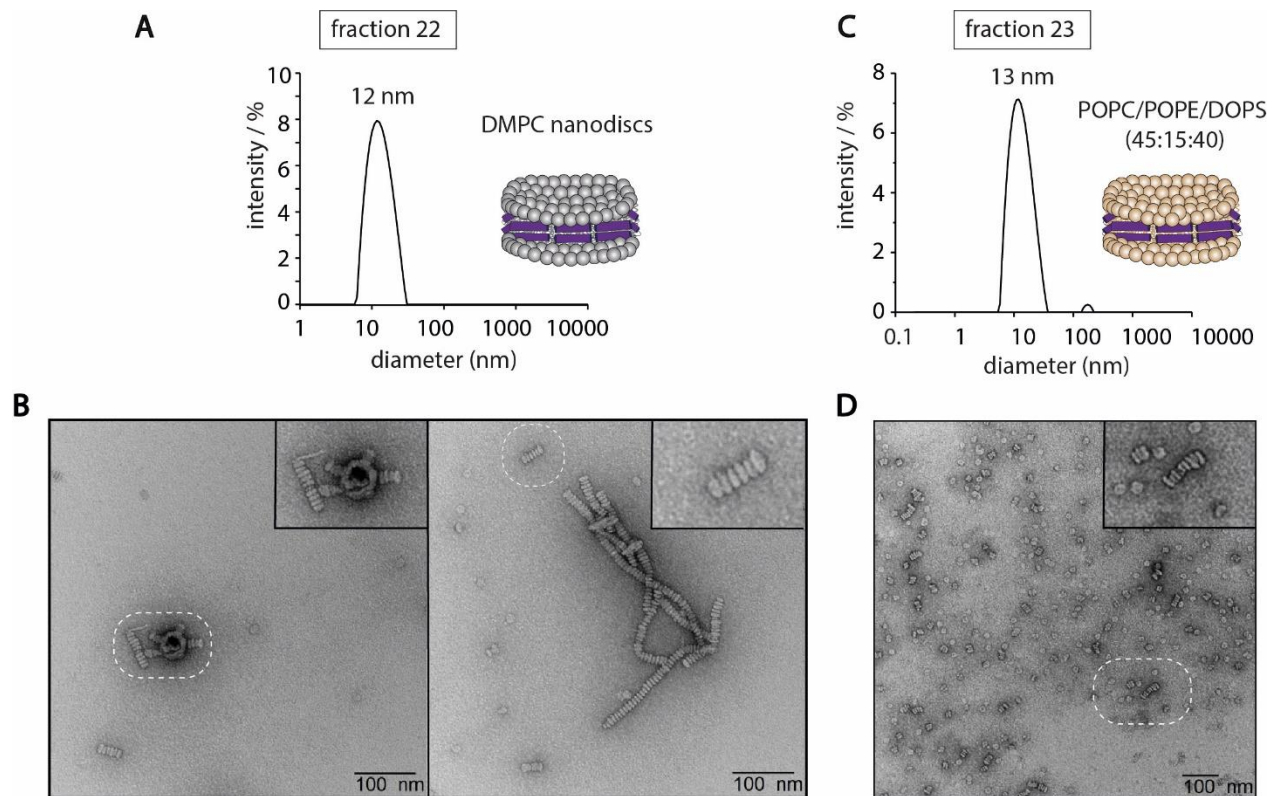


Figure 36: DLS analysis and negative-stain TEM of nanodiscs. DLS spectra show the mean size values for each peak. (A) DLS analysis of SEC fraction 22 of DMPC nanodiscs revealed a mean size distribution at approximately 12 nm diameter corresponding to the purified nanodiscs. (B) Negative-stain TEM of DMPC nanodiscs showed discoidal particles (left image) as well as stacks of nanodiscs (right image). (C) DLS analysis of SEC fraction 23 of multi-component nanodiscs containing POPC, POPE, DOPS (molar ratio 45:15:40) showed a homogeneous size distribution of approximately 12 nm diameter. (D) Negative-stain TEM analysis of nanodiscs containing POPC, POPE and DOPS lipids (molar ratio 45:15:40) revealed discoidal structures and smaller nanodisc stacks. In the top right corner, magnified images of the outlined region are shown.

4.4.3 Establishing Syntaxin-1A nanodiscs

Having established nanodiscs with a natural lipid composition, the next step was to reconstitute a membrane protein into nanodiscs to allow chemical cross-linking of this protein. Note that, chemical cross-linking is only possible if protein domains are accessible to the cross-linker. Accordingly, Syntaxin-1A was chosen as a model protein as it contains domains, that are not buried in the membrane and, therefore, allows

sufficient chemical cross-linking. Syntaxin-1A is a neuronal membrane protein located at the presynaptic membrane. Together with other SNARE proteins i.e., SNAP25-a and Synaptobrevin-2, the so-called SNARE complex is formed. The SNARE complex is responsible for exocytosis of neurotransmitters during signal transmission in neurons²⁴³.

4.4.3.1 Expression and purification of Syntaxin-1A

Syntaxin-1A was first overexpressed in *E.coli* cells and purified (see **Section 3.2.1.4 and 3.2.1.8** for details). The purification protocol for Syntaxin-1A was adapted from Fasshauer et al.²⁴⁴. As a first purification step, the cell lysate containing the N-terminally His-tagged Syntaxin-1A was subjected to IMAC. Collected fractions after affinity chromatography were analyzed by gel electrophoresis and the His-Syntaxin-1A fusion protein was identified (MW 38 kDa) (**Supplementary Figure 9A**). After IMAC purification, the histidine tag was removed by TEV cleavage during dialysis and reverse affinity purification (**Supplementary Figure 9B&C**). To remove unspecifically bound proteins an additional SEC step was performed, and collected fractions were evaluated by gel electrophoresis (**Supplementary Figure 9D**). Fractions containing Syntaxin-1A were pooled, concentrated and subjected to in-gel digestion and LC-MS/MS analysis. Raw data were searched against a database using the MaxQuant software and Syntaxin-1A was identified with a sequence coverage of 81.9 % (**Supplementary Table S3**), confirming successful purification of Syntaxin-1A.

4.4.3.2 Preparation and characterization of Syntaxin-1A nanodiscs

Next, Syntaxin-1A was reconstituted into nanodiscs for chemical cross-linking of an integral membrane protein in a native-like lipid environment. The workflow of nanodisc assembly and cross-linking analysis with reconstituted Syntaxin-1A is shown in **Figure 37**. The reconstitution workflow was adapted from Lee et al.²⁴⁵ and Bao et al.²⁴⁶ Accordingly, lipids containing POPC, POPE, and DOPS at a molar ratio of 45:15:40 were solubilized as described (**Section 3.2.3.3**). MSP1E3D1 and Syntaxin-1A were added at an appropriate MSP1E3D1-Syntaxin-1A-lipid ratio of 1:0.25:120 established previously (see **Section 3.2.3.4** for details). After incubating the protein-to-lipid mixture, nanodisc formation was initiated by incubation with Bio-Beads (**Figure 37, i**).

To remove aggregates nanodiscs were purified by SEC followed by DLS (**Figure 37, ii**) and TEM analysis (**Figure 37, iii**) to determine the size, homogeneity and shape of the nanodiscs. Finally, Syntaxin-1A nanodiscs were cross-linked with BS3 (**Figure 37, v**) and subjected to LC-MS/MS analysis (**Figure 37, iv**).

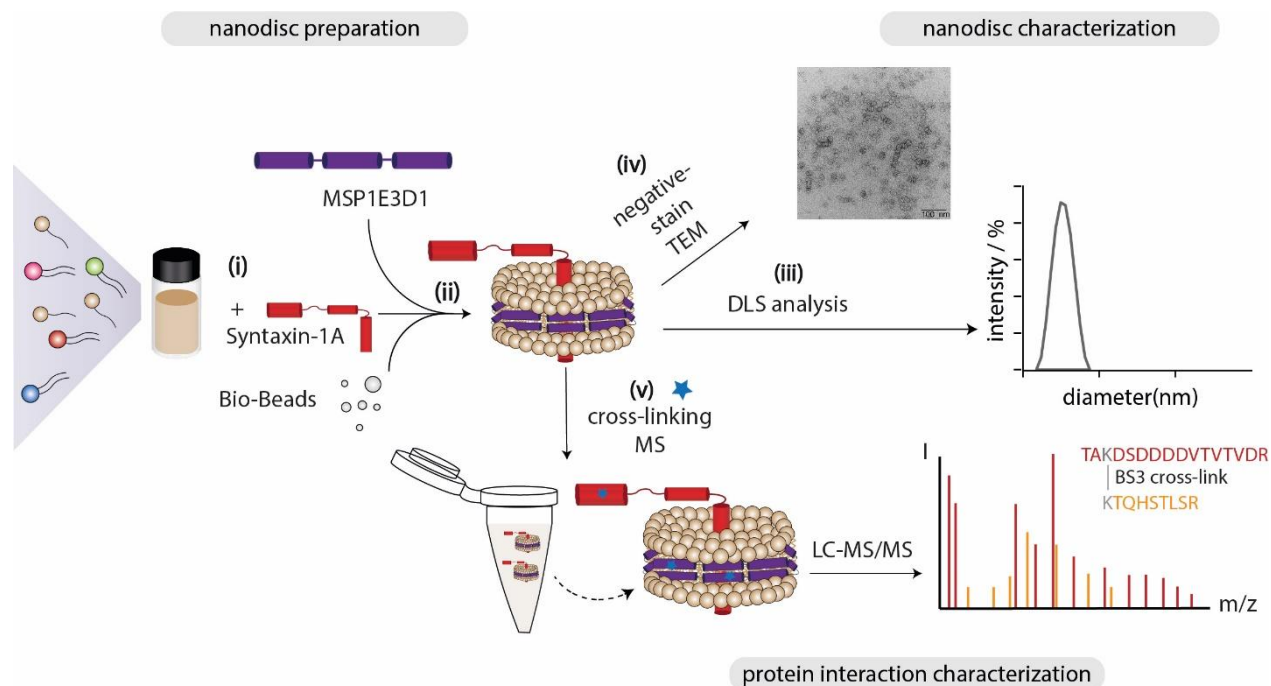


Figure 37: Preparation, characterization and cross-linking of Syntaxin-1A nanodiscs. For nanodisc preparation, lipids were solubilized in detergent followed by the addition of MSP1E3D1 and Syntaxin-1A (i). The self-assembly process was initiated by detergent removal with Bio-Beads (ii). Nanodiscs were characterized by DLS (iii) and TEM (iv). Finally, nanodiscs were cross-linked and analyzed by LC-MS/MS (v).

The SEC chromatogram after nanodisc purification revealed a peak confirming the formation of Syntaxin-1A nanodiscs (**Figure 38A**). Subsequently, fractions after SEC were evaluated by gel electrophoresis and a protein band at a molecular weight of approximately 30 kDa was observed (**Figure 38B**). Note that, this protein band could not unambiguously be assigned as Syntaxin-1A or the MSP1E3D1 as these proteins have similar molecular weights of 35 kDa and 30 kDa, respectively.

To, therefore, confirm the presence of Syntaxin-1A and MSP1E3D1 in these samples and verify the formation of Syntaxin-1A nanodiscs, western blot analysis was performed. For this, Syntaxin-1A nanodiscs after SEC purification were separated by gel electrophoresis and transferred to a blotting membrane.

Blotted proteins were then detected using specific antibodies against Syntaxin-1A and the His-tag of the MSP1E3D1. The antibody against the His-tag was chosen because MSP1E3D1 after purification still contains a His-tag and the antibodies, therefore, serve as a proof that MSP1E3D1 is present in the samples.

Accordingly, western blot analysis confirmed that Syntaxin-1A is present in SEC fractions 19-25 (**Figure 38C**). Western blot analysis against the His-tag of MSP1E3D1 revealed MSP1E3D1 in fractions 19 to 27 (**Figure 38D**). These results, therefore, confirmed that nanodiscs were successfully assembled with reconstituted Syntaxin-1A.

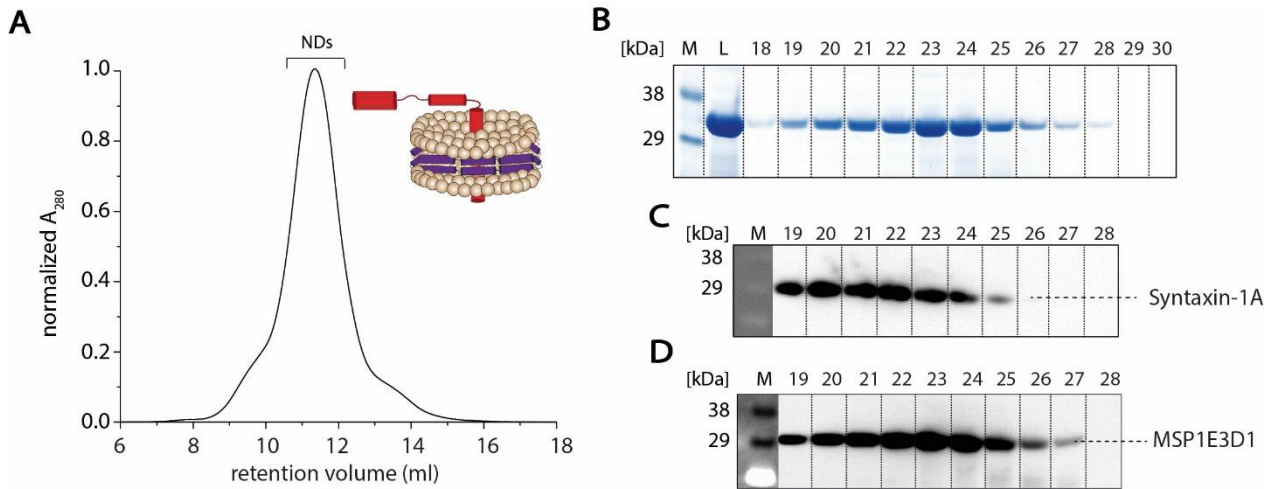


Figure 38: SEC purification and western blot analysis of Syntaxin-1A nanodiscs. (A) SEC purification of Syntaxin-1A nanodiscs revealed a peak corresponding to the nanodiscs. For SEC purification the retention time is plotted against the normalized absorbance. (B) Collected fractions were evaluated by gel electrophoresis showing a protein band at approximately 30 kDa. (C) Western blot analysis of Syntaxin-1A nanodiscs incubated with the antibody against Syntaxin-1A. (D) Western blot analysis of Syntaxin-1A nanodiscs with the antibody against the His-tag of MSP1E3D1. Abbreviations: M (marker), L (load).

4.4.4 DLS analysis and negative-stain TEM of Syntaxin-1A nanodiscs

To verify the shape and homogeneity of Syntaxin-1A nanodiscs after nanodisc purification, DLS and negative-stain TEM were again performed. Based on western blot analysis fractions containing the highest Syntaxin-1A and MSP concentration were chosen and subjected to DLS analysis. DLS analysis of Syntaxin-1A nanodiscs showed mean size distributions of approximately 13 nm diameter in all fractions corresponding to the assembled nanodiscs (**Supplementary Figure S10**). However, as larger and smaller size distributions were also observed in these fractions nanodiscs were not sufficiently assembled.

Nevertheless, fraction 23, revealed the highest concentration of homogeneous nanodiscs (**Figure 39A**) and was, therefore, further analyzed by negative-stain TEM (**Figure 39B**). Negative-stain TEM images of fraction 23 showed discoidal particles suggesting a proper formation of nanodiscs. Interestingly, these images also indicate that less nanodisc stacks are observed compared to the TEM analysis of single- and multi-component nanodiscs shown before, suggesting that Syntaxin-1A reconstitution into nanodiscs might prevent nanodiscs from stacking. Note that, the resolution of the electron microscope used in this thesis was not enough to observe Syntaxin-1A incorporated into nanodiscs. Nevertheless, western blot analysis confirmed the reconstitution of Syntaxin-1A. Additional experiments, for instance, flotation analysis followed by western blot analysis may also be promising to evaluate sufficient binding of Syntaxin-1A to nanodiscs. In conclusion, DLS analysis and negative-stain TEM verify the homogeneity and shape of nanodiscs containing Syntaxin-1A.

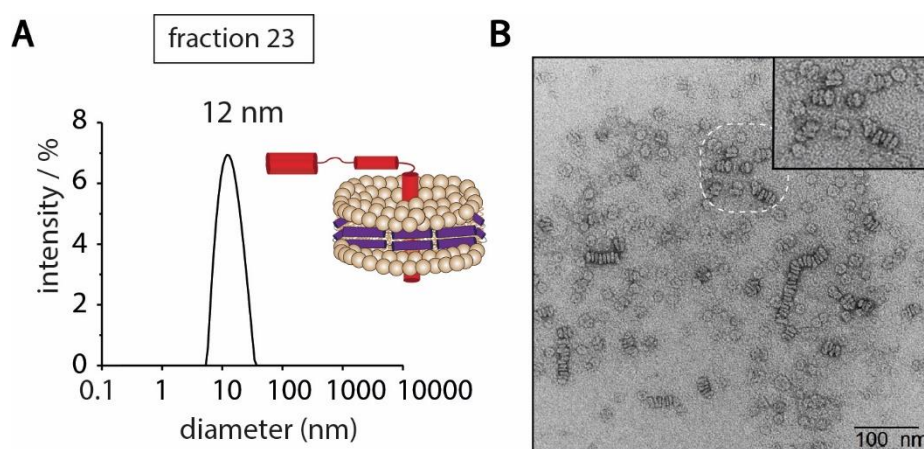


Figure 39: DLS analysis and negative-stain TEM of Syntaxin-1A nanodiscs. (A) DLS analysis of Syntaxin-1A nanodiscs (fraction 23) revealed a homogeneous distribution at approximately 12 nm. DLS analysis reveals the mean size value. (B) Negative-stain TEM of Syntaxin-1A nanodiscs images showed discoidal nanodisc structures as well as nanodisc stacks. In the top right corner a magnified view of the structure in dashed lines is shown.

4.5 Chemical cross-linking of Syntaxin-1A nanodiscs

Having established the reconstitution of Syntaxin-1A into nanodiscs, in the next step, chemical cross-linking was performed to determine the structure of Syntaxin-1A in its natural lipid environment. For this, Syntaxin-1A nanodiscs were cross-linked using the amine-reactive cross-linker BS3, followed by the evaluation of cross-links by gel electrophoresis and LC-MS/MS analysis.

Gel electrophoresis of cross-linked nanodiscs was first utilized to determine the optimal cross-linker concentration for MS analysis. For this, Syntaxin-1A nanodiscs were incubated with increasing BS3 concentrations (0.15 mM to 30 mM). Subsequent gel electrophoresis then revealed protein bands at approximately 35 kDa (**Figure 40**) as well as protein bands at approximately 64 kDa and 96 kDa. Note that, as Syntaxin-1A and MSP1E3D1 have a similar molecular weight, the higher-mass oligomers can either originate from Syntaxin-1A, MSP1E3D1 or mixed complexes. When increasing the cross-linker concentration, the intensity of higher-mass gel bands increases and more oligomers are observed. Moreover, cross-linking with BS3 caused broadening of protein bands presumably reflecting intra-molecular cross-linking of Syntaxin-1A or MSP1E3D1.

Based on these studies, a concentration of 30 mM seems suitable for cross-linking of Syntaxin-1A nanodiscs and was, therefore, employed for the following LC-MS/MS studies. As we suspect that cross-linking of MSP1E3D1 is also possible and cross-links of Syntaxin-1A might, therefore, be prevented, we chose a higher cross-linking concentration of 30 mM to increase the probability of Syntaxin-1A cross-links.

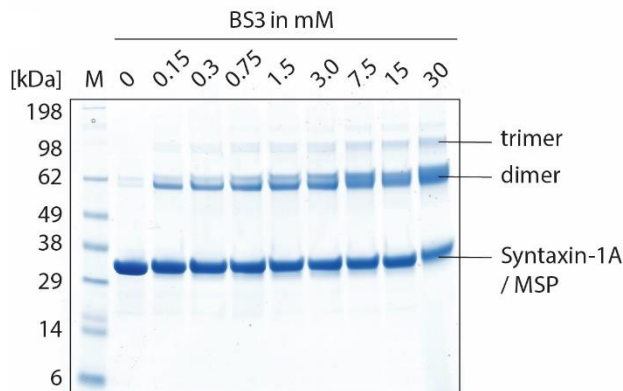


Figure 40: Cross-linking of Syntaxin-1A nanodiscs. 10 μ M of Syntaxin-1A were incubated with increasing concentration of BS3 (0.15 to 30 mM). The control without BS3 (0 mM) showed a protein band at approximately 32 kDa was observed. At increasing BS3 concentrations, signals of higher molecular mass were observed. Abbreviation: M(Marker).

4.5.1 Manual validation of Syntaxin-1A nanodisc cross-links

Having determined the optimal BS3 concentration for sufficient cross-linking, Syntaxin-1A nanodiscs were cross-linked and subsequently analyzed by LC-MS/MS to identify specific interactions within the proteins. For this, Syntaxin-1A nanodiscs were incubated with 30 mM BS3 and hydrolyzed in solution using trypsin. Subsequently, cross-linked peptide pairs were enriched by SEC and fractions containing cross-linked peptide pairs were analyzed by LC-MS/MS. Potential cross-links were identified using the plink2 software and manually validated.

A cross-linked peptide pair was identified if both cross-linked peptides showed a series of at least four consecutive fragment ions. In addition, both peptides must be covered by a series of fragment ions. Furthermore, the signal-to-noise ratio has to be as large as possible.

Accordingly, fragment ions that in addition to the amino acids of one peptide, also contain the mass of the crosslinker and the second peptide, are unambiguously identified as a cross-linked peptide pair. Note that, not only interactions between lysine side chains are possible and side reactions of the BS3 cross-linker with serines, threonines and tyrosines were also identified. Cross-linked peptide pairs that exhibited identical or overlapping peptide sequences were identified as intermolecular cross-links since these sequences can only originate from two copies of a protein.

An example spectrum of an intra-molecular cross-link of Syntaxin-1A is shown in **Figure 41**. The peptides TAKDSDDDDVTVTVDR and KTQHSTLSR are covalently linked through lysine residues at positions three and one, respectively. TAKDSDDDDVTVTVDR showed a series of singly-charged y-ions (y_1 - y_{14} dark blue) and doubly-charged b-ions (b_2 - b_4 , b_6 - b_8 , b_{10} in light blue). For KTQHSTLSR, a series of singly-charged y-ions (y_1 - y_8) as well as doubly-charged b-ions (b_2 - b_4) were assigned. Note that, the cross-linked peptides cover a series of fragment ions. In addition, ions containing fragments of both peptides and the linker allow specific assignment of the position of the cross-linked amino acids.

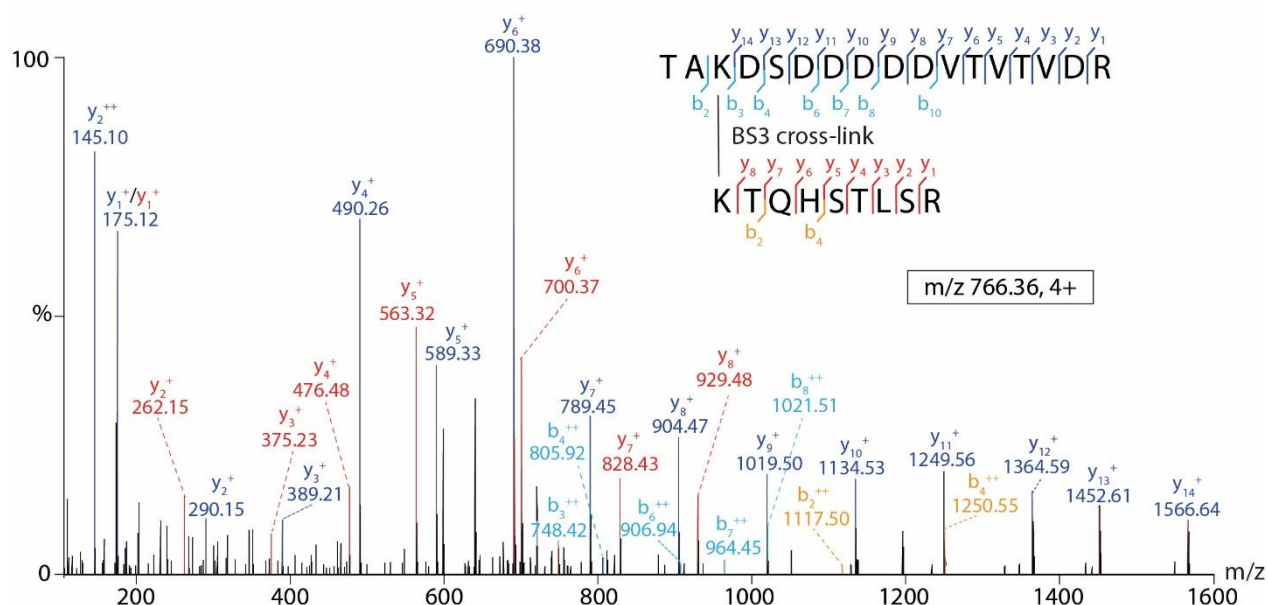


Figure 41: Example spectrum of an intra-molecular cross-link of Syntaxin-1A. The m/z and charge of the precursor ion are indicated (box). For the peptide TAKDSDDDDVTVTVDR y-ions (dark blue) and b-ions (light blue) were assigned. The peptide KTQHSTLSR revealed y-ions (red) and b-ions (yellow).

Since nanodiscs are stabilized by the membrane scaffold protein MSP1E3D1, cross-links of MSP1E3D1 were also identified. An example spectrum of an intra-molecular MSP1E3D1 cross-link is shown in **Figure 42**. The peptides QKLHELQEK and QKVEPLR were covalently linked by lysine residues at position 2. Both peptides show a series of singly-charged y ions. y1 to y8 ions were assigned to the longer sequence of QKLHELQEK and y1 to y6 ions were assigned to the shorter QKVEPLR peptide. b ions were also detected for both peptides. Note that, the triply-charged y-ion, which was assigned to the proline interface, has the highest intensity in this cross-link spectrum. Previous tandem MS experiments showed that the so-called proline effect results in high intense fragment ions which are produced from the cleavage at the N-terminal side of proline^{247,248}. In summary, peptides with a high sequence coverage could be identified allowing an unambiguous assignment of peptide sequences of linkage sites.

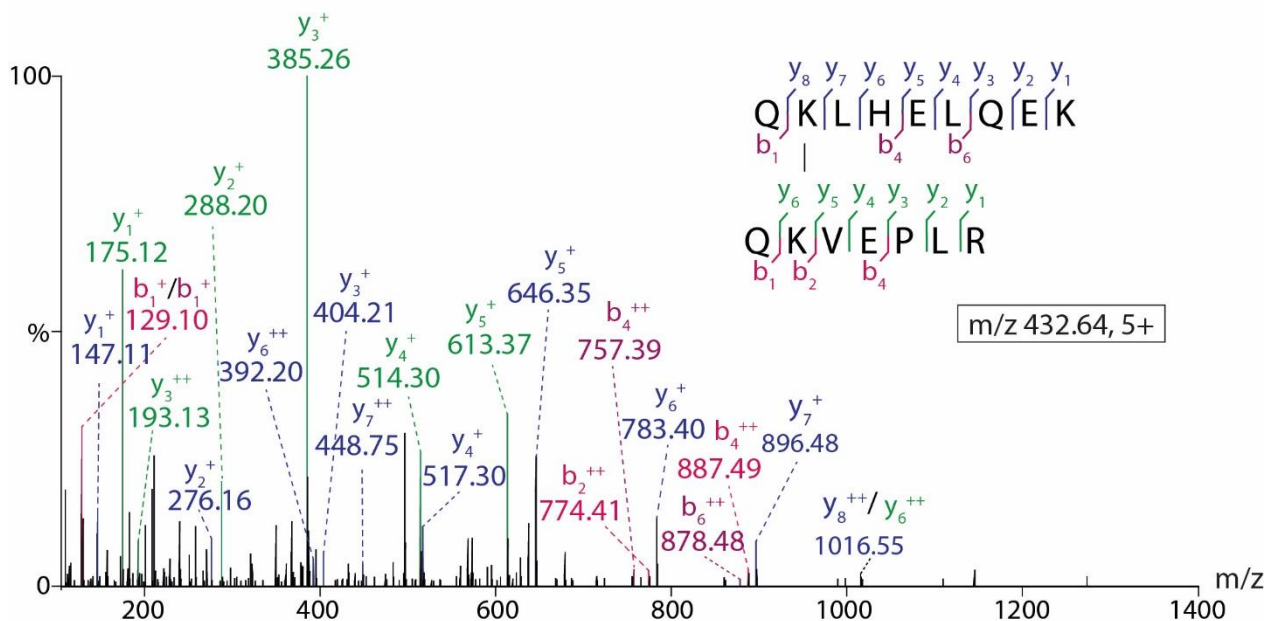


Figure 42: Example spectrum of an intra-molecular cross-link of MSP1E3D1. The m/z and charge of the precursor ion is given (box). For the peptide QKLHELQEK y-ions (blue), b-ions (magenta) were assigned. For the peptide QKVEPLR y-ions (green) and b-ions (pink) are shown.

The cross-link analysis did not only identify intra-molecular cross-links for Syntaxin-1A and MSP1E3D1, but also inter-molecular cross-links between the two proteins. An example spectrum is shown in **Figure 43**. Covalent linkage of the peptides KTQHSTLSR (Syntaxin-1A) and QKVEPLR (MSP1E3D1) was observed between lysine residues at position 1 and the lysine residue at position 2, respectively. In the example spectrum, both peptides were identified by a series of y-ions. In this mass spectrum, the y3+ ion also has the highest intensity, which again is due to the proline effect described earlier, indicating that fragmentation is favored from the N-terminus.

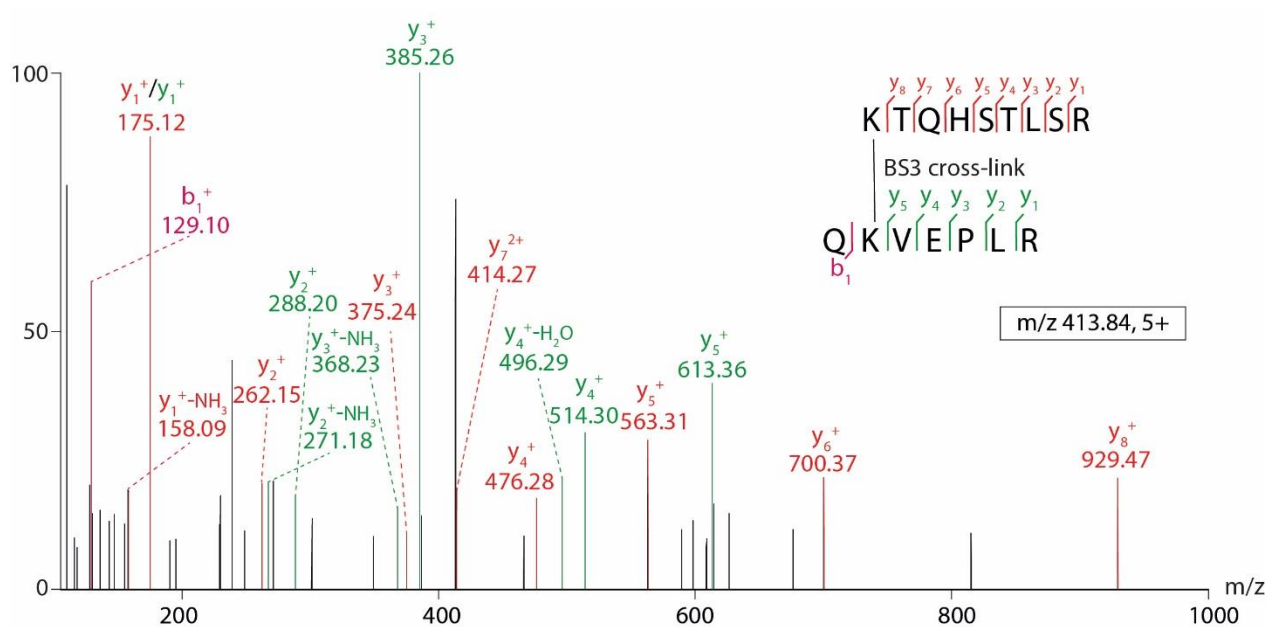


Figure 43: Example spectrum of an inter-molecular cross-link of Syntaxin-1A and MSP1E3D1. The m/z and charge of the precursor ions is given. Characteristic y- (red and green) and b-ions (pink) of both peptides are assigned.

In total, 15 cross-links were identified. Of these, 12 cross-links were identified between lysine residues and three cross-links were identified between serine, threonine and tyrosine residues. These include intra-molecular cross-links of Syntaxin-1A (**Supplementary Table S8**) and MSP1E3D1 (**Supplementary Table S9**) as well as inter-molecular cross-links between Syntaxin-1A and MSP1E3D1 (**Supplementary Table S10**). The results were visualized in a network plot (**Figure 44**) showing intra-molecular cross-links as well as interactions between Syntaxin-1A and MSP1E3D1.

As a rather small amount of intra-molecular cross-links was observed for Syntaxin-1A we assumed, that the Syntaxin-1A cross-links are presumably suppressed by additional cross-linking reactions. For instance, as BS3 reacts towards primary amine groups cross-linking of lipids containing an amine headgroup, like POPE, might also be possible. The intra-molecular cross-link identified for Syntaxin-1A was located between a flexible linker and the Habc domain (**Figure 44A**). This observation agrees with previous studies showing that interactions between the helices of the Habc domain are possible²⁴⁹. MSP1E3D1 cross-links were also identified. Note that MSP1E3D1, as mentioned before, was engineered to adjust larger proteins. The modified version of MSP, therefore, contains an additional sequence of approximately 60 amino acids (**Figure 44A**). Interestingly, however, intra-molecular cross-links found for MSP1E3D1 were only observed in regions of the original MSP structure.

Finally, intermolecular interactions between Syntaxin-1A and MSP1E3D1 were identified. The cross-links observed were mostly observed between different regions of the MSP1E3D1 and the Habc domain or the SNARE-motif (**Figure 44B**).

These observations are supported by previous findings, highlighting that the Habc domain and the SNARE motif are connected through a flexible linker²⁵⁰. Accordingly, we assume that Syntaxin-1A, even though incorporated into nanodiscs contains the flexible linker region which allows a dynamic movement of the protein so that Syntaxin-1A interacts with MSP1E3D1 residues in close proximity.

In summary, chemical cross-linking of Syntaxin-1A nanodiscs provides a first insight into the structural arrangements of Syntaxin-1A in its natural lipid environment. However, one should keep in mind, that cross-linking reactions need to be optimized to allow better validation of interaction sites within Syntaxin-1A. Nevertheless, these experiments show that chemical cross-linking of proteins in nanodiscs is in principle possible, making it a promising tool for future studies on membrane proteins embedded in a native-like lipid environment.

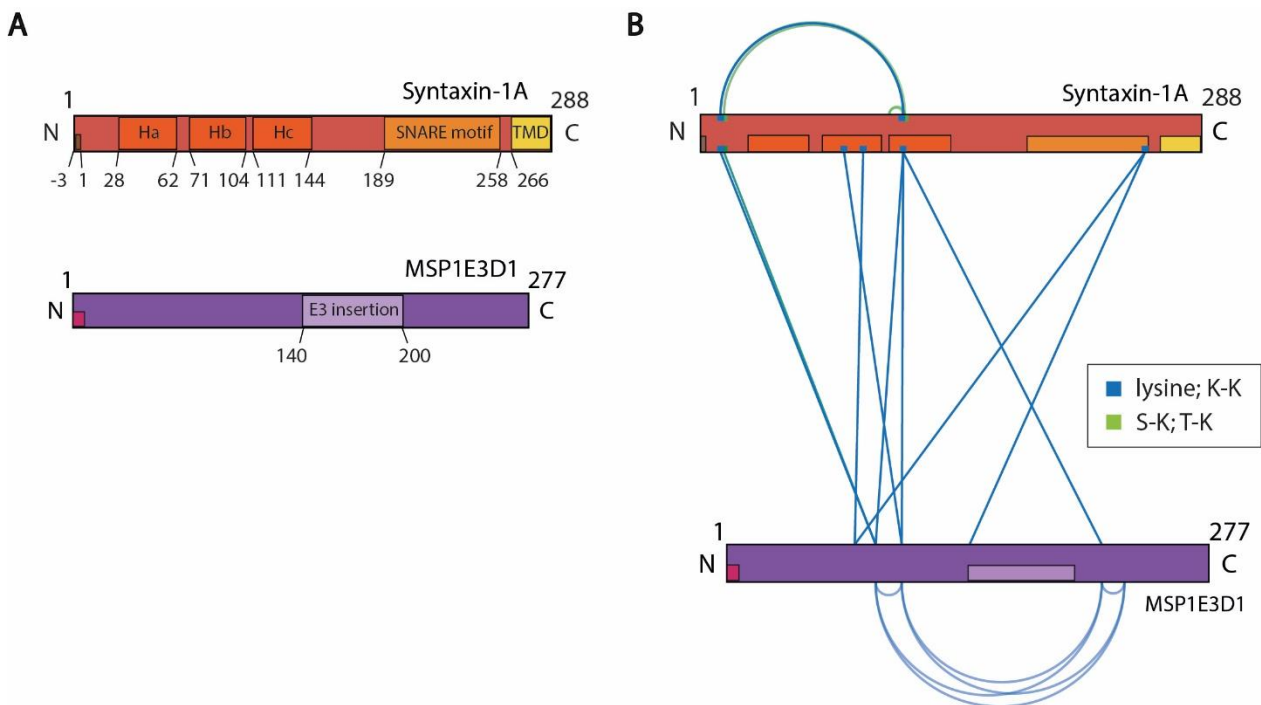


Figure 44: Syntaxin-1A and MSP1E3D1 constructs and network plot of cross-links. (A) Schematic of the Syntaxin-1A and the MSP1E3D1 constructs used in this thesis. The Habc domain, SNARE motif and the transmembrane domain of Syntaxin-1A are highlighted. The histidine-tag and the E3 insertion are shown in the MSP1E3D1 protein. (B) Network plot of protein interactions observed between Syntaxin-1A and MSP1E3D1 after cross-linking of Syntaxin-1A nanodiscs. Intra-molecular interactions of Syntaxin-1A and MSP1E3D1 as well as intra-molecular cross-links between Syntaxin-1A and MSP1E3D1 are shown (blue). Additional intra- and inter-molecular cross-links between threonine-lysine (T-K) and serine-lysine (S-K) are also highlighted (green).

5 Discussion and outlook

5.1 Choosing the right membrane mimetics for analyzing membrane proteins

As the expression of membrane proteins in cells is generally low and biological membranes are highly heterogeneous and insoluble in aqueous solutions²⁵¹, the study of membrane proteins in their native environment has been an ongoing challenge in structural biology. Detergents are typically employed for the solubilization of membrane proteins⁴⁶. However, since they are often used at high concentrations, they often lead to protein unfolding and destabilization²⁵². In addition, detergent micelles are polydisperse and compete with lipids for lipid-binding sites. Accordingly, protein-lipid interactions are hard to be maintained. In addition, with the wide range of detergents available, screening is often required to efficiently solubilize membrane proteins and at the same time preserve their native state.

Therefore, in recent years, membrane mimetics were established to resemble a more native-like environment for membrane proteins⁴⁶. Commonly employed membrane mimetics, which are sorted by their ability to mimic a biological membrane, are shown in **Figure 45**. Accordingly, detergents are the least suitable membrane mimetic as they do not represent a lipid bilayer and liposomes are closely related to biological membranes. As all membrane mimetics have advantages and disadvantages, choosing a suitable membrane mimetic mainly depends on the protein of interest as well as the aim of the experiment. In this work, liposomes and MSP nanodiscs were used for the mass spectrometric analysis of membrane proteins. The reasons for choosing these membrane mimetics and their limitations are discussed in the following section.

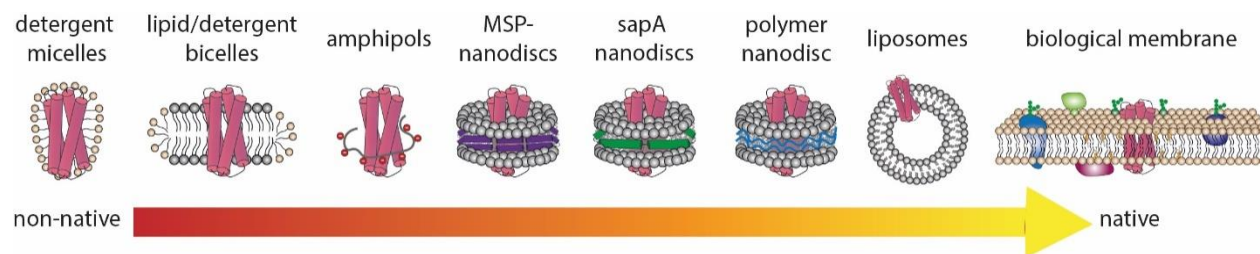


Figure 45: Overview of commonly used membrane mimetics. They are arranged according to their ability to mimic a native membrane. Detergents represent a non-native environment for membrane proteins, while liposomes most natively represent a biological membrane.

5.2 Establishing liposomes for the analysis of membrane-associated proteins by MS

5.2.1 Selection of liposomes as membrane mimetics

Liposomes are spherical vesicles containing one or more lipid bilayers⁵⁰. Although they were initially applied for drug delivery in biomedical research, they are nowadays increasingly used as membrane mimetics for the analysis of membrane proteins in a native-like environment^{172,253–255}. In this work, liposomes were employed to determine structural information on membrane-associated proteins and their interactions with lipids.

The reconstitution of proteins into liposomes has several advantages: First, it allows studying membrane proteins in a native-like environment, thereby avoiding the loss of protein interactions by replacing the lipid bilayer with detergents. Secondly, liposomes represent a continuous membrane environment that is not restricted by membrane scaffolding proteins or polymers. Furthermore, liposomes can be prepared from both native or synthetic phospholipids and their size and composition can be adjusted depending on the protein of interest. Accordingly, large proteins and protein complexes can also be targeted. In contrast to other membrane mimetics, liposomes can be utilized to study the molecular transport performed by membrane proteins. Electrophysiological measurements on liposomes allow a detailed characterization of diffusion mechanisms, which is not possible with other membrane mimetics²⁵⁶. In addition, liposomes have proven useful when applying biochemical techniques. For instance, protein binding to liposomes can be easily verified by flotation on a sucrose gradient²⁵⁷ or co-sedimentation²⁵³.

Although liposomes have many advantages, their application has been limited for a long time by their lack of heterogeneity and stability. Accordingly, liposomes are prone to aggregation and fusion. In this thesis, to exclude aggregation and fusion, liposome size and stability were controlled by DLS. Accordingly, DLS analysis of the majority of single-component (**Figure 12**) and multi-component (**Figure 13**) liposomes revealed homogeneous size distributions. However, DLS analysis of single-component DOPE liposomes showed numerous size distributions (**Figure 12D**). This might be explained by earlier studies describing that DOPE lipids adopt an energetically favorable hexagonal structure in aqueous solutions^{258–260}. Accordingly, to reach an energetically preferred state, DOPE lipids presumably undergo different lamellar transition and aggregation states¹⁹⁷. We, therefore, suggest that the heterogenous size distributions observed by DLS are intermediate transition states of DOPE lipids. Complementary DLS experiments in this thesis, in which liposome size is monitored at different time points, revealed similar results indicating that DOPE liposomes are not stable (**Figure 12E**). DOPC liposomes on the contrary have high stability up to 78 h (**Figure 12F**). Multi-component liposomes containing DOPE lipids, however, showed stable and homogenous size distributions.

This is particularly important for subsequent experiments of this thesis, as it was the goal to prepare and employ liposomes that have a composition best mimicking a biological membrane.

Previous studies showed that the desired orientation of proteins in liposomes is difficult to achieve, resulting in multiple populations (inside-out and outside-out)^{261,262}. The orientation of proteins into liposomes can be investigated by employing, for instance, fluorescence-based methods. Recently, a study describing chemically modified integral membrane proteins allowed a rapid fluorescence-based determination of protein orientation after their reconstitution into liposomes²⁶³. However, as the focus of this thesis was the analysis of membrane-associated proteins, for which orientation does not play a role, studies on orientation were not performed.

Lipid peroxidation and oxidation lead to changes in the structure and biophysical properties of membrane lipids^{264,265}. Oxidation is a modification, which induces changes in membrane fluidity and permeability and thus leads to changes in the structure and activity of membrane proteins. In this thesis, the mass spectra of liposomes did not reveal any signals of oxidized lipids. We, therefore, assume that due to the storage conditions in an inert gas (e.g. argon) and the fresh preparation of liposomes prior to MS analysis, lipid oxidation is not an issue in the experiments.

To conclude, liposomes were initially chosen for this thesis, because they are easy to prepare, can be adapted to the proteins of interest and, most importantly, mimic a well-suited membrane environment. In addition, we also showed that liposomes can be prepared at different compositions, are stable and homogeneous and lipid oxidation can be neglected. Accordingly, in this thesis, liposomes were used for the analysis of membrane-associated proteins and their interactions with lipids.

5.2.2 Methodological considerations

Although liposomes were previously assumed to be too large and heterogeneous¹³⁸ for biophysical studies, in this thesis, we attempted to use liposomes as membrane mimetics to study membrane proteins in their native lipid environment by MS. Previous studies using other membrane mimetics for the investigation of membrane proteins were promising^{64,241,266,267}. Amongst these studies, MS and particularly native MS have proven to be valuable tools to elucidate the structure of membrane proteins and their interactions with^{258–261}. Due to these promising applications and because MS analyses of liposomes and proteoliposomes are missing to date, MS was employed in this thesis to gain new insights into the application of liposomes as membrane mimetics.

Since previous studies using membrane mimetics by MS showed that artificial membranes can be used as detergent-free vesicles for the analysis of membrane proteins in a defined lipid environment, our aim was to explore the application of liposomes. Accordingly, we hypothesized that liposomes dissociate in the gas phase and intact peptides/proteins are released for MS analysis. For the analysis of liposomes and proteoliposomes, two different mass spectrometers were employed, namely the Q Exactive and the Q-ToF mass spectrometers. Note that, in the commercially available Q Exactive mass spectrometer parameters during ionization and transfer into the gas phase are difficult to adjust. Accordingly, the conditions within this mass spectrometer are rather harsh and non-covalent interactions are most likely not preserved. In a previous study, applying a Q Exactive mass spectrometer, we showed that the transfer of liposomes into the gas phase of the mass spectrometer is possible and individual lipids are obtained for subsequent analysis¹⁷². Accordingly, this approach allowed the identification of different lipid species directly from the phospholipid bilayer of liposomes. In addition, the Q-ToF mass spectrometer was employed, which due to its modifications, allows smooth transfer of ions. Accordingly, non-covalent interactions are preserved in the gas phase and protein complexes and protein-ligand interactions are maintained. Previous studies by Hanson et al. employing native MS for the analysis of proteins associated with liposomes, described that liposomes dissociate in the gas phase and lipid interactions between up to 100 lipids are preserved²⁷². In this initial study, protein-lipid interactions from proteoliposomes were detected and the specificity toward lipids was evaluated. Accordingly, in this thesis, native MS was used to preserve non-covalent interactions in the gas phase and thus analyze oligomeric states as well as the interactions of proteins associated with liposomes. The combination of denaturing and native MS was, therefore, used to compare the dissociation of liposomes and proteoliposomes in the gas phase. Accordingly, we assumed that under denaturing gas phase conditions liposome dissociation is facilitated, whereas, under native gas phase conditions, protein-lipid interactions are most likely preserved.

From a technical point of view, liposomes and proteoliposomes were analyzed after direct infusion under denaturing and native gas phase conditions. Note that, direct infusion is often complicated by ion suppression, as all ionizable compounds in a sample are transferred simultaneously into the mass spectrometer and, therefore, compete for charge. In this thesis, experiments were, therefore, performed to investigate whether ion suppression occurs due to high-intense lipid signals. For this, liposomes and proteins were first analyzed individually by MS, following the analysis of soluble proteins mixed with liposomes. By stepwise extending these experiments, we were able to show that lipids and proteins can be analyzed simultaneously in the same mass spectrum. Nevertheless, these experiments also highlight that signals with lower abundance due to the high intense lipid signals are usually difficult to detect.

In addition, data analysis of lipid-lipid and protein-lipid interactions is challenging since complex mass spectra are obtained. In this thesis, calculation and assignment of lipid clusters as well as protein-lipid interactions were performed manually, which is particularly difficult when larger and mixed lipid clusters with different charge states need to be assigned. Accordingly, care must be taken when assigning mass spectra that show overlapping signals. Specialized software, such as Massign¹²², however, can support the assignments.

5.2.3 MS analysis of liposomes

In this thesis, mass spectrometric analysis of single-component (**Figure 14**) and multi-component (**Figure 15**) liposomes revealed that liposomes dissociate into lipid clusters under denaturing as well as native gas phase conditions. Although the exact principle of liposome dissociation and ionization in the gas phase remains unknown, we propose different theories based on our previous knowledge of proteins as well as protein-lipid interactions:

One possible explanation for cluster formation could be, that, during ESI, droplet shrinkage during desolvation leads to an increase in the concentration of the analyte²⁷³. As a result, non-specific ion pairing might occur. This was previously described for two or more analyte molecules which are trapped in the same droplet and interact with each other once the solvent evaporates^{274,275}. Although this was mainly described for proteins injected into the mass spectrometer in the presence of NaCl, non-specific binding was also described in ESI-MS studies of protein-ligand complexes¹⁹⁹. Based on these previous studies, we propose that the detected lipid clusters result from non-specific adduct formation due to droplet shrinkage in the gas phase.

Remarkably, when comparing the mass spectra of multi-component liposomes recorded under denaturing and native gas phase conditions, lipid monomers have the highest signal intensity in the mass spectra acquired under denaturing gas phase conditions (**Figure 15A**), while dimers are mostly observed under native gas phase conditions (**Figure 15B**). We, therefore, assume that due to the presumably harsh conditions within the Q Exactive mass spectrometer, liposomes dissociate more readily. Surprisingly, however, large lipid clusters are also observed under denaturing gas phase conditions, suggesting that the energy of the Q Exactive mass spectrometer is not high enough to dissociate liposomes completely. Note that in the Q Exactive mass spectrometer the ions do not pass through a collision cell on their way to the Orbitrap detector. Accordingly, collision energy cannot be applied without selecting specific ions in the quadrupole and the collision energy for dissociation of liposomes can, therefore, not be adjusted.

Nevertheless, one should keep in mind that lipid-lipid interactions might also be stable enough to survive the transfer from solution to the gas phase in the Q Exactive mass spectrometer. In contrast, the Q-ToF mass spectrometer is modified for the transmission of high masses and the increased pressure of all pumping stages leads to multiple low-energy collisions within the trajectory of the ions, therefore, reducing the internal energy of the ions. This process, known as collisional cooling, previously allowed to maintain non-covalent interactions of large protein complexes^{115,169,276}. We, therefore, speculate that the observed lipid oligomers under native gas phase conditions are presumably stabilized by non-covalent interactions which are preserved due to collisional cooling.²²⁰

These observations, however, raised the question of which interactions stabilize lipid clusters in the gas phase. Previous MS studies showed that non-covalent interactions of proteins are retained during the transfer from solution to the gas phase, however, it must be kept in mind that the gas phase structure of a protein or protein complex might differ from its solution structure. Possible reasons for the different gas phase structures are, for instance, the decreasing pH value during ESI droplet shrinkage²⁷⁷, the heat applied during ESI²⁷⁸, and the loss of the hydration shell²⁷⁹. Molecular dynamics simulations revealed when the proteins are fully desolvated in the gas phase and hydrophobic interactions are lost, that a collapse of charged side chains leads to the formation of a network of electrostatic interactions on the protein. Since the overall structure of the protein remains unchanged in these studies, the newly formed interactions were hypothesized to stabilize the protein²⁸⁰. Additional computational and experimental studies confirmed that the overall structures are retained with only minor differences between the solution and gas phase²⁸⁰⁻²⁸³. Accordingly, under optimized conditions, for instance, under native gas phase conditions, the transfer of proteins and protein complexes by ESI, while maintaining their solution structures, is possible. We, therefore suspect, that during liposome dissociation lipid interactions from solution are preserved under native gas phase conditions and lipid clusters are, therefore, stabilized.

Liposomes were previously described to be stabilized in solution by non-covalent interactions, including hydrophobic, ionic and van der Waals interactions²⁸⁴. Due to the structure of lipids, ionic interactions are formed between their head groups, while van der Waals forces are mainly stabilized by their non-polar fatty acyl chains. Based on previous studies on proteins, we, therefore, hypothesize that lipid clusters are stabilized by these interactions in the gas phase. Under native gas phase conditions, we were indeed able to detect larger clusters at high m/z , confirming that non-covalent bonds are maintained. Since intact liposomes are, however, not preserved and liposomes nonetheless dissociate, we assume that hydrophobic interactions are lost in the gas phase. Based on the protein studies mentioned above, we further speculate that the lipids might undergo a structural rearrangement in the gas phase.

Once the hydration shell is fully removed in the gas phase we, therefore, assume that the lipid headgroups most likely orient towards each other due to their charge attraction. Accordingly, we assume that weak van der Waals interactions are lost, while ionic interactions are maintained. As the internal energy of the ions increases during the transition from solution to the gas phase, this might also lead to a disruption of interactions leaving only a part of the liposome intact. Similar results were observed in the mass spectra obtained under denaturing gas phase conditions applying the Q Exactive mass spectrometer. Note that, larger clusters were observed under native gas phase conditions at higher m/z than possible in the Q Exactive instrument. However, larger clusters could potentially also be detected under denaturing gas phase conditions, if signals were recorded at higher m/z ranges than is possible with the Q Exactive instrument.

The mass spectra of multi-component liposomes, for instance, acquired under native gas phase conditions (**Figure 15D**) also showed that liposomes dissociate into lipid clusters, however, higher intensities were observed for monomeric DOPC lipids compared to DOPE monomers or mixed lipid clusters. Previous studies described the ionization efficiency of lipids in ESI-MS experiments²⁸⁵. Accordingly, the different intensities observed, suggest that DOPC lipids contain a higher ionization efficiency due to their headgroup structure and associated charge. However, it should be noted that the multi-component liposomes prepared in this thesis contain a higher amount of DOPC lipids, likely correlating with higher signal intensities. Interestingly, against our assumptions, lipid clusters containing both DOPC and DOPE have the lowest signal intensities in this mass spectrum (**Figure 15D**). According to previous studies by Hanson et al., the interaction between different lipid molecules under native gas phase conditions is not random and different intensities for lipid clusters can be expected²⁷². Furthermore, they proposed that DOPE lipids as they have a different behavior in membranes due to their headgroup structure do not interact as strongly as DOPC lipids. We, therefore, assume since the liposomes prepared in this thesis contain PE lipids, the different intensities of the lipid clusters observed might also suggest that PE lipids affect cluster formation and dissociation in the gas phase.

In this thesis, cholesterol was not detected in the mass spectra of multi-component liposomes under denaturing or native gas phase conditions (**Figure 15D**). Previous studies describe that effective ionization of neutral sterols such as cholesterol is not observed. Derivatization of cholesterol is therefore required to allow ionization and detection in the gas phase²⁸⁶. Accordingly, in previous studies, cholesterol was converted to cholesterol sulfate, enabling detection in negative ion mode through the formation of ammonium adducts²⁸⁷. We, therefore, hypothesize that cholesterol is not observed in the mass spectra as it cannot be ionized. In addition, we were also not able to observe signals for DOPS or DOPS clusters in the mass spectra of multi-component liposomes (**Figure 15**). As all MS experiments shown in this thesis were

performed in positive ion mode, we assume that during ionization DOPS acquires a negative charge, which is not provided in positive ion mode.

5.2.4 MS analysis of membrane proteins associated with liposomes

MS analysis of p40^{phox}

In this thesis, we employed p40^{phox} to demonstrate the application of liposomes for the study of membrane-associated proteins by MS. For this, p40^{phox} associated with liposomes was studied under denaturing and native gas phase conditions. In our experiments, we observed that liposomes dissociate and signals of lipids as well as p40^{phox} are observed in the same mass spectrum under denaturing and native gas phase conditions (**Figure 24**). However, protein-lipid interactions were not detected.

The mass spectrum of p40^{phox}-proteoliposomes reveals higher charge states of the protein under denaturing gas phase conditions, suggesting that p40^{phox} is unfolded. In contrast, the mass spectrum under native gas phase conditions showed lower charge states for p40^{phox} indicating that non-covalent interactions are most likely preserved and p40^{phox} is maintained in a folded conformation. However, the question arises why protein-lipid interactions are not observed in the acquired mass spectra.

To answer this question, we first inspected the structure and interactions of p40^{phox} bound to membranes. Previous studies proposed that the initial membrane association of p40^{phox} is driven by non-specific electrostatic interactions between the cationic protein surface and the anionic surface of the membrane, followed by specific PI(3)P-triggered membrane penetration of the protein²¹⁴ (**Figure 46A**). In detail, p40^{phox} binds to PI(3)P lipids through hydrogen bonds and salt bridges. Other studies highlighted that within this binding pocket arginine at position 58 (R58) is the most important residue for binding of p40^{phox} to the headgroup of PI(3)P lipids²⁸⁸ (**Figure 46B**). Accordingly, when this residue was mutated to glutamine (Q58), binding was omitted, although the mutation did not affect folding of the protein. Several other interactions support the stabilization of the binding pocket, for instance, the tyrosine residue at position 59 (Y59) which allows hydrophobic contacts with the inositol ring of PI(3)P (**Figure 46B**). Based on these interactions it is rather surprising that protein-lipid interactions were not observed in the mass spectrum obtained under native gas phase conditions. In particular, because earlier studies on peripheral proteins associated with nanodiscs showed that protein interactions with glycolipids are preserved in the gas phase by MS²⁸⁹.

Accordingly, we assume that the main reason for the loss of protein-lipid interactions is that p40^{phox} binding to the membrane is mediated by the specific binding to PI(3)P lipids. As the composition of PI(3)P lipids in the liposomes in our experiments is generally low (1%), we suspect that p40^{phox} does not sufficiently bind

to the liposomes to reveal protein-lipid signals in the mass spectrum. In addition, as lipid signals generally have a higher ionization efficiency in our experiments, signals for protein-lipid complexes are presumably suppressed and, therefore, might be below the detection limit. In addition, as only a few lipids mediate binding of p40^{phox} to liposomes this might also be the reason why less interactions are maintained under native gas phase conditions. In addition, we further assume that the weak binding of p40^{phox} to the membrane described in a previous experiment¹⁸⁵ and liposome rearrangement in the gas phase described before could be the reason why protein-lipid interactions are lost during mass spectrometric analysis.

To however detect protein-lipid interactions in the gas phase, p40^{phox} binding to the liposomes must be adjusted. Accordingly, additional experiments would be beneficial. To increase binding of p40^{phox}, liposomes containing a higher PI(3)P concentration can be prepared. However, note that previous studies showed that p40^{phox} only sufficiently binds as long as the association with the phospholipid bilayer is not disturbed by steric hinderance²¹⁴. Similarly, studies on the peripheral protein cytochrome c described that cardiolipin binding could also not be observed under native gas phase conditions²⁹⁰, suggesting that the study of protein-lipid interactions of peripheral membrane proteins is challenging due to their transient nature²³³. Nevertheless, in this study protein-lipid interactions were confirmed by ion mobility MS²⁹⁰.

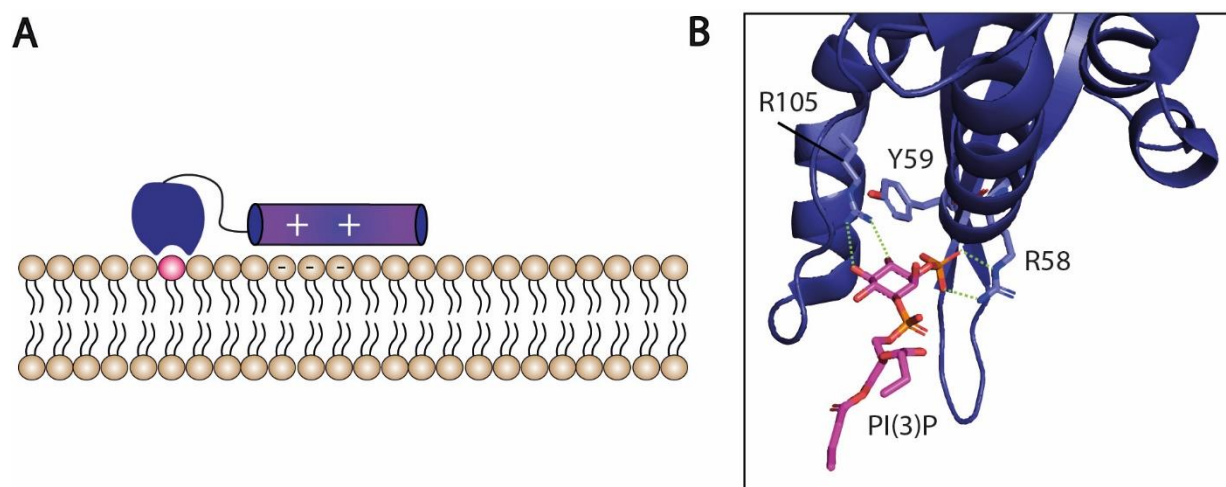


Figure 46: P40^{phox} interactions and p40^{phox} binding pocket. (A) p40^{phox} associates with the membrane through non-specific electrostatic interactions with anionic lipids and through ionic interactions with the PI(3)P headgroup. (B) A detailed representation of the PI(3)P-binding pocket. Interacting residues are drawn as sticks and interactions are shown in dashed lines. The inositol ring of PI(3)P allows hydrophobic contacts with the side chain of tyrosine at position 59 (Y59). Arginine residues 58 and 105 (R58 and R105) form interactions to the headgroup of PI(3)P. PDB ID: 1H6H

To conclude, although we were not able to sufficiently preserve protein-lipid interactions of p40^{phox}, we could show that liposomes dissociate under denaturing and native gas phase conditions and the protein is sufficiently released in its folded conformation. Accordingly, we were able to demonstrate that liposomes are applicable for the mass spectrometric analysis of membrane-associated proteins in their native environment.

Protein-lipid interactions of Melittin

In this thesis, Melittin was used to further demonstrate the application of liposomes for the analysis of membrane-associated peptides/proteins by MS. Again, Melittin-proteoliposomes were studied under denaturing and native gas phase conditions. The mass spectra revealed oligomers of Melittin and importantly, Melittin-lipid interactions. However, due to conflicting views on the physical state of Melittin, which were previously described, the question remains how Melittin associates with biological membranes.

The literature described that Melittin, in the presence of lipids, adopts an alpha-helical conformation, which is either oriented parallel or perpendicular to the membrane plane. Accordingly, a two-step model for pore formation of Melittin was proposed, in which Melittin binds parallel to the membrane at low concentrations and shifts towards the perpendicular orientation at higher concentrations, initiating pore formation^{221,291} (**Figure 47A**). It should be noted that the transition states from parallel to perpendicular orientation are not yet fully understood and previous studies suggest that pore formation depends on the protein-to-lipid ratio²²⁶.

With the protein-to-lipid ratio used in this thesis, we were able to show by flotation analysis that Melittin, for instance, associates with liposomes resembling a eukaryotic membrane composition (**Figure 25B**). Melittin-proteoliposomes analyzed by MS under denaturing gas phase conditions then revealed, as expected, signals for monomeric Melittin since non-covalent interactions of Melittin are lost in the gas phase (**Figure 28A**). Surprisingly, however, Melittin-lipid interactions were preserved under denaturing gas phase conditions, indicating that these interactions are stable enough to survive the transition from solution to the gas phase. Based on these observations, we, therefore, assume that electrostatic interactions are formed between the lipid headgroups and the amino acid side chains of Melittin (see also above).

Flotation analysis (**Figure 25B**) and native MS analysis (**Figure 28B**) of Melittin-proteoliposomes revealed oligomeric states of Melittin. Interestingly, however, as different oligomeric states of Melittin are detected in our experiments, we suggest that pore formation is not yet complete. Accordingly, we assume that the observed non-specific oligomers are intermediate states of Melittin pore formation. In addition, native MS analysis of Melittin-proteoliposomes showed monomeric Melittin interacting with one lipid molecule,

suggesting that amino acid residues mediating protein-lipid interactions are most likely not accessible in oligomeric structures.

Melittin is hydrophobic by nature, except for three residues (Arg-Lys-Arg) near the C-terminal region which are considered hydrophilic²⁹² (**Figure 47B**). Accordingly, Melittin can associate with the phospholipid bilayer of liposomes. In our MS experiments, protein-lipid interactions were observed between Melittin and zwitterionic lipids or zwitterionic lyso-lipids (lyso-DOPE and lyso-DOPC), however, interactions between Melittin and DOPS or lyso-PS lipids were not detected. To further investigate Melittin binding to different lipids, additional flotation assay (**Figure 31**) and monolayer measurements were, therefore, performed (**Figure 32**). Accordingly, Melittin does not sufficiently bind and penetrate phospholipid membranes containing anionic lipids. This agrees with our MS experiments, which showed that Melittin has a strong affinity for zwitterionic lipids, but not for anionic lipids (**Figure 28B**). As Melittin binding to anionic or zwitterionic lipids was previously controversially discussed^{216,227,228,269} we, therefore, assume based on our experiments, that Melittin presumably interacts with anionic lipids, however, stable associates with zwitterionic lipids.

When comparing the mass spectra of Melittin-proteoliposomes obtained under denaturing and native gas phase conditions, more lipids bind to monomeric Melittin under denaturing gas phase conditions, suggesting that potential unfolding of the protein in the gas phase leads to additional binding of lipids in close proximity. Nevertheless, it is important to note that the Q Exactive mass spectrometer which is not modified, does not maintain protein-lipid interactions in the gas phase.

Previous studies showed that cholesterol reduces the association of Melittin with liposomes, as cholesterol has a condensing effect on the phospholipid bilayer of membranes²⁹³. However, in this thesis, we did not observe reduced binding of Melittin to liposomes resembling a eukaryotic membrane composition containing cholesterol (**Figure 15**). Interestingly, when using Melittin-proteoliposomes resembling a prokaryotic membrane composition, fewer interactions were detected by MS (**Figure 29**). Previous studies showed that the PE headgroup reduces bilayer stiffness and increases curvature stress compared to other lipids²⁹⁴. Since prokaryotic membranes are mainly composed of PE lipids²⁹⁵, their smaller headgroup presumably leads to an altered curvature resulting in a lower binding affinity of Melittin suggesting that fewer lipid interactions are preserved in the gas phase. Furthermore, protein-lipid interactions were only detected between the Melittin monomer and lyso-lipids. Since all lipids were cleaved by phospholipase A2 we assume that the lipids of Melittin-proteoliposomes resembling a prokaryotic membrane composition are more accessible to phospholipase A2.

In conclusion, these experiments show that liposomes are promising tools for the structural analysis of membrane-associated proteins by MS. In future experiments, MS studies on proteoliposomes containing integral membrane proteins or membrane complexes are considered. However, one should keep in mind that higher collision energies are possibly required to release an integral membrane protein into the gas phase and the native structures of the proteins may not be sufficiently preserved. Moreover, since lipid signals have a higher ionization efficiency compared to proteins in ESI MS experiments, protein signals and signals of protein-lipid interactions could also be below the detection limit making interpretation of the mass spectra difficult.

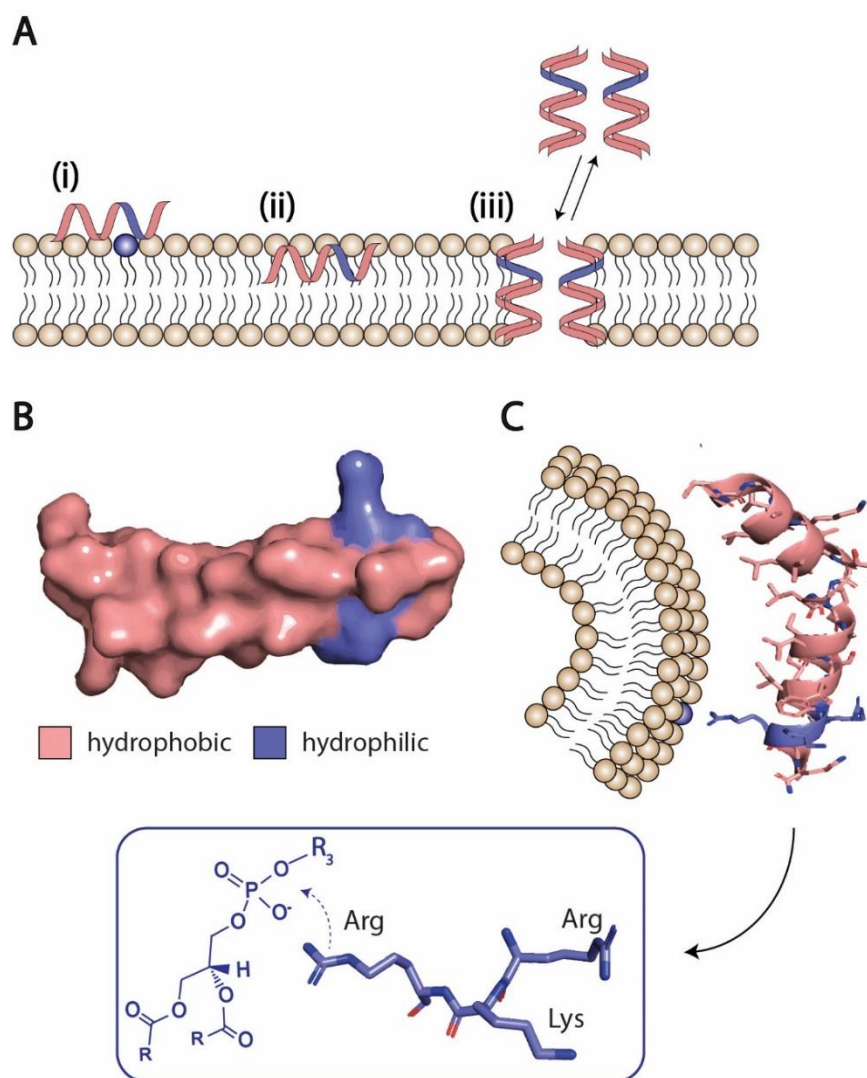


Figure 47: Melittin association with the membrane. (A) Mechanism of Melittin pore formation. (i) Melittin associates with the membrane through electrostatic interactions with anionic lipids. (ii) Melittin inserts into the membrane. (iii) The membrane pore is formed. (B) Hydrophobic (light pink) and hydrophilic (light purple) regions of Melittin. (C) Detailed picture of hydrophilic arginine and lysine residues Melittin interacting with anionic lipids of liposomes.

5.3 Establishing nanodiscs for the analysis of protein-protein interactions

5.3.1 Selection of nanodiscs as membrane mimetics

Classical nanodiscs are disc-shaped lipid bilayers surrounded by a belt of two MSPs⁶⁰. In the past, nanodiscs have been extensively studied using biophysical methods for the structural analysis of membrane proteins^{137,184,241,296}. Although nanodiscs do not perfectly mimic natural membranes, they are advantageous in that their size and lipid content can be controlled by varying the lipid composition and the length of the MSP. Accordingly, previous studies showed that large membrane protein complexes can be successfully reconstituted into nanodiscs¹³⁷. Most importantly, nanodiscs preserve membrane protein integrity and shape⁵⁹, making them particularly advantageous for the analysis of membrane proteins, which are generally unstable.

The use of MSP nanodiscs is usually limited by the need for detergents required for nanodisc assembly which affects the native state of membrane proteins²⁴¹. Furthermore, not all lipid combinations form bilayers that assemble into nanodiscs. In addition, since both sides of nanodiscs are accessible, transport experiments are not possible. In this work, MSP nanodiscs were established to investigate the structure of membrane proteins in their native lipid environment by chemical cross-linking MS. Since the aim was to perform cross-linking experiments on a protein anchored to the lipid membrane, there was no need for transport studies. In addition, the detergent was removed during nanodisc preparation, resulting in a stable lipid environment for membrane proteins. Although previous experiments showed that nanodiscs are promising tools for the structural analysis of proteins and their lipid interactions by native MS^{137,268,297}, chemical cross-linking of membrane proteins to allow their structural investigation in their native lipid environment has not yet been established. Accordingly, we used nanodiscs as they are stable, can be adapted to the protein of interest and previously allowed sufficient structure determination of the membrane proteins in their native environment.

To date, chemical cross-linking is one of the methods of choice to study membrane protein interactions. In particular, in-cell cross-linking allows capturing protein-protein interactions in a native cellular environment^{298,299}. However, these studies are mostly complex and data analysis is difficult. In this thesis, we, therefore, established a simplified approach using nanodiscs to capture the structural properties of membrane proteins in the presence of lipids.

5.3.2 Methodological aspects - Chemical cross-linking of nanodiscs

In these experiments, we analyzed Syntaxin-1A reconstituted into nanodiscs by chemical crosslinking MS. Syntaxin-1A belongs to the SNARE proteins, which are regulatory proteins involved in neuronal exocytosis. Syntaxin-1A consists of a SNARE motif and a neighboring transmembrane helix. In addition, Syntaxin-1A also contains a Habc domain, which is potentially involved in regulating Syntaxin-1A SNARE activity²⁵⁰. Syntaxin-1A was mainly chosen as a model protein as it is well-suited for chemical cross-linking. Accordingly, as Syntaxin-1A is a membrane-anchored protein containing soluble domains, it allows incorporation into the nanodiscs while also providing residues accessibility for chemical cross-linking reagents. In addition, the Habc domain is folded, allowing possible cross-links to be verified with previously described crystal structures. Moreover, from a biological point of view, Syntaxin-1A is an important target for structural biology, as SNARE protein complex assembly and fusion mechanisms are not yet fully understood. By establishing a cross-linking workflow for the analysis of SNARE proteins reconstituted into nanodiscs insights into membrane fusion are potentially gained.

For establishing a nanodisc workflow for the structural analysis of Syntaxin-1A by chemical cross-linking MS, we used a lipid composition that is closely related to the composition found in plasma membranes¹⁹. However, note that cholesterol, even though present in plasma membranes, was omitted in these studies, as previous experiments showed that nanodisc-assembly is more difficult with cholesterol-containing lipid mixtures²³⁹.

In this thesis, BS3 was used for chemical cross-linking of a protein reconstituted into nanodiscs. Previous studies showed that BS3 successfully crosslinks amine-reactive groups of proteins¹⁶⁴. However, cross-linking with BS3 also has drawbacks: We assume that in our experiments BS3 does not only cross-link the amine-reactive groups of our target protein. Accordingly, we suggest that cross-linking reactions between the MSP of the nanodiscs and lipids, containing an ethanolamine headgroup are also possible. Accordingly, lipid cross-links potentially limit the detection of protein-protein interactions. Note that, although BS3 cross-links between lipids and proteins were previously described³⁰⁰, an unambiguous analysis of lipid-lipid cross-links has not yet been possible. Moreover, additional side reactions between lysine, threonine and serine side chains might also lead to a highly complex mixture of cross-linked species.

In addition, the BS3 reaction is also buffer sensitive. Accordingly, ammonium acetate usually used for MS analysis leads to quenching of BS3. This must also be considered during sample preparation. With these limitations in mind, in this thesis, a higher concentration of 30 mM was, accordingly, used for chemical cross-linking of nanodiscs and nanodiscs and proteins were prepared in HEPES buffer to avoid quenching of the cross-linker.

For chemical cross-linking of Syntaxin-1A nanodiscs we applied a previously established cross-linking workflow in which low abundant cross-links were enriched using size exclusion chromatography and data analysis was performed using the software plink2.

5.3.3 Biological aspects - Chemical cross-linking of Syntaxin-1A in nanodiscs

The identification and characterization of the SNARE protein assembly pathway have been of great interest in previous studies. The applied cross-linking strategy of Syntaxin-1A reconstituted in nanodiscs revealed protein interactions of Syntaxin-1A in a native-like lipid environment.

Chemical cross-linking of Syntaxin-1A nanodiscs allowed the identification of intra-molecular cross-links within Syntaxin-1A. However, these cross-links may also be intermolecular, as the different peptides may originate from two copies of the same protein. Accordingly, the observed cross-links can originate from one or two Syntaxin-1A molecules. Previous studies described Syntaxin-1A trimers³⁰¹. In this thesis, gel electrophoresis also revealed protein bands, presumably corresponding to protein dimers and trimers (**Figure 40**). As MSP1E3D1 is known to only form dimers, we, therefore, assume that the trimer protein band corresponds to Syntaxin-1A. However, note that Syntaxin-1A and MSP have similar molecular weights and a clear assignment of the dimers is, therefore, only possible by additional western blot analysis.

Previous experiments with single-molecule multiparameter fluorescence detection assumed that free Syntaxin-1 is in a dynamic equilibrium between the closed and the open conformation and proteins mediating the open or closed conformation were also described²⁴⁵. For instance, binding of SNAP-25 with Munc-13 allows Syntaxin-1A to change into the open conformation, whereas in the presence of Munc18-1, Syntaxin-1A exists in a closed conformation. In the closed conformation, the Habc domain is bound to the SNARE motif, resulting in a four-helix bundle (**Figure 48A**). However, it should be noted that only the open conformation can promote the formation of the SNARE complex and thus membrane fusion.

The intra-molecular cross-links were predominantly observed in the Habc domain of Syntaxin-1A, which is connected to the SNARE motif via a flexible linker region (**Figure 44**). However, it should be noted that the dynamic equilibrium changes very rapidly and cross-links reflecting open and closed conformation are most likely not detected. As only a low number of lysine residues is present in the SNARE motif limited BS3 cross-links are possible. This agrees with our observations, that no cross-links within the SNARE motif were detected. In addition, cross-links were also not observed in the transmembrane domain of Syntaxin-1A, as this region does not contain any lysine, serine or threonine residues.

Finally, intermolecular interactions were observed between Syntaxin-1A and MSP1E3D1. The cross-links were mainly observed between MSP1E3D1 and the Habc domain or the SNARE motif of Syntaxin-1A. The interactions suggest that Syntaxin-1A has a highly dynamic linker region and that the dynamic change results in different cross-links in close proximity (**Figure 48B**).

Interestingly, only a few cross-links were found for Syntaxin-1A, although a high concentration of cross-linker was used. We, therefore, assume that the cross-links were indeed suppressed by undesired side reactions and quenching. As mentioned above, the amine-reactive crosslinker BS3 also crosslinks amine-groups of DOPE lipids or MSP. Note that, in the experiments of this thesis, empty nanodiscs have not yet been separated from nanodiscs containing Syntaxin-1A. However, to ensure better cross-linking efficiencies in the future separation of nanodiscs containing the protein of interest is highly recommended. For this, Syntaxin-1A nanodiscs containing a His-tag should be purified by IMAC. Control experiments with empty nanodiscs should also be performed. By analyzing empty nanodiscs and generating an exclusion list, cross-links of MSP can then successfully be excluded.

In summary, these initial experiments show that nanodiscs are a valuable tool for the analysis of membrane proteins through chemical cross-linking. However, to use nanodiscs for cross-linking studies in the future, additional experiments are still needed. Nevertheless, cross-linking of protein complexes in nanodiscs could potentially allow studying, for instance, SNARE proteins.

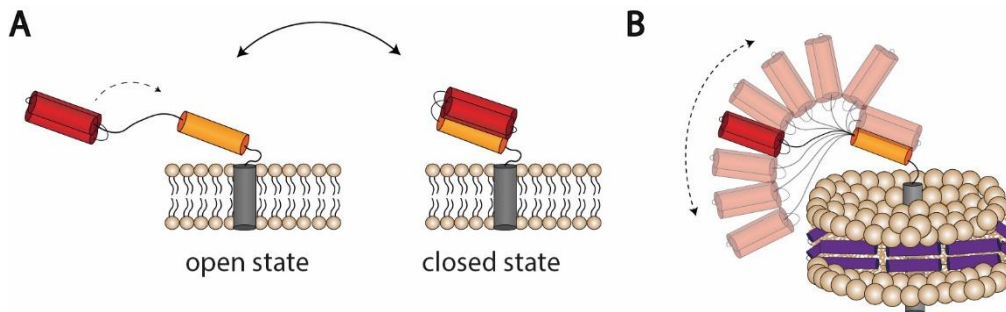


Figure 48: Dynamics of Syntaxin-1A in nanodiscs. (A) Syntaxin-1A is a membrane-anchored protein containing a SNARE motif (yellow) and a Habc domain (red) which undergoes an open-to-closed transition. (B) Syntaxin-1A incorporated into nanodiscs is flexible due to the highly dynamic Habc domain.

6 References

1. Simkiss, K. Cell membranes; barriers, regulators and transducers? in *Comparative Biochemistry and Physiology - A Molecular and Integrative Physiology* **120**, 17–22 (Elsevier Inc., 1998).
2. Guidotti, G. Membrane Proteins. *Annu. Rev. Biochem.* **41**, 731–752 (1972).
3. Singer, S. J. & Nicolson, G. L. *No Title. Science (New York, N.Y.)* **175**, 720–31 (American Association for the Advancement of Science, 1972).
4. Pike, L. J. Lipid rafts: Bringing order to chaos. *Journal of Lipid Research* **44**, 655–667 (2003).
5. Simons, K. & Sampaio, J. L. Membrane organization and lipid rafts. *Cold Spring Harb. Perspect. Biol.* **3**, a004697 (2011).
6. Ishitsuka, R. Imaging Lipid Rafts. *J. Biochem.* **137**, 249–254 (2005).
7. Alberts, B. *et al. Molecular Biology of the Cell. 4th Edition, New York* (2002). doi:10.1091/mbc.E14-10-1437
8. Lee, A. G. How lipids affect the activities of integral membrane proteins. *Biochim. Biophys. Acta - Biomembr.* **1666**, 62–87 (2004).
9. Bienvenüe, A. & Marie, J. Sainte. Modulation of Protein Function by Lipids. *Curr. Top. Membr.* **40**, 319–354 (1994).
10. Hentschel, A., Zahedi, R. P. & Ahrends, R. Protein lipid modifications-More than just a greasy ballast. *Proteomics* **16**, 759–782 (2016).
11. Spiro, R. G. Glycoproteins. *Adv. Protein Chem.* **27**, 349–467 (1973).
12. Quick, M. & Javitch, J. A. Monitoring the function of membrane transport proteins in detergent-solubilized form. *Proc. Natl. Acad. Sci. U. S. A.* **104**, 3603–3608 (2007).
13. Arcizet, D., Meier, B., Sackmann, E., Rädler, J. O. & Heinrich, D. Temporal analysis of active and passive transport in living cells. *Phys. Rev. Lett.* **101**, (2008).
14. Zeuthen, T. Molecular Mechanisms for Passive and Active Transport of Water. *Int. Rev. Cytol.* **160**, 99–161 (1995).
15. Collinson, I. The Dynamic ATP-Driven Mechanism of Bacterial Protein Translocation and the Critical Role of Phospholipids. *Front. Microbiol.* **10**, 1217 (2019).
16. Cournia, Z. *et al. Membrane Protein Structure, Function, and Dynamics: a Perspective from Experiments and Theory. J. Membr. Biol.* **248**, 611–40 (2015).
17. Janmey, P. Chapter 17 Cell membranes and the cytoskeleton. in *Handbook of Biological Physics* **1**, 805–849 (Elsevier, 1995).
18. Watson, H. Biological membranes. *Essays Biochem.* **59**, 43–69 (2015).
19. van Meer, G., Voelker, D. R. & Feigenson, G. W. Membrane lipids: where they are and how they behave. *Nat. Rev. Mol. Cell Biol.* **9**, 112–24 (2008).
20. Harayama, T. & Riezman, H. Understanding the diversity of membrane lipid composition. *Nat. Rev. Mol. Cell Biol.* **19**, 281–296 (2018).

21. Quinn, P. J., Joo, F. & Vigh, L. The role of unsaturated lipids in membrane structure and stability. *Progress in Biophysics and Molecular Biology* **53**, 71–103 (1989).
22. Cullis, P. R., Fenske, D. B. & Hope, M. J. Chapter 1 - Physical properties and functional roles of lipids in membranes. in *Biochemistry of Lipids, Lipoproteins and Membranes* (eds. Vance, D. E. & Vance, J. E. B. T.-N. C. B.) **31**, 1–33 (Elsevier, 1996).
23. Yamakawa, T. & Nagai, Y. Glycolipids at the cell surface and their biological functions. *Trends Biochem. Sci.* **3**, 128–131 (1978).
24. Holdt, S. L. & Kraan, S. Bioactive compounds in seaweed: Functional food applications and legislation. *Journal of Applied Phycology* **23**, 543–597 (2011).
25. Simons, K. & Ehehalt, R. Cholesterol, lipid rafts, and disease. *J. Clin. Invest.* **110**, 597–603 (2002).
26. Gibson Wood, W., Igbavboa, U., Müller, W. E. & Eckert, G. P. Cholesterol asymmetry in synaptic plasma membranes. *J. Neurochem.* **116**, 684–689 (2011).
27. Nyholm, T. K. M. Lipid-protein interplay and lateral organization in biomembranes. *Chemistry and Physics of Lipids* **189**, 48–55 (2015).
28. Kreuzberger, A. J. B. *et al.* Asymmetric Phosphatidylethanolamine Distribution Controls Fusion Pore Lifetime and Probability. *Biophys. J.* **113**, 1912–1915 (2017).
29. Verkleij, A. J. *et al.* The asymmetric distribution of phospholipids in the human red cell membrane. A combined study using phospholipases and freeze-etch electron microscopy. *BBA - Biomembr.* **323**, 178–193 (1973).
30. van Meer, G. Dynamic transbilayer lipid asymmetry. *Cold Spring Harb. Perspect. Biol.* **3**, 1–11 (2011).
31. Escribá, P. V *et al.* Membranes: a meeting point for lipids, proteins and therapies. *J. Cell. Mol. Med.* **12**, 829–75 (2008).
32. E Sackmann & Sackmann E. Physical basis of trigger processes and membrane structures. *Biol. Membr. Academic P*, (1984).
33. Lee, A. . Annular events: lipid-protein interactions. *Trends Biochem.* **2**, 231–233 (1977).
34. Palsdottir, H. & Hunte, C. Lipids in membrane protein structures. *Biochim. Biophys. Acta - Biomembr.* **1666**, 2–18 (2004).
35. East, J. M., Melville, D. & Lee, A. G. Exchange rates and numbers of annular lipids for the calcium and magnesium ion dependent adenosine triphosphatase. *Biochemistry* **24**, 2615–2623 (1985).
36. Marsh, D. & Horváth, L. I. Structure, dynamics and composition of the lipid-protein interface. Perspectives from spin-labelling. *Biochim. Biophys. Acta - Rev. Biomembr.* **1376**, 267–296 (1998).
37. Grigorieff, N., Ceska, T. A., Downing, K. H., Baldwin, J. M. & Henderson, R. Electron-crystallographic Refinement of the Structure of Bacteriorhodopsin. *J. Mol. Biol.* **259**, 393–421 (1996).
38. Shinzawa-Itoh, K. *et al.* Structures and physiological roles of 13 integral lipids of bovine heart cytochrome c oxidase. *EMBO J.* **26**, 1713–25 (2007).
39. Tsukihara, T. *et al.* The whole structure of the 13-subunit oxidized cytochrome c oxidase at 2.8 Å. *Science* **272**, 1136–44 (1996).

40. Yeagle, P. L. Non-covalent binding of membrane lipids to membrane proteins. *Biochimica et Biophysica Acta - Biomembranes* **1838**, 1548–1559 (2014).
41. Contreras, F. X., Ernst, A. M., Wieland, F. & Brügger, B. Specificity of intramembrane protein-lipid interactions. *Cold Spring Harb. Perspect. Biol.* **3**, 1–18 (2011).
42. Hunte, C., Palsdottir, H. & Trumppower, B. L. Protonmotive pathways and mechanisms in the cytochrome bc1 complex. *FEBS Lett.* **545**, 39–46 (2003).
43. Garavito, R. M. & Ferguson-Miller, S. Detergents as Tools in Membrane Biochemistry. *Journal of Biological Chemistry* **276**, 32403–32406 (2001).
44. Raschle, T., Hiller, S., Eitzkorn, M. & Wagner, G. Membrane Proteins. **20**, 471–479 (2011).
45. Yang, Z. *et al.* Membrane protein stability can be compromised by detergent interactions with the extramembranous soluble domains. *Protein Sci.* **23**, 769–789 (2014).
46. Seddon, A. M., Curnow, P. & Booth, P. J. Membrane proteins, lipids and detergents: not just a soap opera. *Biochim. Biophys. Acta* **1666**, 105–117 (2004).
47. Privé, G. G. Detergents for the stabilization and crystallization of membrane proteins. doi:10.1016/j.ymeth.2007.01.007
48. Vestergaard, M., Kraft, J. F., Vosegaard, T., Thøgersen, L. & Schiøtt, B. Bicelles and Other Membrane Mimics: Comparison of Structure, Properties, and Dynamics from MD Simulations. *J. Phys. Chem. B* **119**, 15831–15843 (2015).
49. Hopper, J. T. S. *et al.* Detergent-free mass spectrometry of membrane protein complexes. *Nat. Methods* **10**, 1206–1208 (2013).
50. Akbarzadeh, A., Rezaei-sadabady, R., Davaran, S., Joo, S. W. & Zarghami, N. Liposome : classification , preparation , and applications. *Nanoscale Res. Lett.* **8**, 1 (2013).
51. Rigaud, J. L. & Lévy, D. Reconstitution of Membrane Proteins into Liposomes. *Methods Enzymol.* **372**, 65–86 (2003).
52. Shen, H.-H., Lithgow, T. & Martin, L. L. Reconstitution of Membrane Proteins into Model Membranes: Seeking Better Ways to Retain Protein Activities. *OPEN ACCESS Int. J. Mol. Sci* **14**, 14 (2013).
53. Zhang, H. Thin-film hydration followed by extrusion method for liposome preparation. in *Methods in Molecular Biology* **1522**, 17–22 (Humana Press Inc., 2017).
54. Jesorka, A. & Orwar, O. Liposomes: Technologies and analytical applications. *Annual Review of Analytical Chemistry* **1**, 801–832 (2008).
55. Walde, P., Cosentino, K., Engel, H. & Stano, P. Giant Vesicles: Preparations and Applications. *ChemBioChem* **11**, 848–865 (2010).
56. Quemeneur, F., Rinaudo, M., Maret, G. & Pépin-Donat, B. Decoration of lipid vesicles by polyelectrolytes: Mechanism and structure. *Soft Matter* **6**, 4471–4481 (2010).
57. Rigaud, J.-L. Membrane proteins: functional and structural studies using reconstituted proteoliposomes and 2-D crystals. *Brazilian J. Med. Biol. Res.* **35**, 753–766 (2002).
58. Tunuguntla, R. *et al.* Lipid bilayer composition can influence the orientation of proteorhodopsin in artificial membranes. *Biophys. J.* **105**, 1388–1396 (2013).

59. Denisov, I. G. & Sligar, S. G. Nanodiscs for structural and functional studies of membrane proteins. *Nat. Struct. Mol. Biol.* **23**, 481–6 (2016).
60. Bayburt, T. H., Grinkova, Y. V. & Sligar, S. G. Self-Assembly of Discoidal Phospholipid Bilayer Nanoparticles with Membrane Scaffold Proteins. *Nano Lett.* **2**, 853–856 (2002).
61. Hagn, F., Etzkorn, M., Raschle, T. & Wagner, G. Optimized phospholipid bilayer nanodiscs facilitate high-resolution structure determination of membrane proteins. *J. Am. Chem. Soc.* **135**, 1919–1925 (2013).
62. Flayhan, A. *et al.* Saposin Lipid Nanoparticles: A Highly Versatile and Modular Tool for Membrane Protein Research. *Structure* **26**, 345–355.e5 (2018).
63. Zhou, F. *et al.* Footprinting Mass Spectrometry of Membrane Proteins: Ferroportin Reconstituted in Saposin A Picodiscs. *Cite This Anal. Chem* **93**, 11370–11378 (2021).
64. Dörr, J. M. *et al.* The styrene–maleic acid copolymer: a versatile tool in membrane research. *Eur. Biophys. J.* **45**, 3–21 (2016).
65. Jamshad, M. *et al.* Surfactant-free purification of membrane proteins with intact native membrane environment. *Biochem. Soc. Trans.* **39**, 813 LP – 818 (2011).
66. Knowles, T. J. *et al.* Membrane Proteins Solubilized Intact in Lipid Containing Nanoparticles Bounded by Styrene Maleic Acid Copolymer. *J. Am. Chem. Soc.* **131**, 7484–7485 (2009).
67. Simon, K. S., Pollock, N. L. & Lee, S. C. Membrane protein nanoparticles: the shape of things to come. *Biochem. Soc. Trans.* **46**, 1495–1504 (2018).
68. Mueller, P. K. & Givens, R. G. Dynamic Calibration and Data Interpretation of Light-Scattering Instrument. *J. Air Pollut. Control Assoc.* **11**, 576–584 (2012).
69. Cummins, H. Z., Knable, N. & Yeh, Y. Observation of diffusion broadening of rayleigh scattered light. *Phys. Rev. Lett.* **12**, 150–153 (1964).
70. Lorber, B., Fischer, F., Bailly, M., Roy, H. & Kern, D. Protein analysis by dynamic light scattering: Methods and techniques for students. *Biochem. Mol. Biol. Educ.* **40**, 372–382 (2012).
71. Falke, S. & Betzel, C. Dynamic Light Scattering (DLS). in *Radiation in Bioanalysis* **8**, 173–193 (Nature Publishing Group, 2019).
72. Brenner, S. & Horne, R. W. A negative staining method for high resolution electron microscopy of viruses. *BBA - Biochim. Biophys. Acta* **34**, 103–110 (1959).
73. Thompson, R. F., Walker, M., Siebert, C. A., Muench, S. P. & Ranson, N. A. An introduction to sample preparation and imaging by cryo-electron microscopy for structural biology. *Methods* **100**, 3–15 (2016).
74. De Carlo, S. & Harris, J. R. Negative staining and cryo-negative staining of macromolecules and viruses for TEM. *Micron* **42**, 117–131 (2011).
75. Harris, J. R. & De Carlo, S. Negative staining and cryo-negative staining: Applications in biology and medicine. *Methods Mol. Biol.* **1117**, 215–258 (2014).
76. Lyons, J. A., Bøggild, A., Nissen, P. & Frauenfeld, J. Saposin-Lipoprotein Scaffolds for Structure Determination of Membrane Transporters. in *Methods in enzymology* **594**, 85–99 (2017).
77. Winey, M., Meehl, J. B., O’Toole, E. T. & Giddings, T. H. Conventional transmission electron microscopy. *Molecular Biology of the Cell* **25**, 319–323 (2014).

78. Contreras, F.-X., Ernst, A. M., Wieland, F. & Brügger, B. Specificity of intramembrane protein-lipid interactions. *Cold Spring Harb. Perspect. Biol.* **3**, (2011).
79. Calabrese, A. N. & Radford, S. E. Mass spectrometry-enabled structural biology of membrane proteins. *Methods* **147**, 187–205 (2018).
80. Smith, R., Mathis, A. D., Ventura, D. & Prince, J. T. Proteomics, lipidomics, metabolomics: A mass spectrometry tutorial from a computer scientist's point of view. *BMC Bioinformatics* **15**, S9 (2014).
81. Barrera, N. P. & Robinson, C. V. Advances in the Mass Spectrometry of Membrane Proteins: From Individual Proteins to Intact Complexes. *Annu. Rev. Biochem.* **80**, 247–271 (2011).
82. Landreh, M. & Robinson, C. V. A new window into the molecular physiology of membrane proteins. *J. Physiol.* **593**, 355–362 (2015).
83. Erba, E. B. & Petosa, C. The emerging role of native mass spectrometry in characterizing the structure and dynamics of macromolecular complexes. *Protein Sci.* **24**, 1176–1192 (2015).
84. Yamashita, M. & Fenn, J. B. Electrospray ion source. Another variation on the free-jet theme. *J. Phys. Chem.* **88**, 4451–4459 (1984).
85. Smith, R. D., Loo, J. A., Edmonds, C. G., Barinaga, C. J. & Udseth, H. R. New Developments in Biochemical Mass Spectrometry: Electrospray Ionization. *Anal. Chem.* **62**, 882–899 (1990).
86. Wu, X., Oleschuk, R. D. & Cann, N. M. Characterization of microstructured fibre emitters: In pursuit of improved nano electrospray ionization performance. *Analyst* **137**, 4150–4161 (2012).
87. Rayleigh, Lord. XX. On the equilibrium of liquid conducting masses charged with electricity . *London, Edinburgh, Dublin Philos. Mag. J. Sci.* **14**, 184–186 (1882).
88. Iribarne, J. V & Thomson, B. A. On the evaporation of small ions from charged droplets. *J. Chem. Phys.* **64**, 2287–2294 (1976).
89. Dole, M. *et al.* Molecular Beams of Macroions. *J. Chem. Phys.* **49**, 2240–2249 (1968).
90. Konermann, L. & Douglas, D. J. Unfolding of proteins monitored by electrospray ionization mass spectrometry: A comparison of positive and negative ion modes. *J. Am. Soc. Mass Spectrom.* **9**, 1248–1254 (1998).
91. Benesch, J. L. P., Ruotolo, B. T., Simmons, D. A. & Robinson, C. V. Protein Complexes in the Gas Phase: Technology for Structural Genomics and Proteomics. *Chem. Rev.* **107**, 3544–3567 (2007).
92. Fernandez de la Mora, J. Electrospray ionization of large multiply charged species proceeds via Dole's charged residue mechanism. *Anal. Chim. Acta* **406**, 93–104 (2000).
93. Shevchenko, A., Wilm, M., Vorm, O. & Mann, M. Mass spectrometric sequencing of proteins from silver-stained polyacrylamide gels. *Anal. Chem.* **68**, 850–858 (1996).
94. Michalski, A. *et al.* Mass Spectrometry-based Proteomics Using Q Exactive, a High-performance Benchtop Quadrupole Orbitrap Mass Spectrometer. *Mol. Cell. Proteomics* **10**, M111.011015 (2011).
95. Wolff, M. M. & Stephens, W. E. A pulsed mass spectrometer with time dispersion. *Rev. Sci. Instrum.* **24**, 616–617 (1953).

96. Makarov, A. Electrostatic axially harmonic orbital trapping: A high-performance technique of mass analysis. *Anal. Chem.* **72**, 1156–1162 (2000).
97. Allen, J. S. An improved electron multiplier particle counter. *Rev. Sci. Instrum.* **18**, 739–749 (1947).
98. Tremsin, A. S. *et al.* High-resolution strain mapping through time-of-flight neutron transmission diffraction with a microchannel plate neutron counting detector. *Strain* **48**, 296–305 (2012).
99. Glish, G. L. & Burinsky, D. J. Hybrid Mass Spectrometers for Tandem Mass Spectrometry. *J. Am. Soc. Mass Spectrom.* **19**, 161–172 (2008).
100. Jennings, K. R. Collision-induced decompositions of aromatic molecular ions. *Int. J. Mass Spectrom. Ion Phys.* **1**, 227–235 (1968).
101. Olsen, J. V. *et al.* Higher-energy C-trap dissociation for peptide modification analysis. *Nat. Methods* **4**, 709–712 (2007).
102. Syka, J. E. P., Coon, J. J., Schroeder, M. J., Shabanowitz, J. & Hunt, D. F. Peptide and protein sequence analysis by electron transfer dissociation mass spectrometry. *Proc. Natl. Acad. Sci. U. S. A.* **101**, 9528–9533 (2004).
103. Zubarev, R. A., Kelleher, N. L. & McLafferty, F. W.) *Roepstorff, P.; Fohlman. McLafferty, F. W. Org. Mass Spectrom* **16**, (American Chemical Society, 1983).
104. Mitchell Wells, J. & McLuckey, S. A. B. T.-M. in E. Collision-Induced Dissociation (CID) of Peptides and Proteins. in *Biological Mass Spectrometry* **402**, 148–185 (Academic Press, 2005).
105. Fahy, E., Cotter, D., Sud, M. & Subramaniam, S. Lipid classification, structures and tools. *Biochim. Biophys. Acta - Mol. Cell Biol. Lipids* **1811**, 637–647 (2011).
106. Wu, Z., Shon, J. C. & Liu, K.-H. Mass Spectrometry-based Lipidomics and Its Application to Biomedical Research. *J. Lifestyle Med.* **4**, 17–33 (2014).
107. Brands, M., Gutbrod, P. & Dörmann, P. Lipid Analysis by Gas Chromatography and Gas Chromatography–Mass. in *Methods in Molecular Biology* **2295**, 43–57 (Humana Press Inc., 2021).
108. Cajka, T. & Fiehn, O. LC–MS-based lipidomics and automated identification of lipids using the LipidBlast in-silico MS/MS library. *Methods Mol. Biol.* **1609**, 149–170 (2017).
109. Han, X. & Gross, R. W. Shotgun lipidomics: multidimensional MS analysis of cellular lipidomes. *Expert Rev. Proteomics* **2**, 253–264 (2005).
110. Goto-Inoue, N., Hayasaka, T., Zaima, N. & Setou, M. Imaging mass spectrometry for lipidomics. *Biochimica et Biophysica Acta - Molecular and Cell Biology of Lipids* **1811**, 961–969 (2011).
111. Han, X. & Gross, R. W. Electrospray ionization mass spectroscopic analysis of human erythrocyte plasma membrane phospholipids. *Proc. Natl. Acad. Sci. U. S. A.* **91**, 10635–10639 (1994).
112. Wu, Z., Shon, J. C. & Liu, K.-H. Mass Spectrometry-based Lipidomics and Its Application to Biomedical Research. *J. lifestyle Med.* **4**, 17–33 (2014).
113. Li, A., Hines, K. M. & Xu, L. Lipidomics by HILIC-Ion Mobility-Mass Spectrometry. in *Methods in Molecular Biology* **2084**, 119–132 (Humana Press Inc., 2020).
114. Liebis, G. *et al.* Shorthand notation for lipid structures derived from mass spectrometry. *J. Lipid Res.* **54**, 1523–1530 (2013).

115. Sobott, F., Hernández, H., McCammon, M. G., Tito, M. A. & Robinson, C. V. A tandem mass spectrometer for improved transmission and analysis of large macromolecular assemblies. *Anal. Chem.* **74**, 1402–1407 (2002).
116. Gault, J. *et al.* High-resolution mass spectrometry of small molecules bound to membrane proteins. *Nat. Methods* **13**, 333–336 (2016).
117. Sharon, M. & Robinson, C. V. The Role of Mass Spectrometry in Structure Elucidation of Dynamic Protein Complexes. *Annu. Rev. Biochem.* **76**, 167–193 (2007).
118. Mehmood, S., Allison, T. M. & Robinson, C. V. Mass Spectrometry of Protein Complexes: From Origins to Applications. *Annu. Rev. Phys. Chem.* **66**, 453–474 (2015).
119. Konijnenberg, A., Butterer, A. & Sobott, F. Native ion mobility-mass spectrometry and related methods in structural biology. *Biochimica et Biophysica Acta - Proteins and Proteomics* **1834**, 1239–1256 (2013).
120. Barth, M. & Schmidt, C. Native mass spectrometry – a valuable tool in structural biology. *J. Mass Spectrom.* (2020). doi:10.1002/jms.4578
121. Marty, M. T. *et al.* Bayesian deconvolution of mass and ion mobility spectra: from binary interactions to polydisperse ensembles. *Anal. Chem.* **87**, 4370–6 (2015).
122. Morgner, N. & Robinson, C. V. Massign: An Assignment Strategy for Maximizing Information from the Mass Spectra of Heterogeneous Protein Assemblies. *Anal. Chem.* **84**, 2939–2948 (2012).
123. Jurchen, J. C. & Williams, E. R. Origin of asymmetric charge partitioning in the dissociation of gas-phase protein homodimers. *J. Am. Chem. Soc.* **125**, 2817–2826 (2003).
124. Reading, E. *et al.* The Role of the Detergent Micelle in Preserving the Structure of Membrane Proteins in the Gas Phase. *Angew. Chemie - Int. Ed.* **54**, 4577–4581 (2015).
125. Kundlacz, T., Bender, J. & Schmidt, C. Effects of non-ionic and zwitterionic detergents on soluble proteins during native mass spectrometry experiments. *Int. J. Mass Spectrom.* **468**, 116652 (2021).
126. Barrera, N. P. *et al.* Mass spectrometry of membrane transporters reveals subunit stoichiometry and interactions. *Nat. Methods* **6**, 585–587 (2009).
127. Hoffmann, J. *et al.* ATP synthases: Cellular nanomotors characterized by LILBID mass spectrometry. *Phys. Chem. Chem. Phys.* **12**, 13375–13382 (2010).
128. Zhou, M. *et al.* Mass spectrometry of intact V-type ATPases reveals bound lipids and the effects of nucleotide binding. *Science* **334**, 380–385 (2011).
129. Schmidt, C. *et al.* Comparative cross-linking and mass spectrometry of an intact F-type ATPase suggest a role for phosphorylation. *Nat. Commun.* **4**, 1985 (2013).
130. Schmidt, C. & Urlaub, H. Combining cryo-electron microscopy (cryo-EM) and cross-linking mass spectrometry (CX-MS) for structural elucidation of large protein assemblies. *Current Opinion in Structural Biology* **46**, 157–168 (2017).
131. Liko, I. *et al.* Dimer interface of bovine cytochrome c oxidase is influenced by local posttranslational modifications and lipid binding. *Proc. Natl. Acad. Sci. U. S. A.* **113**, 8230–5 (2016).

132. Housden, N. G. *et al.* Intrinsically disordered protein threads through the bacterial outer-membrane porin OmpF. *Science* (80-.). **340**, 1570–1574 (2013).
133. Landreh, M., Marty, M. T., Gault, J. & Robinson, C. V. A sliding selectivity scale for lipid binding to membrane proteins. *Curr. Opin. Struct. Biol.* **39**, 54–60 (2016).
134. Gupta, K. *et al.* Identifying key membrane protein lipid interactions using mass spectrometry. *Nat. Protoc.* **13**, 1106–1120 (2018).
135. Gupta, K. *et al.* The role of interfacial lipids in stabilizing membrane protein oligomers. *Nature* **541**, 421–424 (2017).
136. Bechara, C. *et al.* A subset of annular lipids is linked to the flippase activity of an ABC transporter. *Nat. Chem.* **7**, 255–62 (2015).
137. Marty, M. T. *et al.* Native mass spectrometry characterization of intact nanodisc lipoprotein complexes. *Anal. Chem.* **84**, 8957–8960 (2012).
138. Marty, M. T., Hoi, K. K. & Robinson, C. V. Interfacing Membrane Mimetics with Mass Spectrometry. *Acc. Chem. Res.* **49**, 2459–2467 (2016).
139. Hebling, C. M. *et al.* Conformational analysis of membrane proteins in phospholipid bilayer nanodiscs by hydrogen exchange mass spectrometry. *Anal. Chem.* **82**, 5415–5419 (2010).
140. Walker, L. R., Marzluff, E. M., Townsend, J. A., Resager, W. C. & Marty, M. T. Native Mass Spectrometry of Antimicrobial Peptides in Lipid Nanodiscs Elucidates Complex Assembly. *Anal. Chem.* **91**, 9284–9291 (2019).
141. Walker, L. R. & Marty, M. T. Revealing the Specificity of a Range of Antimicrobial Peptides in Lipid Nanodiscs by Native Mass Spectrometry. *Biochemistry* **59**, 2135–2142 (2020).
142. Chorev, D. S. *et al.* Protein assemblies ejected directly from native membranes yield complexes for mass spectrometry. *Science* **362**, 829–834 (2018).
143. Montenegro, F. A., Cantero, J. R. & Barrera, N. P. Combining mass spectrometry and X-ray crystallography for analyzing native-like membrane protein lipid complexes. *Front. Physiol.* **8**, (2017).
144. Novikova, I., Zhou, M., Shaw, J., Hellmann, H. & Evans, J. E. Dual Native MS and Cryo-EM Approach to Resolve Heteromeric Protein Assemblies and Subunit Stoichiometry. *Microsc. Microanal.* **25**, 1214–1215 (2019).
145. Politis, A. & Schmidt, C. Structural characterisation of medically relevant protein assemblies by integrating mass spectrometry with computational modelling. *Journal of Proteomics* **175**, 34–41 (2018).
146. O'Reilly, F. J. & Rappsilber, J. Cross-linking mass spectrometry: methods and applications in structural, molecular and systems biology. *Nature Structural and Molecular Biology* **25**, 1000–1008 (2018).
147. Chen, Z. A. *et al.* Architecture of the RNA polymerase II-TFIIF complex revealed by cross-linking and mass spectrometry. *EMBO J.* **29**, 717–726 (2010).
148. Greber, B. J. *et al.* The complete structure of the large subunit of the mammalian mitochondrial ribosome. *Nature* **515**, 283–286 (2014).

149. Schopper, S. *et al.* Measuring protein structural changes on a proteome-wide scale using limited proteolysis-coupled mass spectrometry. *Nat. Protoc.* **12**, 2391–2410 (2017).
150. Staros, J. V. N-Hydroxysulfosuccinimide Active Esters: Bis(N-hydroxysulfosuccinimide) Esters of Two Dicarboxylic Acids Are Hydrophilic, Membrane-impermeant, Protein Cross-Linkers. *Biochemistry* **21**, 3950–3955 (1982).
151. Müller, F., Graziadei, A. & Rappsilber, J. Quantitative Photo-crosslinking Mass Spectrometry Revealing Protein Structure Response to Environmental Changes. *Anal. Chem.* **91**, 9041–9048 (2019).
152. Vanherck, K., Koeckelberghs, G. & Vankelecom, I. F. J. Crosslinking polyimides for membrane applications: A review. *Progress in Polymer Science* **38**, 874–896 (2013).
153. Tan, D. *et al.* Trifunctional cross-linker for mapping protein-protein interaction networks and comparing protein conformational states. *Elife* **5**, (2016).
154. Es-Haghi, H., Bouhendi, H., Bagheri Marandi, G., Zohurian-Mehr, M. J. & Kabiri, K. An investigation into novel multifunctional cross-linkers effect on microgel prepared by precipitation polymerization. *React. Funct. Polym.* **73**, 524–530 (2013).
155. Leitner, A. *et al.* Expanding the chemical cross-linking toolbox by the use of multiple proteases and enrichment by size exclusion chromatography. *Mol. Cell. Proteomics* **11**, (2012).
156. Rinner, O. *et al.* Identification of cross-linked peptides from large sequence databases. *Nat. Methods* **5**, 315–318 (2008).
157. Schnirch, L. *et al.* Expanding the Depth and Sensitivity of Cross-Link Identification by Differential Ion Mobility Using High-Field Asymmetric Waveform Ion Mobility Spectrometry. *Anal. Chem.* **92**, 10495–10503 (2020).
158. Chen, Z. L. *et al.* A high-speed search engine pLink 2 with systematic evaluation for proteome-scale identification of cross-linked peptides. *Nat. Commun.* **10**, 1–12 (2019).
159. Chen, Z. L. *et al.* A high-speed search engine pLink 2 with systematic evaluation for proteome-scale identification of cross-linked peptides. *Nat. Commun.* **10**, 1–12 (2019).
160. Du, X. *et al.* Xlink-Identifier: An automated data analysis platform for confident identifications of chemically cross-linked peptides using tandem mass spectrometry. *J. Proteome Res.* **10**, 923–931 (2011).
161. Mendes, M. L. *et al.* An integrated workflow for crosslinking mass spectrometry. *Mol. Syst. Biol.* **15**, (2019).
162. Götze, M. *et al.* Automated assignment of MS/MS cleavable cross-links in protein 3d-structure analysis. *J. Am. Soc. Mass Spectrom.* **26**, 83–97 (2014).
163. Kukačka, Z. *et al.* LinX: A Software Tool for Uncommon Cross-Linking Chemistry. *J. Proteome Res.* **20**, 2021–2027 (2021).
164. Yu, C. & Huang, L. Cross-Linking Mass Spectrometry: An Emerging Technology for Interactomics and Structural Biology. *Analytical Chemistry* **90**, 144–165 (2018).
165. Michalski, A. *et al.* Mass spectrometry-based proteomics using Q exactive, a high-performance benchtop quadrupole orbitrap mass spectrometer. *Mol. Cell. Proteomics* **10**, (2011).

166. Miller, P. E. & Denton, M. B. The quadrupole mass filter: Basic operating concepts. *J. Chem. Educ.* **63**, 617 (1986).
167. Makarov, A. *et al.* Performance evaluation of a hybrid linear ion trap/orbitrap mass spectrometer. *Anal. Chem.* **78**, 2113–2120 (2006).
168. Thomson, B. A. 1997 McBryde Medal Award Lecture Radio frequency quadrupole ion guides in modern mass spectrometry. *Can. J. Chem.* **76**, 499–505 (1998).
169. Krutchinsky, A. N., Chernushevich, I. V., Spicer, V. L., Ens, W. & Standing, K. G. Collisional damping interface for an electrospray ionization time-of-flight mass spectrometer. *J. Am. Soc. Mass Spectrom.* **9**, 569–579 (1998).
170. Tolmachev, A. V., Udseth, H. R. & Smith, R. D. Radial stratification of ions as a function of mass to charge ratio in collisional cooling radio frequency multipoles used as ion guides or ion traps. *Rapid Commun. Mass Spectrom.* **14**, 1907–1913 (2000).
171. Leney, A. C. & Heck, A. J. R. Native Mass Spectrometry: What is in the Name? *J. Am. Soc. Mass Spectrom.* **28**, 5–13 (2017).
172. Frick, M., Hofmann, T., Haupt, C. & Schmidt, C. A novel sample preparation strategy for shotgun lipidomics of phospholipids employing multilamellar vesicles. *Anal. Bioanal. Chem.* **410**, 4253–4258 (2018).
173. Liebisch, G. *et al.* Shorthand notation for lipid structures derived from mass spectrometry. *J. Lipid Res.* **54**, 1523–1530 (2013).
174. Bender, J. & Schmidt, C. The CroCo cross-link converter: A user-centred tool to convert results from cross-linking mass spectrometry experiments. *Bioinformatics* **36**, 1296–1297 (2020).
175. Perkins, D. N., Pappin, D. J. C., Creasy, D. M. & Cottrell, J. S. Probability-based protein identification by searching sequence databases using mass spectrometry data. in *Electrophoresis* **20**, 3551–3567 (Wiley-VCH Verlag, 1999).
176. MassLynx MS-Software. *Waters Corp.*
177. Cox, J. & Mann, M. MaxQuant enables high peptide identification rates, individualized p.p.b.-range mass accuracies and proteome-wide protein quantification. *Nat. Biotechnol.* **26**, 1367–1372 (2008).
178. Morgner, N. & Robinson, C. V. Mass ign: An assignment strategy for maximizing information from the mass spectra of heterogeneous protein assemblies. *Anal. Chem.* **84**, 2939–2948 (2012).
179. Origin. 2003. Origin 7.5. OriginLab Corp., Northampton, M. No Title.
180. Li, D. *et al.* pFind: A novel database-searching software system for automated peptide and protein identification via tandem mass spectrometry. *Bioinformatics* **21**, 3049–3050 (2005).
181. Yang, B. *et al.* Identification of cross-linked peptides from complex samples. *Nat. Methods* **9**, 904–906 (2012).
182. Grimm, M., Zimniak, T., Kahraman, A. & Herzog, F. XVis: A web server for the schematic visualization and interpretation of crosslink-derived spatial restraints. *Nucleic Acids Res.* **43**, W362–W369 (2015).
183. Benchling [Biology Software]. Retrieved from <https://benchling.com>. No Title. (2022).

184. Malhotra, K. & Alder, N. N. Reconstitution of mitochondrial membrane proteins into nanodiscs by cell-free expression. in *Methods in Molecular Biology* **1567**, 155–178 (Humana Press Inc., 2017).
185. Chandra, M. *et al.* Classification of the human phox homology (PX) domains based on their phosphoinositide binding specificities. *Nat. Commun.* **10**, (2019).
186. Ma, C., Su, L., Seven, A. B., Xu, Y. & Rizo, J. Reconstitution of the vital functions of Munc18 and Munc13 in neurotransmitter release. *Science (80-.)*. **339**, 421–425 (2013).
187. Chen, X. *et al.* SNARE-mediated lipid mixing depends on the physical state of the vesicles. *Biophys. J.* **90**, 2062–2074 (2006).
188. Gasteiger, E. *et al.* *Protein Analysis Tools on the ExPASy Server* 571–571 From: *The Proteomics Protocols Handbook Protein Identification and Analysis Tools on the ExPASy Server*.
189. Walker, J. M. *The Proteomics Protocols Handbook*. (2005).
190. Shi, L. *et al.* SNARE proteins: One to fuse and three to keep the nascent fusion pore open. *Science (80-.)*. **335**, 1355–1359 (2012).
191. Shi, L. *et al.* Preparation and characterization of SNARE-containing nanodiscs and direct study of cargo release through fusion pores. *Nat. Protoc.* **8**, 935–948 (2013).
192. Sobott, F., Hernández, H., McCammon, M. G., Tito, M. A. & Robinson, C. V. A tandem mass spectrometer for improved transmission and analysis of large macromolecular assemblies. *Anal. Chem.* **74**, 1402–1407 (2002).
193. Konermann, L. Addressing a Common Misconception: Ammonium Acetate as Neutral pH “Buffer” for Native Electrospray Mass Spectrometry. *J. Am. Soc. Mass Spectrom.* **28**, 1827–1835 (2017).
194. Nele, V. *et al.* Effect of Formulation Method, Lipid Composition, and PEGylation on Vesicle Lamellarity: A Small-Angle Neutron Scattering Study. *Langmuir* **35**, 6064–6074 (2019).
195. Janmey, P. A. & Kinnunen, P. K. J. Biophysical properties of lipids and dynamic membranes. *Trends in Cell Biology* **16**, 538–546 (2006).
196. Van Den Brink-Van Der Laan, E., Antoinette Killian, J. & De Kruijff, B. Nonbilayer lipids affect peripheral and integral membrane proteins via changes in the lateral pressure profile. *Biochimica et Biophysica Acta - Biomembranes* **1666**, 275–288 (2004).
197. Siegel, D. P. & Epand, R. M. *The Mechanism of Lamellar-to-Inverted Hexagonal Phase Transitions in Phosphatidylethanolamine: Implications for Membrane Fusion Mechanisms*. *Biophysical Journal* **73**, (1997).
198. Yang, S.-T., Kreuzberger, A. J. B., Lee, J., Kiessling, V. & Tamm, L. K. The role of cholesterol in membrane fusion. *Chem. Phys. Lipids* **199**, 136–143 (2016).
199. Banerjee, S. & Mazumdar, S. Electrospray Ionization Mass Spectrometry: A Technique to Access the Information beyond the Molecular Weight of the Analyte. *Int. J. Anal. Chem.* **2012**, 1–40 (2012).
200. Furey, A., Moriarty, M., Bane, V., Kinsella, B. & Lehane, M. Ion suppression; A critical review on causes, evaluation, prevention and applications. *Talanta* **115**, 104–122 (2013).

201. King, R., Bonfiglio, R., Fernandez-Metzler, C., Miller-Stein, C. & Olah, T. Mechanistic investigation of ionization suppression in electrospray ionization. *J. Am. Soc. Mass Spectrom.* **11**, 942–950 (2000).
202. Riordan, J. F. Angiotensin-I-converting enzyme and its relatives. *Genome Biology* **4**, 225 (2003).
203. Esther, C. R. *et al.* The critical role of tissue angiotensin-converting enzyme as revealed by genotargeting in mice. *J. Clin. Invest.* **99**, 2375–2385 (1997).
204. Pickart, C. M. & Eddins, M. J. Ubiquitin: Structures, functions, mechanisms. *Biochimica et Biophysica Acta - Molecular Cell Research* **1695**, 55–72 (2004).
205. Sun, L. & Chen, Z. J. The novel functions of ubiquitination in signaling. *Current Opinion in Cell Biology* **16**, 119–126 (2004).
206. Martín-Villanueva, S., Gutiérrez, G., Kressler, D. & de la Cruz, J. Ubiquitin and ubiquitin-like proteins and domains in ribosome production and function: Chance or necessity? *International Journal of Molecular Sciences* **22**, (2021).
207. Nikš, M., Otto, M., Bušová, B. & Štefanović, J. Quantification of proliferative and suppressive responses of human T lymphocytes following ConA stimulation. *J. Immunol. Methods* **126**, 263–271 (1990).
208. Senear, D. F. & Teller, D. C. Thermodynamics of Concanavalin A Dimer-Tetramer Self-Association: Sedimentation Equilibrium Studies. *Biochemistry* **20**, 3076–3083 (1981).
209. Light-Wahl, K. J., Winger, B. E. & Smith, R. D. Observation of the Multimene Forms of Concanavalin A by Electrospray Ionization Mass Spectrometry. *Journal of the American Chemical Society* **115**, 5869–5870 (1993).
210. McKenzie, G. H., Sawyer, W. H. & Nichol, L. W. The molecular weight and stability of concanavalin A. *BBA - Protein Struct.* **263**, 283–293 (1972).
211. Giese, S. H., Belsom, A., Sinn, L., Fischer, L. & Rappsilber, J. Noncovalently Associated Peptides Observed during Liquid Chromatography-Mass Spectrometry and Their Affect on Cross-Link Analyses. *Anal. Chem.* **91**, (2019).
212. Chandra, M. *et al.* Classification of the human phox homology (PX) domains based on their phosphoinositide binding specificities. *Nat. Commun.* **10**, 1–14 (2019).
213. Teasdale, R. D. & Collins, B. M. Insights into the PX (phox-homology) domain and SNX (sorting nexin) protein families: Structures, functions and roles in disease. *Biochemical Journal* **441**, 39–59 (2012).
214. Stahelin, R. V., Burian, A., Bruzik, K. S., Murray, D. & Cho, W. Membrane binding mechanisms of the PX domains of NADPH oxidase p40phox and p47phox. *J. Biol. Chem.* **278**, 14469–14479 (2003).
215. Habermann, E. Bee and Wasp Venoms. *Science (80-.)*. **177**, 314–322 (1972).
216. Jamasbi, E. *et al.* Melittin peptides exhibit different activity on different cells and model membranes. *Amino Acids* **46**, 2759–2766 (2014).
217. Gauldie, J., Hanson, J. M., Rumjanek, F. D., Shipolini, R. A. & Vernon, C. A. The Peptide Components of Bee Venom. *Eur. J. Biochem.* **61**, 369–376 (1976).

218. Popplewell, J. F., Swann, M. J., Freeman, N. J., McDonnell, C. & Ford, R. C. Quantifying the effects of melittin on liposomes. *Biochim. Biophys. Acta - Biomembr.* **1768**, 13–20 (2007).
219. Bello, J., Bello, H. R. & Granados, E. Conformation and Aggregation of Melittin: Dependence on pH and Concentration. *Biochemistry* **21**, 461–465 (1982).
220. Barylyuk, K. *et al.* What happens to hydrophobic interactions during transfer from the solution to the gas phase? The case of electrospray-based soft ionization methods. *J. Am. Soc. Mass Spectrom.* **22**, 1167–1177 (2011).
221. Lee, M. T., Sun, T. L., Hung, W. C. & Huang, H. W. Process of inducing pores in membranes by melittin. *Proc. Natl. Acad. Sci. U. S. A.* **110**, 14243–14248 (2013).
222. Raghuraman, H. & Chattopadhyay, A. Melittin: A membrane-active peptide with diverse functions. *Bioscience Reports* **27**, 189–223 (2007).
223. Walker, L. R., Marzluff, E. M., Townsend, J. A., Resager, W. C. & Marty, M. T. Native Mass Spectrometry of Antimicrobial Peptides in Lipid Nanodiscs Elucidates Complex Assembly. *Anal. Chem.* **91**, 9284–9291 (2019).
224. Lin, J. H. & Baumgaertner, A. Stability of a melittin pore in a lipid bilayer: A molecular dynamics study. *Biophys. J.* **78**, 1714–1724 (2000).
225. Klocek, G., Schulthess, T., Shai, Y. & Seelig, J. Thermodynamics of melittin binding to lipid bilayers. Aggregation and pore formation. *Biochemistry* **48**, 2586–2596 (2009).
226. Lee, M. T., Hung, W. C., Chen, F. Y. & Huang, H. W. Mechanism and kinetics of pore formation in membranes by water-soluble amphipathic peptides. *Proc. Natl. Acad. Sci. U. S. A.* **105**, 5087–5092 (2008).
227. Benachir, T. & Lafleur, M. Study of vesicle leakage induced by melittin. *BBA - Biomembr.* **1235**, 452–460 (1995).
228. Kuchinka, E. & Seelig, J. Interaction of Melittin with Phosphatidylcholine Membranes. Binding Isotherm and Lipid Head-Group Conformation. *Biochemistry* **28**, 4216–4221 (1989).
229. Bayburt, T. H., Grinkova, Y. V. & Sligar, S. G. Self-Assembly of Discoidal Phospholipid Bilayer Nanoparticles with Membrane Scaffold Proteins. *Nano Lett.* **2**, 853–856 (2002).
230. Denisov, I. G., Grinkova, Y. V., Lazarides, A. & Sligar, S. G. Directed Self-Assembly of Monodisperse Phospholipid Bilayer Nanodiscs with Controlled Size. *Nano Lett.* 3477–3487 (2004). doi:10.1021/ja0393574
231. Denisov, I. G., McLean, M. A., Shaw, A. W., Grinkova, Y. V. & Sligar, S. G. Thermotropic phase transition in soluble nanoscale lipid bilayers. *J. Phys. Chem. B* **109**, 15580–15588 (2005).
232. Henrich, E. *et al.* Analyzing native membrane protein assembly in nanodiscs by combined non-covalent mass spectrometry and synthetic biology. *Elife* **6**, (2017).
233. Sahin, C., Reid, D. J., Marty, M. T. & Landreh, M. Scratching the surface: native mass spectrometry of peripheral membrane protein complexes. *Biochem. Soc. Trans.* **48**, 547–558 (2020).
234. Nath, A., Atkins, W. M. & Sligar, S. G. Applications of phospholipid bilayer nanodiscs in the study of membranes and membrane proteins. *Biochemistry* **46**, 2059–2069 (2007).

235. Bayburt, T. H. & Sligar, S. G. Membrane protein assembly into Nanodiscs. *FEBS Letters* **584**, 1721–1727 (2010).
236. Denisov, I. G., Grinkova, Y. V., Lazarides, A. A. & Sligar, S. G. Directed Self-Assembly of Monodisperse Phospholipid Bilayer Nanodiscs with Controlled Size. *J. Am. Chem. Soc.* **126**, 3477–3487 (2004).
237. Schuler, M. A., Denisov, I. G. & Sligar, S. G. Nanodiscs as a new tool to examine lipid-protein interactions. *Methods Mol. Biol.* **974**, 415–33 (2013).
238. Ritchie, T. K. *et al.* Chapter 11 Reconstitution of Membrane Proteins in Phospholipid Bilayer Nanodiscs. *Methods in Enzymology* **464**, 211–231 (2009).
239. Li, M. J., Atkins, W. M. & McClary, W. D. Preparation of Lipid Nanodiscs with Lipid Mixtures. *Curr. Protoc. Protein Sci.* **98**, e100 (2019).
240. Jakubec, M. *et al.* Cholesterol-containing lipid nanodiscs promote an α -synuclein binding mode that accelerates oligomerization. *FEBS J.* **288**, 1887 (2021).
241. Etzkorn, M., Viegas, A., Viennet, T. & Aldino Viegas, R. The power, pitfalls and potential of the nanodisc system for NMR-based studies. *Biol. Chem* **397**, (2016).
242. Li, M. J., Atkins, W. M. & McClary, W. D. Preparation of Lipid Nanodiscs with Lipid Mixtures. *Curr. Protoc. Protein Sci.* **98**, e100 (2019).
243. Han, J., Pluhackova, K. & Böckmann, R. A. The multifaceted role of SNARE proteins in membrane fusion. *Frontiers in Physiology* **8**, 5 (2017).
244. Fasshauer, D., Otto, H., Eliason, W. K., Jahn, R. & Brünger, A. T. Structural changes are associated with soluble N-ethylmaleimide-sensitive fusion protein attachment protein receptor complex formation. *J. Biol. Chem.* **272**, 28036–28041 (1997).
245. Lee, S. *et al.* Munc18-1 induces conformational changes of syntaxin-1 in multiple intermediates for SNARE assembly. *Sci. Rep.* **10**, 11623 (2020).
246. Bao, H. *et al.* Exocytotic fusion pores are composed of both lipids and proteins. *Nat. Struct. Mol. Biol.* **23**, 67–73 (2016).
247. Raulfs, M. D. M. *et al.* Investigations of the mechanism of the ‘proline effect’ in tandem mass spectrometry experiments: The ‘pipecolic acid effect’. *J. Am. Soc. Mass Spectrom.* **25**, 1705–1715 (2014).
248. Bleiholder, C., Suhai, S., Harrison, A. G. & Paizs, B. Towards Understanding the Tandem Mass Spectra of Protonated Oligopeptides. 2: The Proline Effect in Collision-Induced Dissociation of Protonated Ala-Ala-Xxx-Pro-Ala (Xxx = Ala, Ser, Leu, Val, Phe, and Trp). *J. Am. Soc. Mass Spectrom* **22**, 1032–1039 (2011).
249. Fasshauer, D., Bruns, D., Shen, B., Jahn, R. & Brünger, A. T. A structural change occurs upon binding of syntaxin to SNAP-25. *J. Biol. Chem.* **272**, 4582–4590 (1997).
250. Margittai, M., Fasshauer, D., Jahn, R. & Langen, R. The Habc domain and the SNARE core complex are connected by a highly flexible linker. *Biochemistry* **42**, 4009–4014 (2003).
251. Products, A. Detergents and their uses in membrane protein science. 1–17 (2007). doi:10.1093/toxsci/kfp097

252. Reading, E. *et al.* The effect of detergent, temperature, and lipid on the oligomeric state of MscL constructs: Insights from mass spectrometry. *Chem. Biol.* **22**, 593–603 (2015).
253. Larsson, E., Hubert, M. & Lundmark, R. Analysis of protein and lipid interactions using liposome co-sedimentation assays. in *Methods in Molecular Biology* **2169**, 119–127 (Humana Press Inc., 2020).
254. Yao, X., Fan, X. & Yan, N. Cryo-EM analysis of a membrane protein embedded in the liposome. *Proc. Natl. Acad. Sci. U. S. A.* **117**, 18497–18503 (2020).
255. Unilamellar, G. in vitro membrane systems Reconstitution of transmembrane proteins in liposomes. 1–7
256. Kreir, M., Farre, C., Beckler, M., George, M. & Fertig, N. Rapid screening of membrane protein activity: Electrophysiological analysis of OmpF reconstituted in proteoliposomes. *Lab Chip* **8**, 587–595 (2008).
257. Busse, R. A. *et al.* Qualitative and quantitative characterization of protein-phosphoinositide interactions with liposome-based methods. *Autophagy* **9**, 770–777 (2013).
258. Ramezanpour, M. *et al.* Structural Properties of Inverted Hexagonal Phase: A Hybrid Computational and Experimental Approach. *Langmuir* **36**, 6668–6680 (2020).
259. Di Gregorio, G. M. & Mariani, P. Rigidity and spontaneous curvature of lipidic monolayers in the presence of trehalose: A measurement in the DOPE inverted hexagonal phase. *Eur. Biophys. J.* **34**, 67–81 (2005).
260. Marrink, S. J. & Mark, A. E. Molecular view of hexagonal phase formation in phospholipid membranes. *Biophys. J.* **87**, 3894–3900 (2004).
261. Luis G. Cuello, ‡, Jesus G. Romero, ‡, D. Marien Cortes, ‡ and & Perozo*, E. pH-Dependent Gating in the Streptomyces lividans K⁺ Channel†. (1998). doi:10.1021/BI972997X
262. Iwahashi, Y. & Nakamura, T. Orientation and reactivity of NADH kinase in proteoliposomes. *J. Biochem.* **105**, 922–926 (1989).
263. Deutschmann, S., Rimle, L. & Ballmoos, C. Rapid Estimation of Membrane Protein Orientation in Liposomes. *ChemBioChem* **23**, e202100543 (2022).
264. Catalá, A. Lipid peroxidation modifies the assembly of biological membranes – The Lipid Whisker Model – #157; *Front. Physiol.* **5**, 520 (2015).
265. Catalá, A. & Díaz, M. Editorial: Impact of Lipid Peroxidation on the Physiology and Pathophysiology of Cell Membranes. *Front. Physiol.* **7**, 423 (2016).
266. Leney, A. C., McMorran, L. M., Radford, S. E. & Ashcroft, A. E. Amphipathic polymers enable the study of functional membrane proteins in the gas phase. *Anal. Chem.* **84**, 9841–9847 (2012).
267. Dürr, U. H. N. N., Gildenberg, M. & Ramamoorthy, A. The magic of bicelles lights up membrane protein structure. *Chem. Rev.* **112**, 6054–6074 (2012).
268. Hellwig, N. *et al.* Native mass spectrometry goes more native: investigation of membrane protein complexes directly from SMALPs. *Chem. Commun. (Camb)*. **54**, 13702–13705 (2018).
269. Walker, L. R., Marzluff, E. M., Townsend, J. A., Resager, W. C. & Marty, M. T. Native Mass Spectrometry of Antimicrobial Peptides in Lipid Nanodiscs Elucidates Complex Assembly. *Anal. Chem.* **91**, 9284–9291 (2019).

270. Martens, C., Shekhar, M., Lau, A. M., Tajkhorshid, E. & Politis, A. Integrating hydrogen–deuterium exchange mass spectrometry with molecular dynamics simulations to probe lipid-modulated conformational changes in membrane proteins. *Nat. Protoc.* **14**, 3183–3204 (2019).
271. Laganowsky, A., Reading, E., Hopper, J. T. S. & Robinson, C. V. Mass Spectrometry of Intact Membrane Protein Complexes. *Nat. Protoc.* **8**, 639–651 (2014).
272. Hanson, C. L. *et al.* Phospholipid complexation and association with apolipoprotein C-II: insights from mass spectrometry. *Biophys. J.* **85**, 3802–3812 (2003).
273. Konermann, L., Metwally, H., Duez, Q. & Peters, I. Charging and supercharging of proteins for mass spectrometry: Recent insights into the mechanisms of electrospray ionization. *Analyst* **144**, 6157–6171 (2019).
274. Konermann, L., Ahadi, E., Rodriguez, A. D. & Vahidi, S. Unraveling the Mechanism of Electrospray Ionization. (2012). doi:10.1021/ac302789c
275. Metwally, H., McAllister, R. G. & Konermann, L. Exploring the mechanism of salt-induced signal suppression in protein electrospray mass spectrometry using experiments and molecular dynamics simulations. *Anal. Chem.* **87**, 2434–2442 (2015).
276. Landreh, M. *et al.* Controlling release, unfolding and dissociation of membrane protein complexes in the gas phase through collisional cooling. *Chem. Commun.* **51**, 15582–15584 (2015).
277. Assessment, U. E. N. C. for E. ACIDITY DETERMINATION IN DROPLETS FORMED BY ELECTROSPRAYING METHANOL-WATER SOLUTIONS. (2009).
278. Mirza, U. A. & Chait, B. T. Do proteins denature during droplet evolution in electrospray ionization? *Int. J. Mass Spectrom. Ion Process.* **162**, 173–181 (1997).
279. Wolynes, P. G. Biomolecular folding in vacuo!!!(?). *Proceedings of the National Academy of Sciences of the United States of America* **92**, 2426–2427 (1995).
280. Steinberg, M. Z., Elber, R., McLafferty, F. W., Gerber, R. B. & Breuker, K. Early Structural Evolution of Native Cytochrome c after Solvent Removal. *ChemBioChem* **9**, 2417–2423 (2008).
281. Steinberg, M. Z., Breuker, K., Elber, R. & Gerber, R. B. The dynamics of water evaporation from partially solvated cytochrome c in the gas phase. *Phys. Chem. Chem. Phys.* **9**, 4690–4697 (2007).
282. Wytenbach, T. & Bowers, M. T. Structural stability from solution to the gas phase: Native solution structure of ubiquitin survives analysis in a solvent-free ion mobility-mass spectrometry environment. *J. Phys. Chem. B* **115**, 12266–12275 (2011).
283. Bakhtiari, M. & Konermann, L. Protein Ions Generated by Native Electrospray Ionization: Comparison of Gas Phase, Solution, and Crystal Structures. *J. Phys. Chem. B* **123**, 1784–1796 (2019).
284. Sabín, J., Prieto, G., Ruso, J. M., Hidalgo-´ Alvarez, R. & Sarmiento, F. Size and stability of liposomes: A possible role of hydration and osmotic forces. *Eur. Phys. J. E* **20**, 401–408 (2006).
285. Koivusalo, M., Haimi, P., Heikinheimo, L., Kostianen, R. & Somerharju, P. Quantitative determination of phospholipid compositions by esi-ms: Effects of acyl chain length, unsaturation, and lipid concentration on instrument response. *J. Lipid Res.* **42**, 663–672 (2001).
286. Higashi, T. & Shimada, K. Derivatization of neutral steroids to enhance their detection characteristics in liquid chromatography-mass spectrometry. *Analytical and Bioanalytical Chemistry* **378**, 875–882 (2004).

-
287. Sandhoff, R., Brügger, B., Jeckel, D., Lehmann, W. D. & Wieland, F. T. Determination of cholesterol at the low picomole level by nano- electrospray ionization tandem mass spectrometry. *J. Lipid Res.* **40**, 126–132 (1999).
288. Bravo, J. *et al.* The crystal structure of the PX domain from p40phox bound to phosphatidylinositol 3-phosphate. *Mol. Cell* **8**, 829–839 (2001).
289. Zhang, Y. *et al.* Protein-glycosphingolipid interactions revealed using catch-and-release mass spectrometry. *Anal. Chem.* **84**, 7618–7621 (2012).
290. Szymkowicz, L., Lento, C. & Wilson, D. J. Impact of Cardiolipin and Phosphatidylcholine Interactions on the Conformational Ensemble of Cytochrome *c*. *Biochemistry* **58**, 3617–3626 (2019).
291. van den Bogaart, G., Guzmán, J. V., Mika, J. T. & Poolman, B. On the mechanism of pore formation by melittin. *J. Biol. Chem.* **283**, 33854–33857 (2008).
292. Raghuraman, H. & Chattopadhyay, A. Melittin: A membrane-active peptide with diverse functions. *Bioscience Reports* **27**, 189–223 (2007).
293. Wessman, P., Strömstedt, A. A., Malmsten, M. & Edwards, K. Melittin-lipid bilayer interactions and the role of cholesterol. *Biophys. J.* **95**, 4324–4336 (2008).
294. Yang, Q., Guo, Y., Li, L. & Hui, S. W. *Effects of Lipid Headgroup and Packing Stress on Poly(Ethylene Glycol)-Induced Phospholipid Vesicle Aggregation and Fusion*. *Biophysical Journal* **73**, (1997).
295. Raetz, C. R. H. *Molecular genetics of membrane phospholipid synthesis*. (1986).
296. Bayburt, T. H., Grinkova, Y. V. & Sligar, S. G. Assembly of single bacteriorhodopsin trimers in bilayer nanodiscs. *Arch. Biochem. Biophys.* **450**, 215–222 (2006).
297. Sobott, F., Hernández, H., McCammon, M. G., Tito, M. A. & Robinson, C. V. A tandem mass spectrometer for improved transmission and analysis of large macromolecular assemblies. *Anal. Chem.* **74**, 1402–1407 (2002).
298. Debelyy, M. O., Waridel, P., Quadroni, M., Schneiter, R. & Conzelmann, A. Chemical crosslinking and mass spectrometry to elucidate the topology of integral membrane proteins. *PLoS One* **12**, (2017).
299. Larance, M. *et al.* Global membrane protein interactome analysis using in vivo crosslinking and mass spectrometry-based protein correlation profiling. *Mol. Cell. Proteomics* **15**, 2476–2490 (2016).
300. Scacioc, A. *et al.* Structure based biophysical characterization of the PROPPIN Atg18 shows Atg18 oligomerization upon membrane binding. *Sci. Rep.* **7**, 14008 (2017).
301. Poirier, M. A. *et al.* Protease resistance of syntaxin-SNAP-25-VAMP complexes: Implications for assembly and structure. *J. Biol. Chem.* **273**, 11370–11377 (1998).

7 Appendix

7.1 Supplementary figures

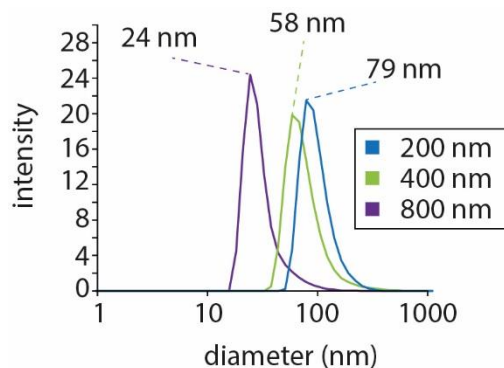


Figure S1: DLS analysis of multi-component liposomes differing in size. Liposomes composed of DOPC, DOPE, DOPS and cholesterol (molar ratio 5:2:2:1) and extruded through membranes of different pore sizes 200 nm, 400 nm, 800 nm. Liposomes extruded through membranes of 800 nm pore size (purple) revealed a size of approximately 24 nm diameter, liposomes extruded through polycarbonate membranes of 400 nm pore size (green) revealed approximately 58 nm diameter and liposomes extruded through a pore membrane of 200 nm pore size (blue) showed a size of approximately 79 nm diameter.

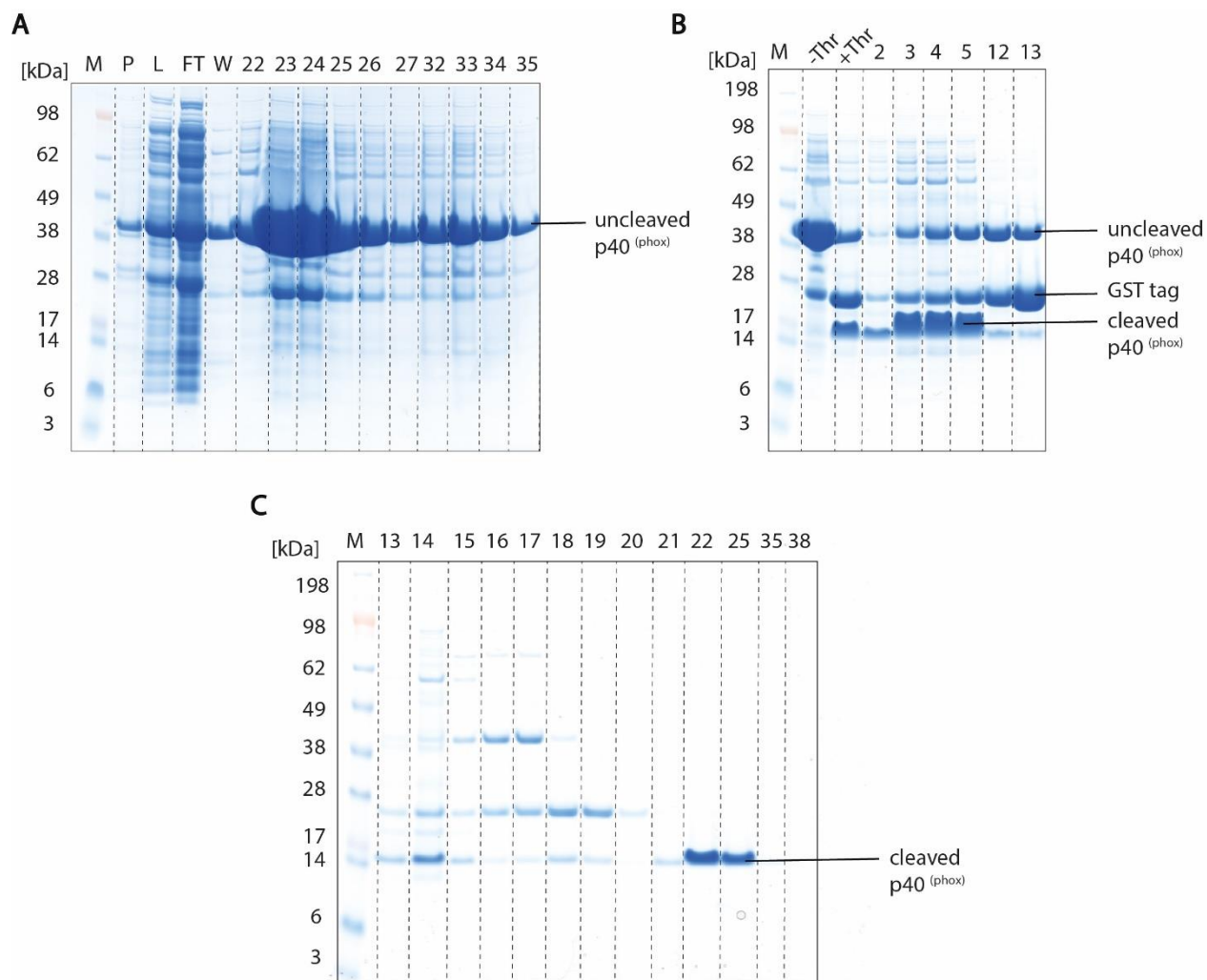


Figure S2: Protein purification of p40^{phox}. (A) Collected fractions after GST-affinity chromatography were applied to gel electrophoresis. Fractions containing the GST-p40^{phox} fusion protein (22-35) were pooled and subjected to further purification. (B) Gel electrophoresis from reverse GST-affinity chromatography after thrombin cleavage and dialysis. Fractions containing p40^{phox} were pooled and subjected to SEC. (C) Elution fractions (22 to 25) of SEC revealed a molecular weight of approximately 16 kDa. Fractions with highest protein concentration were concentrated. Abbreviations: M (marker), P (pellet), L (load), FT (flowthrough), W (wash), - Thr (before thrombin cleavage), + Thr (after thrombin cleavage).

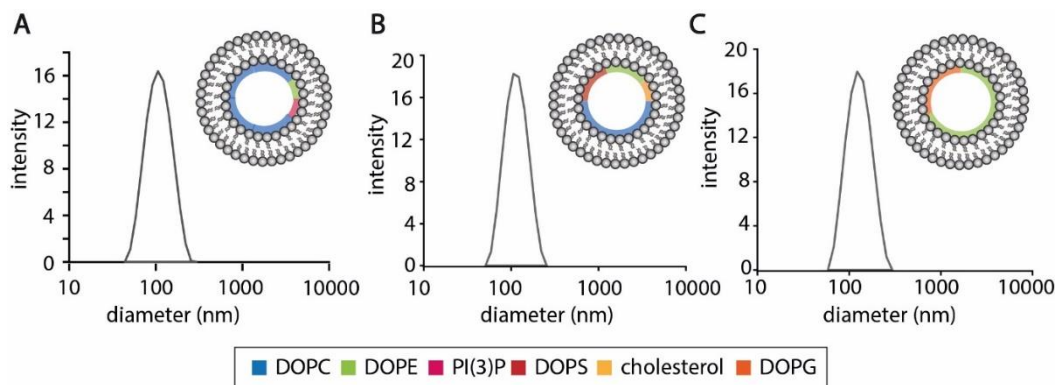


Figure S3: DLS analysis of multi-component liposomes with different compositions. See figure legend for color scheme. Size distributions of liposomes containing (A) DOPC, DOPE and PI(3)P (molar ratio 8:1:1). (B) DOPC, DOPE, DOPS and cholesterol (molar ratio: 5:2:2:1) and (C) DOPG and DOPE (molar ratio 5:2). Liposomes revealed homogeneous size distributions of approximately 100 nm diameter.

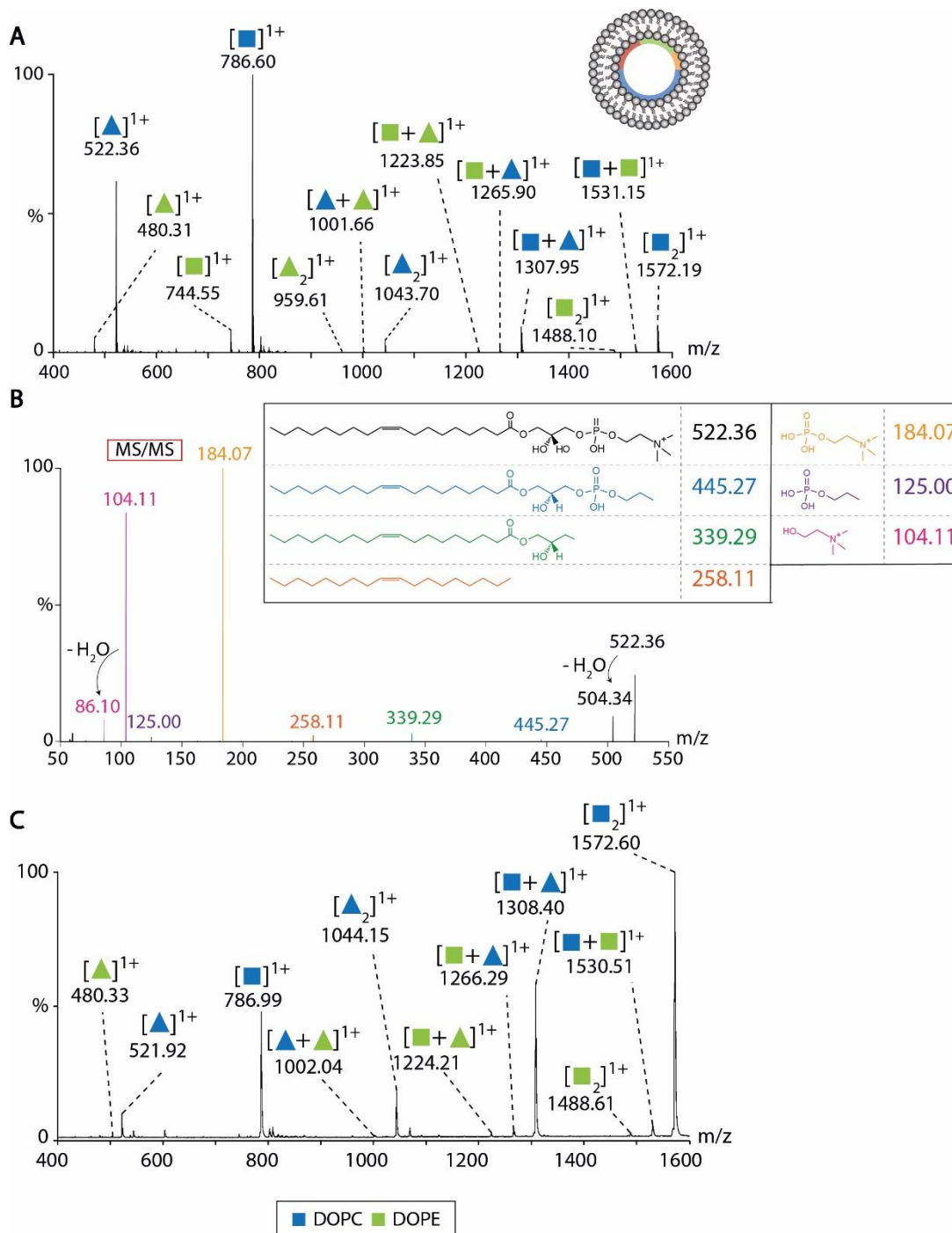


Figure S4: MS analysis of liposomes resembling a eukaryotic membrane composition incubated with phospholipase A2. Liposomes composed of DOPC, DOPE, DOPS and cholesterol (molar ratio 5:2:2:1) See figure legend for color scheme. **(A)** Mass spectrum of liposomes obtained under denaturing gas phase conditions. DOPE, DOPC, lyso-PE and lyso-PC as well as lipid clusters are assigned. **(B)** Tandem mass spectrum (MS/MS) of lyso-PC (m/z 522.36). Fragments specific to the lipid head group and the acyl chain are highlighted. **(C)** Native mass spectrum of liposomes. DOPE, DOPC, lyso-PE, lyso-PC and clusters thereof are assigned.

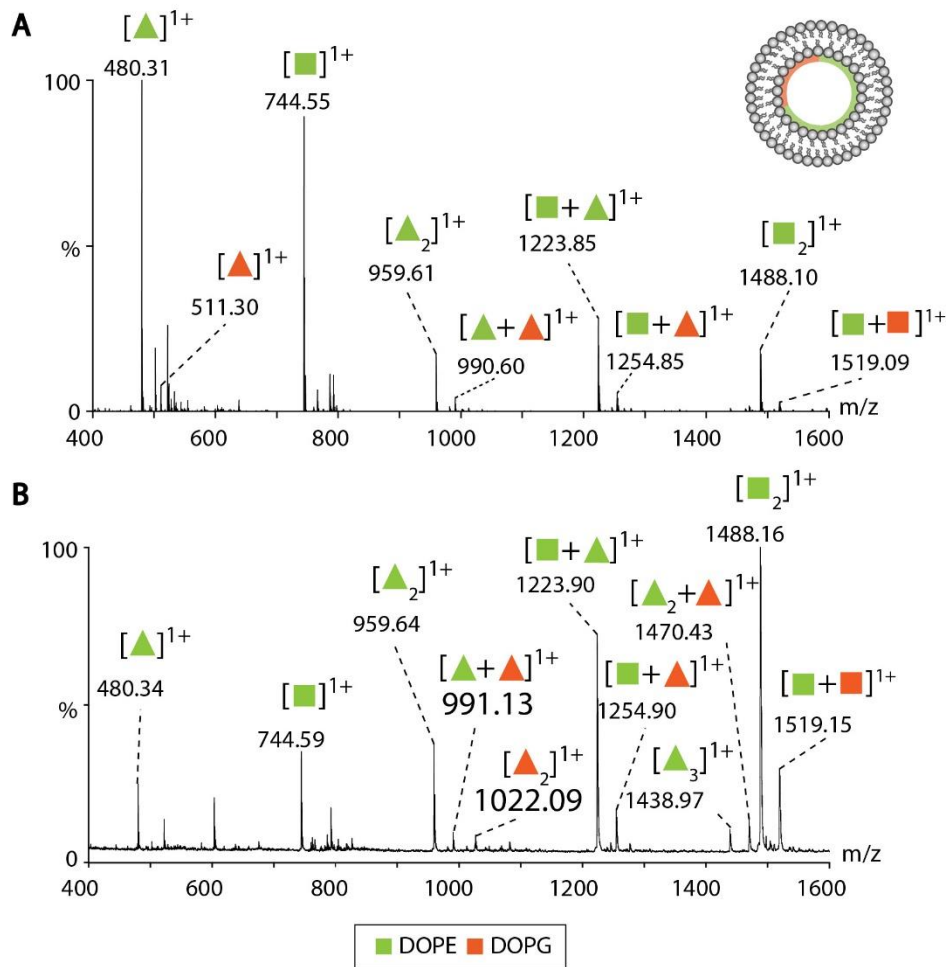


Figure S5: MS analysis of liposomes resembling a prokaryotic membrane composition incubated with phospholipase A2. Liposomes composed of DOPE and DOPG (molar ratio 5:2). See figure legend for color scheme. **(A)** Mass spectrum of liposomes under denaturing gas phase conditions. DOPE, DOPG, lyso-PE and lyso-PG as well as lipid clusters are assigned. **(B)** Native mass spectrum of liposomes. The mass spectrum revealed signals for DOPE, DOPG, lyso-PE, lyso-PG and lipid clusters.

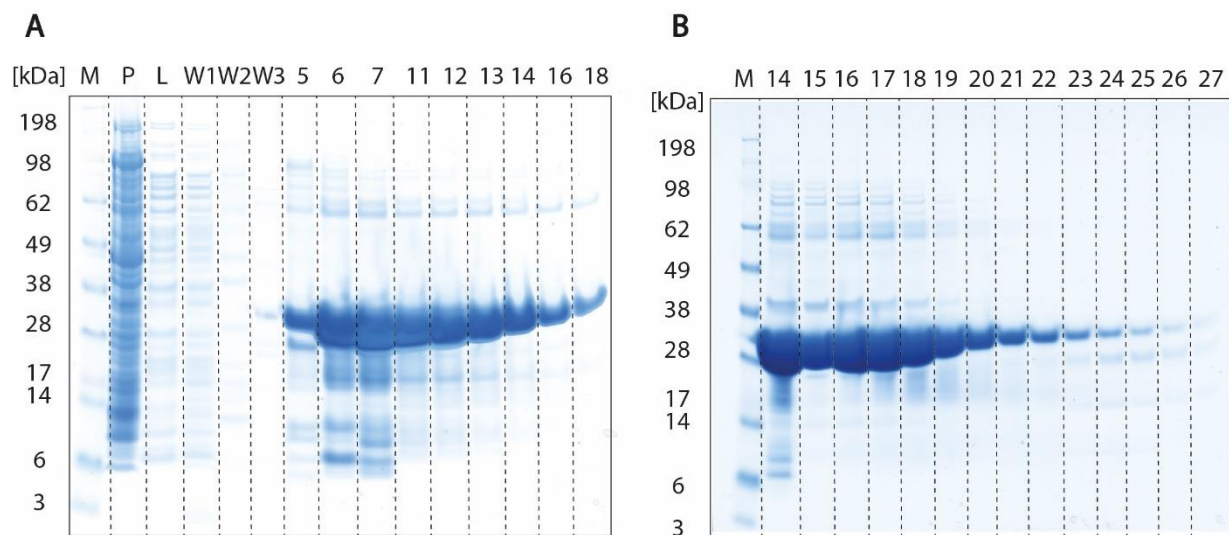


Figure S6: Protein purification of MSP1E3D1. (A) After protein expression, the cell lysate containing the MSP1E3D1 protein is purified using an IMAC column. Collected fractions are analyzed by gel electrophoresis. MSP1E3D1 is observed at approximately 30 kDa. (B) Elution fractions (5-18) are pooled, concentrated and subjected to SEC. Gel electrophoresis after SEC purification reveals MSP1E3D1 at a molecular weight of approximately 30 kDa. Fractions 19-21 are concentrated and used for nanodiscs assembly. Abbreviations: M (marker), P (pellet), L (load), W1-W3 (wash 1-3).

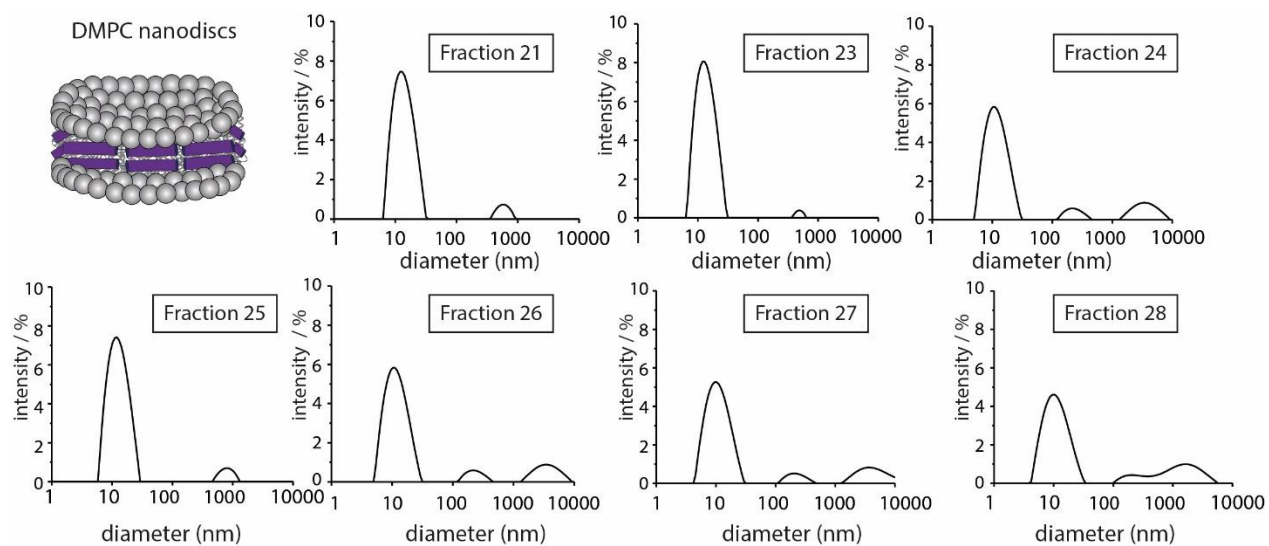


Figure S7: DLS analysis of single-component nanodiscs. Nanodiscs are composed of DMPC lipids. DLS analysis of SEC fractions containing the highest protein concentration. DLS analysis revealed mean size distributions of approximately 13 nm corresponding to the purified nanodiscs. Additional aggregates at higher size distributions are also observed, suggesting insufficient nanodisc assembly.

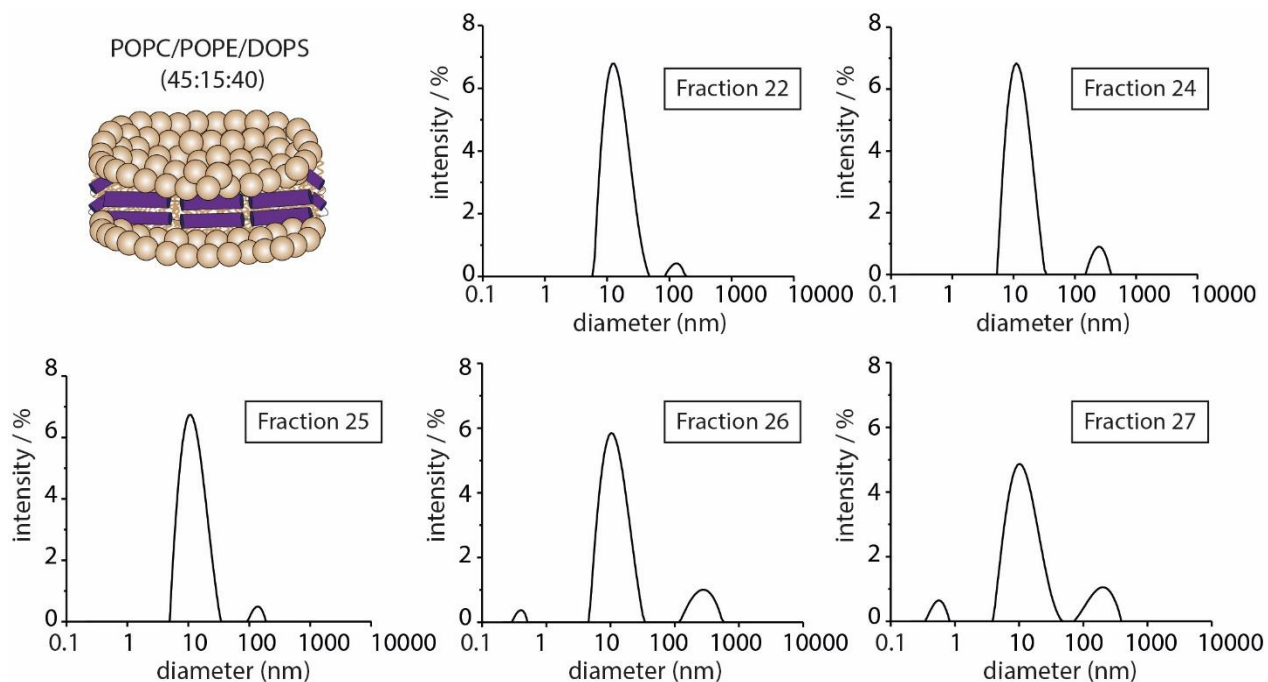


Figure S8: DLS analysis of multi-component nanodiscs. Nanodiscs are composed of DOPC, DOPE and DOPS (molar ratio: 45:15:40). DLS analysis of SEC fractions containing the highest protein concentration revealed mean size distributions of approximately 13 nm corresponding to the assembled nanodiscs. The additional aggregates at higher and lower size distributions suggest insufficient nanodisc assembly.

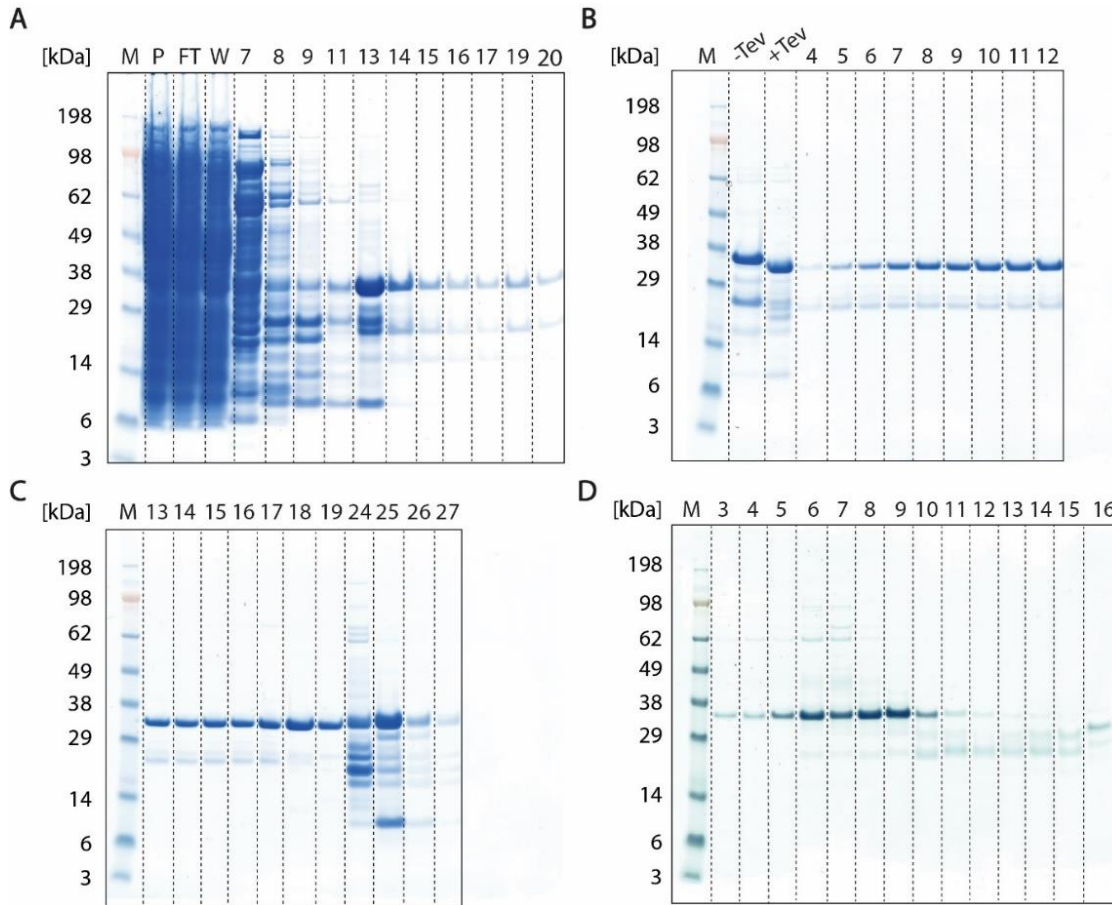


Figure S9: Protein purification of Syntaxin-1A. (A) After protein expression, the cell lysate containing Syntaxin-1A is purified by IMAC. Collected fractions are analyzed by gel electrophoresis and Syntaxin-1A containing the His-tag is observed at 38 kDa (B-C) Gel electrophoresis of reverse IMAC. Elution fractions (5-19) are pooled, concentrated, and subjected to SEC. (D) Gel electrophoresis of fractions from SEC. Fractions containing the highest protein concentration (fraction 5-9) are pooled and concentrated. Abbreviations: M (marker), P (pellet), (FT) flow through, W (wash), -TEV (before TEV cleavage), +TEV (after TEV cleavage).

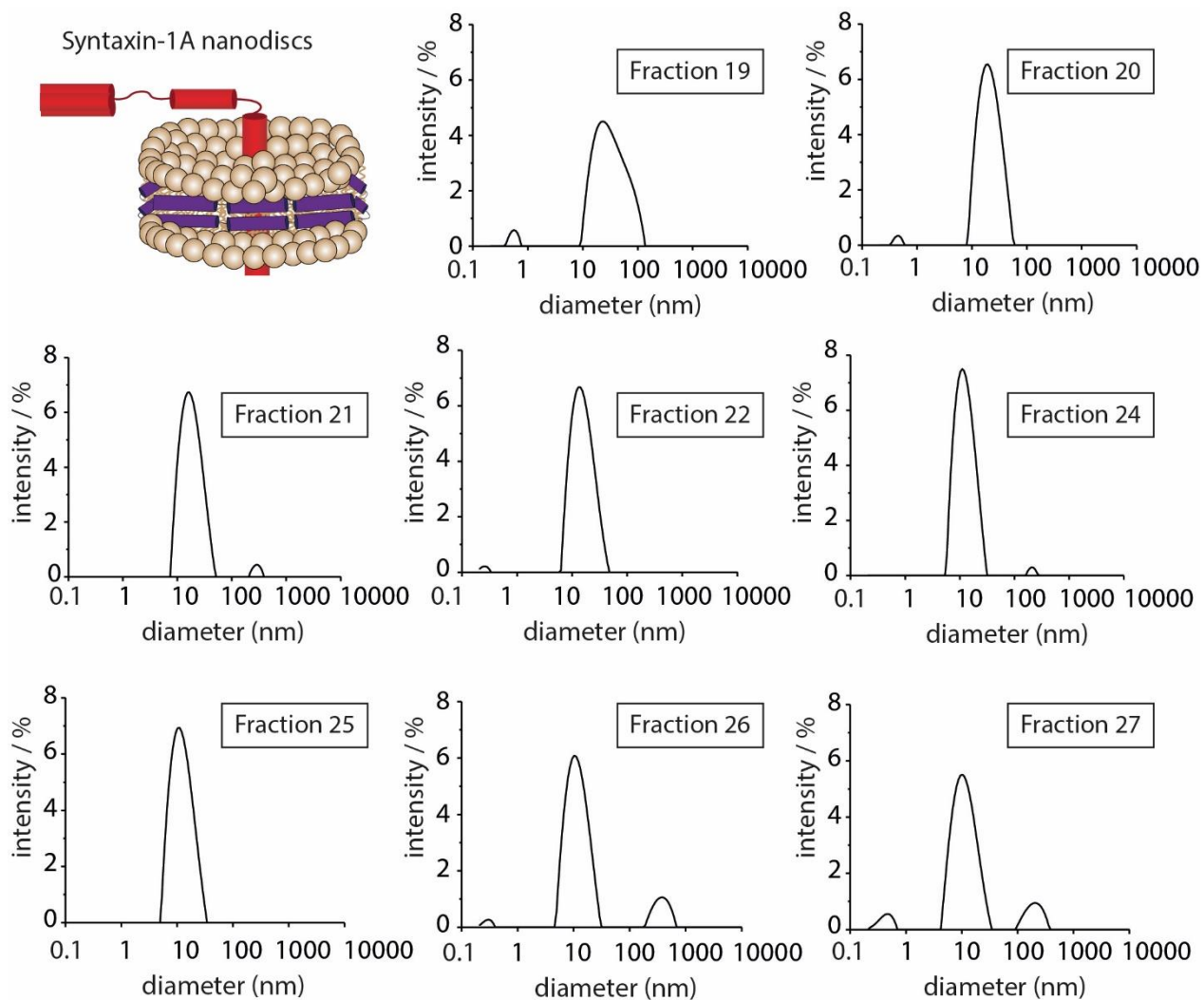


Figure 10: DLS analysis of Syntaxin-1A nanodiscs. Fractions after SEC containing the highest protein concentration were inspected by DLS analysis. Mean size distribution of a diameter of approximately 12 nm was observed in all fractions. Higher size distributions presumably correspond to liposome species or insufficient nanodisc assembly. Note that, the DLS analysis of fraction 25 also revealed a high homogeneity, however, was not used for further experiments, as this fraction did not contain the highest Syntaxin-1A and MSP concentration.

7.2 Supplementary Tables

Table S1: m/z ratios of single-component liposomes in denaturing MS experiments (see Figure 14A).

composition	m/z experimental	m/z theoretical
[DOPC ₅] ²⁺	1966.00	1966.26
[DOPC ₃] ¹⁺	2358.80	2359.35
[DOPC ₇] ²⁺	2752.90	2752.40
[DOPC ₁₁] ³⁺	2883.53	2883.42
[DOPC ₁₂] ³⁺	3145.40	3145.46
[DOPG ₅ +(NH ₄) ₃] ²⁺	1963.91	1963.10
[DOPG ₃ +NH ₄] ¹⁺	2342.67	2341.12
[DOPG ₇ +(NH ₄) ₃] ²⁺	2738.96	2737.13
[DOPG ₈ +(NH ₄) ₂] ²⁺	3118.22	3115.15
[DOPS ₅] ²⁺	1970.85	1969.80
[DOPS ₈] ³⁺	2102.45	2101.09
[DOPS ₃] ¹⁺	2364.63	2363.60
[DOPS ₁₀] ³⁺	2627.48	2626.11
[DOPS ₁₄] ⁴⁺	2758.90	2757.36
[DOPS ₁₁] ³⁺	2890.32	2888.61
[DOPS ₁₆] ⁴⁺	3153.17	3151.12
[DOPE ₃] ¹⁺	2232.60	2230.11
[DOPE ₇] ²⁺	2604.87	2601.63
[DOPE ₁₀] ³⁺	2480.78	2477.79
[DOPE ₁₁] ³⁺	2728.63	2725.45
[DOPE ₁₂] ³⁺	2977.15	2973.14
[DOPE ₁₃] ³⁺	3224.66	3220.82
[DOPE ₁₄] ³⁺	3473.17	3468.50
[DOPE ₁₅] ³⁺	3721.69	3716.18

Table S2: m/z ratios of single-component liposomes in native MS experiments (see Figure 14B).

composition	m/z experimental	m/z theoretical
[DOPC ₅] ²⁺	1965.73	1964.99
[DOPC ₃] ¹⁺	2358.46	2357.78
[DOPC ₇] ²⁺	2751.73	2750.58
[DOPC ₄] ¹⁺	3145.11	3143.38
[DOPC ₅] ¹⁺	3930.89	3928.97
[DOPG ₃] ¹⁺	2328.85	2323.12
[DOPG ₄] ¹⁺	3104.68	3097.15
[DOPG ₅] ¹⁺	3878.56	3871.19
[DOPS ₅] ²⁺	1970.63	1969.83
[DOPS ₃] ¹⁺	2364.79	2363.60
[DOPS ₁₀] ³⁺	2627.83	2627.11
[DOPS ₇] ²⁺	2759.07	2757.36
[DOPS ₁₁] ³⁺	2890.74	2888.62
[DOPS ₄] ¹⁺	3153.34	3151.13
[DOPS ₁₃] ³⁺	3416.33	3413.64
[DOPS ₉] ²⁺	3547.18	3544.89
[DOPS ₁₄] ³⁺	3678.24	3676.15
[DOPS ₁₅] ³⁺	3941.21	3938.66
[DOPE ₃] ¹⁺	2232.90	2230.11
[DOPE ₄] ¹⁺	2977.37	2973.14
[DOPE ₉] ²⁺	3349.31	3344.66
[DOPE ₅] ¹⁺	3720.78	3716.18

Table S3: Results of MaxQuant database search for protein identification.

Protein	Score	Molecular weight (Da)	Spectra	Peptides	Sequence coverage (%)
P40 ^{phox}	323.21	16000	480	33	100
Melittin	26.876	2847	18	3	84.6
MSP1E3D1	323.21	32599	554	40	87.7
Syntaxin-1A	323.21	33067	1135	50	81.9

Table S4: m/z ratios of p40^{phox}-proteoliposomes in denaturing MS experiments (see Figure 24A).

composition	m/z experimental	m/z theoretical
[P40 ^{phox}] ⁹⁺	1841.95	1834.06
[DOPC ₂ + DOPE ₃] ²⁺	1902.92	1901.92
[DOPC ₃ + DOPE ₂] ²⁺	1923.94	1922.94
[DOPC ₄ + DOPE] ²⁺	1944.97	1943.97
[DOPC ₅] ²⁺	1965.99	1964.99
[P40 ^{phox}] ⁸⁺	2071.95	2054.12
[DOPC ₃ + DOPE ₃] ²⁺	2296.22	2294.72
[DOPC ₄ + DOPE ₂] ²⁺	2316.75	2315.74
[DOPC ₅ + DOPE] ²⁺	2337.77	2336.76
[DOPC ₆] ²⁺	2358.60	2357.79

Table S5: m/z ratios of p40^{phox}-proteoliposomes in native MS experiments (see Figure 24B).

composition	m/z experimental	m/z theoretical
[DOPC ₅] ²⁺	1967.15	1964.99
[P40 ^{phox}] ⁸⁺	2073.00	2054.12
[DOPC ₄ + DOPE ₂] ²⁺	2317.58	2315.74
[DOPC ₅ + DOPE] ²⁺	2338.57	2336.76
[DOPC ₆] ²⁺	2359.64	2357.79
[P40 ^{phox}] ⁷⁺	2368.58	2347.42

Table S6: m/z ratios of Melittin (M)-proteoliposomes in denaturing MS experiments (see Figure 28A).

Liposomes are composed of DOPC, DOPE, DOPS and cholesterol.

composition			m/z experimental	m/z theoretical
[M+DOPC+		lysoPE] ⁴⁺	1029.16	1029.10
[M+DOPC+	lysoPC] ⁴⁺	1039.68	1039.62
[lysoPC ₂] ¹⁺	1043.70	1043.70
[M+	lysoPC+lysoPE ₂]	⁴⁺	1083.18	1082.87
[M+DOPC+		lysoPE ₂] ⁴⁺	1093.84	1093.61
[M+		lysoPE] ³⁺	1109.69	1109.94
[M+		lysoPC] ³⁺	1123.71	1123.95
[M+	DOPE+lysoPC+lysoPE]	⁴⁺	1149.24	1148.93
[M+DOPC+	lysoPC+lysoPE]	⁴⁺	1159.75	1159.44
[M+DOPC] ³⁺	1212.12	1212.04
[DOPE+	lysoPE] ¹⁺	1223.86	1223.86
[DOPE+lysoPC] ¹⁺	1265.90	1265.90
[DOPC+	lysoDOPC] ¹⁺	1307.95	1307.95

Table S7: m/z ratios of Melittin (M)-proteoliposomes in native MS experiments (see Figure 28B).

Liposomes are composed of DOPC, DOPE, DOPS and cholesterol.

composition			m/z experimental	m/z theoretical
[M+	lysoDOPC] ³⁺	1123.57	1123.95
[M+	DOPE] ³⁺	1196.78	1198.02
[M+DOPC] ³⁺	1211.51	1212.03
[M ₃] ⁷⁺	1222.84	1221.36
[M ₄] ⁹⁺	1266.82	1266.55
[DOPC+	lysoDOPC] ¹⁺	1307.58	1307.95

Table S8: Cross-links Syntaxin-1A

Cross-linking lysine				
Protein 1	Protein 2	Cross-linking		Score
		Position 1	Position 2	
Syntaxin-1A	Syntaxin-1A	10	117	3.11E-04
Cross-linking serine, threonine, tyrosine				
Syntaxin-1A	Syntaxin-1A	12	118	2.90E-02
Syntaxin-1A	Syntaxin-1A	117	109	5.85E-02
Syntaxin-1A	Syntaxin-1A	118	109	5.66E-03
Syntaxin-1A	Syntaxin-1A	12	117	3.11E-04
Syntaxin-1A	Syntaxin-1A	14	117	1.61E-05

Table S9: Cross-links MSP1E3D1

Cross-linking lysine				
Protein 1	Protein 2	Cross-linking		Score
		Position 1	Position 2	
MSP1E3D1	MSP1E3D1	229	101	2
MSP1E3D1	MSP1E3D1	101	86	2
MSP1E3D1	MSP1E3D1	216	86	1
MSP1E3D1	MSP1E3D1	229	86	1
MSP1E3D1	MSP1E3D1	229	216	1
MSP1E3D1	MSP1E3D1	216	101	1

Table S10: Cross-links of syntaxin-1A and MSP1E3D1

Cross-linking lysine				
Protein 1	Protein 2	Cross-linking		Score
		Position 1	Position 2	
MSP1E3D1	Syntaxin-1A	101	83	2.9E-01
MSP1E3D1	Syntaxin-1A	74	256	17.1E-01
MSP1E3D1	Syntaxin-1A	140	256	1.37E-01
MSP1E3D1	Syntaxin-1A	216	117	1.3E-01
MSP1E3D1	Syntaxin-1A	74	94	1.04E-01
Syntaxin-1A	MSP1E3D1	117	86	1.7E-03
MSP1E3D1	Syntaxin-1A	101	117	4.19E-05
Syntaxin-1A	MSP1E3D1	12	86	7.98E-10
Cross-linking serine, threonine, tyrosine				
Syntaxin-1A	MSP1E3D1	14	86	2.58E-11

Acknowledgment

First and foremost, I want to express my great appreciation and gratitude to Jun.-Prof. Dr. Carla Schmidt for giving me the opportunity to deepen my knowledge in the field of mass spectrometry. Her encouragement and supervision have guided me on this journey to successfully complete my dissertation. I would also like to thank her for the many opportunities throughout my dissertation as I was able to attend several international and national conferences and publish papers.

Carla, little did we know that an internship 6 years ago would make me stay by your side for this long. However, the enthusiasm you carry for your research is contagious. Thank you for your continuous support, for being my mentor, for your wisdom, useful critiques, valuable feedback, your eagerness to bring out the best in me and for always having your door open.

Second, I would like to thank the second and third reviewer for reviewing this thesis.

I am sincerely grateful to PD Dr. Annette Meister for performing the negative-stain TEM experiments, that gave valuable insight into the shape and structure of nanodiscs. I also want to thank her for fruitful discussions and all questions I was able to ask related to liposomes and nanodiscs.

A special thank you also goes to Dr. Christian Schwieger for introducing me to lipid monolayers, for the many discussions, valuable feedback and for providing monolayer experiments to this thesis.

I would also like to thank Claudia Müller as she was the first person to introduce me to the world of lipids and liposomes. Throughout the years I was always able to rely on her.

Next, I would like to thank the whole group including current and former members: Marie Alfes (former Barth), Julian Bender, Dr. Caroline Haupt, Julia Hesselbarth, Dr. Tommy Hofmann, Leonie Jaster, Susann Kostmann, Til Kundlacz, Dr. Christian Schwieger and Sabine Wittig for fruitful discussions and for sharing wonderful memories throughout the years, including retreats, conferences, lunch, cake and coffee breaks, Christmas parties, and so much more. To everyone who was involved in critically reading this thesis thank you for all the useful comments and for providing valuable feedback.

To all the members of the graduate school “Beyond Amphiphilicity, Self-organization of Soft Matter via multiple Noncovalent Interactions” (BEAM RTG 2670), especially to Prof. Dr. Dariush Hinderberger and Dr. Imme Sakwa-Waltz, thank you for giving me the opportunity to present my work at BEAM meetings and for giving me the opportunity to be the first spokesperson of the d-colloquium

(weekly colloquium for PhD students). I also want to thank them for allowing me to attend many inspiring workshops and lectures.

To all my master, bachelor and internship students including Lea Steen, Danny Knobloch-Sperlich and Phuong Anne Günther thank you for letting me share this exciting field of research with you. A special thanks also goes to Danny Knobloch-Sperlich for providing liposome experiments to this thesis.

Next, I would also like to thank my friends for their ongoing support and encouragement throughout the years. A special thanks goes to Robert Broneske and Johanna Nordmeier for their helpful discussions during these past years.

At last, a very special thank you goes to my family, especially to my mom, my sister and my brother. You have all been my rocks. Thank you for your encouragement and for always being my biggest cheerleaders. I love you.

Curriculum vitae

Personal data

Name Melissa Elena Frick
Nationality German, Canadian
Date of birth January 17th, 1993
Place of birth Bad Homburg vor der Höhe

Education

09/2018 - present **PhD student**
Institute of Biochemistry and Biotechnology, Martin Luther University
Halle-Wittenberg, Interdisciplinary Research Center HALOmem, Charles
Tanford Protein Center, Halle (Germany)
Group of Jun.- Prof. Dr. Carla Schmidt, *Biophysikalische
Charakterisierung von medizinisch relevanten Membranproteinen*

10/2016 -05/ 2018 **Master of Science, Biochemistry**
Institute of Biochemistry and Biotechnology, Martin Luther University
Halle-Wittenberg, Halle (Germany)
Title of master thesis: *Exploring Liposomes for Mass Spectrometry*

09/2013-09/2014 **Study abroad**
Trent University, Peterborough (Canada)

10/2011 – 08/2016 **Bachelor of Science, Biochemistry**
Institute of Biochemistry and Biotechnology, Martin Luther University
Halle-Wittenberg, Halle (Germany)
Title of bachelor thesis: *Mass Spectrometric studies on
bMunc13- 2/Calmodulin interaction*

2011 **Highschool diploma (Abitur)**
Albert-Einstein-Gymnasium, Schwalbach (Germany)

Publication list

Frick M, Schwieger C, Schmidt C., (2021) Liposomes as Carriers of Membrane-Associated Proteins and Peptides for Mass Spectrometric Analysis. **Angew Chem Int Ed Engl** 60(20), 11523-11530 **Hot paper, Cover story**

Frick M, Schmidt C., (2019) Mass spectrometry-A versatile tool for characterizing the lipid environment of membrane protein assemblies. **Chem Phys Lipids** 221, 145-157.

Frick, M, Schmidt, C., (2019) Massenspektrometrische Analyse von Phospholipiden aus Liposomen. **Biospektrum** 25, 167–169

Frick M, Hofmann T, Haupt C, Schmidt C., (2018) A novel sample preparation strategy for shotgun lipidomics of phospholipids employing multilamellar vesicles. **Anal Bioanal Chem** 410, 4253-4258.

Manuscripts in preparation

Julian Bender, Til Kundlach, Lucas S. Powell-Rudden, **Melissa Frick**, Christian Schwieger, Matteo T. Degiacomi, Carla Schmidt. Lipid binding of Synaptotagmin-1, **manuscript in preparation**.

Oral presentations

EMBO Workshop, Hamburg, virtual (29.11 – 01.12.2021)

Liposomes as carriers of membrane-associated proteins and peptides for mass spectrometric analysis

HALOmem Retreat, Lutherstadt Wittenberg (15. – 17.07.2021)

Exploring nanodiscs for membrane fusion

HALOmem supergroup meeting, Halle, virtual (27.05.2021)

Liposomes as carriers of membrane-associated proteins and peptides for mass spectrometric analysis

6th Statusseminar HALOmem, Halle, virtual (12.11.2020)

Liposomes as carriers of peripheral membrane proteins for mass spectrometric analysis

D-colloquium BEAM GRK 2670, Halle, virtual (30.06.2020)

Membrane Mimetics – How liposomes and nanodiscs support the structural analysis of membrane proteins

5th Statusseminar HALOmem, Halle (8.11.2018)

Mass spectrometry of liposomes

Poster presentations

Frick, Schwieger, Schmidt. Liposomes as carriers of membrane-associated proteins and peptides for mass spectrometric analysis. EMMTJ, Graz (Austria), 2021

Frick, Schmidt. Establishing proteoliposomes for the analysis of membrane proteins by mass spectrometry. ASMS, Houston (USA), 2020

Frick, Bender, Schmidt. Establishing proteoliposomes for the analysis of membrane proteins. DGMS, Münster (Germany), 2020

Frick, Haupt, Schmidt. Exploring (proteo-) liposomes for mass spectrometry. 63rd Biophysical Society Annular Meeting, Baltimore (USA), 2019

Frick, Bender, Schmidt. Establishing proteoliposomes for the analysis of membrane proteins directly from the phospholipid bilayer. EMBO Workshop, Hamburg (Germany), 2019

Frick, Bender, Schmidt. Establishing proteoliposomes for the analysis of membrane proteins directly from the phospholipid bilayer. International HALOmem Meeting, Halle (Germany), 2019

Frick, Bender, Schmidt. Establishing proteoliposomes for the analysis of membrane proteins directly from the phospholipid bilayer. SSP, Göttingen (Germany), 2019

Frick, Hofmann, Haupt, Schmidt. Exploring liposomes for mass spectrometry. European Lipidomics Meeting, Leipzig (Germany), 2018

Frick, Schmidt. Exploring liposomes for mass spectrometry. SSP, Berlin (Germany), 2018

Frick, Hofmann, Haupt, Schmidt. Mass spectrometry of liposomes. Lipidomics Forum, Borstel (Germany) 2017

Frick, Hofmann, Haupt, Schmidt. Mass spectrometry of liposomes. Status report meeting HALOmem, Halle (Germany), 2017

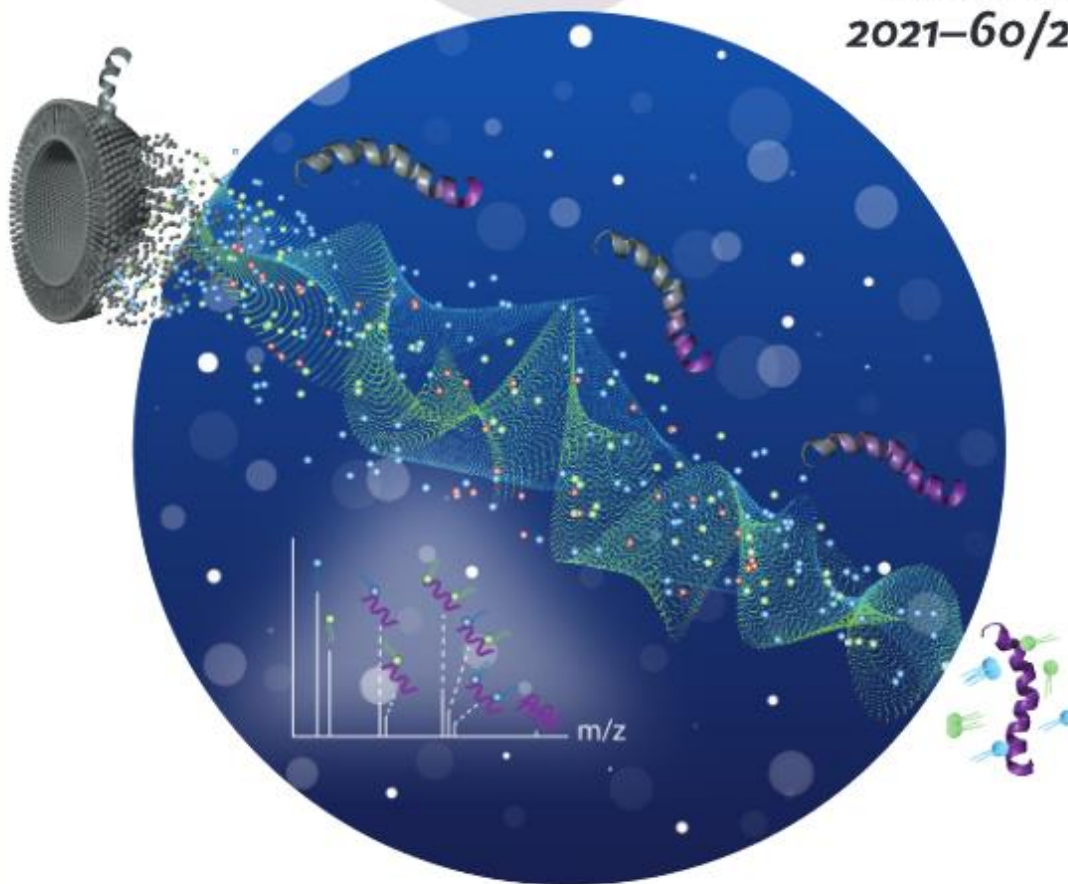
A Journal of the German Chemical Society

Angewandte Chemie

GDCh
International Edition

www.angewandte.org

2021–60/20



Cover Picture

Carla Schmidt et al.

Liposomes as Carriers of Membrane-Associated Proteins and Peptides
for Mass Spectrometric Analysis

ACEFS 60 (20) 10997–11532 (2021) · ISSN 1433–7851 · Vol. 60 · No. 20

WILEY-VCH

Affidavit

I hereby declare that this thesis has been written independently and with no other sources and aids than quoted. Parts directly or indirectly obtained from foreign sources are indicated. In addition, material provided, or experiments performed by other persons are indicated. The submitted written version of this thesis corresponds to that on the electronic storage medium. Furthermore, I assure that this doctoral thesis has not been submitted as a thesis elsewhere. I have not submitted any other doctoral thesis before this thesis.

Halle (Saale),

Melissa Frick

Eidesstattliche Erklärung

Hiermit versichere ich, dass ich die vorliegende Arbeit selbstständig und ohne fremde Hilfe angefertigt habe und keine anderen Quellen und Hilfsmittel verwendet habe. Die aus fremden Quellen direkt oder indirekt übernommenen Stellen sind als solche kenntlich gemacht. Ebenfalls sind alle von anderen Personen bereitgestellten Materialien oder erbrachten Experimente als solche gekennzeichnet. Die eingereichte schriftliche Fassung der Arbeit entspricht der auf dem elektronischen Speichermedium. Weiterhin versichere ich, dass die vorliegende Promotionsarbeit noch nicht als Abschlussarbeit an anderer Stelle eingereicht wurde. Ich habe vor dieser Arbeit keine andere Promotionsarbeit eingereicht.

Halle (Saale), den

Melissa Frick